Novel derivatives of nicotinamide adenine dinucleotide (NAD) and their biological evaluation against NAD-Consuming Enzymes

Giulia Pergolizzi

University of East Anglia
School of Pharmacy

Thesis submitted for the degree of Doctor of Philosophy
July, 2012

ABSTRACT

Nicotinamide adenine dinucleotide (β-NAD^+) is a primary metabolite involved in fundamental biological processes. Its molecular structure with characteristic functional groups, such as the quaternary nitrogen of the nicotinamide ring, and the two high-energy pyrophosphate and nicotinamide *N*-glycosidic bonds, allows it to undergo different reactions depending on the reactive moiety. Well known as a redox substrate owing to the redox properties of the nicotinamide ring, β-NAD^+ is also fundamental as a substrate of NAD^+-consuming enzymes that cleave either high-energy bonds to catalyse their reactions. In this study, a panel of novel adenine-modified NAD^+ derivatives was synthesized and biologically evaluated against different NAD^+-consuming enzymes. The synthesis of NAD^+ derivatives, modified in position 2, 6 or 8 of the adenine ring with aryl/heteroaryl groups, was accomplished by Suzuki-Miyaura cross-couplings. Their biological activity as inhibitors and/or non-natural substrates was assessed against a selected range of NAD^+-consuming enzymes. The fluorescence of 8-aryl/heteroaryl NAD^+ derivatives allowed their use as biochemical probes for the development of continuous biochemical assays to monitor NAD^+-consuming enzyme activities. The introduction of different substituents in position 8 on the adenine ring allowed the modulation of their fluorescence, resulting in the development of more sensitive and alternative probes compared to the known fluorophore ε-NAD^+. The different substitutions introduced on the adenine ring also allowed us to probe the active site of an NAD^+-dependent bacterial DNA ligase. The selective activity of 8-aryl/heteroaryl NAD^+ derivatives against different NAD^+-consuming enzymes offers excellent opportunities for their application as tool compounds in *in-vitro*/*in-vivo* studies, and as inhibitor templates for drug discovery.

Parts of this thesis have already been published in scientific journals, and presented at scientific conferences.

- A novel fluorescent probe for NAD-consuming enzymes

Giulia Pergolizzi, Julea N. Butt, Richard P. Bowater and Gerd K. Wagner
Chemical Communications, **2011**, 47, 12655-12657.

- Two-Step Synthesis of Novel, Bioactive Derivatives of the Ubiquitous Cofactor Nicotinamide Adenine Dinucleotide (NAD)

Thomas Pesnot, Julia Kempter, Jörg Schemies, Giulia Pergolizzi, Urszula Uciechowska, Tobias Rumpf, Wolfgang Sippl, Manfred Jung, and Gerd K. Wagner
Journal of Medicinal Chemistry, **2011**, 54, 3492-3499.

3^{th} – 8^{th} July 2011: Synthesis and biological evaluation of novel fluorescent NAD^+ analogues. Giulia Pergolizzi, oral communication, European School of Medicinal Chemistry (ESMEC) (Urbino, Italy).

April 2011: Base-modified NAD^+ derivatives – Novel Chemical Tools for the Investigation of NAD^+-consuming Enzymes. Giulia Pergolizzi, Julea N. Butt, Richard P. Bowater and Gerd K. Wagner, poster presentation, RSC Carbohydrate and Bioorganic Meeting (5^{th} April) & RSC Bioorganic Postgraduate Symposium (15^{th} April) (London, UK).

July – September 2010: Novel NAD^+ derivatives modified at the adenine base: synthesis and biological applications. Giulia Pergolizzi, Julea N. Butt, Richard P. Bowater and Gerd K. Wagner, poster presentation, 6^{th} Nucleic Acids Forum Meeting (2^{nd} July, Liverpool, UK) & 8^{th} NACON (Nucleic Acid Conference) (12^{th} – 16^{th} September, Sheffield, UK).

TABLE OF CONTENTS

List of Figures

List of Schemes

List of Tables

List of Figures in Appendix

List of Tables in Appendix

Abbreviations

Φ	quantum yield
δ	chemical shift
°C	degree Celsius
2″(3″)-OAc-ADPR	2″(3″)-acetate-adenosine diphosphate ribose
2″-FNAD$^+$	2″-fluoro-nicotinamide adenine dinucleotide (ox.form)
2-AP	2-amino purine
2-F-ADPR	2-fluoro adenosine diphosphate ribose
2-F-NAD$^+$	2-fluoro nicotinamide adenine dinucleotide (ox. form)
2HPC	2-hydroxy-3-pyridinecarboxaldehyde
3AcPAD$^+$	3-acetyl pyridine adenine dinucleotide (ox. form)
3AlPAD$^+$	3-aldehyde pyridine adenine dinucleotide (ox. form)
3HAO	3-hydroxyanthranilate-3,4-dioxygenase
Å	angstrom
AAD	*bis*-adenine dinucleotide
Ac	acetyl
acetyl-CoA	acetyl coenzyme A
ACN	acetonitrile
AcOH	acetic acid
Ado	adenosine
ADP	adenosine diphosphate
ADPR	adenosine diphosphate ribose
ADPRC	adenosine diphosphate ribosyl cyclase
ADPRNH$_2$	1″-amino adenosine diphosphate
ADPR-*p*NP	adenosine diphosphate ribose *para*-nitro phenol
AMC	7-amino-4-methyl coumarin
AMP	adenosine 5′-monophosphate
ara-2″-FNAD$^+$	nicotinamide 2″-deoxy-2″-fluoroarabinoside adenine dinucleotide (ox. form)
ara-2″-FNMN	nicotinamide 2″-deoxy-2″-fluoroarabinoside mononucleotide
ara-NAD$^+$	nicotinamide arabinoside adenine dinucleotide (ox. form)
Arg	arginine

ART	adenosine diphosphate ribosyl transferase
ATP	adenosine triphosphate
BAD	benzamide adenine dinucleotide
Boc	*tert*-butyloxycarbonyl
bp	base pair
br s	broad singlet
BRCT	breast cancer carboxy-terminal
BSA	bovin serum albumin
Bu	butyl
*c*ADPR	cyclic adenosine diphosphate ribose
*c*ADPRP	2′-phosphate cyclic adenosine diphosphate ribose
*c*AMP	3′,5′-cyclic adenosine monophosphate
carba-NAD^+	carba-nicotinamide adenine dinucleotide (ox. form)
Cbz	carboxybenzyl
*c*GDPR	cyclic guanine diphosphate ribose
CICR	Ca^{2+}-induced Ca^{2+}-release
*c*IDPR	cyclic inosine diphosphate ribose
cm	centimetre
CN	cyanide
C-NAD	C-nicotinamide adenine dinucleotide
C-PAD	C-picolinamide adenine dinucleotide
*c*XDPR	cyclic xanthosine diphosphate ribose
Cys	cysteine
*c*εADPR	cyclic 1,N^6-etheno-adenosine diphosphate ribose
d	doublet
*d*AMP	deoxy adenosine monophosphate
DCI	4,5-dicyanoimidazole
dd	doublet of doublets
DDR	DNA damage response
*d*GMP	deoxy guanosine monophosphate
DH	dehydrogenase
DIPEA	diisopropylethylamine

DMAP	4-dimethylamino pyridine
DME	dimethyl ether
DMF	dimethylformamide
DMSO	dimethylsulfoxide
DMT	dimethoxy
DNA Lig	deoxy ribonucleic acid ligase
DNA	deoxy ribonucleic acid
DTT	dithiothreitol
E	glutamic acid
E. coli	*Escherichia coli*
E. faecalis	*Enterococcus faecalis*
EcLigA	*Escherichia coli* DNA ligase
EDTA	ethylenediaminetetraacetic acid
ENPP	ecto-nucleotide pyrophosphatase
equiv	equivalent
ESI	electrospray ionization
EtOAc	ethyl acetate
FAM	6-carboxy fluorescein
FRET	Förster (fluorescence) resonance energy transfer
g	gram
Grad	gradient
HAT	histone acetyl transferase
HCV	hepatitis C virus
HDAC	histone deacetylase
HEPES	4-(2-hydroxyethyl)-1-piperazineethanesulfonic acid
HHD	*bis*-hypoxanthine dinucleotide
HhH	helix-hairpin-helix
His	histidine
HOBt	hydroxybenzotriazole
HOMO	highest occupied molecular orbital
HPLC	high pressure liquid chromatography
HR-MS	high resolution mass spectra

Hz	hertz
IC	internal conversion
IC_{50}	half maximal inhibitory concentration
IDA	iminodiacetic acid
IDO	indoleamine-2,3-dioxygenase
Ile	isoleucine
IP_3	inositol 1,4,5-triphosphate
iPA	isopropanol
IPTG	isopropil β-D-1-tiogalattopiranoside
ISC	inter system crossing
J	coupling constant
K	kelvin
K3H	kynurenine 3-hydroxylase
kcal	kilocalorie
k_{cat}	enzymatic turnover number
kDa	kilodalton
KFase	kynurenine formamidase
K_i	inhibition constant for competitive inhibitor
K_i'	inhibition constant for uncompetitive inhibitor
K_m	Michaelis-Menten constant
Kyase	kynureninase
LB	Luria Bertani
LC	liquid chromatography
LUMO	lowest unoccupied molecular orbital
Lys	lysine
M	molar
m	multiplet
m/z	mass to charge ratio
MAL	*tert*-butyloxycarbonyl 1-(4-methyl-2-oxo-2H-chromen-7-ylcarbamoyl)-5-acetamidopentylcarbamate (*Boc*-Lys[Ac]-AMC)
Me	methyl
MeOH	methanol

mer	polymer unit
mg	milligram
MHz	megahertz
mL	millilitre
mM	millimolar
mm	millimetre
mol	mole
MS	mass spectra
N	normal
NA	nicotinic acid
NADase	nicotinamide adenine dinucleotide glycohydrolase
NADK	nicotinamide adenine dinucleotide kinase
NaM	nicotinamide
NAMN	nicotinic acid mononucleotide
NAMNAT	nicotinic acid mononucleotide adenylyl transferase
NaMPRT	nicotinamide phospho-ribosyl transferase
NaOAc	sodium acetate
NAPRT	nicotinic acid phospho-ribosyl transferase
NFD^+	nicotinamide formycin dinucleotide (ox. form)
NGD^+	nicotinamide guanine dinucleotide (ox. form)
NHD^+	nicotinamide hypoxanthine dinucleotide (ox. form)
nm	nanometre
nM	nanomolar
NMNAT	nicotinamide mononucleotide adenylyl transferase
NMR	nuclear magnetic resonance
NNS	non-natural substrate
NOE	nuclear Overhauser effect
NOESY	nuclear Overhauser effect spectroscopy
NPP	nucleotide pyrophosphatase
NR	nicotinamide ribonucleoside
NRK	nicotinamide ribonucleoside kinase
NS	natural substrate

NTase	nucleotidyl transferase
NXD^+	nicotinamide xanthine dinucleotide (ox. form)
OAc	acetate
OB	oligonucleotide binding
OD	optical density
PAGE	polyacrylamide gel electrophoresis
PAH	polycyclic aromatic hydrocarbon
PARG	polyadenosine diphosphate ribosyl glycohydrolase
PARP	polyadenosine diphosphate ribosyl polymerase
PDB	protein data bank
Ph	phenyl
P_i	phosphate
pK_a	acid dissociation constant
ppb	parts per billion
PPh_3	triphenylphosphine
PP_i	diphosphate, or pyrophosphate
ppm	parts per million
PPP_i	triphosphate
PTS	polyoxyethanyl α-tocopheryl sebacate
q	quartet
QA	quinolic acid
QAPRT	quinolic acid phospho-ribosyl transferase
RCSB	research collaboratory for structural bioinformatics
R_f	retention factor
RFU	relative fluorescence unit
RNA	ribonucleic acid
ROS	reactive oxygen species
RP	reverse phase
rt	room temperature
s	singlet
SD	standard deviation
SDS	sodium dodecyl sulphate

S_EAr	aromatic electrophilic substitution
Sir	silent information regulator
SIRT	sirtuin
$S_N1(2)$	nucleophilic substitution
S_NAr	aromatic nucleophilic substitution
T	threonine
$t_{1/2}$	half life
TAMRA	tetramethyl rhodamine
TBAF	tetrabutylammonium fluoride
TBE	tris/borate/EDTA
^{t}Bu	*tert*-butyl
^{t}BuOH	*tert*-butanol
^{t}BuOOH	*tert*-butyl hydroperoxide
TDO	tryptophan-2,3-dioxygenase
TEA	triethylamine
TEAB	triethylammonium bicarbonate buffer
TFA	trifluoroacetic acid
TGS	tris/glycine/SDS
THF	tetrahydrofurane
thio-NAD^+	thio-nicotinamide adenine dinucleotide (ox. form)
TIPS	triisopropylsilyl
TLC	thin layer chromatography
TPPTS	triphenylphosphine trisulfonate
Tris	tris(hydroxymethyl)aminomethane
tRNA	transfer ribonucleic acid
Trp	tryptophan
TXPTS	trixylylphosphine trisulfonate
U	enzyme unit
V	volt
V_0	initial velocity
V_{max}	maximum velocity
V_w	van der Waals volume

W	tryptophan
Y	tyrosine
Z-MAL	benzyl 1-(4-methyl-2-oxo-2H-chromen-7-ylcarbamoyl)-5-acetamidopentylcarbamate (*Cbz*-Lys[Ac]-AMC)
ZML	benzyl 1-(4-methyl-2-oxo-2H-chromen-7-ylcarbamoyl)-5-aminopentylcarbamate (*Cbz*-Lys-AMC)
α-NAD^+	α-nicotinamide adenine dinucleotide (ox. form)
β-$NAAD^+$	β-nicotinic acid adenine dinucleotide (ox. form)
β-$NAADP^+$	2′-phosphate β-nicotinic acid adenine dinucleotide (ox. form)
β-NAD^+	β-nicotinamide adenine dinucleotide (ox. form)
β-NADH	β- nicotinamide adenine dinucleotide (red. form)
β-$NADP^+$	2′-phosphate β-nicotinamide adenine dinucleotide (ox. form)
β-NADPH	2′-phosphate β-nicotinamide adenine dinucleotide (red. form)
β-NMN	β-nicotinamide mononucleotide
ΔE^0	difference of standard reduction potential
ε-ADP	1,N^6-etheno-adenosine diphosphate
ε-ADPR	1,N^6-etheno-adenosine diphosphate ribose
ε-AMP	1,N^6-etheno-adenosine monophosphate
ε-ATP	1,N^6-etheno-adenosine triphosphate
ε-hy^4$PdAD^+$	1,N^6-etheno-4-hydrazinocarbonyl pyridine adenine dinucleotide (ox. form)
ε-NAD^+	1,N^6-etheno-nicotinamide adenine dinucleotide
ε-$PdAD^+$	1,N^6-etheno-pyridine adenine dinucleotide (ox. form)
η	refractive index
λ_{em}	emission wavelength
λ_{ex}	excitation wavelength
µg	microgram
µL	microlitre
µm	micrometre
µM	micromolar
µmol	micromole
ψ carba-NAD^+	*pseudo* carba-nicotinamide adenine dinucleotide (ox. form)

Acknowledgements

I would like to thank my supervisors, Dr Gerd Wagner, Dr Richard Bowater and Prof Julea Butt, for encouraging, supporting and believing in me during the whole period of my PhD, and for contributing to my knowledge as a scientist. I would also like to thank UEA for the studentship and KCL for the financial support, which enabled me to carry out this PhD.

I wish to thank all the teaching and technical staff at the KCL for their warm welcome in the new institute. I wish to extend my gratitude to Andrew Atkinson (KCL), Shirley Fairhurst (JIC), Colin MacDonald (UEA) and Martin Rejzek (JIC) for their assistance with obtaining NMR data. I am grateful to the EPSCR National Mass Spectrometry Service Centre in Swansea for the recording of Mass Spectra. I am also grateful to Manfred Jung and his group for the biological testing of candidate molecules. I would like to thank Sebastian Gehrke for its help in the docking studies, and Sarah Zähringer for its help in the synthetic part of this project. Special thanks to Lauren for proofreading this thesis.

I wish to thank my very special housemates and best friends, Doroty and Lorina, who shared with me so many moments and emotions along these four years. Special thanks go to Thomas for its great help as friend and mate in the laboratory, and to Simone for being my "punch ball".

I wish to thank all past and present members of the Wagner group: Alice, Andy E., Ferdinand, George, Karine, Lauren, Niina, Sebastian and Sarah for their help and company in and outside the laboratory. And more, my colleagues, Andrew and Andy G. for their support during my work in BIO (UEA). I would like to thank my dear friends, Francesca and Andrea, who always made me smile, and all friends I have met along these years, Alberto, Annalisa, Chiara, Eva, Ewelina, Fatima, Giovanna, Huiying, Kristel, Sam, Simona and Yongmin. I wish also to thank all my friends back home, in particular Paolo, Dario, Giovanna, Valentina and Irene, for their support.

Last but not least, very special thanks to my parents and my sister for their tireless and wholehearted support during my studies, which allowed me to arrive until here.

1 β-NAD+: AN ESSENTIAL BIOLOGICAL MOLECULE

1.1 β-NAD+ structure

Nicotinamide adenine dinucleotide, β-NAD+, is a ubiquitous biological molecule found in all living cells that is involved in many major biological processes. Its structure consists of two nucleotides, adenosine 5′-monophosphate (AMP) and β-nicotinamide mononucleotide (β-NMN), joined by a pyrophosphate bond through their phosphate groups (Figure 1.1).[1]

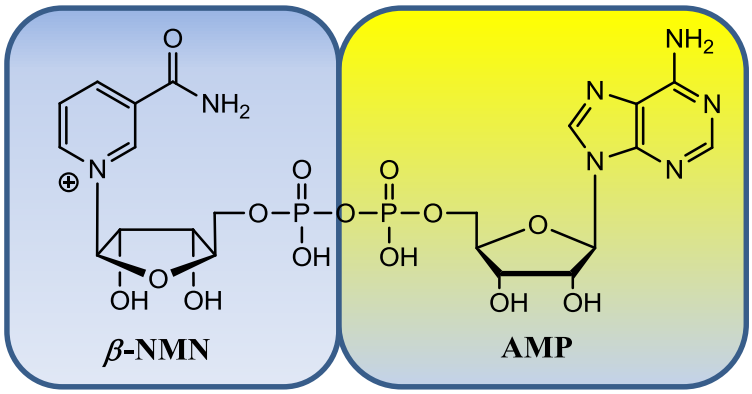

Figure 1.1 β-NAD+ structure. AMP (yellow box) and β-NMN (blue box) joined by a pyrophosphate bond.

Its discovery and structure assignment in the 1930s attributed to β-NAD+ the main function of reversible hydride donor/acceptor because of the ability of the nicotinamide (NaM) ring to shuttle between the oxidized and reduced form by the transfer of a proton and two electrons (Figure 1.2). Because of this property, β-NAD+ was classified as a redox co-substrate for enzymes catalyzing redox reactions. The reduction potential for the β-NAD+/β-NADH couple, $\Delta E^0_{NAD+/NADH}$, is equal to -0.320 V; therefore, the oxidation of β-NADH to β-NAD+ is strongly favoured compared to its reduction and this makes β-NADH a strong reducing agent (Figure 1.2).[2]

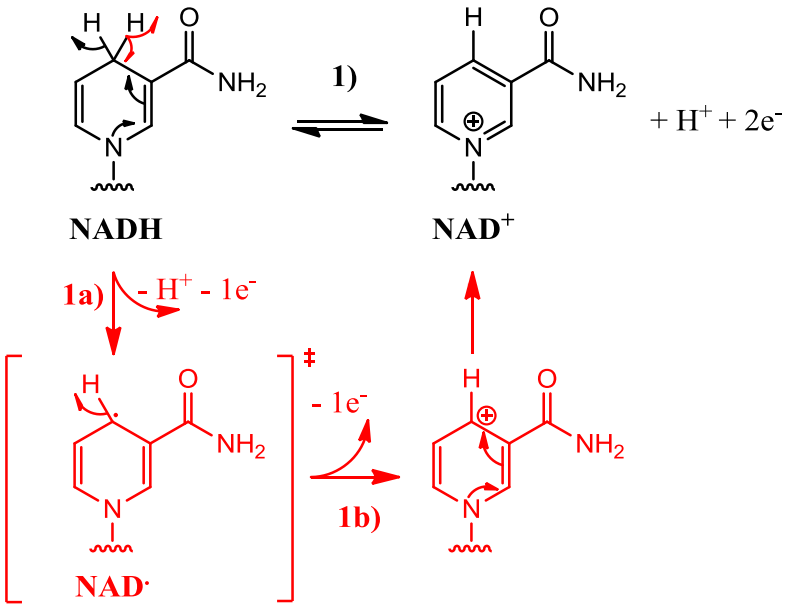

Figure 1.2 β-NAD$^+$/β-NADH redox reaction. The redox reaction can go through a two-electron mechanism (**1**, in black) or a one-electron mechanism (**1a**, **1b**, in red), depending on the redox potential of the coupled substrate, and, in case of enzymatic reactions, on the pH, the polarity of the solvent and steric requirement.[2, 3] Generally, enzymatic reactions proceed *via* **1**, where the enantiotopic protons, *pro*-R and *pro*-S, can be preferentially transferred depending on the enzymes. The one-electron reduction potential for the couple β-NAD$^{\cdot}$/β-NADH is $\Delta E^0_{NAD\cdot/NADH}$ = 0.282 V (**1a**); for the couple β-NAD$^+$/ β-NAD$^{\cdot}$, it is $\Delta E^0_{NAD+/NAD\cdot}$ = -0.922 V (**1b**). The overall reaction (**1**) generates β-NAD$^+$ from β-NADH by the loss of a proton and two electrons ($\Delta E^0_{NAD+/NADH} = (\Delta E^0_{NAD\cdot/NADH} + \Delta E^0_{NAD+/NAD\cdot})/2$ = -0.320 V).

Besides its redox property, the structure of β-NAD$^+$ is characterized by two high-energy bonds, the nicotinamide *N*-glycosidic bond and the pyrophosphate bond, and cleavage of either releases a substantial amount of energy (Figure 1.3). The cleavage of the nicotinamide *N*-glycosidic bond (**a**) results in the formation of NaM and adenosine diphosphate ribose (ADPR); on the other hand, cleavage of the pyrophosphate bond (**b**) generates β-NMN and AMP. These bonds, extremely labile and unstable, make β-NAD$^+$ easily susceptible to enzymatic and chemical hydrolytic degradation.

The enzymatic cleavage of either high-energy bond in the structure of β-NAD$^+$ is catalyzed by NAD$^+$-consuming enzymes.[4-7] These enzymes use β-NAD$^+$ as a substrate to generate important signalling molecules (*e.g.* cyclic ADPR, or *c*ADPR, and ADPR), or covalently modify the acceptors involved in their enzymatic reactions.

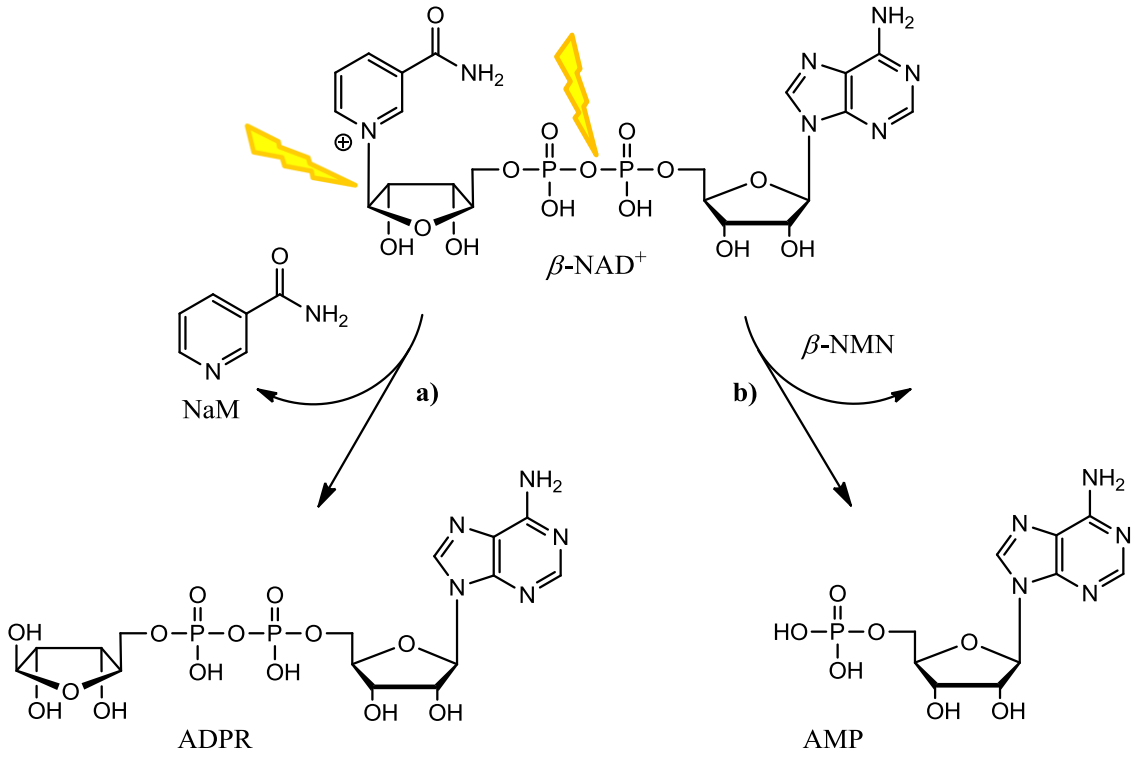

Figure 1.3 β-NAD$^+$ and its high-energy bonds. The cleavage of nicotinamide *N*-glycosidic bond (**a**) generates NaM and ADPR; the cleavage of pyrophosphate bond (**b**) generates β-NMN and AMP.

Regarding its chemical hydrolytic degradation, β-NAD$^+$ is very unstable under basic conditions, while relatively stable under acidic conditions.[8] It has been shown that, at concentrations below 1 M KOH, the main hydrolytic reaction is the cleavage of the nicotinamide *N*-glycosidic bond (Figure 1.3 **a**, Figure 1.4 **a**). Indeed, under these conditions the ionization of the ribose diol (pK_a = 11.9) would accelerate the release of NaM because of the electron-donating ability of the anion that stabilizes the oxocarbenium ion intermediate; evidence of this effect is given by the stability of *O*-isopropylidene protected nicotinamide ribonucleoside (NR) to the cleavage of the nicotinamide *N*-glycosidic bond. At concentrations above 1 M KOH, the primary reaction would become the nucleophilic attack of the hydroxide on the nicotinamide ring to generate 2-hydroxy-3-pyridinecarboxaldehyde (2HPC) by ring opening, elimination and reclosing (Figure 1.4 **b**).[9-11]

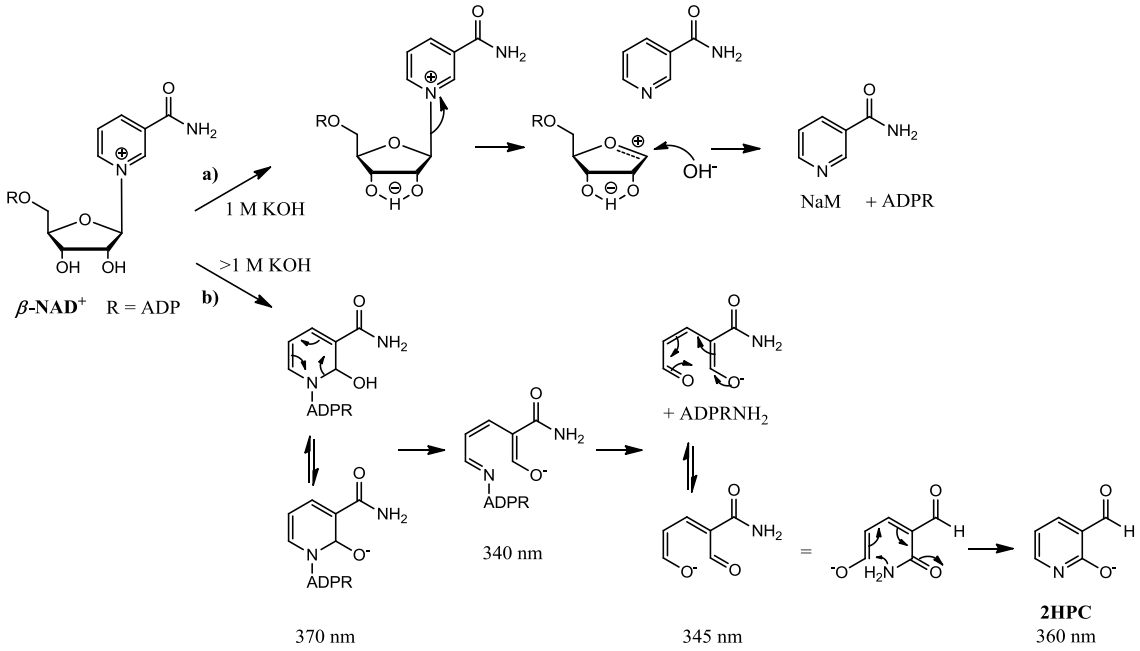

Figure 1.4 β-NAD$^+$ decomposition pathways in basic conditions. **a)** The cleavage of nicotinamide *N*-glycosidic bond with formation of NaM and ADPR occurs at concentration ≤ 1 M KOH. **b)** The hydroxylation of NaM, ring opening, release of 1′′-amino adenosine diphosphate ribose ($ADPRNH_2$), ring closing with formation of 2HPC occurs at concentration > 1 M KOH.

1.1.1 Redox properties of β-NAD$^+$

Owing to its reversible redox activity, β-NAD$^+$(H) is involved in fundamental metabolic processes occurring in prokaryotes and eukaryotes, such as glycolysis, the Krebs cycle and cellular respiration (Figure 1.5).[1] During the oxidative catabolism of different substances (*e.g.* carbohydrates, lipids, proteins) to a common intermediate (acetyl coenzyme A, or acetyl-CoA), the energy released can be used to reduce β-NAD$^+$ to β-NADH (endergonic reduction) in the cytosol. β-NADH molecules are then re-oxidized into β-NAD$^+$ at the surface of the mitochondrial membrane in eukaryotes, generating electrons that are transferred to the electron transport chain, comprising an enzymatic series of redox reactions across the mitochondrial inner membrane, to finally reduce O_2 to H_2O. During the reactions occurring in the electron transport chain, a proton gradient across the mitochondrial membrane is generated, providing the energy to catalyze the endergonic synthesis of adenosine triphosphate, ATP, from adenosine diphosphate, ADP, and phosphate, P_i (oxidative phosphorylation).[1]

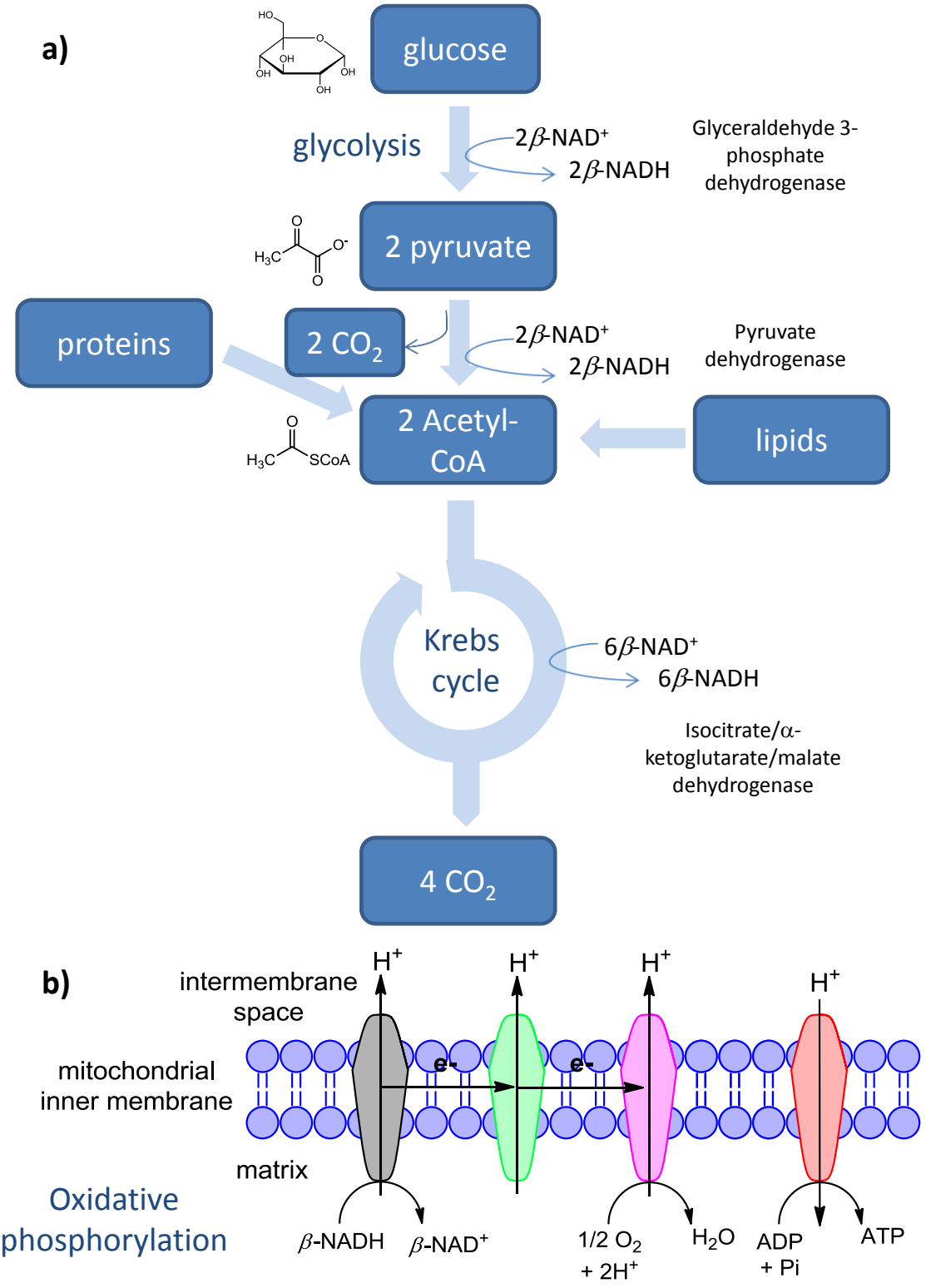

Figure 1.5 Glucose metabolism and enzymatic reactions involving β-NAD$^+$(H) as a redox substrate. **a)** refers to processes occurring in the cytosol, **b)** to the oxidative phosphorylation occurring in eukaryotes at the interface with the mitochondrial membrane.

Enzymes using β-NAD^+(H) as a redox substrate keep constant the cytosolic concentration of the dinucleotide that shuttles between its oxidized and reduced form. The β-NAD^+:β-NADH ratio is connected to the intracellular redox state and influences several metabolic processes; changes in this ratio reflect metabolic changes in the cells,[12] hence the importance to cellular functions to monitor the β-NAD^+:β-NADH ratio.

Intracellular β-NAD^+(H) can be present in the free and enzyme-bound form; the total (free + bound) intracellular β-NAD^+:β-NADH ratio fluctuates between 0.1 and 10 in different organisms, while the cytosolic free β-NAD^+:β-NADH ratio is around 500, since most β-NADH is in its enzyme-bound form.[12, 13] The β-NAD^+:β-NADH ratio has been estimated in different cellular compartments, for example in the cytosol and the mitochondria, showing quite similar values, with the oxidized form favoured to the reduced form.[12] The preference for a substantial free pool of β-NAD^+ compared to β-NADH reflects the requirement of β-NAD^+ in the catabolic processes occurring in the cytosol.

1.1.2 β-NAD^+ catabolism and NAD^+-consuming enzymes

As mentioned in 1.1.1, the use of β-NAD^+(H) as a substrate by redox enzymes does not alter its concentration in living cells. By contrast, β-NAD^+ is used up by NAD^+-consuming enzymes,[7] strictly involved in the catabolism of β-NAD^+.

ADP-ribosyl cyclases (ADPRCs), NAD^+-glycohydrolases (NADases), ADP-ribosyl transferases (ARTs), polyADP-ribosyl polymerases (PARPs) and sirtuins all share the same substrate/co-substrate, β-NAD^+, and catalyze the cleavage of the nicotinamide *N*-glycosidic bond with consequent release of NaM as a reaction product. In ADPRCs and NADases, β-NAD^+ is the only enzyme substrate and it is used to generate *c*ADPR and ADPR (Figure 1.6). In addition, ADPRCs can also catalyze the exchange of the nicotinamide ring with the nicotinic acid (NA) from β-$NAD(P)^+$, or (2′-phosphate) nicotinamide adenosine dinucleotide, to generate β-$NAAD(P)^+$, or (2′-phosphate) nicotinic acid adenosine dinucleotide, not consuming the β-NAD^+ scaffold. All these molecules have been shown to be involved in Ca^{2+} signalling, although through

completely different pathways (Figure 1.6).[4, 6, 7, 13] ARTs and PARPs use β-NAD^+ as a co-substrate in their reactions, where they catalyze respectively the transfer of one unit of ADPR, or many branched polymers of ADPR, to amino acid protein residues (Figure 1.6). Protein modification by ARTs would have a regulatory and signalling role, acting by inhibition of the normal activities of the protein acceptors. Regarding PARPs, a variety of these enzymes have been found in mammals; the best studied is PARP-1, for which the modification of the protein is triggered by breaks in the DNA and, therefore, it is involved in the DNA repair response and transcriptional activation. Another important PARP is tankyrase-1, which regulates the maintenance of telomere length (Figure 1.6).[4, 6, 7] Finally, sirtuins use β-NAD^+ as a co-substrate to mainly catalyze the deacetylation of proteins and generate NaM and 2″(3″)-acetate-ADPR, or 2″(3″)-OAc-ADPR (Figure 1.6). The deacetylation of proteins is a fundamental regulatory biological process; hence, the interest toward sirtuins has increased since they appear to be involved in epigenetic, ageing and several human diseases.[5, 6] In addition, the reaction product, 2″(3″)-OAc-ADPR, seems to be a signalling molecule involved again in Ca^{2+} release.[6, 7, 13] Sirtuins could also have a secondary activity as ARTs, but it is still not clear in which conditions this activity would be stimulated (Figure 1.6).[14]

Nucleotide pyrophosphatases (NPPs) and NAD^+-dependent DNA ligases use β-NAD^+ respectively as a substrate and a co-substrate.[15, 16] Indeed, both enzymes catalyze the cleavage of the pyrophosphate bond to generate AMP and β-NMN (Figure 1.6); in the case of the DNA ligases, this reaction is in conjunction with the ligation of a single strand DNA break. With respect to AMP generated from NPPs, which are generally ecto-enzymes with the catalytic site in the extracellular space, this can be recycled by ecto-5′-nucleotidases to obtain adenosine, involved in purinergic signalling (Figure 1.6).[17] The other reaction product, β-NMN, is not a direct precursor of β-NAD^+ in its biosynthesis, as will be shown in 1.1.3; nevertheless, there is evidence for the existence of enzymes that would generate precursors of β-NAD^+ from β-NMN, such as NR or NaM.[18, 19] These enzymes have not been well characterized yet in humans but highlight the existence of many pathways for the biosynthesis of β-NAD^+.

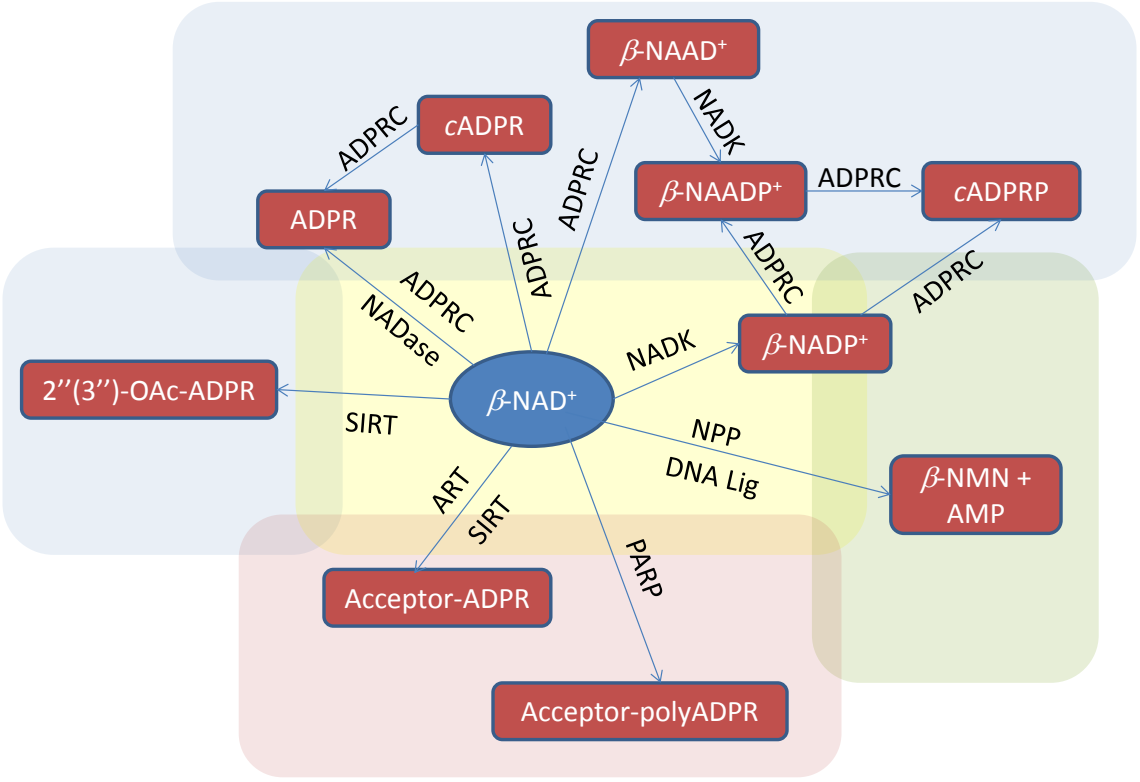

Figure 1.6 NAD^+ derivatives from NAD^+-consuming enzymes activities and their functions. Ca^{2+}-signalling messengers in the blue boxes; purinergic signalling messenger from AMP, and β-NAD^+ precursors from β-NMN in the green box; regulatory protein modifications (*e.g.* DNA repair, transcription activation, ageing) in the red box. The overlap between the boxes indicates the strong relations occurring between the activities of all these enzymes. Abbreviations used: NAD^+, nicotinamide adenine dinucleotide; ADPR, adenosine diphosphate ribose; *c*ADPR, cyclic ADPR; *c*ADPRP, 2′-phosphate *c*ADPR; $NADP^+$, 2′-phosphate NAD^+; $NAADP^+$, 2′-phosphate nicotinic acid adenine dinucleotide; 2″(3″)-OAc-ADPR, 2″(3″)-acetate-ADPR; ADPRC, ADPR cyclase; NADase, NAD^+-glycohydrolase; NADK, NAD^+ kinase; NPP, nucleotide pyrophosphate; PARP, polyADPR polymerase; ART, ADPR transferase; SIRT, sirtuins; DNA Lig, DNA ligase.

Extremely important among the enzymes that transform but do not consume the β-NAD^+ scaffold is the NAD^+ kinase (NADK); this enzyme catalyzes the phosphorylation of β-NAD^+ on 2′-OH to give β-$NADP^+$ (Figure 1.6).[13] In turn, two other fundamental Ca^{2+}-signalling messengers, β-$NAADP^+$ and *c*ADPRP (2′-phosphate cyclic ADPR), can be generated from β-$NADP^+$ by the action of ADPRCs (Figure 1.6).

β-$NADP^+$, having the same reduction potential as β-NAD^+, can undergo reduction on the nicotinamide ring to obtain β-NADPH. The concentration of the two dinucleotide couples is regulated by set of different enzymes; in particular, the concentration of β-$NADP^+$ is generally much lower than β-NAD^+ for similar concentrations of β-NADPH and β-NADH (Table 1.1). Therefore, the β-$NADP^+$:β-NADPH ratio is in favour of the

reduced form, in contrast to what is observed for the β-NAD^+:β-NADH ratio.[13, 20] This fact reflects the importance of β-$NADP^+$(H) on the balance of the intracellular redox state in response to cellular oxidative stress; indeed, the substantial free pool of β-NADPH compared to β-NADH is needed to react and inactivate the reactive oxygen species (ROS), that are responsible for oxidative stress and, therefore, a significant cause of cellular damages.

Metabolite	*Concentration [M]*
β-NAD^+	2.6×10^{-3}
β-NADH	8.3×10^{-5}
β-$NADP^+$	2.1×10^{-6}
β-NADPH	1.2×10^{-4}

Table 1.1 Intracellular metabolite concentrations in *E. coli*.[20]

When extensive DNA damage occurs in cells, it triggers a cascade of enzyme activities responsible for DNA repair; PARP-1, one of the most important DNA-repair enzymes in mammals, begins to produce very long ADPR branches as part of its function, almost completely depleting the intracellular free pool of β-NAD^+, and substantially altering the intracellular β-NAD^+:β-NADH ratio. This change would dramatically reflect on the intracellular lack of β-NADH, hence in ROS protection; therefore, this underscores the importance of the free pool of β-NADPH to respond to cellular oxidative stress.[13]

Moreover, the different ratios of β-NAD^+(H) and β-$NADP^+$(H) reflect another important difference between the two dinucleotide couples. While β-NAD^+(H) is mostly in its oxidized form, hence it is used in oxidative catabolic reactions, β-$NADP^+$(H), mostly present in its reduced form, is almost exclusively used in reductive anabolic reactions, where complex substances (*e.g.* carbohydrates, lipids, proteins) are formed by reductive steps from acetyl-CoA (Figure 1.7). This is a fascinating example of how nature has developed independent catabolic and anabolic pathways depending respectively on similar dinucleotides exploiting differently their reversible redox activity.[1]

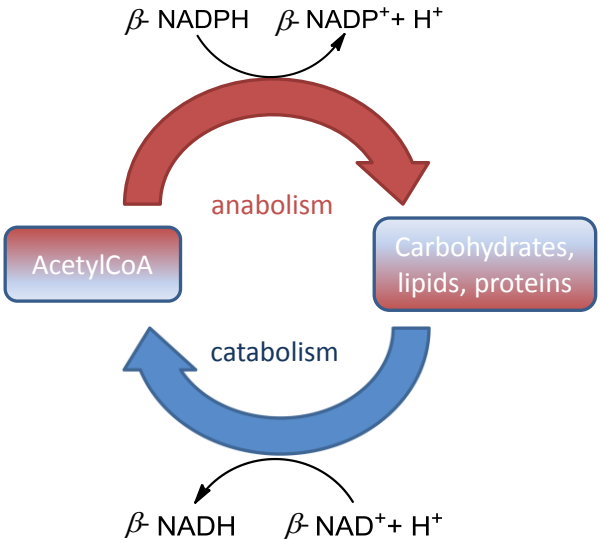

Figure 1.7 Catabolic processes (blue arrow) mainly involving the reduction of β-NAD^+ to β-NADH; anabolic processes (red arrow) involving the oxidation of β-NADPH to β-$NADP^+$.

1.1.3 β-NAD^+ biosynthesis

Since redox enzymes keep the β-NAD^+(H) concentration constant while NAD^+-consuming enzymes use it in their reactions and decrease its concentration, β-NAD^+(H) homeostasis in living cells is maintained by two different biosynthetic pathways that regenerate β-NAD^+. These pathways are classified as the *de novo* pathway, in which β-NAD^+ is generated from tryptophan (Trp) by different enzyme-catalyzed steps, and the *salvage* pathway, where β-NAD^+ is formed from recycling products, such as NaM, NA, also known as niacin or vitamin B3, and NR, which come from the depletion of β-NAD^+ or are introduced by diet into the cells (Figure 1.8).[18, 21] The two different pathways converge at a certain point and share the same enzymes to give the final β-NAD^+.

Different organisms show different preferences towards the *de novo* and *salvage* pathway; generally, the *salvage* pathway is preferred to the *de novo* one. In addition, different organisms exhibit clear preferences toward *salvage* pathway precursors: for instance, yeast prefers NA to NaM, since it expresses the enzyme nicotinamide deamidase, which deamidates NaM to NA, which is not present in mammals. In yeast and bacteria, another salvage precursor can be NR, which can be converted into β-NMN by NRK (NR kinase).

In the *salvage* pathway of mammals, the precursor NaM is directly transformed to *β*-NMN by the action of NaMPRT (NaM phospho-ribosyl transferase), which undergoes the coupling with AMP by NMNAT (NMN adenylyl transferase) to give *β*-NAD^+. In yeast, NA, obtained from NaM by nicotinamide deamidase, is transformed in nicotinic acid mononucleotide (NAMN) by NAPRT (NA phospho-ribosyl transferase); then, NAMN is coupled to AMP by NAMNAT (NAMN adenylyl transferase) to give *β*-$NAAD^+$, which is amidated by NAD^+-synthetase to finally give *β*-NAD^+ (Figure 1.8).

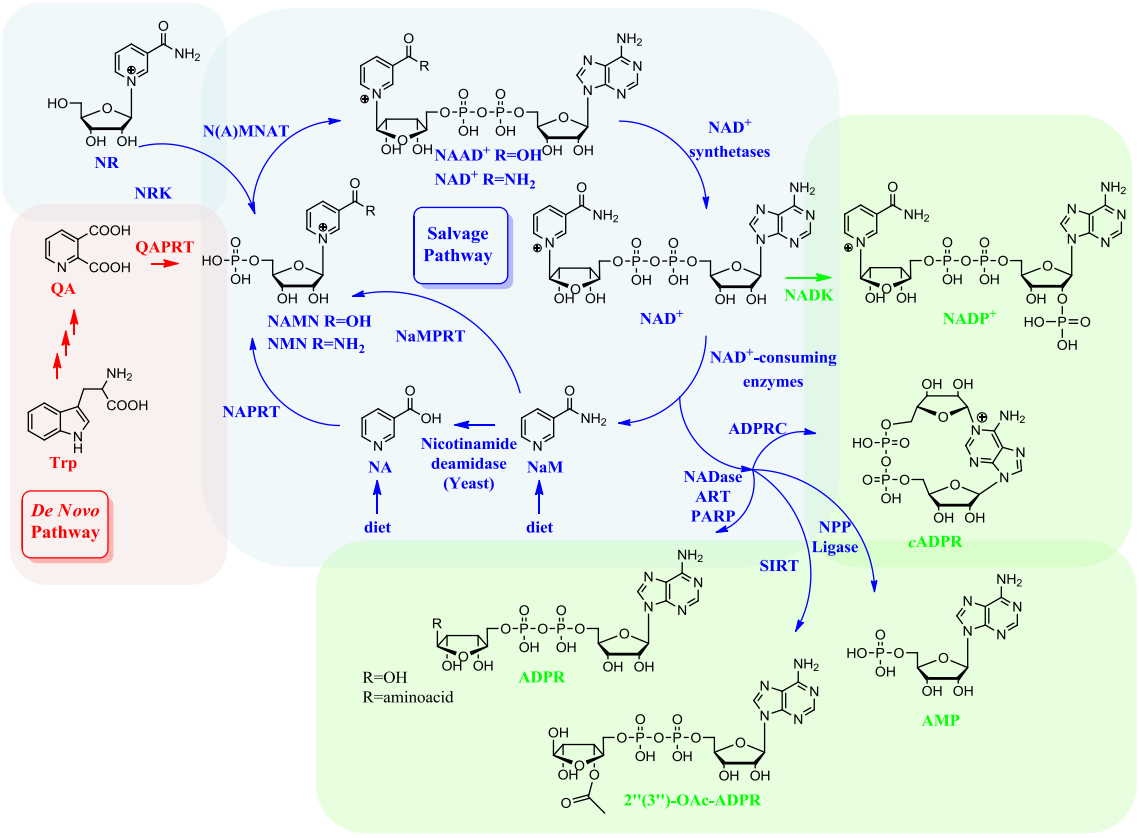

Figure 1.8 *β*-NAD^+ biosynthesis and metabolism. *De novo* pathway (red box); *salvage* pathway (blue boxes); products from NAD^+ metabolism (green boxes). Abbreviations used: Trp, tryptophan; QA, quinolic acid; QAPRT, QA phospho-ribosyl transferase; NA, nicotinic acid; NaM, nicotinamide; NAMN, nicotinic acid mononucleotide; NMN, NaM mononucleotide; NR, NaM ribonucleoside; NRK, NR kinase; N(A)MNAT, NaM (NA) mononucleotide adenylyltransferase; $NAAD^+$, NA adenine dinucleotide; NAD^+, NaM adenine dinucleotide; NAPRT, NA phospho-ribosyl transferase; NaMPRT, NaM phospho-ribosyl transferase; NADK, NaM adenine dinucleotide kinase; $NADP^+$, 2′-phosphate NaM adenine dinucleotide; ADPR, adenine diphosphate ribose; ADPRC, ADPR cyclase; *c*ADPR, cyclic ADPR; NPP, nucleotide pyrophosphatase; AMP, adenosine monophosphate; SIRT, sirtuins; 2″(3″)-OAc-ADPR, 2″(3″)-acetate-ADPR; NADase, NAD^+-glycohydrolase; ART, ADPR transferase; PARP, polyADPR polymerase.

Therefore, each organism has a similar set of enzymes (*e.g.* phospho-ribosyl transferases and adenylyl transferases) to perform the *salvage* pathway but with specificity depending on the favoured precursor. Structural studies of the active site of mammalian, yeast and bacterial enzymes involved in *salvage* pathways have shown substantial differences responsible for the different substrate specificity in spite of their same function; hence, although the sequence of reactions is conserved among different organisms, an evolutionary divergence has allowed them to differentiate the pathway specificity.[22]

In the human *salvage* pathway the rate-limiting enzyme is NaMPRT, which catalyzes the phosphoribosylation of NaM from 5-phosphoribosyl-1-pyrophosphate with release of *β*-NMN and pyrophosphate, PP_i. This enzyme is crucially involved in the *β*-NAD^+ biosynthesis and, therefore, in the activity of NAD^+-consuming enzymes, responsible for many biological processes involved in human diseases; hence, there is an increasing interest toward NaMPRT as a therapeutic target.[21, 23] Less crucial, but still important, is NMNAT, which catalyzes the adenylation of *β*-NMN from ATP with release of *β*-NAD^+ and PP_i; also the control of its activity could potentially influence the metabolism of *β*-NAD^+ and, therefore, have an impact on the cure of some human diseases.[21]

In mammals, NA is essential due to its role as a precursor of *β*-NAD^+. It can be obtained by diet or synthesized from Trp; consequently, lack of NA or Trp in the diet can cause pellagra in humans, a deficiency disease. Hence, the *de novo* pathway is fundamental to provide NA from Trp and *β*-NAD^+ in mammals in the case of restricted NA availability. The *de novo* pathway synthesizes *β*-NAD^+ starting from Trp through the kynurenine pathway (Scheme 1.1).[18] The opening of the pyrrole ring of Trp in conjuction with its oxidation, catalyzed by indoleamine-2,3-dioxygenase (IDO) in most tissues and tryptophan-2,3-dioxygenase (TDO) in the liver, generates formylkynurenine; the latter is hydrolysed to L-kynurenine by kynurenine formamidase (KFase). L-Kynurenine undergoes hydroxylation in position 3 by kynurenine-3-hydroxylase (K3H) to give 3-hydroxykynurenine, which is converted to 3-hydroxyanthranilic acid and L-alanine by kynureninase (kyase). Then, 3-hydroxyanthranilate-3,4-dioxygenase (3HAO) catalyzes the opening of the phenyl ring and its oxidation by insertion of molecular oxigen to give 2-amino-3-carboxy muconate semialdehyde, which spontaneously cyclizes into

quinolinic acid (QA). The latter is transformed to NAMN by the action of quinolinate phospho-ribosyl transferase (QAPRT) (Figure 1.8); hence, the *de novo* pathway converges on the *salvage* pathway to finally give β-NAD$^+$.

The rate-limiting steps in the *de novo* pathway are the reactions catalyzed by IDO/TDO and QAPRT; the rates of these reactions influence the rate of the *de novo* pathway and strictly forces it toward the conjunction with the *salvage* pathway.[18] IDO and K3H have shown to be potential therapeutic targets toward a wide class of human diseases.[21]

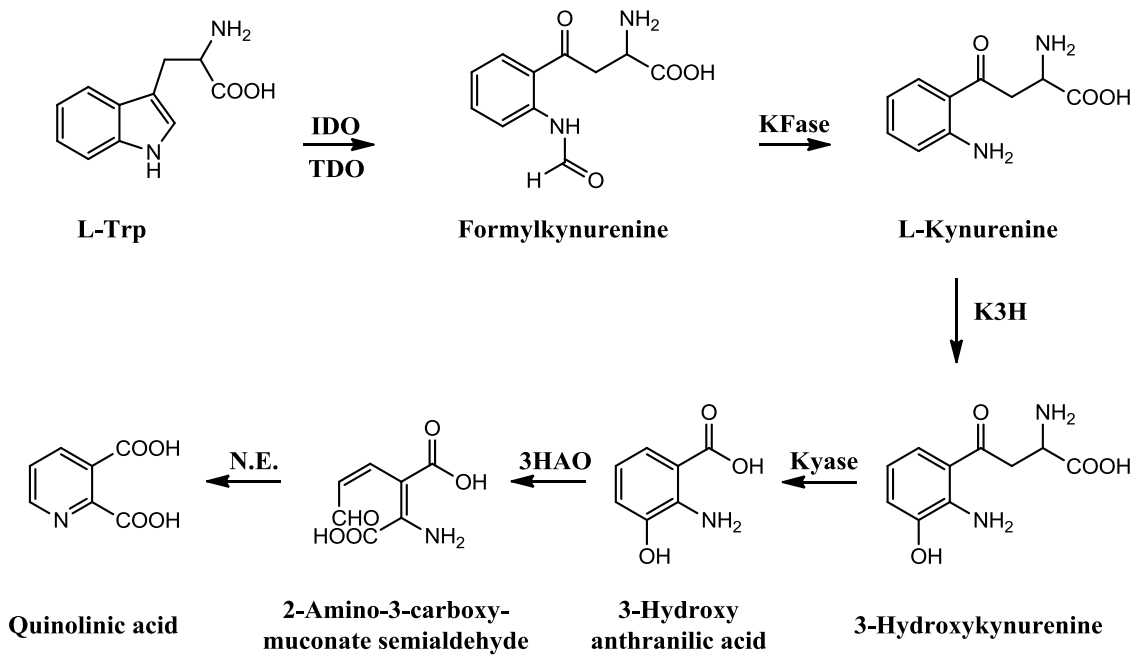

Scheme 1.1 *De novo* pathway. Abbreviations used: L-Trp, L-tryptophan; IDO, indoleamine-2,3-dioxygenase; TDO, tryptophan-2,3-dioxygenase; KFase, kynurenine formamidase; K3H, kynurenine-3-hydroxylase; kyase, kynureninase; 3HAO, 3-hydroxyanthranilate-3,4-dioxygenase; N.E., not enzymatic.

1.2 NAD$^+$-consuming enzymes

The main NAD$^+$-consuming enzymes, their activities and reaction products have been highlighted in 1.1.2. Since the main product released from the activity of NAD$^+$-consuming enzymes is NaM, the principal *salvage* precursor for the biosynthesis of β-NAD$^+$ in mammals (Figure 1.8), it is clear that a strong relationship exists between the activity of these enzymes and the biosynthesis of β-NAD$^+$; hence, every enzymatic

reaction and its substrates and products are connected in a delicate equilibrium which controls the homeostasis of such an essential molecule as β-NAD^+.[4-7, 18]

Herein, the attention will be focused on the relationship existing between the activities of NAD^+-consuming enzymes, discussing how they influence each other and the extracellular and intracellular homeostasis of β-NAD^+. Later, this chapter will present a short review of the existing synthetic NAD^+ derivatives and their use as inhibitors for drug therapies, or biochemical tools for the development of assays to monitor the activity of NAD^+-consuming enzymes. In this context, the project and its objectives will be introduced as an alternative and innovative solution to solve biochemical questions involving the NAD^+-consuming enzymes.

1.2.1 NAD^+-consuming enzymes: similarities and relationships

The majority of NAD^+-consuming enzymes catalyze the cleavage of the nicotinamide *N*-glycosidic bond with consequent release of NaM. The cleavage of this bond is an exergonic reaction;[24] in particular, the energy released is equal to -8.2 kcal·mol^{-1} (for comparison, the cleavage of ATP to generate ADP and P_i,[25] a very well known exergonic reaction occurring in biochemical processes, is equal to -7.3 kcal·mol^{-1}). Within cells, exergonic reactions are generally coupled with endergonic processes but, in the case of NAD^+-consuming enzyme activities, it is not always clear what the energy released is used for. Indeed, the reaction products from their activities do not keep the energy released under the form of high-energy bonds, as often occurs in reactions using ATP; moreover, the catalytic mechanisms of NAD^+-consuming enzymes do not justify the release of such a large amount of free energy.

NAD^+-consuming enzymes catalyzing the cleavage of the nicotinamide *N*-glycosidic bond have in common an NAD^+-glycohydrolase activity; then, other enzymatic reactions can be coupled to this common one, for instance the cyclization of ADPR to *c*ADPR (ADPRCs), the transfer of ADPR to protein acceptors (ARTs, PARPs), and protein deacetylation (sirtuins). The cleavage of the nicotinamide *N*-glycosidic bond by these enzymes occurs *via* a two-step mechanism resembling its chemical hydrolysis, where the ionization of the ribose diol stabilizes the formation of an oxocarbenium

intermediate accelerating the release of NaM (Figure 1.4). In the enzymatic catalysis, the interaction of 2″-OH and 3″-OH of the nicotinamide ribose with a carboxylic residue in the active site, would form a partial negative charge on the diol (Figure 1.9). The latter would exert an electron-donating effect on the ribose ring destabilizing the nicotinamide *N*-glycosidic bond and, therefore, favouring the release of NaM and the formation of an oxocarbenium intermediate.[8] This intermediate, stabilized on the nicotinamide ribose by H-bonds, would then undergo different fates.

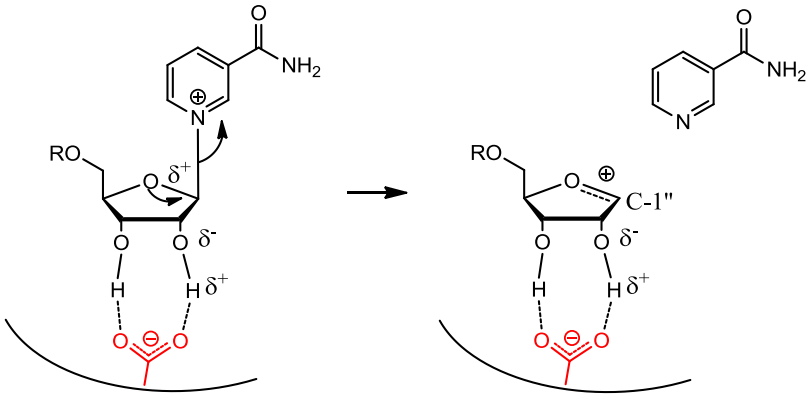

Figure 1.9 Formation of an oxocarbenium intermediate during the NAD^+-glycohydrolase activity of NAD^+-consuming enzymes. A carboxylic acid residue stabilizes the oxocarbenium intermediate by H-bonds, which can evolve afterwards into different compounds by nucleophilic attack on C-1″.

ADPRCs, NADases, PARPs, and ARTs mechanisms all proceed *via* the hypothetical oxocarbenium intermediate, as demonstrated by the presence in each of these enzymes of highly conserved glutamate residues.[8, 26-30] Still controversial is the mechanism adopted by sirtuins; indeed, it could involve an S_N1 reaction *via* the oxocarbenium intermediate,[31] or an S_N2 reaction with concurrent nucleophilic attack and elimination of NaM.[32] The energy released by the cleavage of the nicotinamide *N*-glycosidic bond is temporarily conserved in the highly reactive oxocarbenium intermediate; however, the following transformations in which it is involved are not very endergonic reactions. For instance, in ADPRCs the cyclization of the intermediate into *c*ADPR requires the adenine ring to turn from *anti* into *syn* conformation (Chapter 4, see 4.2.3);[26] in NADases, the intermediate can undergo nucleophilic attack by water (hydrolysis) to form ADPR, or by other nucleophiles to undergo an exchange reaction;[24] in ARTs and

PARPs the intermediate reacts with the nucleophilic residues of a protein acceptor to give an ADP-ribosylated acceptor;[28] and, finally, in sirtuins the eventual oxocarbenium intermediate undergoes acetylation on 2″(3″)-OH to give 2″(3″)-OAc-ADPR and the corresponding deacetylated protein.[31] Therefore, the energy conserved in the oxocarbenium intermediate is thought in part to be used for the former transformations, even if not highly endergonic, but also to be coupled to other biological processes, not immediately connected to the enzyme catalytic mechanisms. Hence, in the human ADPRC, CD38, it has been shown the necessity for this ecto-enzyme, that binds *β*-NAD^+ from the extracellular space, to dimerize to actively produce *c*ADPR and transport it inside the cells (Figure 1.12); this process would require energy, which could come from the cleavage of the nicotinamide *N*-glycosidic bond.[33] Furthermore, in PARPs the formation of ADPR branches as post-transcriptional modification is required as a signal to actively recruit other proteins involved in DNA repair, and energy would be needed in this process;[7] in addition, but not yet fully demonstrated, the ADPR branches could be used as a source to synthesize ATP.[34] Finally, in sirtuins the deacetylation of histones, proteins required for the compacting of chromatin, would be coupled to chromatin condensation, an active process for which the energy released could be used.[25]

In contrast to ADPRCs, NADases, PARPs, ARTs and sirtuins, NPPs and NAD^+-dependent DNA ligases catalyze the exergonic cleavage of the *β*-NAD^+ pyrophosphate bond; in both enzymes, the energy released is conserved by the formation of active enzyme-AMP complexes in the first step of their catalytic mechanisms. Afterwards, NPPs release AMP with an apparent loss of free energy (see 4.1, Scheme 4.1); by contrast, DNA ligases transfer the energy from the active enzyme-AMP complex to the active DNA-AMP complex, to eventually form the phosphodiester bond on the nicked DNA strand (see 5.1, Scheme 5.1). In the case of NPPs, the apparent loss of energy could be coupled to more complex biological processes, such as the formation of adenosine from AMP and, therefore, be linked to its role in purinergic signalling.[17]

It is interesting to study the complex relationship existing between the different NAD^+-consuming enzymes and how they influence major biological processes connected to many human diseases; a summary of the main effects exerted by these connections will be provided. An aspect shared by all those enzymes with NAD^+-glycohydrolase activity (ADPRCs, NADases, PARPs, ARTs and sirtuins) is the inhibitory effect exerted by NaM, their reaction product, on their activities. High concentrations of NaM from the activity of any NAD^+-consuming enzyme inhibit the activities of all the others; hence, the depletion of NaM *via* the *salvage* β-NAD^+ biosynthetic pathway[5, 18] is fundamental (Figure 1.10). In mammals, the activity of PARPs and CD38,[35] having both ADPRC and NADase activities, is responsible for the depletion of large amounts of β-NAD^+ at a very fast rate.[7] Therefore, NaM produced by these enzymes can strongly inhibit sirtuins, which activity can be re-established by removal of NaM through the action of NaMPRT in mammals,[23] or NaM deamidase (PNC1) in yeast[7] to form precursors of β-NAD^+. Since sirtuins are proposed to be involved in many critical biological processes (glucose, fat and insulin metabolism, ageing and life span increase, DNA transcription and repair, apoptosis), the regulation of their activity seems crucial; hence, it is important to develop sirtuins inhibitors/activators, or CD38/PARPs inhibitors to block the depletion of β-NAD^+ that inhibits sirtuins.[35] Since the activities of all these enzymes are important in cells, the choice of the process to block with a drug is crucial to avoid possible side effects.

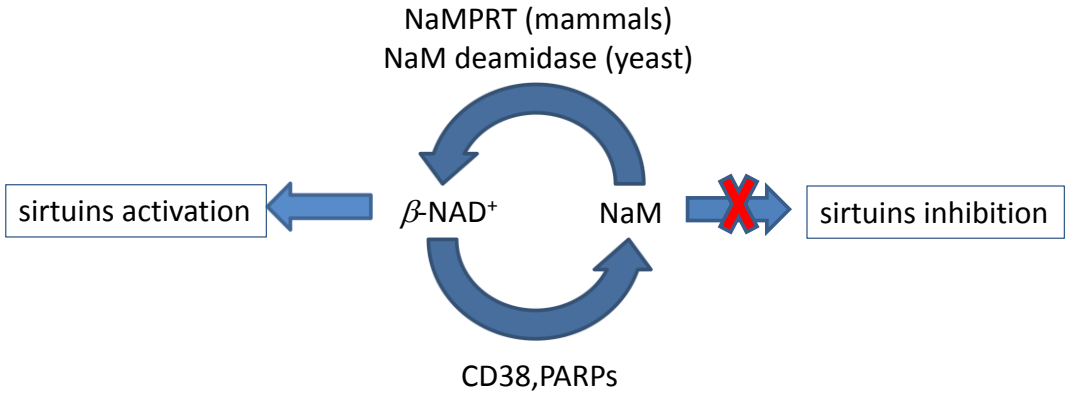

Figure 1.10 β-NAD^+ metabolism and its influence on the activity of sirtuins. Abbreviations used: NAD^+, nicotinamide adenine dinucleotide; NaM, nicotinamide; PARP, polyADPR polymerase; NaMPRT, NaM phospho-ribosyl transferase.

Sirtuins, PARPs and DNA ligases are intracellular enzymes involved in DNA repair processes (Figure 1.11).[36] When DNA damages occur in the cells, PARP-1 starts immediately its ADP-ribosylation or that of other proteins as a signal to trigger the recruitment to the DNA break of all proteins involved in DNA repair process (**1**). The formation of branches of ADPR, up to 200 units in length, occurs in a very short time and almost completely depletes the free intracellular β-NAD^+ pool with a huge increase of NaM concentration in the proximity of the DNA break.[7] The latter affects the activity of sirtuins, strongly inhibited by NaM (**2**), which therefore are not able to deacetylate histones (**3**).[5] Therefore, the DNA is unwound because of the fully acetylated histones in chromatin and the proteins for the DNA repair, including DNA ligases, can move close to the DNA and interact with it to fix its damage. When ADPR branches have reached the critical length, PARP-1 decreases its activity and, consequently, the NaM concentration near to the DNA break decreases as well; then, sirtuins can deacetylate histones re-compacting again the chromatin (**4**).[36] However, the inhibition of sirtuins can affect the activity of other biological processes. For instance, sirtuins can deacetylate p53, a protein responsible for DNA repair or apoptosis when the DNA damage is irreparable; p53 acetylation (**7**), in the case of the inhibition of sirtuins, corresponds to its activation and, therefore, to cell apoptosis (**8**). On the other hand, sirtuins can deacetylate FOXO transcription factors, involved as well as p53 in apoptotic processes; oppositely to the effect exerted on p53, FOXO acetylation (**5**), in the case of the inhibition of sirtuins, corresponds to their deactivation and, therefore, to cell survival (**6**).

Moreover, a PARP-overstimulation leads directly to cell apoptosis (**9**) because of the complete depletion of the intracellular β-NAD^+ pool, which cannot be formed in a short time by the β-NAD^+ biosynthetic pathways. Conversely, the inhibition of PARPs can be connected to cell survival (**18**), despite the loss in DNA repair response, because it leads to the activation of sirtuins (**11**). The latter effect can in turn lead to apoptosis or cell survival depending on the activity exerted respectively on FOXO transcription factors (**14**) or p53 (**16**)/histones (**12**). Hence, the inhibition/activation of sirtuins by PARP activity can result in completely different cellular fates depending on the main cellular

responses and their activation times compared to the DNA repair processes (Figure 1.11).[36]

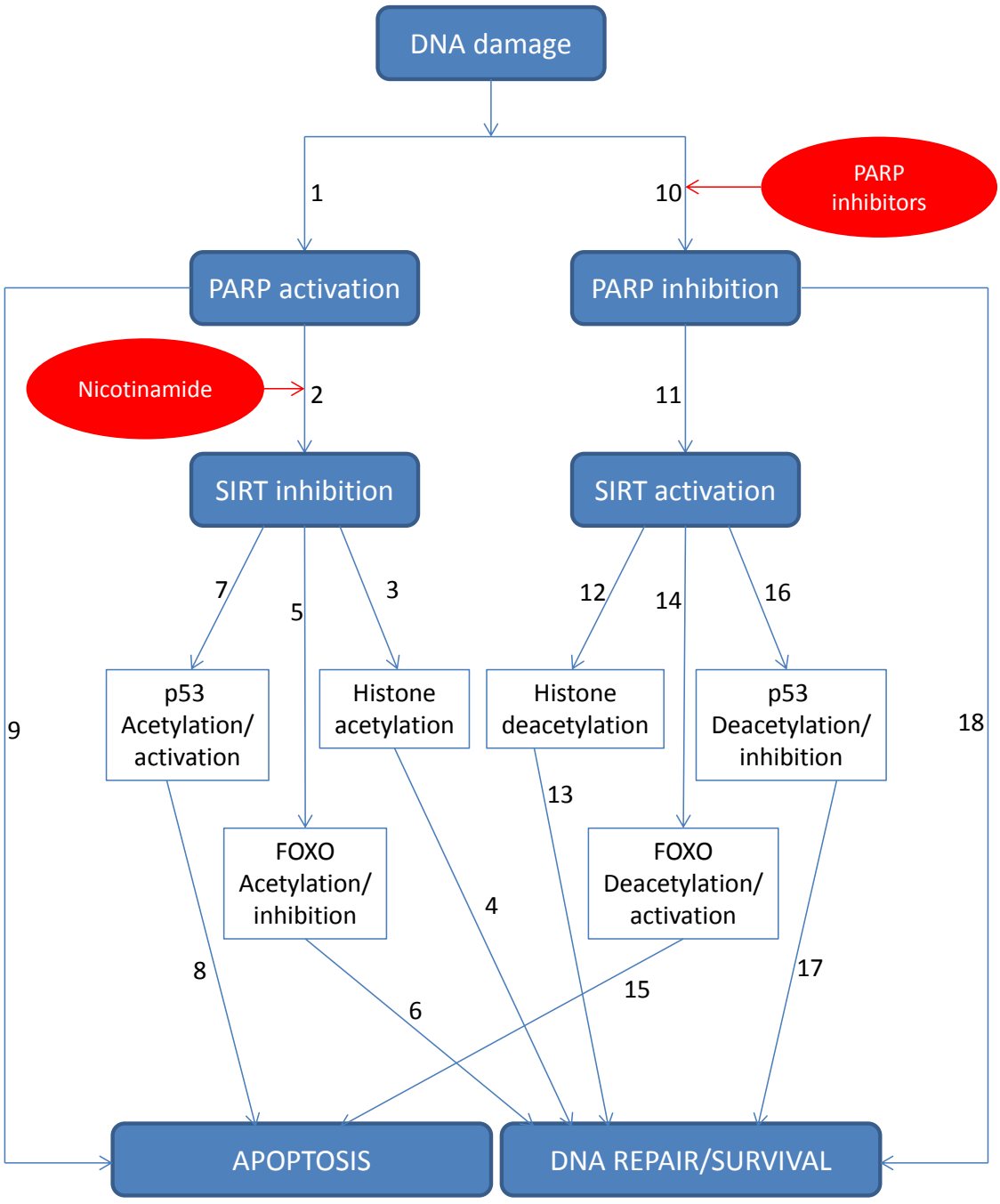

Figure 1.11 Inhibition/activation of sirtuins by the activity of PARPs in response to DNA damage. Cells can undergo different fates (1-18) depending on the related activities of sirtuins and PARPs and their modes of action. FOXO (Forkhead box proteins, class O) are involved in cellular proliferation, lifespan and stress tolerance. p53 (protein 53) is a tumor suppressor.

1.2.2 Intracellular and extracellular β-NAD^+ balance

A delicate balance exists between extracellular and intracellular β-NAD^+ concentration in multicellular organisms to regulate the functions of such a fundamental biological molecule.[37] It has been estimated that in multicellular organisms extracellular β-NAD^+ concentration is normally in the order of submicromolar range (10 – 50 nM), much lower than the intracellular one (0.1 – 3 mM).[7] These concentrations are the result of the activities of an intricate network of nucleoside/nucleotide receptors and NAD^+-consuming enzymes that keep a constant extracellular balance between β-NAD^+ and its degradation products, regulating the release of intracellular β-NAD^+ and its degradation outside the cells (Figure 1.12).[38, 39]

The main cause of intracellular β-NAD^+ release and, consequently, extracellular β-NAD^+ increase is cellular apoptosis and lysis. In addition, β-NAD^+ transporters (Connexin 43 transmembrane hemi channels) have recently been identified as responsible for the influx/efflux of β-NAD^+ into/outside the cells, allowing the regulation of its concentration in response to different biological processes, and to modulate intercellular communications.[40] Indeed, it has been shown that extracellular β-NAD^+ concentration substantially increases during inflammatory responses, since β-NAD^+ can act as a cytokine that triggers signalling cascade responses through its binding to specific purinergic receptors. For instance, its binding to P2Y11 causes an elevated intracellular Ca^{2+} release and *c*AMP (cyclic AMP) changes leading to anti-inflammatory responses (Figure 1.12).[37, 39, 41]

Extracellular β-NAD^+ homeostasis is further controlled by its degradation through the activities of some NAD^+-consuming enzymes, for instance mammalian ADPRC (CD38), NADases, ARTs and NPPs. All these enzymes belong to the ecto-enzyme class, characterized by the presence of their catalytic active site in the extracellular space. As discussed in 1.1.2, they catalyze the cleavage of extracellular β-NAD^+ to generate signalling molecules (*e.g.* *c*ADPR, ADPR, β-$NAADP^+$) or protein ADP-ribosyl modifications that potentially act in the intracellular space. Hence, it emerges the paradox of these enzymes, that are active in the extracellular space but involved in intracellular processes (*e.g.* Ca^{2+} release, post-transcriptional modifications, regulation

of intracellular sirtuins and PARPs activities).[7] The first issue in solving this paradox is due to the low extracellular β-NAD^+ concentration, below the K_m of NAD^+-consuming enzymes, which makes their activity rate very low. However, this allows to modulate finely their activity, since even small increases in extracellular β-NAD^+ concentration by the action of β-NAD^+ transporters,[40] favouring the release of intracellular β-NAD^+ in the extracellular space, could dramatically increase the activity of ecto NAD^+-consuming enzymes.

Another issue is the connection between the extracellular activity of these enzymes and the triggered intracellular processes. In the case of the cyclase activity of CD38, mostly present as an ecto-enzyme, the extracellular β-NAD^+ is bound into the catalytic site to generate *c*ADPR, which stimulates intracellular Ca^{2+} release from the endoplasmic reticulum. The discovery of the dimerization and internalization of CD38 to catalyze the enzymatic reaction and actively transport the product inside the cell explained the link between the extracellular β-NAD^+ binding site and the intracellular product release.[33] Moreover, specific *c*ADPR-transporters have been found in the cellular membrane, responsible for the intracellular uptake of *c*ADPR.[42] Regarding the NADase activity of CD38, it generates extracellular ADPR, which promotes intracellular Ca^{2+} release[41] *via* pathways mediated by IP_3 (inositol 1,4,5-triphosphate), possibly binding to the extracellular P2Y purinergic receptor.[43] This process is completely independent from the Ca^{2+}-permeable TRPM2 channel transport, which mediates intracellular Ca^{2+} release from internal compartments and/or Ca^{2+} influx from the extracellular space by the action of second messengers, such as intracellular ADPR (produced by degradation of ADPR branches), *c*ADPR, 2″(3″)-OAc-ADPR (produced by sirtuins) and β-$NAADP^+$.[43] The extended activation of this non-selective cation channel causes cell death. β-$NAADP^+$, generated by the exchange activity of CD38 from extracellular β-$NADP^+$, can be, in turn, transported inside the cells *via* specific β-$NAADP^+$ transporters (Figure 1.12).[44]

Mammalian ARTs have been discovered quite recently and most of them are classified as ecto-enzymes, therefore acting in the extracellular space and generating ADP-ribosyl modifications of extracellular proteins; in particular, they are involved in receptor modifications and triggering signalling cascades during immune and inflammatory

responses.[7] For instance, in mouse T-cells the ADP-ribosylation of the purinergic receptor P2X7 by ART2 induces its activation and a cascade of signalling processes, finally leading to cell death.[37] A large number of intracellular proteins undergo ADP-ribosylation, which cannot be ascribed to ecto-ARTs; therefore, the existence of intracellular ARTs or the secondary ART activity of sirtuins[14] would be responsible for intracellular modifications (Figure 1.12).[7]

Finally, NPPs, as well as the previous enzymes, belong to the ecto-enzymes class. The presence of NPPs on the cellular surface is fundamental for the recycling of extracellular nucleotides and for keeping the balance between nucleotides/nucleosides. For instance, the CD38-generated ADPR can be transformed by NPPs into AMP, which in turn can be hydrolysed into adenosine (Ado), which is able to bind to purinergic receptors and stimulate signalling responses (Figure 1.12).

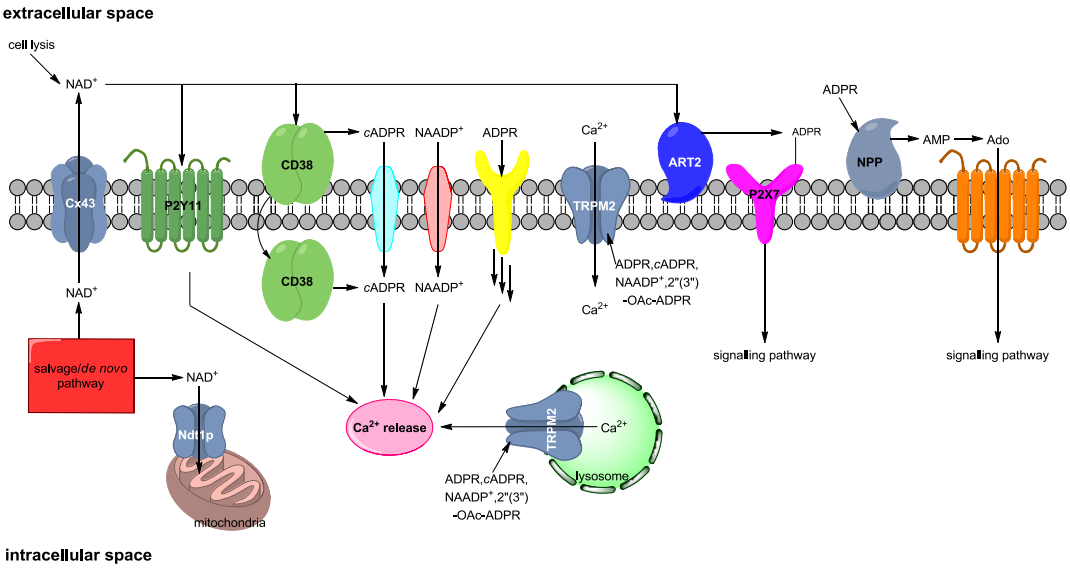

Figure 1.12 Pathways for the extracellular/intracellular β-NAD$^+$ balance. Abbreviations used: NAD$^+$, nicotinamide adenine dinucleotide; ADPR, adenosine diphosphate ribose; *c*ADPR, cyclic ADPR; NAADP$^+$, 2′-phosphate nicotinic acid adenine dinucleotide; 2″(3″)-OAc-ADPR, 2″(3″)-acetate-ADPR; AMP, adenosine monophosphate; Ado, adenosine; Cx43, Connexin 43; ART2, ADPR transferase 2; NPP, nucleotide pyrophosphatase.

All these ecto-enzymes are therefore involved, not only in the homeostasis of extracellular β-NAD$^+$, but in fundamental signalling pathways, where activation triggers anti-inflammatory and immunosuppressive responses. The increased extracellular β-

NAD^+ concentration in connection with increased expression of NAD^+-consuming ecto-enzymes and purinergic receptors is the effect observed following cellular stress at the beginning of inflammatory responses; tumor cells seem to modulate these interactions to escape the immune response.[39]

Intracellular β-NAD^+, as already shown in 1.1.3, is synthesized in the cytosol by the *salvage* or *de novo* pathways and used by intracellular enzymes, such as redox (NAD^+-dependent dehydrogenases) and NAD^+-consuming enzymes (PARPs, sirtuins, NAD^+-dependent DNA ligases). Some of these enzymes perform their crucial activities inside the mitochondria, where an appropriate β-NAD^+:β-NADH ratio is fundamental for a variety of biological processes; however, for a long time it was thought that β-NAD^+(H) was unable to permeate the mitochondrial membrane. Recently, a mitochondrial β-NAD^+ transporter, Ndt1p, has been identified in *Saccharomyces cerevisiae* as a specific β-NAD^+ carrier. It imports β-NAD^+ into the mitochondria preferentially by exchange with mitochondrial deoxy-AMP (*d*AMP) and deoxy-GMP (*d*GMP), and to a small extent by uniport reaction (Figure 1.12).[45]

1.3 NAD^+ derivatives as mechanistic probes for NAD^+-dependent enzymes

As shown in the previous sections, NAD^+-dependent enzymes play a fundamental role in many biological processes and alterations and modifications to their normal status are linked to several human diseases. Therefore, the necessity to investigate and, eventually, modulate or block NAD^+-dependent enzymes has led to the development of NAD^+ derivatives that mimic the natural substrate (NS) and act either as non-natural substrates (NNSs) for biochemical applications or potential enzyme inhibitors for drug discovery.

In general, designing derivatives of the natural substrates requires minor modifications of the natural molecule scaffold in order to keep intact the essential groups interacting with the enzymes and allowing its binding to the catalytic sites. Then, depending on the modifications, it is possible to generate NNSs, that are metabolized with the same fashion as the NS, and are consequently its competitive inhibitors; or, simply, enzyme inhibitors, if the modifications allow their binding but not their metabolism by the enzymes. In the development of NAD^+ derivatives it is therefore necessary to look at the natural β-NAD^+ structure and identify the chemical groups that can be subjected to

modifications; then, depending on the need of inhibitors or NNSs, the right modifications have to be considered.

In the design of inhibitors, if the enzyme structure and mechanism are well known, the modifications are aimed to block essential groups for the catalytic reactions. In contrast, in the design of NNSs, the modifications are needed to investigate and monitor the enzyme structure and/or the related mechanism, without consequently affecting the essential interactions responsible for the enzymatic catalytic mechanisms. For instance, an ideal NNS should have an enzyme affinity similar or higher compared to the NS ($K_{m\ NNS} \leq K_{m\ NS}$) to bind properly in the active site. In addition, a k_{cat} (turnover number) lower than the NS ($k_{cat\ NNS} < k_{cat\ NS}$) would allow a slower metabolism of NNS by the enzyme, permitting in some cases easier kinetic studies and mechanism visualizations without altering the reaction mechanism itself. By definition, NNSs are competitive inhibitors of the NS; however, if their K_m and k_{cat} are similar to the NS, the enzyme activity will not be inhibited overall, since both substrates can be used with the same efficacy. If their K_m and k_{cat} are lower (higher affinity and slow turnover) compared to the NS, then the final effect will be a slowdown of the enzymatic reaction and, therefore, inhibition; hence, under such conditions, NNSs can be potentially used as enzyme inhibitors or modulators, or at least give the basis for the design of new inhibitors. In addition, in the design of NNS, the labelling of the natural molecule scaffold by groups monitored by sensitive techniques, such as fluorescence, UV absorbance and immunoanalytical methods, can be extremely useful for the development of assays that are more sensitive compared to those using the NS. The labelling of nucleosides/nucleotides with the purpose to generate fluorescent probes will be discussed in detail in Chapter 3, where the attention will be focused on the nucleobase substitutions; however, the ribose or phosphate conjugation with fluorophores by linkers,[46-48] where the length is crucial to avoid steric hindrances with the substrate, is a common labelling method. Also, the introduction of biotin on the natural molecule scaffold represents a useful labelling method, allowing very sensitive detections and selective purification due to the strong affinity of biotin and streptavidin.[49]

The structure of β-NAD$^+$ is characterized by a variety of functional groups, that are involved differently in enzyme recognitions and activities; therefore, their modifications lead to different responses to different enzymes (Figure 1.13).

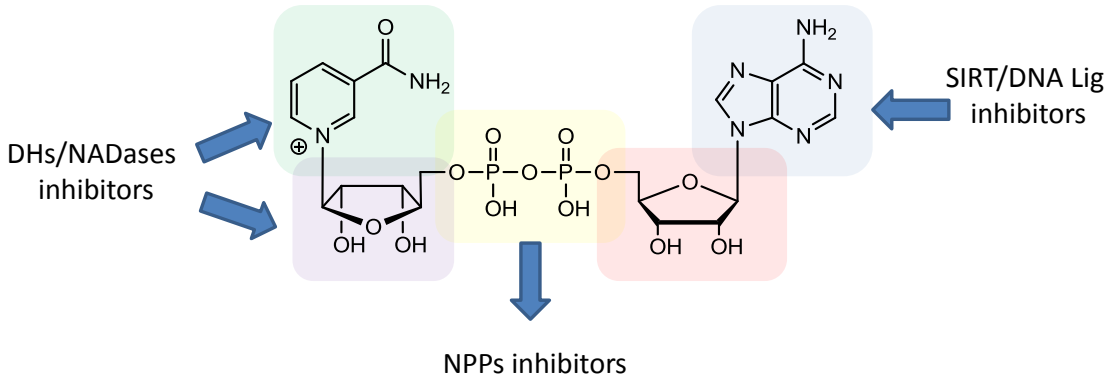

Figure 1.13 Relationship between group modifications on β-NAD$^+$ structure and specific enzyme responses. NaM (green box) and nicotinamide ribose (purple box) modifications lead to the inhibition of dehydrogenases (DHs) and enzymes with NAD$^+$-glycohydrolase activity (ADPRCs, NADases, ARTs, PARPs, sirtuins). Pyrophosphate bond (yellow box) modifications lead to the inhibition of nucleotide pyrophosphatases (NPPs). Adenine (blue box) modifications lead to the inhibition of sirtuins (SIRT) and NAD$^+$-dependent DNA ligases.

Dehydrogenases (DHs), which use the nicotinamide ring for its redox activity, are mainly inhibited by its modification. NAD$^+$-consuming enzymes that share the NADase activity (ADPRCs, NADases, ARTs, PARPs, sirtuins, see 1.2.1) are especially inhibited by NaM/NR modifications, since the formation of an oxocarbenium intermediate is crucial for their catalytic mechanisms (Figure 1.9). NPPs are mainly inhibited by pyrophosphate bond modifications, since they catalyze its cleavage. Finally, NAD$^+$-dependent DNA ligases and sirtuins, which closely interact with the adenine moiety of β-NAD$^+$ in their catalytic sites (see Chapter 5, respectively 5.1 and 5.2), can be inhibited by adenine modification in particular positions. By aiming for selective inhibitions following specific modifications, hypothetically it should be possible to design NNSs of NAD$^+$-dependent enzymes by modifying the chemical groups not involved in their inhibition.

1.3.1 NAD^+ derivatives as inhibitors of NAD^+-dependent enzymes

1.3.1.1 Nicotinamide modification

NaM is an essential component of β-NAD^+, required for its recognition/binding to several enzymes as well as for their activities. Indeed, the nicotinamide portion is responsible for the β-NAD^+ redox activity, hence for its use as a co-substrate by DHs; in addition, its positive charge makes the nicotinamide *N*-glycosidic bond extremely labile, allowing the use of β-NAD^+ as a substrate/co-substrate of NAD^+-consuming enzymes. The modification of NaM is effective in generating inhibitors, NAD^+-like or not, for NAD^+-dependent DHs and NAD^+-consuming enzymes. A variety of studies aimed at the discovery of inhibitors for important DHs have been focused on the nicotinamide substitution within the β-NAD^+ structure with a variety of aryl/heteroaryl rings (Figure 1.14, benzamide **1**, C-nicotinamide **2**, picolinamide **3**, isonicotinamide **4**, thiazole-4-carboxamide **5**, and many others). These main substitutions, in combination with ribose and pyrophosphate bond modifications, have successfully brought the development of effective inhibitors of DHs.[50, 51] Some of the DH inhibitors have been found to inhibit also NADK, responsible for the phosphorylation of the 2′-OH of β-NAD^+ to generate β-$NADP^+$.[52]

As mentioned in 1.2.1, NaM, the reaction product of ARTs, PARPs, sirtuins, ADPRCs and NADases activities, is a common inhibitor for these enzymes, in particular as a competitive inhibitor for ARTs and PARPs,[53, 54] a non-competitive inhibitor for sirtuins,[55] and a mixed inhibitor for ADPRCs[56] and NADases.[24] Many nicotinamide derivatives have been developed as potential inhibitors for these enzymes (*e.g.* **8**-**13**) (Figure 1.14). All the developed nicotinamide derivatives contain in their structure essential features to act as inhibitors of ARTs, PARPs and sirtuins. For instance, a primary or secondary amide, responsible for the interactions between NaM and the enzyme active sites, is engaged in H-bonding by its carbonyl and amine groups,[31] and its *anti* conformation is specifically required for the compounds activity toward ARTs and PARPs. In addition, an aromatic ring more electron-rich than the pyridine, and a non cleavable bond contribute to the inhibitory activity of nicotinamide derivatives.[53, 54] β-NADH (**14**) and β-$NAAD^+$ (**15**), where NaM is substituted with the reduced pyridine

ring and NA respectively, act as inhibitors of sirtuins.[57] Moreover, BAD (**1**), AAD (**16**) and HHD (**17**) inhibit ADPRCs activity (Figure 1.14).[58] All these inhibitors give an example of the essential nature of the nicotinamide portion for the activity of NAD^+-dependent enzymes.

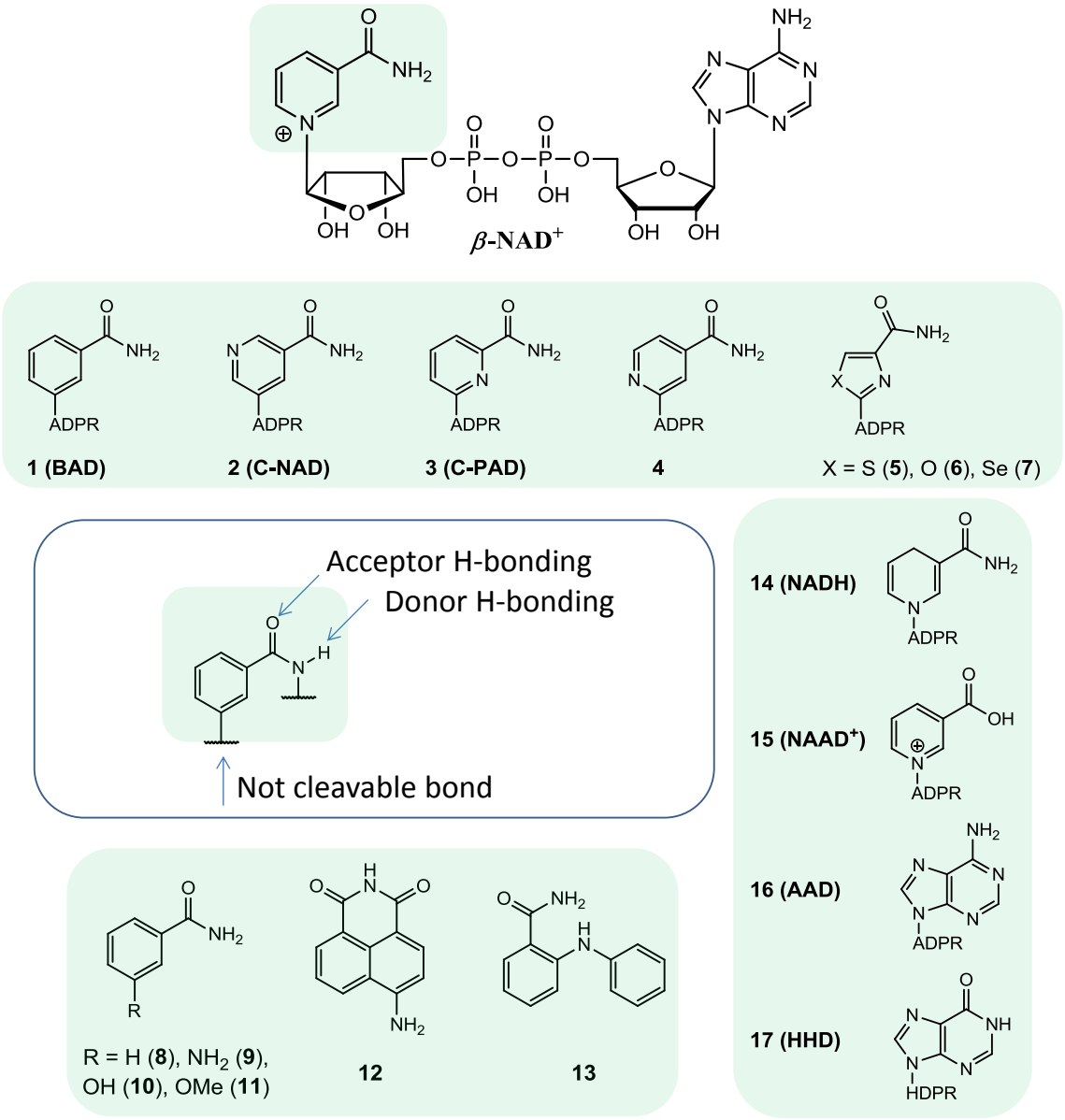

Figure 1.14 Inhibitors of DHs, NADKs, ARTs, PARPs, sirtuins, ADPRCs and NADases based on nicotinamide modifications. Abbreviations used: NAD^+, nicotinamide adenine dinucleotide; BAD, benzamide adenine dinucleotide; C-NAD, C-nicotinamide adenine dinucleotide; C-PAD, C-picolinamide adenine dinucleotide; NADH, nicotinamide adenine dinucleotide (reduced form); $NAAD^+$, nicotinic acid adenine dinucleotide; AAD, *bis*-adenine dinucleotide; HHD, *bis*-hypoxanthine dinucleotide.

1.3.1.2 Nicotinamide ribose modification

The nicotinamide ribose plays a fundamental role in the activities of NAD^+-dependent enzymes. In particular, as shown in 1.2.1, it is actively involved in the reaction mechanisms of NAD^+-consuming enzymes with a common NADase activity due to the formation of a stabilized oxocarbenium intermediate. Its modification has been undertaken to generate inhibitors for NAD^+-consuming enzymes, such as ARTs, PARPs, sirtuins, ADPRCs and NADases. However, it has also been targeted to improve the efficacy of inhibitors for DHs[50] and NADKs.[52] The most common modifications of the nicotinamide ribose have been suggested by the knowledge of the reaction mechanism for enzymes with NADase activity (Figure 1.9). The substitution of O-1 of the ribose with a methylene group (CH_2) causes the loss of stabilization of the oxocarbenium intermediate by the oxygen lone pairs; therefore, the replacement of the ribose ring with a 2,3-dihydroxycyclopentane ring generates a dinucleotide diastereomers mixture, containing carba-NAD^+ (**1**, with D-2,3-dihydroxycyclopentane ring) and *pseudo* carba-NAD^+ (**2**, ψ carba-NAD^+, with L-2,3-dihydroxycyclopentane ring) (Figure 1.15).[59] In particular, ψ carba-NAD^+ is more active than carba-NAD^+ as an inhibitor of ARTs, PARPs, sirtuins, NADases and CD38,[54, 60] while both derivatives are inactive toward ADPRC from *Aplysia californica*,[60] shown to be insensitive to ribose modifications.[58] By contrast to its inhibitory properties toward enzymes with NADase activities, carba-NAD^+ acts as a NNS for DHs, while ψ carba-NAD^+ is completely inactive.[59]

The substitution of the 2″-OH of the nicotinamide ribose with a fluorine (F) deletes its H-bonding interactions with glutamate residues or electron-withdrawing groups in the active site, which help in stabilizing the oxocarbenium intermediate. Further modifications, such as the change of the ribose with arabinose, where the 2″-OH (F) points toward the other face of the ribose; or the removal of the 2″-OH in 2″-deoxy nicotinamide ribonucleoside derivatives,[61] achieve the same destabilizing effect on the oxocarbenium intermediate. Therefore, 2″-deoxy nicotinamide ribonucleoside derivatives (**3**-**5**), 2″-FNAD^+ (**6**), *ara*-NAD^+ (**7**), *ara*-2″-FNAD^+ (**8**) and *ara*-2″-FNMN (**9**) are all good inhibitors of NAD^+-dependent enzymes (Figure 1.15), in particular of DHs, in combination with nicotinamide modifications,[50] NADKs,[52] NADases,[62] and

CD38.[30, 61, 63] Finally, the change of nicotinamide ribose conformation from β-D-ribose to α-D-ribose generates α-NAD$^+$ that inhibits sirtuins.[57]

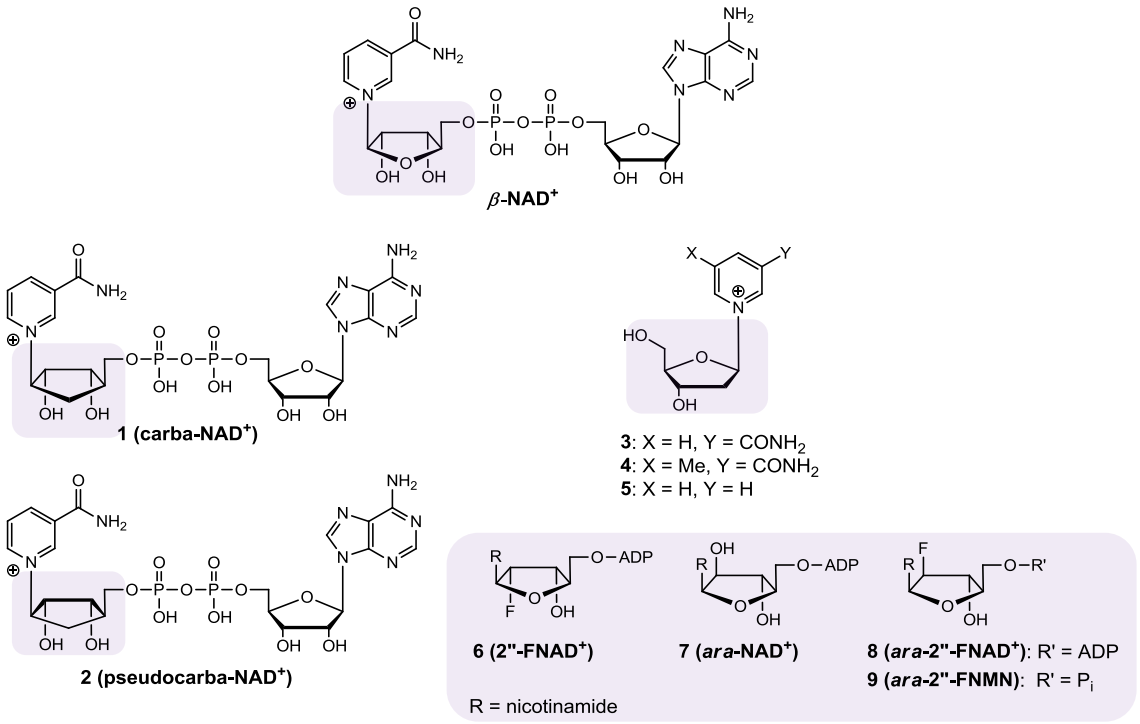

Figure 1.15 Inhibitors of DHs, NADKs, sirtuins and NADases based on nicotinamide ribose modifications. Abbreviations used: NAD$^+$, nicotinamide adenine dinucleotide; 2″-FNAD$^+$, 2″-fluoroNAD$^+$; *ara*-NAD$^+$, arabinose-NAD$^+$; *ara*-2″-FNAD$^+$, arabinose-2″-fluoroNAD$^+$; *ara*-2″-FNMN, arabinose-2″-fluoro nicotinamide mononucleotide.

1.3.1.3 Pyrophosphate bond modification

The β-NAD$^+$ structure is largely dynamic because of the variety of flexible bonds and rotational angles that it can assume in generating different conformations.[64] The pyrophosphate bond that joins the two nucleosides is the most flexible part of the molecule because of the three dihedral angles, ζ, α and γ, able to rotate and confer different orientations and conformations to the nucleosides (Figure 1.16). Due to its high flexibility, the pyrophosphate bond is generally not strictly involved in recognition by enzymes. However, its modification in the synthesis of dinucleotide derivatives is very important because it confers stability to potential inhibitors or NNSs against *in vivo* enzymatic degradation by nucleases, which are often responsible for the cleavage of

nucleic acid phosphodiester or dinucleotide pyrophosphate bonds. Therefore, modifications of the pyrophosphate bond have been used to inhibit nucleases, or, in the particular case of β-NAD^+, NPPs.[65] However, its coupling to other modifications has allowed generation of effective DHs, NADKs and NAD^+-consuming enzyme inhibitors. The most common modifications on the pyrophosphate bond (Figure 1.16) involve the substitution of the oxygen bridge between the two phosphates with a CH_2 or difluoromethylene (CF_2) group to generate phosphonate derivatives (**1**, **2**).[50, 66] These modifications do not alter the three-dimensional shape of the molecule since the size of these groups is similar to the oxygen, but they do provide resistance to attack by nucleases and make the dinucleotides more lipophilic and able to penetrate inside cells. Moreover, CF_2 is a better bioisostere than CH_2, since the electron-withdrawing effect of the fluorine atoms increases the pK_a of the phosphate groups, making them more similar to the natural pyrophosphate bond. Other substitutions[67] can be the introduction of phosphatephosphonate groups (**3**, **4**), sulphonamide groups (**5**), amidephosphonate groups (**6**), thioethylenephosphonate (**7**) or disulphide[68] (**8**) groups.

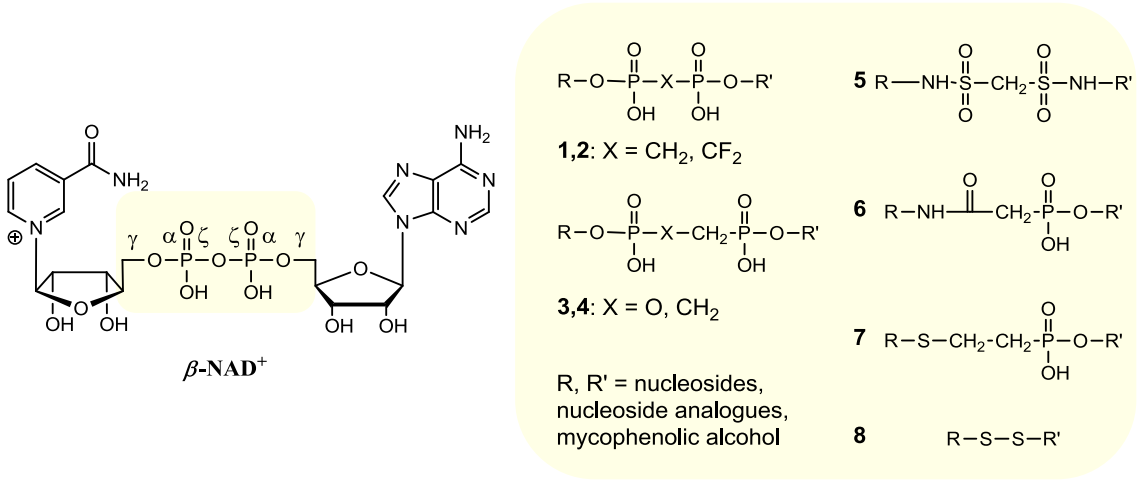

Figure 1.16 Inhibitors of DHs, NADKs and NPPs based on pyrophosphate bond modifications. Abbreviations used: NAD^+, nicotinamide adenine dinucleotide.

1.3.1.4 Adenine modification

The adenine moiety in β-NAD^+ is fundamental for recognition and binding by enzymes. With the exception of NAD^+-dependent DNA ligases, sirtuins and ADPRCs, DHs, NADKs and all other NAD^+-consuming enzymes do not actively involve the adenine moiety in their catalytic mechanisms. Therefore, its modification within the β-NAD^+ structure is generally aimed at the synthesis of NNSs for these enzymes. As discussed in 1.3, the NNS activity implies a competitive inhibition with β-NAD^+. Hence, from the design of NNSs with high affinity for the enzyme (low K_m) and slow turnover (low k_{cat}), it is possible to generate effective inhibitors. The latter is a common case and a good example is given by NNSs for ADPRC from *Aplysia californica*. This enzyme has shown broad substrate tolerance related to the adenine moiety, which has been substituted with guanine (**1**), hypoxanthine (**2**), xanthine and ε-adenine to generate NNSs which are also good inhibitors for ADPRC (Figure 1.17).[58, 69]

Whilst the NNS activity often coincides with the competitive inhibition of the NS, the reverse is not always true. For instance, 8-aryl/heteroaryl NAD^+ derivatives are inhibitors but not NNSs for sirtuins (**3**, Figure 1.17),[70] indicating that the substitutions in position 8 on the adenine ring allow the binding of the compounds to the enzyme active site but inhibit their metabolism (see 5.2.2). Another example is given by 2-fluoroNAD^+ (2-$FNAD^+$) (**4**, Figure 1.17);[71] indeed, this compound is cleaved by ADPRC from *Aplysia californica* on the nicotinamide *N*-glycosidic bond, but its cyclization is inhibited by the fluorine in position 2 on the adenine ring, with consequent release of 2-FADPR. Therefore, the compound acts as a substrate for the NADase activity of ADPRC, but as an inhibitor toward its main cyclase activity.

Beyond the adenine-modified NAD^+ derivatives, adenine-based compounds (**5**) and adenine-modified adenosine derivatives (**6**, **7**) (Figure 1.17) have been developed, respectively, as inhibitors of sirtuins[72] and NAD^+-dependent DNA ligases,[73, 74] indicating the strong influence of the adenine moiety in both enzymes.

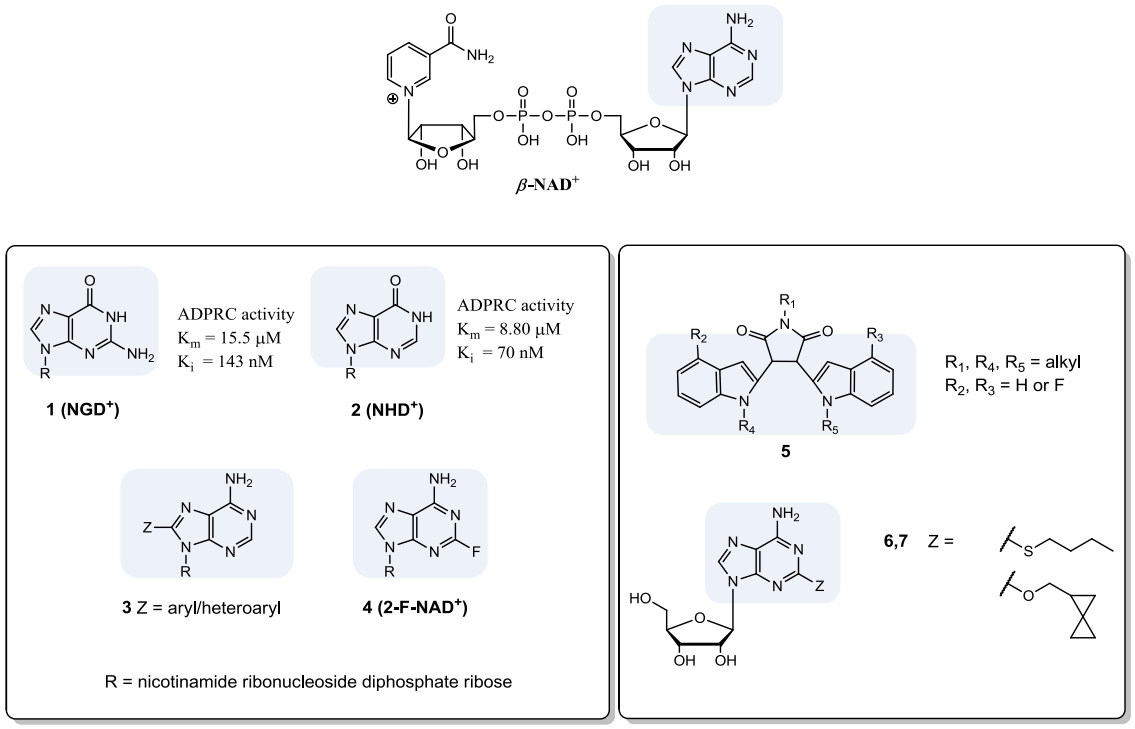

Figure 1.17 Inhibitors of ADPRCs, NPPs, sirtuins and DNA ligases based on adenine modifications. Abbreviations used: NAD^+, nicotinamide adenine dinucleotide; NGD^+, nicotinamide guanine dinucleotide; NHD^+, nicotinamide hypoxanthine dinucleotide; 2-$FNAD^+$, 2-fluoroNAD^+.

1.3.2 NAD^+ derivatives as non-natural substrates of NAD^+-dependent enzymes

The development of NNSs can help to investigate the active sites and catalytic mechanisms of enzymes. Therefore, targeted modifications and labelling are required to generate useful biochemical tools. As mentioned in 1.3.1.4, the adenine modifications are generally aimed at the synthesis of NNSs for NAD^+-dependent enzymes. The adenine base has been modified preferentially in a few favourite positions, such as N-1, NH_2 in 6 position and C-8 position. The correlation between different NNS activities and the modifications in different positions highlight the structure and the fundamental interactions occurring between the β-NAD^+ scaffold and the active sites of enzymes. However, modifications on the nicotinamide ring can also generate NNSs for NAD^+-dependent enzymes, as long as they keep unchanged the labile *N*-glycosidic bond or the redox activity of the nicotinamide ring that is still used as a substrate.

NNSs for DHs have mostly been modified in N-1 (**4**-**6**), NH_2 in 6 position (**1**, **2**, **7**-**9**) or both (**3**) on the adenine ring (Figure 1.18).[75, 76] Other NAD^+ derivatives have been synthesized substituting the amide group on the pyridine ring (**14**-**18**), still maintaining its redox activity (Figure 1.18).[77, 78] Different DHs have shown selective specificities toward the differently substituted NAD^+ derivatives, demonstrating the existence of structural differences within the same class of enzymes.

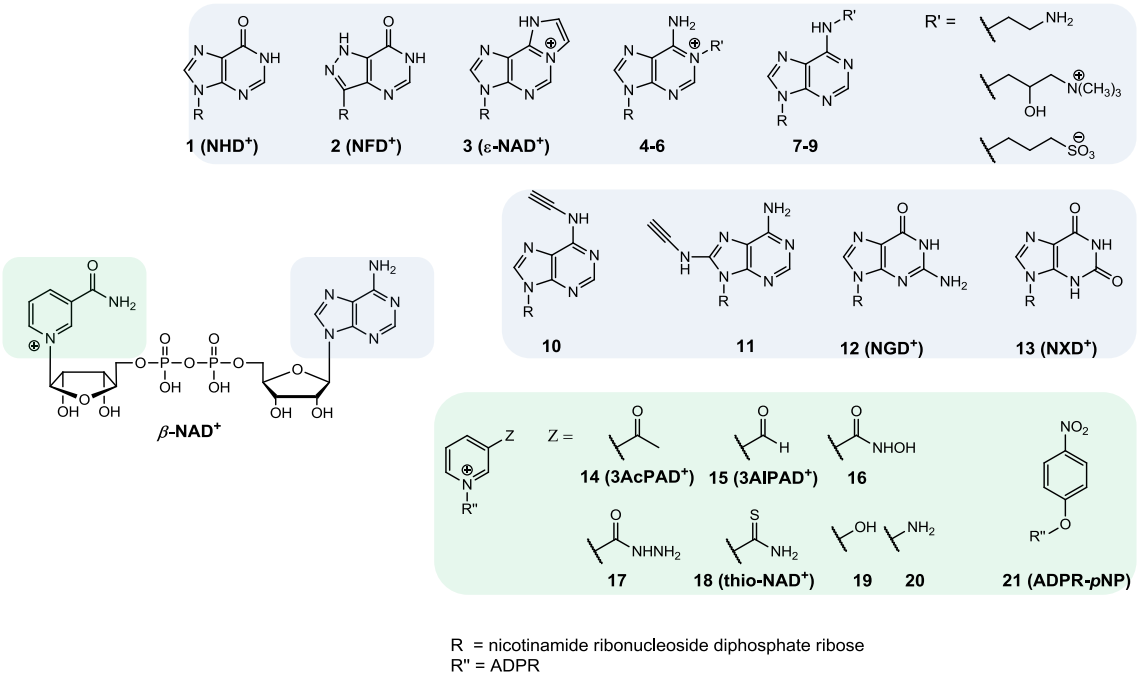

Figure 1.18 NAD^+ derivatives with NNS activities toward NAD^+-dependent enzymes. Abbreviations used: NAD^+, nicotinamide adenine dinucleotide; NHD^+, nicotinamide hypoxanthine dinucleotide; NFD^+, nicotinamide formycin dinucleotide; ε-NAD^+, 1,N^6-etheno-NAD^+; NGD^+, nicotinamide guanine dinucleotide; NXD^+, nicotinamide xanthine dinucleotide; $3AcPAD^+$, 3-acetyl pyridine adenine dinucleotide; $3AlPAD^+$, 3-aldehyde pyridine adenine dinucleotide; thio-NAD^+, thio-nicotinamide adenine dinucleotide; ADPR-*p*NP, adenosine diphosphate ribose *para*-nitrophenol.

NNSs for NAD^+-consuming enzymes have mostly been modified on the adenine ring (**1**, **3**, **10**-**13**, Figure 1.18). Also in this case, each enzyme has shown preferences toward particular substrates depending on their active site. For example, PARPs has shown preferences toward **12** compared to **1** or **3**,[79] indicating the importance of a free amino group on the adenine ring; and, furthermore, PARPs, sirtuins and NADases have higher affinity for **10** compared to **11**.[14, 80, 81] In addition, some of the pyridine-modified derivatives have been used as NNSs for sirtuins (**14**, **18**, **19**),[57] and PARPs (**21**).[82] Many

substitutions introduced in the NNSs shown in Figure 1.18 have allowed the development of binding and kinetic assays for NAD^+-dependent enzymes, as discussed in the next section.

At this point it is worth to introduce the most common NNS of β-NAD^+, 1,N^6-etheno-NAD^+ (ε-NAD^+, Figure 1.19), which has been used since the 1970s to investigate many NAD^+-dependent enzymes.[83] Its structure is characterized by the introduction of an etheno bridge between the N-1 and the exocyclic amino group in 6 position on the adenine ring; this modification, extending the electron delocalization along the adenine ring, makes the latter strongly fluorescent. Owing to this property, ε-NAD^+ has been extensively used as a fluorescent probe for NAD^+-dependent enzymes; indeed, the small modification on the adenine ring does not generally interfere with binding to enzyme active sites, allowing structural studies of the relevant enzymes. Moreover, changes in fluorescence following the enzymatic metabolism of the compound by the action of NAD^+-consuming enzymes have allowed the development of fluorescence-based assays for accurate kinetic and mechanistic studies, which will be examined later in this chapter; the characteristic fluorescence properties of this compound and its derivatives will also be considered further in Chapter 3 (see 3.7.1).

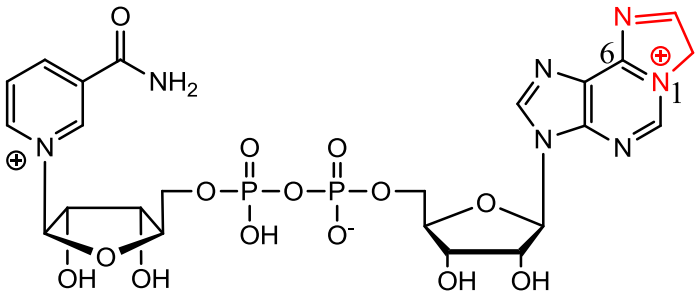

ε–NAD$^+$

Figure 1.19 Chemical structure of ε-NAD^+.

Despite its extensive use for the study of many NAD^+-dependent enzymes, ε-NAD^+ has shown some limitations due to its modification on the adenine ring. Indeed, as will be shown later, ε-NAD^+ is not a good substrate for PARPs (see 1.4.2), ADPRC from *Aplysia kurodai*[56] and some NPPs (see 4.1.2). Moreover, its use for the investigation of

sirtuins and NAD^+-dependent DNA ligases has never been reported, indicating its unsuitability to act as an inhibitor and/or NNS toward these enzymes. Hence, the development of novel classes of NAD^+ derivatives with different features compared to ε-NAD^+ would provide a better insight into the knowledge of many NAD^+-dependent enzymes.

1.4 Assays for NAD^+-consuming enzymes

The investigation of enzyme structures, reaction mechanisms and kinetic measurements is fundamental to the understanding of the enzyme activities and how they correlate to major biological processes. Therefore, the development of NNSs as biochemical probes allows us to answer several biochemical questions. As previously discussed, the chemical modification of different positions on adenine or pyridine rings, and how they influence the corresponding NNS activities, provides an improved understanding of the active site structure and the requirement of fundamental moieties in the natural molecule scaffold. Moreover, the labelling of NNSs with groups that are detectable by sensitive techniques allows the development of more sensitive binding, kinetic and screening assays, compared to those using the NS. These assays generally exploit the labelled NNSs or the corresponding reaction products to monitor their consumption/formation in a continuous or non-continuous format by sensitive techniques. Alternatively, the labelling of the remaining *β*-NAD^+ or reaction products can be performed in a second step of the assay to provide steady-state/endpoint measurements of the enzymatic activities.

Herein, attention will be focused on the existing assays and their principles to monitor the activities of NAD^+-consuming enzymes. As will be shown, assays in a continuous format have been generally developed for those enzymes having *β*-NAD^+ as the only substrate. In contrast, steady-state/endpoint assays have been the only way to monitor the activity of NAD^+-consuming enzymes that have more than one substrate involved in their reaction. Indeed, the different complexities of the reaction mechanisms involving one or more substrates reflects on the substrate/co-substrate binding specificity, which becomes higher if the enzyme has to coordinate the entrance, binding in the active site and metabolism of more than one substrate. Therefore, the development of labelled

NNSs which are tolerated by enzymes with complex reaction mechanisms is an open challenge. In this perspective, novel classes of NAD^+ derivatives with NNS activities toward NAD^+-consuming enzymes could be exploited for the development of new advantageous assays.

1.4.1 Cyanide and dehydrogenase assays

One of the oldest methods to detect NAD^+-consuming enzyme activities is the reaction of the quaternary nitrogen of NaM in β-NAD^+ with cyanide to form a complex that absorbs at 325 nm (Figure 1.20).[84] Adenine nitrogens, free NaM, or dihydronicotinamide in β-NADH do not interfere with this reaction, which is specific for quaternary amines. Moreover, β-NMN can react with cyanide and give a complex with the same spectral properties of β-NAD^+, thus interfering with the assay. While the activity of NADases can be monitored by an absorbance decrease at 325 nm, proportional to the consumption of β-NAD^+, the activity of NPPs cannot be detected, since β-NAD^+ and NPP's reaction product, β-NMN, give exactly the same absorbance reading.

A parallel method to detect changes in β-NAD^+ concentration consists of the reaction of the remaining β-NAD^+ with DHs to generate β-NADH, formation of which can be monitored by absorbance at 340 nm or emission at 475 nm (Figure 1.20),[84] where β-NAD^+ does not interfere. Indeed, β-NAD^+ and β-NADH are both characterized by a maximum absorbance at 260 nm with an extinction coefficient of 16900 $M^{-1}\cdot cm^{-1}$ due to the adenine ring; in addition, β-NADH has another absorbance peak at 340 nm with an extinction coefficient of 6220 $M^{-1}\cdot cm^{-1}$, due exclusively to the reduced nicotinamide ring. Exciting β-NAD^+ and β-NADH at 360 nm, the compounds emit respectively at 445 and 475 nm; however, β-NAD^+ emission is very weak compared to that of β-NADH and, therefore, working with *in vivo* concentrations is possible to fluorimetrically detect only β-NADH.[85, 86]

Identical values for the activity of NADases are obtained by the measurements *via* both cyanide and DH methods, unless β-NAD^+ contains β-NMN impurities that give negative interference. A combination of cyanide and DH methods allows determination of

whether NPPs, NADases or both activities are responsible for the β-NAD^+ consumption. Indeed, a positive absorbance difference between the readings obtained with cyanide and DH methods indicates the presence of NPPs activity beyond that of the NADases.

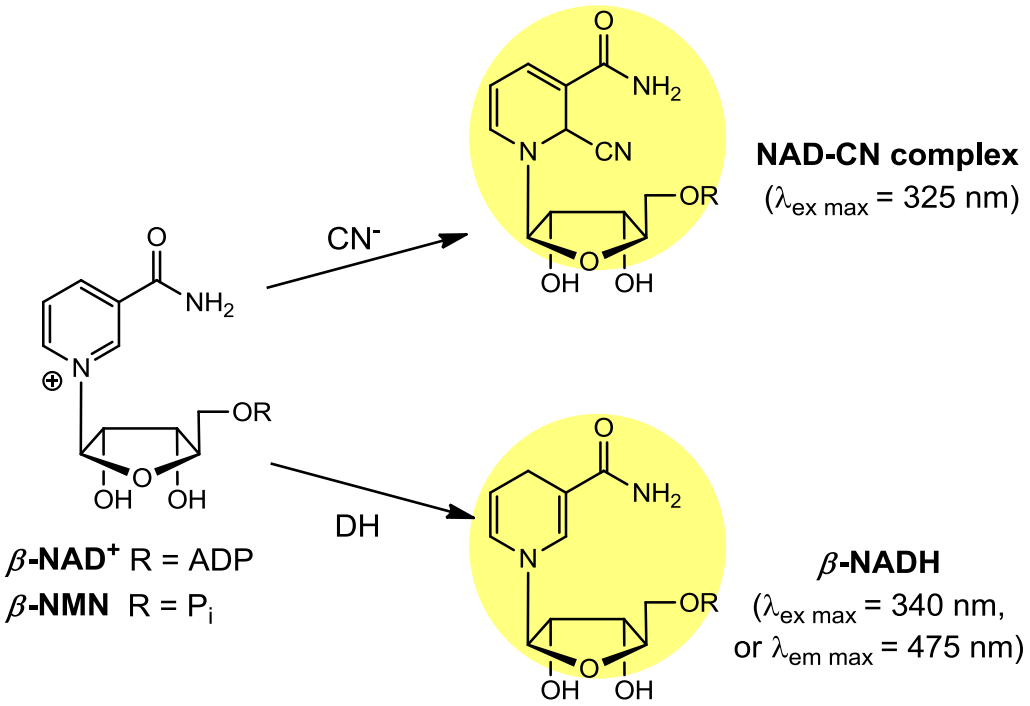

Figure 1.20 Cyanide and dehydrogenase (DH) assays to detect NAD^+-consuming activities. Abbreviations used: NAD^+, nicotinamide adenine dinucleotide; NMN, nicotinamide mononucleotide; ADP, adenosine diphosphate; P_i, phosphate; NAD-CN, NAD-cyanide complex; NADH, reduced NAD^+.

1.4.2 ε-NAD^+ and its application for NAD^+-consuming enzyme assays

ε-NAD^+ (Figure 1.21), as mentioned in 1.3.2 and discussed in detail in Chapter 3, has been largely employed as a fluorescent NNS to monitor the activity of NAD^+-consuming enzymes. Its fluorescence properties, more than its absorbance properties, have been used for the development of continuous or steady-state fluorescence-based assays depending on the examined enzymes, or to gain more sensitivity in HPLC analysis. As will be discussed in more detail in Chapter 3, ε-NAD^+ is characterized by a strong internal fluorescence quenching due to stacking interactions between the ε-adenine and the nicotinamide rings in the intact β-NAD^+ structure.[83, 87, 88] When the ε-NAD^+ structure is disrupted by the activities of NAD^+-consuming enzymes, the fluorescence of the ε-adenine moiety is re-established with a consequent fluorescence

increase, which can be spectroscopically monitored. NPPs,[89] ADPRCs,[69, 90] NADases[87, 91] and ARTs[92, 93] activities can be evaluated by ε-NAD^+ continuous fluorescence-based assays. Indeed, all enzymatic products from the activity of these enzymes are more fluorescent than ε-NAD^+ because of the disruption of the internal quenching between the aromatic rings (Figure 1.21). Therefore, a fluorescence increase during the enzymatic reactions can be detected at 410 nm (λ_{ex} = 300 nm), allowing monitoring of enzyme activities and kinetic measurements.

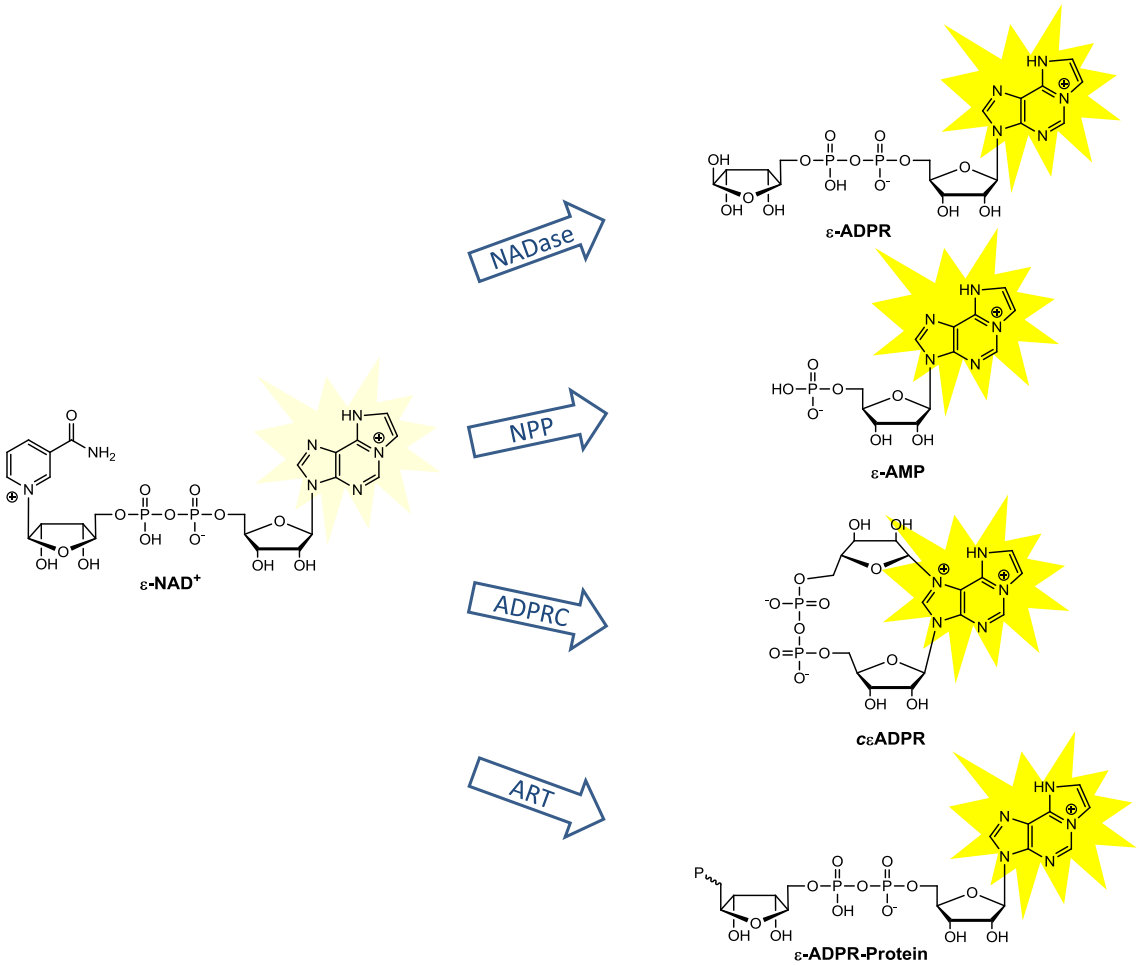

Figure 1.21 ε-NAD^+ as a NNS of NADases, NPPs, ADPRCs and ARTs for the development of continuous fluorescence-based assays. A fluorescence increase is monitored at 410 nm (λ_{ex} = 300 nm) during the enzymatic reactions of the above NAD^+-consuming enzymes. Abbreviations used: ε-NAD^+, 1,N^6-etheno-nicotinamide adenine dinucleotide; ε-ADPR, 1,N^6-etheno-adenosine diphosphate ribose; ε-AMP, 1,N^6-etheno-adenosine monophosphate; *c*εADPR, cyclic 1,N^6-etheno-adenosine diphosphate ribose.

Unfortunately, because all these enzymes use ε-NAD^+ as a NNS, it is not possible simply by fluorescence measurements to distinguish the single enzymatic activities when they are all present. In addition, since these enzymes belong to the same class of ecto-enzymes, this causes a lack of enzyme compartment differentiation, not allowing any enzymatic activity distinction *in vitro*/*in vivo*. Consequently, only the discovery of fluorescent NNSs selective for particular enzymes or HPLC analysis can allow the distinction of the different enzymatic activities *in vitro*/*in vivo*. Hence, modifications to the ε-NAD^+ structure have been performed in the attempt to generate specific substrates for different enzymes. For example, ε-$PdAD^+$ and ε-hy^4PdAD^+ (Figure 1.22) have similar fluorescent properties to ε-NAD^+, with ε-$PdAD^+$ acting as a specific substrate toward NPPs, but not toward NADases.[89] Moreover, the fluorescent properties of ε-NAD^+ and its different enzymatic products have allowed the development of HPLC assays with fluorescence detection, which are much more sensitive than those using the natural *β*-NAD^+.[92, 94]

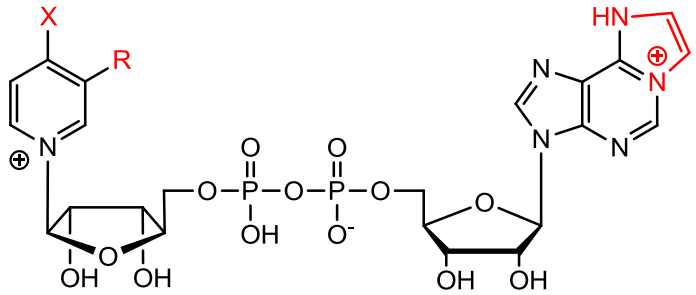

ε–NAD^+ R = $CONH_2$, X = H
ε–$PdAD^+$ R = H, X = H
ε–hy^4PdAD^+ R = H, X = $CONHNH_2$

Figure 1.22 ε-NAD^+ and its derivatives. Abbreviations used: ε-NAD^+, 1,N^6-etheno-nicotinamide adenine dinucleotide; ε-$PdAD^+$, 1,N^6-etheno-pyridine adenine dinucleotide; ε-hy^4PdAD^+, 1,N^6-etheno-4-hydrazinocarbonyl-pyridine adenine dinucleotide.

PARPs use ε-NAD^+ as a NNS, but they do not have a very good affinity for it since the formation of poly(ε-ADPR) is very slow and the length of the polymers much shorter compared to those from *β*-NAD^+.[79] In principle, a fluorescence increase should be observed in relation to the activity of PARPs that catalyzes the removal of NaM and,

therefore, the disruption of the internal quenching in ε-NAD^+. However, a strong fluorescence quenching occurs in the polymers of ε-ADPR, not allowing a continuous monitoring of the activity of PARPs by increase in fluorescence emission.[95] By contrast, the degradation of poly(ε-ADPR) generates a fluorescence increase due to the release of ε-ADPR units, which gives information about the extent of PARPs activity.[79] The poly(ε-ADPR) degradation can be performed by phosphodiesterases, but not by NADases or PARP-glycohydrolases (PARGs);[79, 96] the latter enzymes are indeed inhibited by poly(ε-ADPR).[96] To avoid the slow formation of poly(ε-ADPR) using ε-NAD^+ as a NNS for PARPs, poly(ε-ADPR) can be generated *in situ* from poly(ADPR), obtained by the reaction of PARPs with the natural *β*-NAD^+, by staining with chloroacetaldehyde.[79, 96] Alternatively, poly(ADPR) can be degraded by NPPs to ADPR units, which can be stained *in situ* with chloroacetaldehyde to obtain ε-ADPR.[97] Since the activity of PARPs cannot be directly monitored by fluorescence changes using ε-NAD^+ as a NNS, an immunohistochemical reaction between the ε-adenosine moiety and a specific antibody has been developed to detect *in situ* the formation of poly(ε-ADPR);[95] this method is more sensitive and specific than another immunohistochemical reaction involving the natural adenosine moiety and allowing the *in situ* detection of poly(ADPR).[98]

1.4.3 NGD^+, NHD^+ and NXD^+ for ADPRC fluorescence-based assays

NGD^+, NHD^+ and NXD^+ have been used for the development of continuous fluorescence-based assays to monitor the activity of ADPRCs.[69] Indeed, these compounds, not fluorescent in the form of dinucleotides, become strongly fluorescent after their cyclization by ADPRCs (Figure 1.23).

The acquired fluorescence properties seem to be due to the cyclization of the compounds in N-7, generating a different electron delocalization along the ring because of the generated positive charge. Therefore, a fluorescence increase during the enzymatic reaction can be detected at 410 nm (λ_{ex} = 300 nm), allowing monitoring of the activity of ADPRCs and estimation of kinetic inhibition parameters for this enzyme. Detailed discussions about these NNSs for ADPRC from *Aplysia californica* and their assays will be provided in Chapter 4 (see 4.2.3).

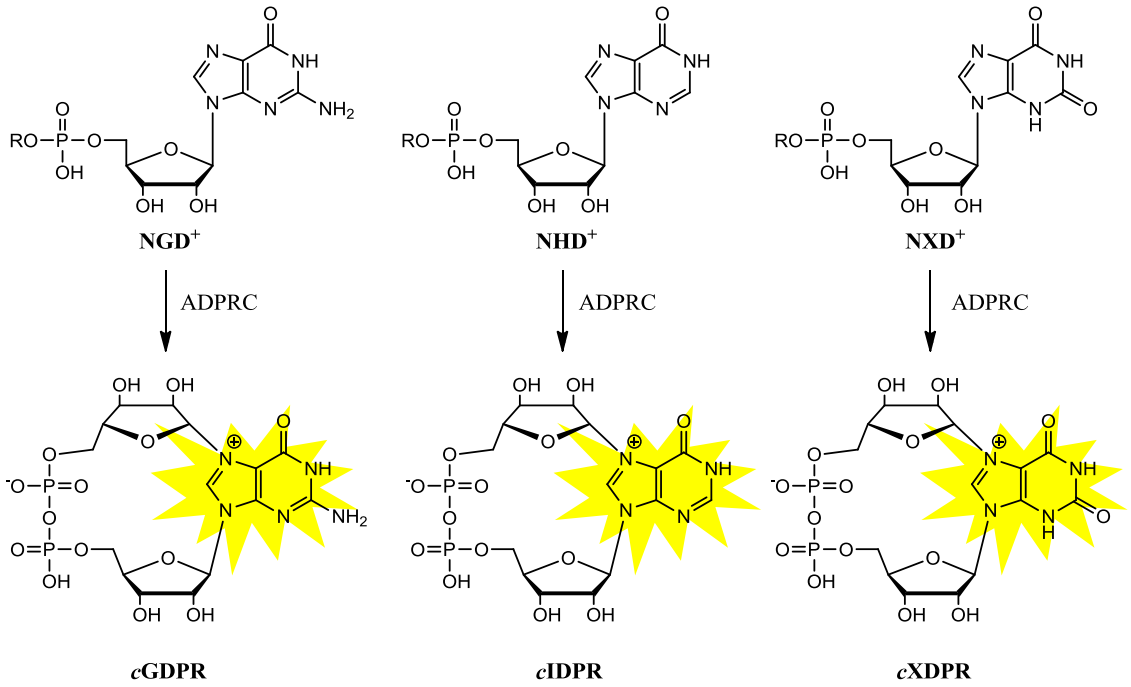

Figure 1.23 NGD^+, NHD^+ and NXD^+ as NNSs of ADPRCs for the development of continuous fluorescence-based assays. A fluorescence increase is monitored at 410 nm (λ_{ex} = 300 nm) during the enzymatic reaction of ADPRCs with NGD^+, NHD^+ and NXD^+. Abbreviations used: *β*-NMN, nicotinamide mononucleotide; NGD^+, nicotinamide guanine dinucleotide; NHD^+, nicotinamide hypoxanthine dinucleotide; NXD^+, nicotinamide xanthine dinucleotide; *c*GDPR, cyclic guanosine diphosphate ribose; *c*IDPR, cyclic inosine diphosphate ribose; *c*XDPR, cyclic xanthosine diphosphate ribose.

1.4.4 6 and 8-alkyne NAD^+ for NADase activity assays

As discussed in 1.2.1, NADases, ARTs, PARPs and sirtuins are characterized by NADase activity since they all cleave the nicotinamide *N*-glycosidic bond with release of NaM. Then, the generated oxocarbenium intermediate can react in different ways depending on the considered enzyme.

A new assay has been developed by Lin and co-workers involving the use of 6 or 8-alkyne NAD^+ as NNSs to label and monitor the activities and the targets of NADase (CD38), ARTs, PARPs and sirtuins.[14, 80, 81] The principle of the assay is based on the labelling of the different ADPR enzymatic products by reaction of the alkyne moiety, introduced in the 6 or 8 position on the adenine ring, with rhodamine or biotin tagged

azides *via* click chemistry (Figure 1.24). Generally, 6-alkyne NAD^+ has been shown to be a better substrate than 8-alkyne NAD^+ for the enzymes examined.

In the case of the activities of ARTs and PARPs, the labelling of mono-ADPR or poly-ADPR acceptors *via* rhodamine has allowed their detection in gel electrophoresis by fluorescence; by contrast, the labelling *via* biotin has allowed their isolation and purification by affinity chromatography, with identification by LC-MS/MS.[80] In the case of sirtuins, the assay has been used to monitor their suspected ART activity. However, even if 6 or 8-alkyne NAD^+ have been shown to be NNSs for the deacetylation activity, they were not able to detect any ART activity exerted by sirtuins, probably because of its weakness compared to the deacetylation process.[14] Finally, the alternative substrates have been used to covalently label CD38.[81] Indeed, it is known that *ara*-2″-$FNAD^+$ inhibits CD38 by covalently binding the ADPR moiety by C-1″ to a glutamate residue.[63] The introduction of a 6 or 8-alkyne moiety on *ara*-2″-$FNAD^+$ has therefore allowed fluorescent labelling of CD38 in living cells.

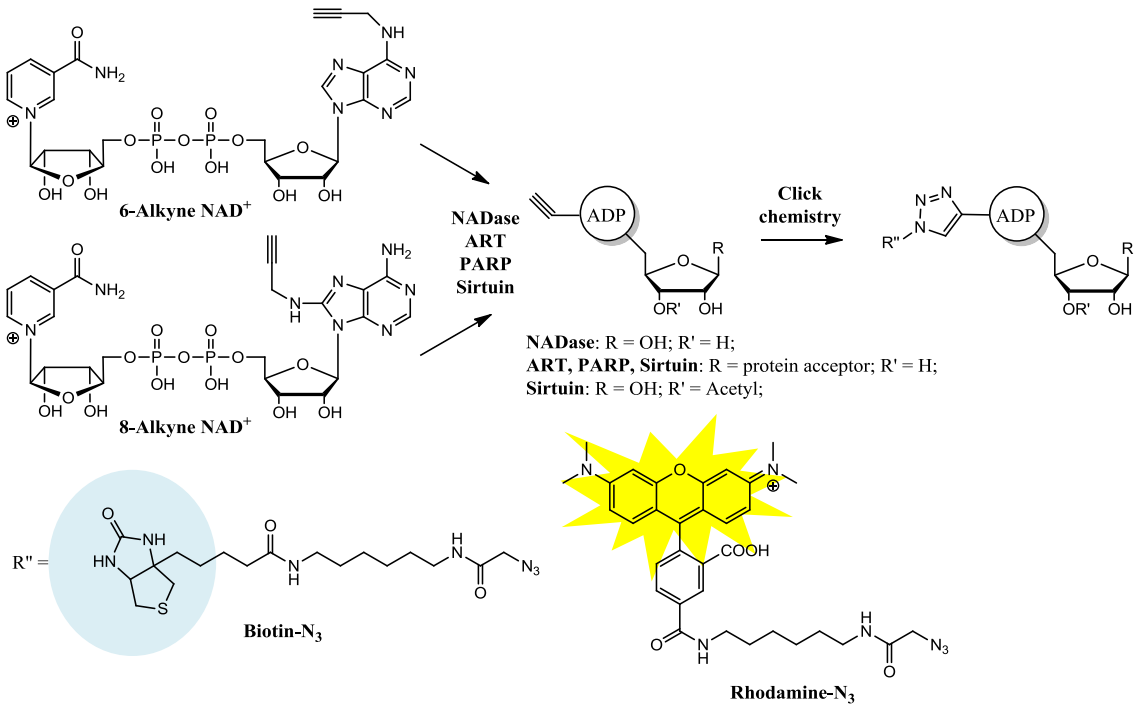

Figure 1.24 6 and 8-alkyne NAD^+ as NNSs of NADases, ARTs, PARPs and sirtuins for the development of fluorescence or immunohistochemical assays. After the enzymatic reaction using 6 or 8-alkyne NAD^+ as NNSs, the different enzymatic products can undergo click chemistry to introduce the biotin or the rhodamine tag.

1.4.5 β-NAD$^+$ quantification by reaction with acetophenone

Another non-continuous assay to monitor the activity of PARPs and sirtuins is based on the quantification of the unreacted β-NAD$^+$ by its reaction with acetophenone to generate a fluorescent NAD$^+$ derivative (**1**, Figure 1.25).[99-101] The treatment of the enzymatic reactions with solutions of KOH and acetophenone, followed by addition of formic acid and heating, leads to the formation of a cyclized fluorescent product, **1**, which can be detected by fluorescence emission at 444 nm (λ_{ex} = 372 nm); at this wavelength, β-NAD$^+$ and NaM do not have any intrinsic fluorescence, therefore they cannot interfere with the assay. Even though it is an endpoint assay requiring different reaction steps, the possibility to perform it on 96 well-plates is a great advantage in terms of large screening of inhibitors.

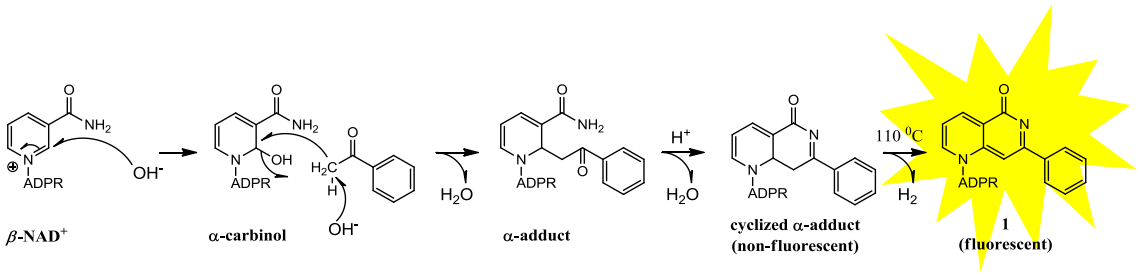

Figure 1.25 Quantification of the unreacted β-NAD$^+$ by its reaction with acetophenone to generate the fluorescent NAD$^+$ derivative, **1**. A KOH solution is added to the enzymatic reaction to generate the α-carbinol intermediate. Then, the addition of acetophenone generates a highly reactive α-adduct, which spontaneously cyclizes to a cyclized non-fluorescent α-adduct; the latter, after heating at 110 °C, dehydrogenates to give the fluorescent NAD$^+$ derivative, **1**.

1.4.6 A continuous colourimetric assay for the detection of PARP activity

A continuous colourimetric assay has been developed for the study of the activity of PARPs; its principle is based on the colour changes occurring during the enzymatic reaction of an NAD$^+$ derivative, used as a NNS of PARPs, in which the nicotinamide ring is substituted with a *para*-nitrophenol ring.[82] The latter is a well known pH indicator, indeed, it is colourless at acidic/neutral pH and bright yellow at basic pH (pK_a = 7.16), when it is in the form of *para*-nitrophenolate. PARPs are able to cleave the *O*-glycosidic bond between the C-1″ of the ribose and the *para*-nitrophenol ring, which is released under its phenolate form to be monitored by absorbance increase at 405 nm (Figure 1.26).

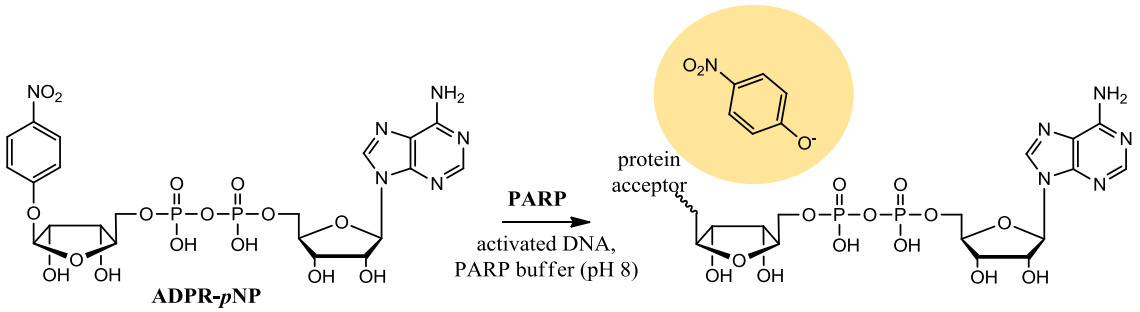

Figure 1.26 ADPR-*para*-nitrophenol (ADPR-*p*NP) as a NNS of PARPs for the development of a continuous colourimetric assay. During the enzymatic reaction, the release of the yellow *para*-nitrophenolate can be monitored at 405 nm.

1.4.7 Alternative assays for the detection of sirtuins activity

Many assays have been developed in the past years to test the activity of sirtuins. Most of the initial assays involved the use of radioactive *β*-NAD^+, labelled with $^{14}C/^{32}P$ on the nicotinamide ring or the pyrophosphate bond, or, alternatively, radioactive acetylated peptides, labelled with ^{3}H on the acetate group.[102] However, radioactive measurements, despite their sensitivity, involve a considerable health hazard, cost and waste issues. More recently, several non-continuous fluorescence-based assays to monitor the activity of sirtuins have been developed: one of them, described in 1.4.5, is based on the detection of the unreacted *β*-NAD^+ by transformation of the latter in a fluorescent derivative. Other assays rely on fluorescence changes during the enzymatic reaction of internally quenched fluorescent peptide substrates. A common assay based on this principle is the Fluor de Lys, commercially available in kits, which uses as a substrate a peptide comprising amino acids 379-382 of human p53 (Arg-His-Lys-Lys[Ac]), containing at the C terminus the fluorophore AMC (7-amino-4-methylcoumarin). Other assays are based on the same principle, using as substrates MAL (*Boc*-Lys[Ac]-AMC)[103] or Z-MAL (*Cbz*-Lys[Ac]-AMC).[104] In the first step of the assay, sirtuins are incubated with *β*-NAD^+ and the fluorescent quenched acetylated peptide substrate (for instance, Z-MAL, Figure 1.27) in the reaction buffer. The peptide, deacetylated by the activity of sirtuins, ZML, is a trypsin substrate; therefore, after the addition into the reaction mixture of a stop solution containing trypsin, the fluorescent product, AMC is released in solution with consequent fluorescence increase. The developed fluorescence is proportional to the deacetylation performed by sirtuins.[103, 104] This assay has been

used for the biological evaluation of 8-aryl/heteroaryl substituted NAD^+ derivatives described in Chapter 5.

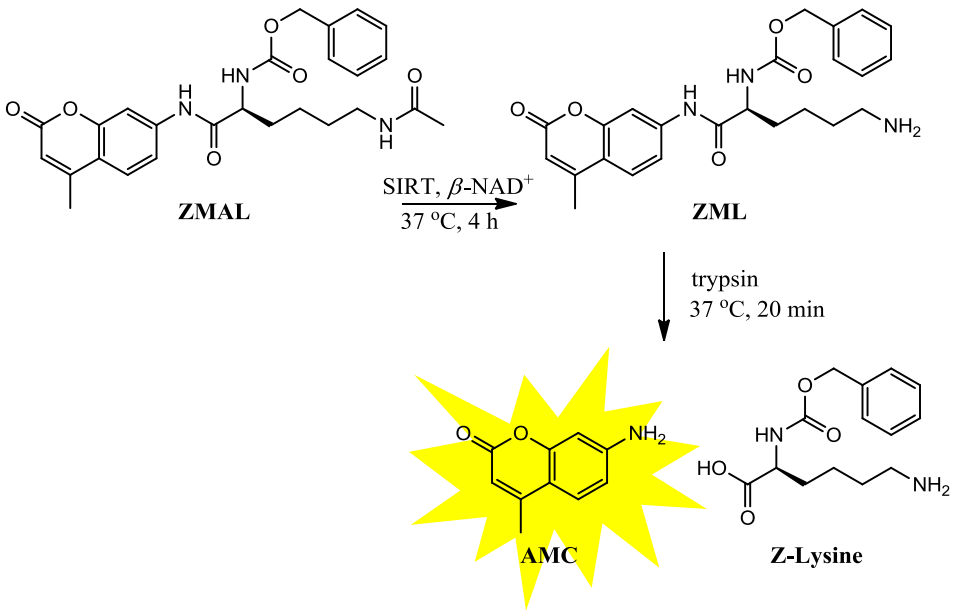

Figure 1.27 Fluorescence-based assay for sirtuins activity. Z-MAL (*Cbz*-Lys[Ac]-AMC) is incubated with sirtuins and β-NAD^+ to give the deacetylated product, ZML (*Cbz*-Lys-AMC). The latter is hydrolysed by trypsin to release the fluorophore, AMC (7-amino-4-methylcoumarin), and Z-lysine. The fluorescence is proportional to the deacetylation exerted by sirtuins.

1.4.8 Assays for the detection of DNA ligase activity

The gel electrophoresis technique is commonly used to monitor the DNA ligation experiments. Its principle is based on the detection of fluorescently or radioactively labelled single strand nicked DNA and its corresponding eventually joined DNA, migrating differently on the gel because of their different molecular sizes. This technique, exploiting a fluorescently labelled single strand nicked DNA, has been used to evaluate the NAD^+ derivatives synthesized in Chapter 2 (more details in Chapter 5, see 5.1.1) toward the ligation activity of EcLigA. However, the gel electrophoresis technique is generally time-consuming and laborious, especially in the screening of many compounds, and its results strongly depend on the batches of enzyme activity and DNA substrates. For this reason, other assays for high-throughput screening of potential inhibitors of DNA ligases have been developed to simplify and overcome the

limitations of the gel electrophoresis assay. Some of them are based on FRET (fluorescence resonance energy transfer) signals generated upon ligation of DNA strands carrying a fluorescence donor and acceptor (Figure 1.28 **a**);[73] others on the fluorescence changes upon ligation of molecular beacons carrying a fluorophore (Figure 1.28 **b**),[105] or a fluorophore and a quencher at the extremities.[106] These assays, although non-continuous and involving different steps (*e.g.* ligation reaction, denaturation, washing), allow high-throughput screening of potential inhibitors of DNA ligases in 96 well-plates with great accuracy and reproducibility.

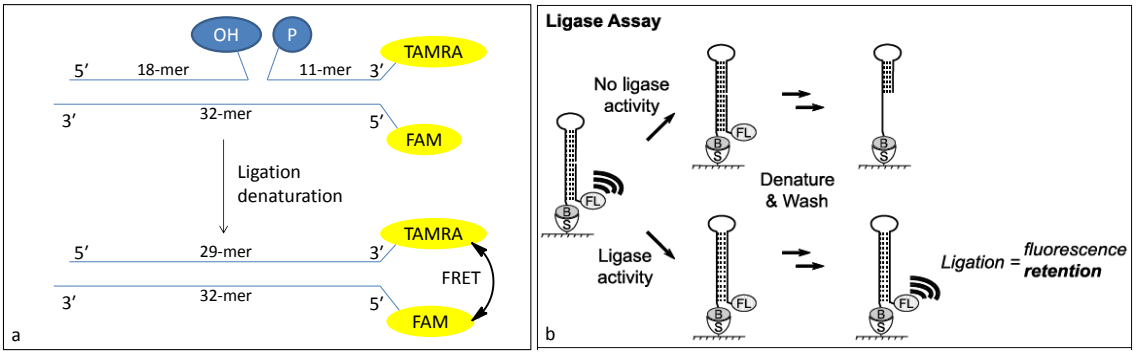

Figure 1.28 Ligation assays based on the generation of FRET signals (**a**), or on the fluorescence detection of ligated molecular beacons[105] (**b**) upon ligation and denaturation conditions.

1.5 Project Objectives

Interest towards NAD^+-consuming enzymes has increased in the past years since a deeper knowledge of fundamental biological processes has shown the involvement of this class of enzymes in their regulation and, consequently, in a number of human diseases. Therefore, the necessity to further investigate their structure and catalytic mechanism and, eventually, to modulate or block their activities has brought an admirable scientific effort in the development of efficient and accurate assays to monitor their enzymatic reactions and screen large numbers of inhibitors.

As reviewed within this chapter, many improvements have been made in targeting and regulating these enzymes. Since β-NAD^+ is the common substrate of NAD^+-consuming enzymes, a major effort has been made in generating NAD^+ derivatives that could act as

inhibitors and/or NNSs for these enzymes. A continuous increase and updating of information about the reaction mechanism and active site structure of NAD^+-consuming enzymes has allowed more specific design of compounds that could show some biological activity toward them.

At the outset of this project, a review of the existing NAD^+ derivatives and their activities toward NAD^+-consuming enzymes has shown that, among the different modifications on the β-NAD^+ scaffold, those on the adenine ring can generate different biological activities depending on the enzymes examined. For example, the adenine modifications are tolerated by a large number of NAD^+-consuming enzymes, such as NADases, ADPRCs, ARTs and PARPs, generating NNSs that have been exploited for the development of binding and kinetic assays. On the other hand, two interesting classes of enzymes, such as NAD^+-dependent DNA ligases and sirtuins, belonging to the NAD^+-consuming enzymes but characterized by complex reaction mechanisms, had shown a strong involvement of the adenine moiety in the enzyme binding and reaction mechanism, suggesting that its modifications can generate potential inhibitors interfering with their activities.

This project has been developed on the basis of these arguments, in an attempt to generate novel adenine-modified NAD^+ derivatives, that could provide new biochemical information about NAD^+-consuming enzymes. The main objectives proposed in this project are summarised below and in Figure 1.29.

- Synthesis of novel NAD^+ derivatives, modified in the position 2, 6 or 8 of the adenine ring with aryl/heteroaryl groups by palladium-mediated cross-couplings (Figure 1.29 **a**) (see Chapter 2). The successful application of these couplings would offer the opportunity to insert many different chemical groups on the adenine ring, keeping intact its skeleton. These modifications, although already applied to the synthesis of nucleosides, nucleotides and DNA derivatives, have never been used for the synthesis of NAD^+ derivatives.

- Spectroscopic analysis of the novel NAD^+ derivatives in view of their potential activity as NNSs for NAD^+-consuming enzymes and, therefore, their application to the development of sensitive assays based on spectroscopic techniques (see Chapter 3).

- Evaluation of the novel NAD^+ derivatives toward NAD^+-consuming enzymes as inhibitors for drug discovery and/or NNSs for the development of advantageous, continuous or non-continuous, assays as an alternative to those already existing (Figure 1.29 **b**). NPPs, NADases and ADPRCs were chosen as model enzymes to test the activities of the NAD^+ derivatives because of the simplicity of their reaction mechanism, involving β-NAD^+ as the only substrate (see Chapter 4). In contrast, NAD^+-dependent DNA ligases and sirtuins were chosen as examples of complex NAD^+-consuming enzymes, using β-NAD^+ as a co-substrate (see Chapter 5).

a

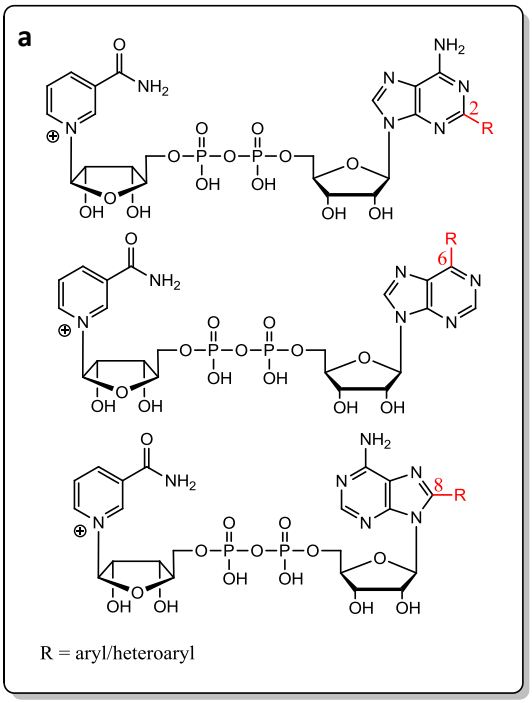

b

β-NAD⁺	*NAD⁺-consuming enzyme*
substrate	NPP
	NADase
	ADPRC
co-substrate	NAD^+-dependent DNA ligase
	sirtuins

Figure 1.29 Synthetic (**a**) and biological (**b**) targets of the project. The synthetic targets (**a**) are represented by the novel NAD^+ derivatives, modified in the position 2, 6 or 8 of the adenine ring with aryl/heteroaryl substituents (R). The biological targets (**b**) are represented by the listed NAD^+-consuming enzymes, divided in two classes depending on the activity of β-NAD^+ as a substrate/co-substrate in their reactions.

- Analysis of the different activities exerted on different enzymes by NAD^+ derivatives substituted in the same position on the adenine ring and, therefore, their ability to target specific biological processes. The enzyme specificity is a fundamental requirement in the drug development for *in vitro*/*in vivo* studies (see Chapter 6).

Therefore, the development of novel adenine-modified NAD^+ derivatives as biochemical probes for NAD^+-consuming enzymes provides new tools for the investigation of this important class of enzymes.

2 SYNTHESIS OF ARYL/HETEROARYL ADENINE-MODIFIED NAD$^+$ DERIVATIVES

2.1 Synthetic strategies to aryl/heteroaryl adenine-modified NAD$^+$ derivatives

β-NAD$^+$ is a fundamental biological molecule found in all living cells and used by a variety of enzymes involved in many different biological processes. Its structure with two labile high-energy bonds, *i.e.* the pyrophosphate and the nicotinamide *N*-glycosidic bond (see 1.1), underpins the biological activity of β-NAD$^+$ as a substrate/co-substrate of NAD$^+$-consuming enzymes, but also makes it an extremely fragile molecule.[5, 7, 13] Indeed, β-NAD$^+$ can be subject to degradation even under mild conditions, which complicates its chemical synthesis and derivatisation. Nevertheless, given the importance of β-NAD$^+$ in biology, the development of NAD$^+$ derivatives is of considerable interest and importance, as such derivatives can be used as biochemical tools to investigate NAD$^+$-dependent enzymes, their reaction mechanisms and their biological roles.

Owing to its limited chemical stability, the chemical modification of β-NAD$^+$ is not always straightforward. Only a few reactions have been reported in the literature where a modification is applied directly on the β-NAD$^+$ scaffold,[70, 83, 107-109] generally involving the introduction of substituents on the nucleobases or the riboses. However, because of the extreme fragility of β-NAD$^+$, the most common method to obtain NAD$^+$ derivatives substituted on the nucleobases, the riboses or the pyrophosphate bond, consists of the introduction of a modification on a stable precursor of the β-NAD$^+$ scaffold, such as the nucleoside/nucleotide moieties, and the following synthesis of the NAD$^+$ target.

As discussed in Chapter 1 (see 1.5), the project aim was the synthesis of NAD$^+$ derivatives modified on C-2, C-6 or C-8 of the adenine ring with aryl/heteroaryl groups, and their following biological evaluation toward NAD$^+$-consuming enzymes. Therefore, the synthesis of adenine-modified NAD$^+$ derivatives was explored. The most common pathway toward adenine-modified NAD$^+$ derivatives is the multistep synthesis (pathway a, Scheme 2.1), which starts with the substitution of the adenosine in the desired

position, subsequently undergoing the phosphorylation of 5′-OH, the phosphate activation and the final coupling with β-NMN to generate the pyrophosphate bond.[110-112] Alternative routes were explored to shorten the synthesis of adenine-modified NAD^+ derivatives: the pathway b (Scheme 2.1) *via* nucleoside phosphoramidite intermediates gives in one step the phosphorylation/phosphate activation of substituted adenosines for their following coupling with β-NMN;[113] the pathway c (Scheme 2.1) allows bromination and substitution by Suzuki-Miyaura cross-coupling in one-pot, on position 8 of the natural β-NAD^+.[70]

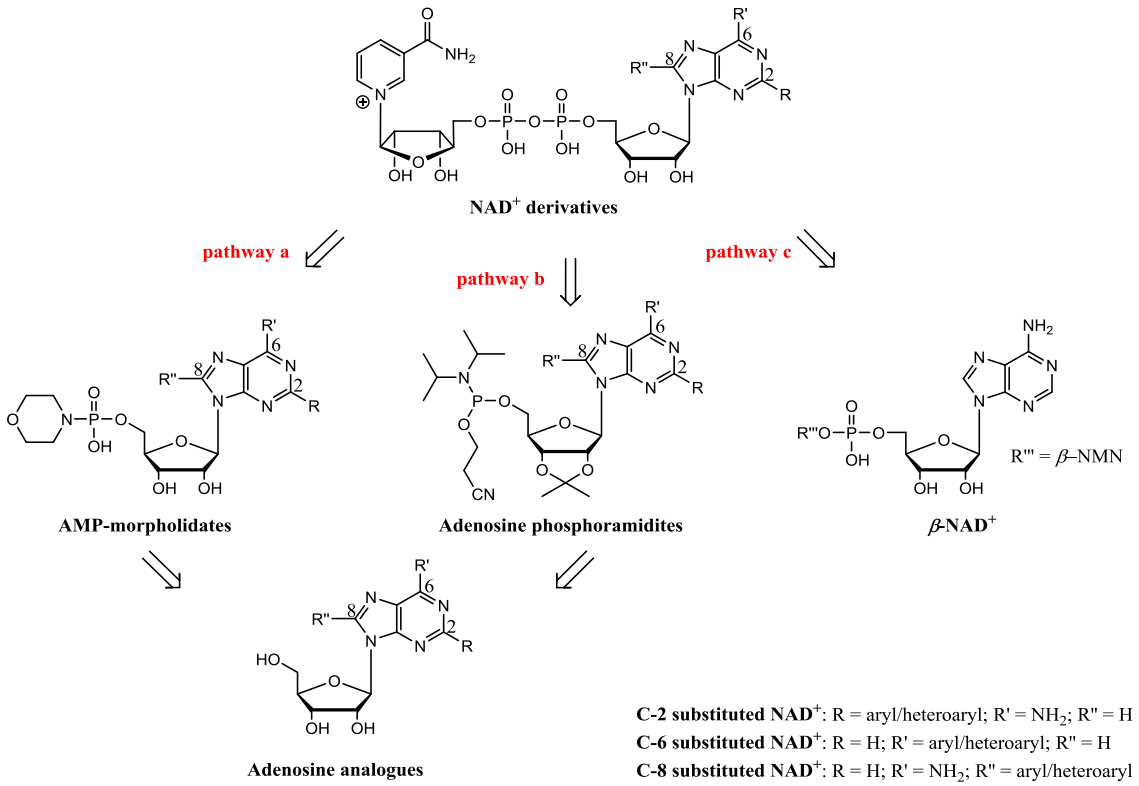

Scheme 2.1 General synthetic pathways to aryl/heteroaryl adenine-modified NAD^+ derivatives. Pathway **a)** *via* AMP-morpholidates; pathway **b)** *via* nucleoside phosphoramidites; pathway **c)** *via* one-pot, two-step synthesis of 8-substituted NAD^+ derivatives. Abbreviations used: β-NAD^+, nicotinamide adenine dinucleotide; AMP, adenosine monophosphate; β-NMN, nicotinamide mononucleotide.

The pathway a, though more laborious and time-consuming, is the most flexible to successfully obtain different substitutions on the β-NAD^+ scaffold, since even the modifications requiring harsh reaction conditions are introduced on the stable adenosine precursors. Indeed, this pathway was used to synthesize all the final NAD^+ derivatives

studied in this thesis. Through substitution of the adenosine on C-2, C-6 or C-8 of the adenine ring and phosphorylation of the 5′-OH, the NAD^+ multistep synthesis converges to two final steps, in common for all the substituted adenosines, leading to the final NAD^+ derivatives. This route will be discussed first, starting with the synthesis of the differently adenine-modified AMP derivatives (see 2.3, 2.4 and 2.5), converging then to the common steps to obtain the final NAD^+ derivatives (see 2.6). The pathway b and c will be explored as well, though subject to many future further studies (see 2.7).

2.2 Substitution of the adenine ring by palladium-mediated cross-couplings

Since the 1940s and 1950s, the study of nucleosides, nucleotides and their derivatives has become more and more important, in parallel with the improved and deeper knowledge of DNA and metabolic processes involving these compounds. Their several biological roles have made them a constant source of interest as therapeutics and molecular probes to understand biological systems. From the first attempts to modify the natural substrates on the nucleobase or the ribose, to the most successful attempts to substantially change the structure, improving the derivatives stability and selectivity, an extensive study to new approaches for these modifications has been undertaken resulting in the development of many useful synthetic pathways.[114]

Since this project aimed to synthesize of NAD^+ derivatives modified on the adenine ring, attention was mainly focused on the modified purines, also found in nature, well known for their extremely various and important biological properties.[115] Several have therapeutic activity as modulators of adenosine receptors or stimulators of plant cell growth and division (cytokinines); others inhibit DNA polymerases exhibiting antiviral, antibacterial, anticancer properties. Moreover, purines modified by metabolically activated mutagens and carcinogens introduced in the cells by dietary and environmental exposure, can cause DNA alteration, and even oncogenesis. Indeed, the modification of the purine ring in different positions can substantially alter the normal nucleoside/nucleotide conformation, the H-bonding ability and, consequently, the intercalation in DNA and the interaction with proteins.

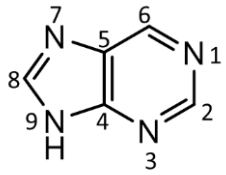

Figure 2.1 Purine structure and numbering.

The purine ring, which skeleton is given by the fusion of imidazole and pyrimidine rings (Figure 2.1), can be substituted on C-2, C-6 and C-8 and on N-1, N-3, N-7 and N-9.[116] Substituted purines can be obtained by different methods:

- Heterocyclization from pyrimidine or imidazole; however, in particular cases the methods are not efficient and require many reaction steps with quite low yield;[115, 117]
- S_NAr, where halogenated electrophilic purines can undergo displacement of the halogen with a good nucleophile;[118]
- S_EAr, where nucleophilic purines can be substituted with electrophilic reagents (*e.g.* alkylation).[119]

The last two methods require particular electronic properties and drastic reaction conditions; consequently, other easier synthetic pathways have been explored. The recent development of metal-mediated couplings has considerably facilitated the synthesis of purine derivatives.[114, 120, 121] In general, metal-catalyzed couplings are economically advantageous; in addition, they are suitable for introducing a broad range of substituents. A wide variety of palladium-mediated reactions, such as Sonogashira, Heck, Stille and Suzuki-Miyaura cross-couplings, has been developed since the 1960s, and adapted and optimized to prepare respectively alkynyl, alkenyl and aryl/heteroaryl purine derivatives.[114, 116, 120-127]

The synthetic part of this project was focused on the substitution of C-2, C-6 or C-8 of the adenine ring in adenosine and/or adenosine monophosphate with aryl/heteroaryl groups, as intermediates to synthesize the final targets, the corresponding adenine-modified NAD^+ derivatives. In particular, the introduction of phenyl and pyrrolyl groups in different positions on the adenine ring was considered in order to screen and

compare eventual structural and biological differences caused by the hydrophobic interactions exerted by the phenyl group, with those due to H-bonding formation of the pyrrolyl group. In addition, the substitution of the adenine with a pyrrolyl group could be particularly interesting because of the presence of pyrrole units in many biological molecules.

Suzuki-Miyaura and Stille cross-couplings were the most suitable palladium-mediated reactions for our purposes. They catalyze respectively the C-C bond formation between aryl/heteroaryl boronic acids, $XB(OH)_2$, or stannanes, $XSnBu_3$, and activated aromatic halides (Scheme 2.2). Owing to the commercial availability and relatively easy halogenation of purine nucleosides/nucleotides (**1**-**3**), the general cross-coupling strategy uses the halogenated nucleosides/nucleotides in the favoured position as starting materials (**4**-**6**), followed by the coupling with boronic acids (a) or stannanes (b) *via* palladium-mediated reactions. Palladium-mediated cross-couplings can be performed directly on adenosine, avoiding the halogenation step, although this generally requires harsh reaction conditions; only recently, mild reaction conditions have been found, also suitable for the direct substitution of the unstable and unprotected 2′-deoxyadenosine.[128-130]

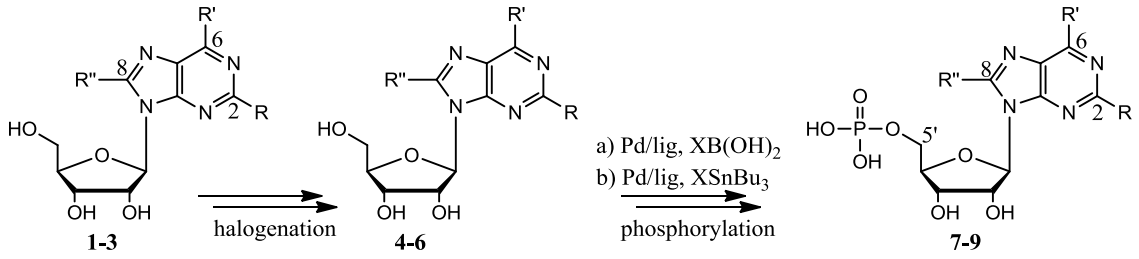

1-3 **4-6** **7-9**

1: R=NH_2, R'=OH, R"=H
2: R=H, R'=OH, R"=H
3: R=H, R'=NH_2, R"=H

4: R=I, R'=NH_2, R"=H
5: R=H, R'=Cl, R"=H
6: R=H, R'=NH_2, R"=Br

7: R=X, R'=NH_2, R"=H
8: R=H, R'=X, R"=H
9: R=H, R'=NH_2, R"=X

Scheme 2.2 General synthetic strategy to aryl/heteroaryl adenine-modified nucleotides. Guanosine (**1**) as starting material for 2-substituted adenosine monophosphate (**7**); inosine (**2**) as starting material for 6-substituted purine nucleotide (**8**); adenosine (**3**) as starting material for 8-substituted adenosine monophosphate (**9**). After the halogenation of the nucleosides, **1**-**3**, in the favoured positions, **4**-**6** undergo Suzuki-Miyaura (a) or Stille cross-coupling (b) by Pd/lig catalyst (lig = phosphine) to introduce the aryl/heteroaryl group, X. The following phosphorylation generates the corresponding nucleotides, **7**-**9**.

The Suzuki-Miyaura[131] and Stille[132] cross-couplings proceed *via* a catalytic cycle, involving an oxidative addition, transmetallation and reductive elimination (Scheme 2.3). In the first step, the reactive species, Pd(0), is oxidized to Pd(II) after the addition of an organic halide, R-X, forming a *cis* complex, that rapidly isomerizes to *trans*: this is generally the rate-limiting step in the catalytic cycle, depending on the reactivity of the halide and the σ-donating ability of the ligands coordinating Pd(0). During the transmetallation step, the second organic group, R′, is transferred to Pd(II) from another metallic species. In the Suzuki-Miyaura cross-coupling this is a boronic acid, while in the Stille cross-coupling it is an organic stannane. The use of a base in the Suzuki-Miyaura cross-coupling is fundamental to activate the organic boronic acid during the transmetallation step; indeed, the organic group on the boron, because of the predominantly covalent B-C bond, would not otherwise be nucleophilic enough to take part in the transmetallation step. In contrast, the organic stannanes do not need any activation because of the weaker Sn-C bond. The last step in the catalytic cycle, the reductive elimination, requires a slow isomerization of the *trans* Pd(II) complex to *cis* with elimination of the cross-coupled product, R-R′, and the re-establishment of the reactive species, Pd(0).

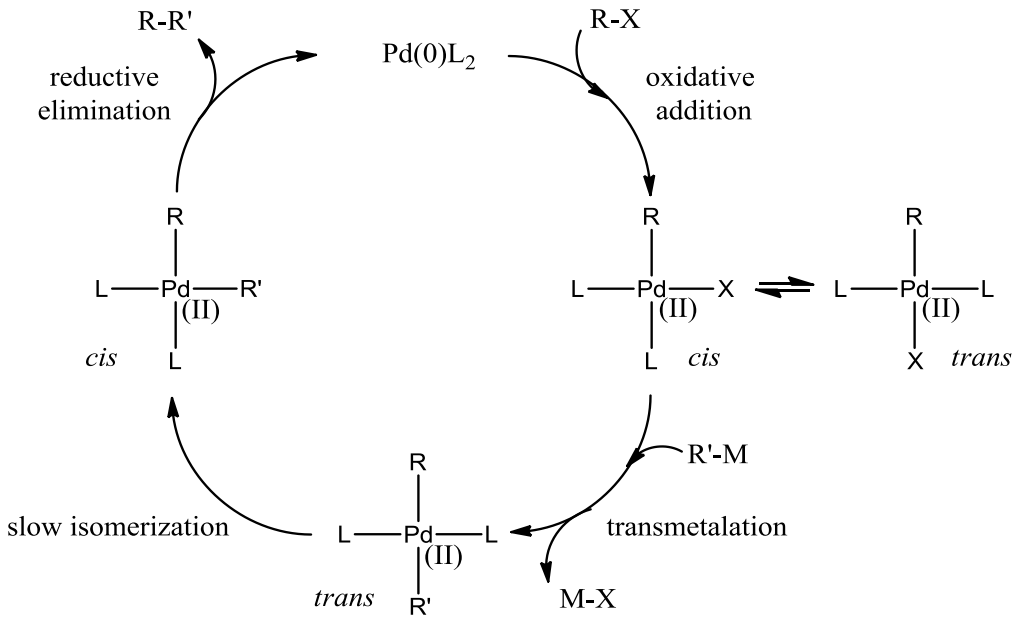

Scheme 2.3 Catalytic cycle of palladium-mediated cross-couplings.

The toxicity of stannanes and their difficult disposal, compared to the high stability, easy handling, low toxicity and huge variety of available boronic acids has favoured the development of the Suzuki-Miyaura cross-coupling compared to the Stille cross-coupling. Nevertheless, in some cases only the Stille cross-couplings are really effective for the formation of certain types of C-C bonds.[131-133]

2.3 Synthetic route to 2-aryl/heteroaryl AMP derivatives

The synthetic route to 2-aryl/heteroaryl AMP derivatives starts with the halogenation of C-2 on the adenine ring in order to form the organic halide, which will undergo the Suzuki-Miyaura or Stille cross-coupling for the introduction of the aryl/heteroaryl substituent.

The most common substitutions on C-2 are normally achieved by halogenation of this position, followed by nucleophilic aromatic substitutions, formation of palladium-catalyzed C-N bonds, or Sonogashira cross-couplings; the latter is an alternate copper-catalyzed palladium-mediated cross-coupling to obtain 2-alkynyl adenine derivatives.[134, 135] Very few examples of Suzuki-Miyaura and Stille cross-couplings on C-2 of adenosine are present in the literature.[127, 136-138] Most of these substitutions start from guanosine (**1**) and proceed *via* the installation of an iodine on C-2, as this generates the most reactive halide (**4**) (Scheme 2.2). Indeed, the substitutions on C-2 of the adenine ring are complicated by the low reactivity of this position, which is on the electron-poor pyrimidine ring of the purine skeleton; hence, the introduction of a very good leaving group is necessary. To date, the cross-coupling reactions described in the literature for the 2-substitution have only been applied on the adenosine, but not on the adenosine monophosphate. Indeed, these reactions are carried out in organic phase with apolar reagents and solvents, requiring for this reason the protection of the hydroxyl groups of adenosine with different protecting groups.[127, 136-138]

Our synthetic strategy aimed at the synthesis of 2-iodo AMP (**7a**), 2-phenyl AMP (**7b**) and 2-(*N*-Me-pyrrol-2-yl) AMP (**7c**). It proceeded through the iodination of adenosine on C-2 (**4**) and the protection of the 2′, 3′-OH on the ribose with acetone to form the isopropylidene protecting group (**4a**). After the Pd-mediated cross-couplings for the introduction of phenyl and *N*-Me-2-pyrrolyl groups (**4a-c**), the phosphorylation of 5′-OH *via* phosphoramidite intermediates (**4d-f**) or by $POCl_3$ afforded **4g-i**, finally deprotected to give the final compounds (**7a-c**) (Scheme 2.4).

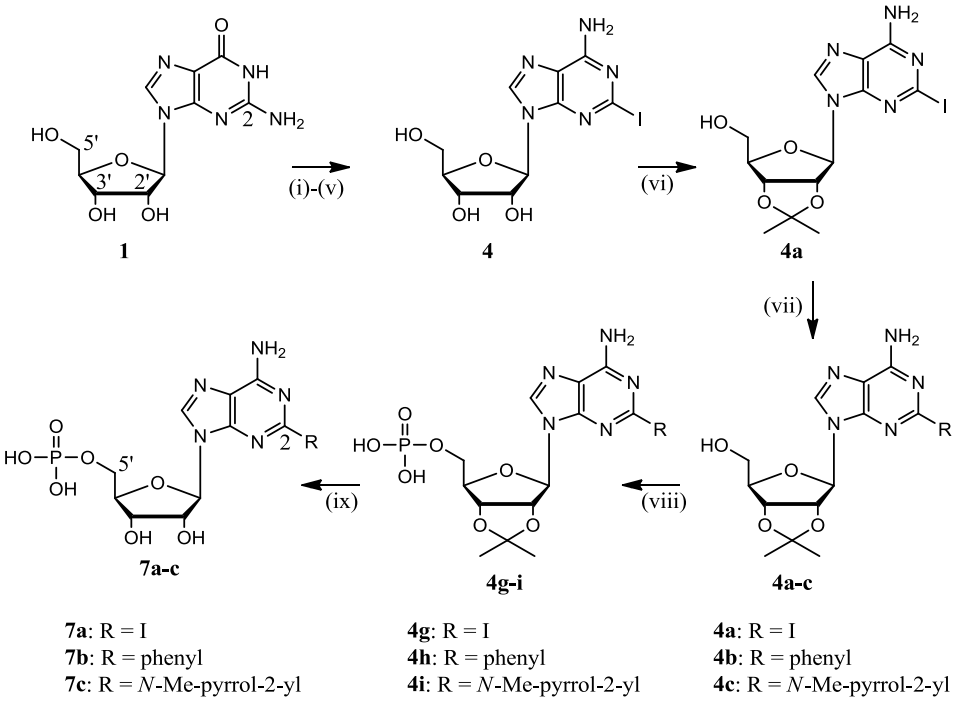

Scheme 2.4 Synthetic route to 2-substituted AMP derivatives. (i)-(v) Iodination of adenosine on C-2 from guanosine (**1**); (vi) 2′,3′-*O*-isopropylidene protection; (vii) palladium-mediated cross-coupling; (viii) phosphorylation of 5′-OH; (ix) deprotection of 2′,3′-OH.

2.3.1 Iodination of C-2 and 2′,3′-*O*-isopropylidene protection of adenosine

The first step in the synthesis of 2-substituted AMP derivatives is the iodination of C-2 in adenosine, particularly required to have the most reactive halide in the following Suzuki-Miyaura and Stille cross-couplings. The halogenation of aromatic rings is generally achieved by S_EAr; in the case of the adenine ring, the halogenation in position 2 is less straightforward than that in position 8 because of a lower reactivity of C-2

compared to C-8 in S_EAr. For this reason, the iodination of C-2 is generally achieved by a long synthetic strategy, well described in the literature, which avoids the use of S_EAr. It starts from guanosine (**1**), converting it to the fully acetylated 2-amino-6-chloro purine nucleoside (**1a**); the latter is converted by diazotization-iodine substitution in the fully acetylated 2-iodo-6-chloro purine nucleoside (**1b**), which undergoes amination and deprotection to finally give the 2-iodo adenosine (**4**) (Scheme 2.5).[134, 139, 140]

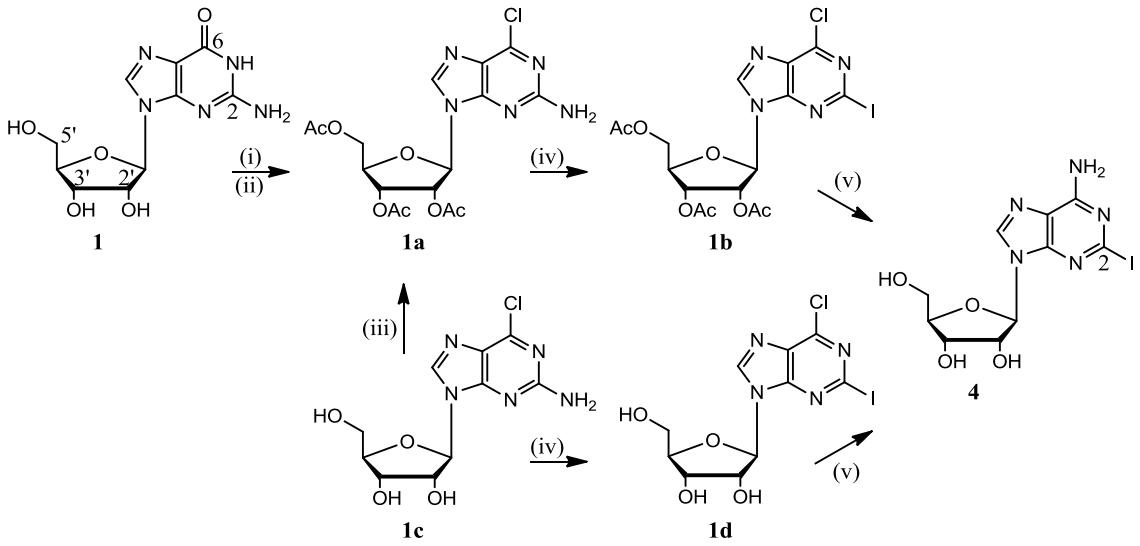

Scheme 2.5 Iodination of adenosine on C-2 from **1**. (i) Acetic anhydride, DMF, pyridine, 75 °C, 4 h, 87%; (ii) $POCl_3$, *N*,*N*-dimethylaniline, 100 °C, 10 min, 85%; (iii) acetic anhydride, DMAP, TEA, acetonitrile, rt, 1 h, 89%; (iv) CuI, I_2, CH_2I_2, isoamyl nitrite in THF, 70 °C, 4 – 12 h, 85% from **1a**, 51% from **1c**; (v) NH_3/MeOH, 60 °C, 12 h, 40% from **1b**, 30% from **1d**; 33% overall from **1a**, 21% overall from **1c**.

Our synthesis, described in Scheme 2.5, started from the commercially available 2-amino-6-chloro purine nucleoside (**1c**), which was fully protected by acetylation to obtain **1a** (89%). Afterwards, the next reactions were carried out on the protected nucleosides as described in the literature, until the final amination/deprotection step, which gave compound **4** with 33% yield overall (compared to 70% yield in the literature).[139] The same pathway was performed on the unprotected nucleosides, starting with the diazotization-iodine substitution of **1c** to give **1d** (51%), finally converted in the compound **4** with 21% yield overall. Therefore, this pathway, although giving product **4** in lower yields, allowed to avoid the protection/deprotection steps.

Afterwards, the obtained 2-iodo adenosine (**4**) had to be protected on the ribose to undergo the subsequent palladium-mediated cross-coupling in organic phase. Because of our synthetic strategy, the isopropylidene protecting group was the most convenient to install. Indeed, because of its acetal nature, it was resistant to the basic conditions of the Suzuki-Miyaura cross-coupling, and allowed the protection of the vicinal hydroxyl groups in C-2′ and C-3′, leaving the primary alcohol in C-5′ free for the subsequent phosphorylation.

The 2′,3′-*O*-isopropylidene protecting group can be introduced by reaction of the nucleoside with acetone in acidic conditions (Scheme 2.6);[135, 141] the acetal formation is a reversible equilibrium, hence the deprotection occurs again in acidic conditions. The 2′,3′-*O*-isopropylidene protection of **4** was carried out as described in the literature, affording the desired product **4a** with 98% yield.

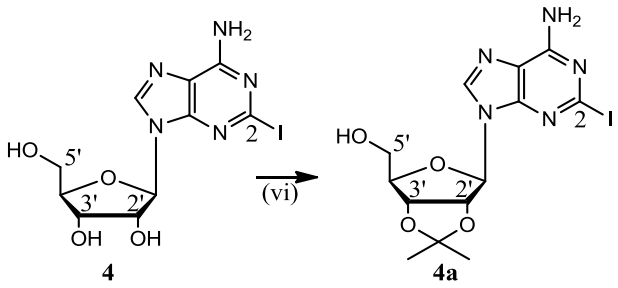

Scheme 2.6 2′,3′-*O*-isopropylidene protection of 2-iodo adenosine, **4**. (vi) Acetone, 70% $HClO_4$, rt, 1 h; then, NH_4OH, rt, 3 h, 98%.

2.3.2 Suzuki-Miyaura and Stille cross-couplings on C-2 of 2′,3′-*O*-isopropylidene-2-iodo adenosine

As mentioned in 2.3, the reactivity of C-2 on the adenine ring toward palladium-mediated cross-couplings is lower compared to other positions, due to the electron-poor nature of the pyrimidine ring; indeed, the electrophilicity of the organic iodide is decreased because of a strong mesomeric effect competing with the inductive effect.

In the literature, the optimized conditions for the Suzuki-Miyaura cross-coupling on the protected 2-iodo adenosine (**4a**) allow the successful coupling with simple aryl boronic acids,[127, 136-138] such as phenyl or biphenyl boronic acids; $Pd(OAc)_2$, (2-biphenyl)dicyclohexylphosphine, K_3PO_4, in anhydrous 1,4-dioxane at 100 °C is the optimal catalytic system, affording the desired products in 60% yield.[136] In this project, these conditions using phenyl boronic acid were successfully applied to obtain the 2′,3′-*O*-isopropylidene-2-phenyl adenosine (**4b**) in 43% yield (Scheme 2.7).

No references in the literature have been found on Suzuki-Miyaura cross-couplings at C-2 with heteroaryl boronic acids. The installation of a pyrrolyl group on the adenine ring by Suzuki-Miyaura cross-coupling would require the use of 2-pyrrole boronic acid. However, the latter is a difficult substrate because it can dimerize or protodeboronate, and the free amino group can coordinate Pd(0) inhibiting the catalytic cycle[142, 143]. The protection of the amino group of the pyrrole with different protecting groups (*Boc*, *TIPS*) has solved these problems in many cases affording the pyrrolyl cross-coupled products with quite good yields. Nevertheless, the Suzuki-Miyaura cross-coupling on C-2 of the 2′,3′-*O*-isopropylidene-2-iodo adenosine (**4a**) with the *N*-Boc-2-pyrrole boronic acid failed using the optimized conditions for the phenyl substitution.[136]

The only example found in the literature for the synthesis of 2-heteroaryl substituted protected adenosine has used the Stille cross-coupling to introduce thienyl and furanyl groups[137] on the fully *tert*-butyldimethylsilyl protected 2-iodo adenosine. In the context of this project, the commercially available tributyl-(*N*-Me-pyrrol-2-yl) stannane was used to test the Stille cross-coupling conditions on 2′,3′-*O*-isopropylidene-2-iodo adenosine (**4a**), requiring $PdCl_2(PPh_3)_2$ as catalyst. Effectively, under these conditions, using anhydrous 1,4-dioxane instead of anhydrous THF, about 43% of **4a** was converted in **4c**, slightly improved to 50% when anhydrous LiCl was added to the reaction; indeed, the addition of chloride in Stille cross-couplings can often accelerate the catalytic reaction during the transmetallation step (Scheme 2.7). However, the purification by silica gel chromatography of the product **4c** from the excess of stannane was unsuccessful, causing a substantial stannane contamination of the reaction product even after several purifications; therefore, the next synthetic steps were performed on the crude mixture.

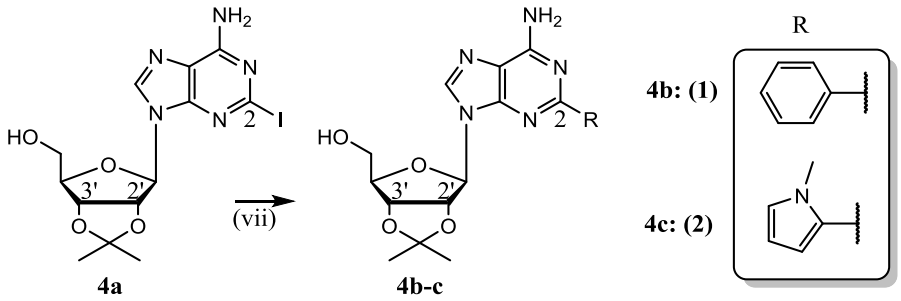

Scheme 2.7 Palladium-mediated cross-couplings on C-2 of 2′,3′-*O*-isopropylidene-2-iodo adenosine, **4a**. Suzuki-Miyaura cross-coupling (**1**): phenyl boronic acid, $Pd(OAc)_2$, (2-biphenyl)dicyclohexylphosphine, K_3PO_4 in anhydrous 1,4-dioxane, 100 °C, 24 h, 43% for **4b**. Stille cross-coupling (**2**): tributyl-(*N*-Me-pyrrol-2-yl) stannane, optional anhydrous LiCl, $PdCl_2(PPh_3)_2$ in anhydrous 1,4-dioxane, 100 °C, 48 h, 43-50% conversion for **4c**.

2.3.3 Phosphorylation of 5′-OH of 2′,3′-*O*-isopropylidene-2-substituted adenosine and subsequent deprotection to 2-aryl/heteroaryl AMP derivatives

A common method to phosphorylate the 5′-OH of protected and/or unprotected nucleosides uses $POCl_3$ as phosphorylating agent (method 1). In the past, many studies have been performed to optimize this reaction affording quite good yields, even in the difficult case of the phosphorylation of unprotected nucleosides, where the selective phosphorylation of 5′-OH is required. The optimized reaction conditions require the addition of a base to the reaction mixture to buffer the acidic pH generated along the reaction course; indeed, adenosine is subjected to depurination under acidic conditions. Moreover, the solvents commonly used are acetonitrile or triethylphosphate, the latter accelerating the phosphorylation in a selective way towards the 5′-OH.[144-146]

In this study, when the phosphorylation was performed on 2′,3′-*O*-isopropylidene-2-phenyl adenosine (**4b**) using $POCl_3$, proton sponge as a base and triethylphosphate as solvent, the conversion was so low that, in some cases, no product could be recovered. In addition, when the reaction failed, the recovery of the starting material was complicated because of the difficult purification from triethylphosphate and proton sponge. The phosphorylation by $POCl_3$ was also attempted on 2′,3′-*O*-isopropylidene-2-iodo adenosine (**4a**), substituting the triethylphosphate with acetonitrile and removing the proton sponge to facilitate the purification step. However, a poor conversion was observed also in this case, probably due to a substantial substitution of the iodide with the chloride generated in the course of the reaction (Scheme 2.8).

Because of the unsatisfactory results obtained in the phosphorylation of **4a** and **4b** by $POCl_3$, this phosphorylation method was not applied on the crude 2′,3′-*O*-isopropylidene-2-(*N*-Me-pyrrol-2-yl) adenosine (**4c**).

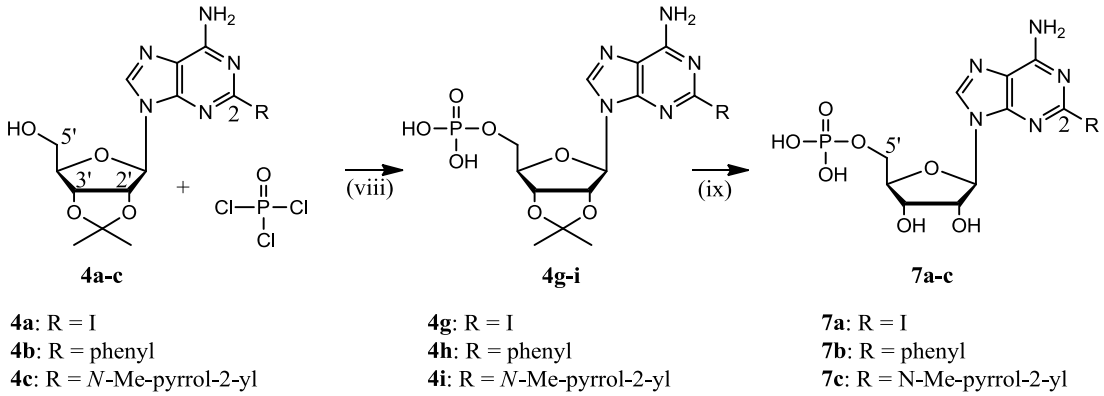

4a-c **4g-i** **7a-c**

4a: R = I
4b: R = phenyl
4c: R = *N*-Me-pyrrol-2-yl

4g: R = I
4h: R = phenyl
4i: R = *N*-Me-pyrrol-2-yl

7a: R = I
7b: R = phenyl
7c: R = N-Me-pyrrol-2-yl

Scheme 2.8 Phosphorylation of 5′-OH of 2′,3′-*O*-isopropylidene-2-substituted adenosine by $POCl_3$ (method 1). (viii) Optional proton sponge, triethylphosphate or anhydrous acetonitrile, 0 °C, 12 h, 9% from **4a**; (ix) Dowex 88 (H^+), rt, 12 h, 36% for **7a**; 3% overall for **7a**.

Therefore, an alternative phosphorylation method was chosen using the phosphoramidite as a highly reactive phosphorylating agent (method 2).[113] The new phosphorylation strategy required the reaction of 2′,3′-*O*-isopropylidene-2-substituted adenosines (**4a-c**) with 2-cyanoethyl *N*,*N*-diisopropylchlorophosphoramidite to obtain the phosphoramidite nucleoside intermediates (**4d-f**). These could then be oxidized to the phosphate intermediates by ^{t}BuOOH, and deprotected from 2-cyanoethyl and *N*,*N*-diisopropyl groups by treatment with NH_4OH, to afford the 2′,3′-*O*-isopropylidene-2-substituted adenosines 5′-monophosphate (**4g-i**). After removal of the *O*-isopropylidene protecting group by treatment with Dowex 88 (H^+), the final 2-substituted AMP derivatives (**7a-c**) were obtained (Scheme 2.9).

This synthetic route, though involving more steps compared to the $POCl_3$ method and the use of an expensive reagent in the form of 2-cyanoethyl *N*,*N*-diisopropylchlorophosphoramidite, turned out to be successful in the phosphorylation of 2′,3′-*O*-isopropylidene-2-substituted adenosines (**4a-c**), affording **7a** and **7b** in 19% and 17% yield overall respectively.

Unfortunately, **7c** was never recovered pure, even after several purifications, due to the stannane contamination from the previous Stille cross-coupling.

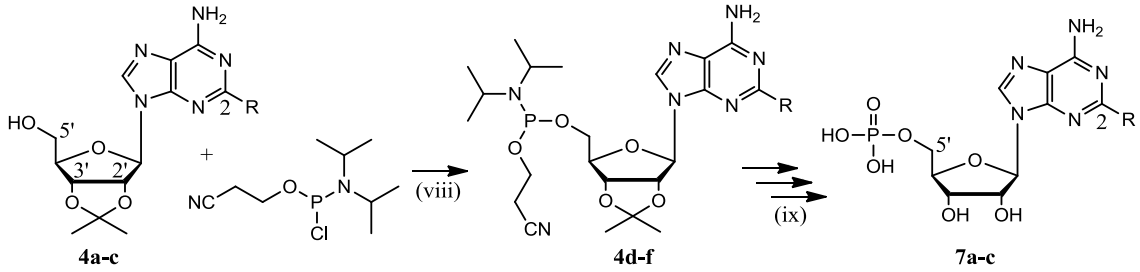

4a-c **4d-f** **7a-c**

4a: R = I
4b: R = phenyl
4c: R = *N*-Me-pyrrol-2-yl

4d: R = I
4e: R = phenyl
4f: R = *N*-Me-pyrrol-2-yl

7a: R = I
7b: R = phenyl
7c: R = *N*-Me-pyrrol-2-yl

Scheme 2.9 Phosphorylation of 5′-OH of 2′,3′-*O*-isopropylidene-2-substituted adenosine *via* phosphoramidite (method 2). (viii) DIPEA, anhydrous CH_2Cl_2, rt, 1 h; then, 5.0 – 6.0 M ^{t}BuOOH in nonane, rt, 1 h; NH_4OH, rt, 3 h; (ix) Dowex 88 (H^+), rt, 12 h; 19% overall for **7a**, 17% overall for **7b**; yield not estimated for **7c**.

As will be discussed in 2.7.1, the phosphoramidite strategy could be used to form the pyrophosphate bond between the activated phosphite intermediates and *β*-NMN, to generate the final NAD^+ targets. However, this route still needs further investigations and optimizations.

2.4 Synthetic route to 6-aryl/heteroaryl AMP derivatives

The synthetic strategy to 6-phenyl and 6-(pyrrol-2-yl) AMP derivatives, respectively **8a** and **8b**, started with the Suzuki-Miyaura cross-coupling on the commercially available 6-chloro purine nucleoside (**5**), that could be otherwise readily synthesized from inosine (**2**) by treatment with $POCl_3$ and *N*,*N*-diethylaniline.[140] To avoid the difficult phosphorylation step on unprotected nucleosides, the 6-substituted purine nucleosides (**5a-b**) were protected on the 2′, 3′-OH by *O*-isopropylidene protecting group (**5c-d**). Then, these intermediates were phosphorylated on the 5′-OH *via* phosphoramidite intermediates (**5e-f**) or by $POCl_3$ to afford **5g-h**, then finally deprotected to obtain the 6-substituted AMP derivatives (**8a-b**) (Scheme 2.10).

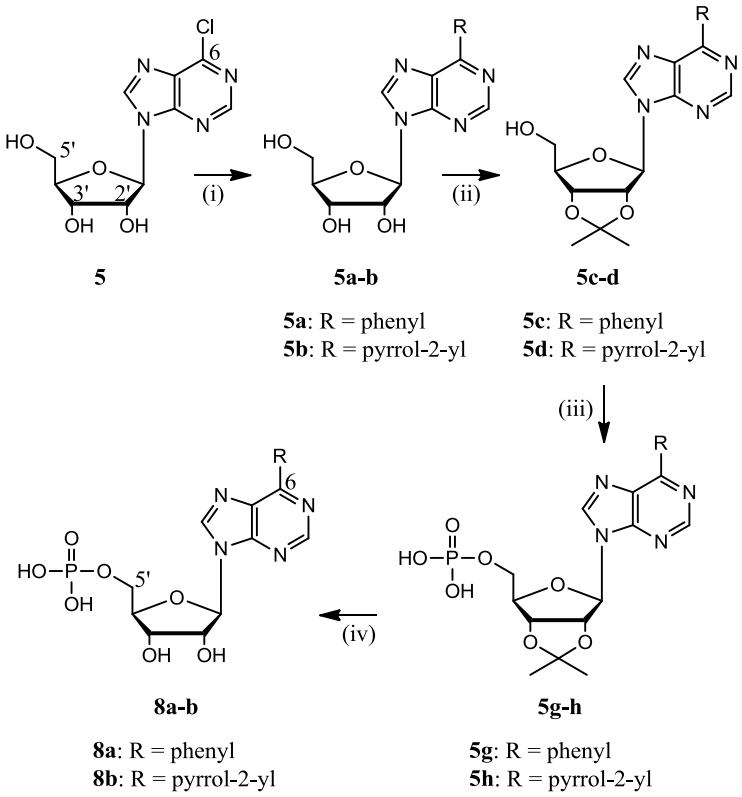

Scheme 2.10 Synthetic route to 6-aryl/heteroaryl AMP derivatives. (i) Suzuki-Miyaura cross-coupling; (ii) 2′,3′-*O*-isopropylidene protection; (iii) phosphorylation of 5′-OH; (iv) deprotection of 2′,3′-OH.

2.4.1 Suzuki-Miyaura cross-coupling on C-6 of 6-chloro purine nucleoside

The Suzuki-Miyaura cross-coupling on C-6 of purine nucleosides is well described in the literature and remarkable improvements have been achieved in the optimization of its conditions. The first examples of substitutions on C-6 concerned the cross-coupling of simple substituted aryl groups on the protected purine nucleosides.[147] Since the unprotected compounds showed cytostatic activities, the scientific interest toward these substitutions enhanced. Later, the attention was focused on the introduction of heteroaryl groups that exhibited, in addition to the cytostatic activities, strong anti-HCV (Hepatitis C Virus) activities.[148] Hence, a large number of heteroaryl substituents have been introduced on the fully protected purine nucleosides using different methods, such as the Suzuki-Miyaura cross-coupling, the heterocyclization by 1,3-dipolar cycloadditions, or the palladium-mediated Negishi cross-coupling, involving organozinc reagents.[148, 149] More recently, Suzuki-Miyaura cross-couplings on the unprotected 6-chloro purine nucleoside (**5**) have been successfully carried out in the aqueous phase for

the introduction of some heteroaryl or unprotected phenylalanine substituents.[149, 150] However, no references have been found for the Suzuki-Miyaura cross-coupling on the unprotected 6-chloro purine nucleoside (**5**) in an aqueous phase with *N*-Boc-2-pyrrole boronic acid.

In this project, the aqueous cross-coupling conditions described in the literature for the synthesis of unprotected 8-substituted adenosine and guanosine, requiring Na_2PdCl_4, TPPTS and K_2CO_3 as catalytic system,[144, 151, 152] were applied to the synthesis of the 6-phenyl (**5a**) and 6-(pyrrol-2-yl) (**5b**) purine nucleosides, affording the desired products in 50% and 37% yield respectively (Scheme 2.11). Interestingly, during the synthesis of **5b**, the *Boc*-deprotection of the pyrrolyl substituent occurred directly under the basic cross-coupling conditions.[153, 154]

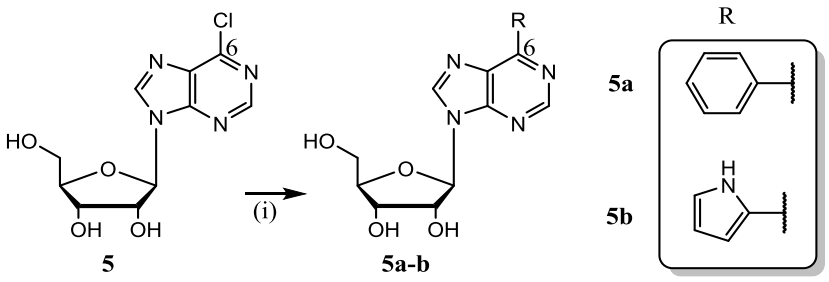

Scheme 2.11 Suzuki-Miyaura cross-coupling on C-6 of 6-chloro purine nucleoside, **5**. Phenyl or *N*-Boc-2-pyrrole boronic acid, Na_2PdCl_4, TPPTS, K_2CO_3 in water, 100 °C, 1 h (**5a**), 24 h (**5b**); 50% for **5a**, 37% for **5b**.

Substantial differences in polarity between the phenyl (**5a**) and the pyrrolyl (**5b**) substituted purine nucleosides were noticed during their purifications. Indeed, **5a** was isolated and purified from the reaction mixture by extraction in organic phase and following recrystallization from water. By contrast, **5b** was soluble in water and needed to be purified by ion-pair chromatography. Moreover, the reaction mixture from the cross-coupling with the *N*-Boc-2-pyrrole boronic acid was quite complex, and only a very slow gradient during the ion-pair purification allowed the separation between a multitude of different peaks. These were not isolated and analysed, but some of them could potentially be attributed to the dimer of the pyrrole,[142] or to the *N*-arylated

product, formed by coupling of the nitrogen of the pyrrole with the chlorine of the 6-chloro purine nucleoside.[149]

2.4.2 2′,3′-*O*-isopropylidene protection and phosphorylation of 5′-OH of 6-substituted purine nucleosides, with subsequent deprotection to 6-aryl/heteroaryl AMP derivatives

The 2′,3′-*O*-isopropylidene protection of 6-substituted purine nucleosides (**5a-b**) was carried out with the same conditions described in 2.3.1, affording **5c-d** with 85% and 39% yield respectively. Afterwards, the phosphorylation of 5′-OH of 2′,3′-*O*-isopropylidene-6-substituted purine nucleosides (**5c-d**) was performed by $POCl_3$ (method 1) and *via* the phosphoramidite (method 2), as previously described in 2.3.3 (Scheme 2.12).

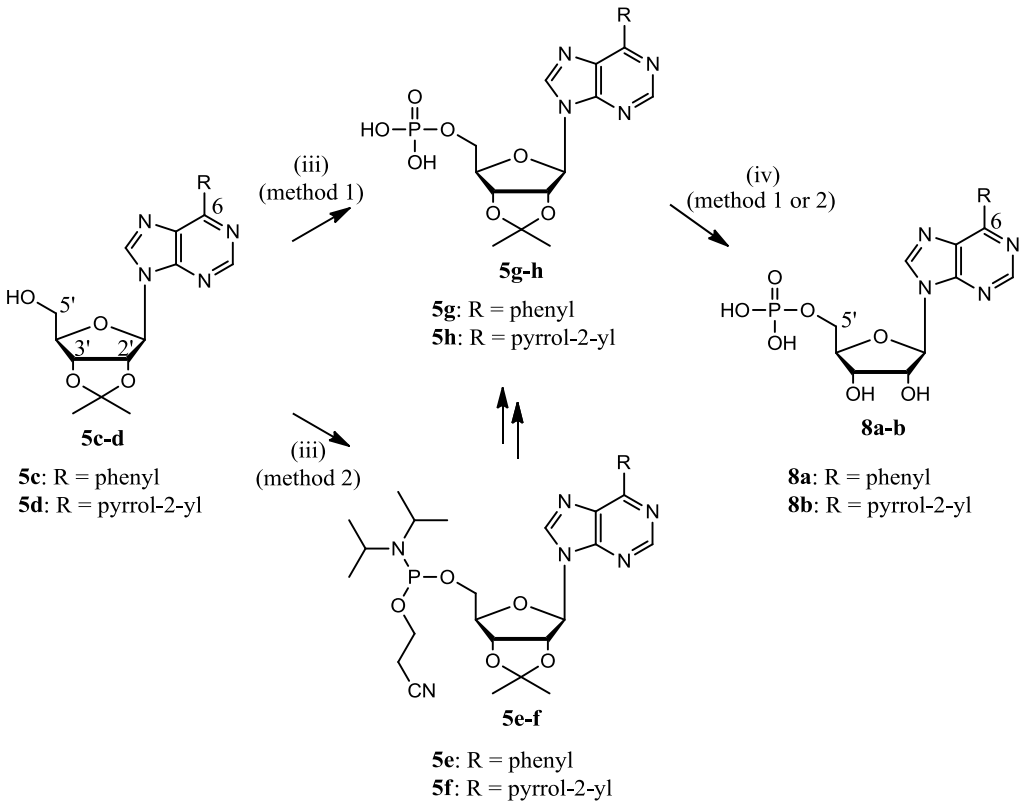

Scheme 2.12 Phosphorylation of 5′-OH and following deprotection of 2′,3′-*O*-isopropylidene-6-substituted purine nucleosides. (iii) Method 1 by $POCl_3$: $POCl_3$, anhydrous acetonitrile, 0 °C, 12 h. (iii) Method 2 *via* phosphoramidite: 2-cyanoethyl *N*,*N*-diisopropylchlorophosphoramidite, DIPEA, anhydrous CH_2Cl_2, rt, 1 h; then, 5.0 – 6.0 M ^tBuOOH in nonane, rt, 1 h; NH_4OH, rt, 3 h. (iv) (Method 1): Dowex 88 (H^+), rt, 12 h, 30% for **8a**. (iv) (Method 2): AcOH/H_2O (1:9), 90 °C, 3 h, complete conversion for **8b**; 28% for **8a** and 50% for **8b** overall *via* phosphorylation method 1; 7% for **8a** overall *via* phosphorylation method 2.

The phosphoramidite method, selected for the phosphorylation of 2′,3′-*O*-isopropylidene-2-substituted adenosines, allowed the phosphorylation of the 2′,3′-*O*-isopropylidene-6-phenyl purine nucleoside (**5c**), affording the desired product **8a** with 7% yield overall. By contrast, when the same phosphorylation method was applied to the 2′,3′-*O*-isopropylidene-6-(pyrrol-2-yl) purine nucleoside (**5d**), no product was recovered after the different deprotection steps. In particular, the final treatment with Dowex 88 (H^+) to remove the *O*-isopropylidene protecting group on the ribose seemed to be responsible for the loss of the material. Indeed, **5h**, especially if present in small amounts, could have remained attached to resin; hence, the use of a weak acid cation exchange resin could have allowed an easier and more efficient recovery of the material.

Owing to the poor yields obtained for the phosphorylation *via* phosphoramidite (method 2), the method with $POCl_3$ (method 1) was reconsidered and slightly modified to allow, in case of failure, the recovery of the starting materials. Therefore, the reactions were performed in anhydrous acetonitrile without the additional proton sponge to simplify the purification step. Under these conditions, a partial deprotection of the *O*-isopropylidene protecting group occurred because of the acidic pH developed during the reaction course. Then, the complete *O*-isopropylidene deprotection of **5g** was carried out by the usual treatment with Dowex 88 (H^+). However, a new deprotection method was used for **5h**, requiring its treatment with an acetic acid solution at 90 °C for 3 h, yielding a complete deprotection. Compounds **8a**-**b** were obtained in 28% and 50% yield overall respectively (Scheme 2.12).

2.5 Synthetic route to 8-aryl/heteroaryl AMP derivatives

The synthetic strategy to 8-aryl/heteroaryl AMP derivatives started with the bromination of adenosine (**3**) or adenosine monophosphate (**3a**) in position 8 of the adenine ring; this reaction is selective for C-8, as this position is very reactive to S_EAr, as mentioned in 2.3.1.[155, 156]

The subsequent Suzuki-Miyaura cross-coupling in position 8 is very well documented in the literature and a large variety of aryl/heteroaryl groups have been introduced in this position. The development of hydrophilic ligands and palladium sources has

allowed its performance in aqueous phase with unprotected nucleosides/nucleotides, avoiding time-consuming protection and deprotection steps.[144, 150-152, 157-159]

Two routes can be followed to obtain the final 8-aryl/heteroaryl AMP derivatives (**9**) (Scheme 2.13). The longest route starts from adenosine (**3**), *via* its bromination in position 8 to give **6**. The latter can alternatively undergo the phosphorylation of 5′-OH by $POCl_3$ to obtain **9a**, or the Suzuki-Miyaura cross-couplings to obtain the 8-aryl/heteroaryl adenosine derivatives. These intermediates can be further phosphorylated on 5′-OH to give the final 8-aryl/heteroaryl AMP derivatives (**9**). The shortest route starts from adenosine monophosphate (**3a**), *via* its bromination in position 8 to give **9a**. The latter can directly undergo the Suzuki-Miyaura cross-coupling to give the final 8-aryl/heteroaryl AMP derivatives (**9**). In this project, the choice to follow the shortest synthetic route led in a short period of time to the synthesis of a small library of 8-aryl/heteroaryl AMP derivatives (**9b-n**).

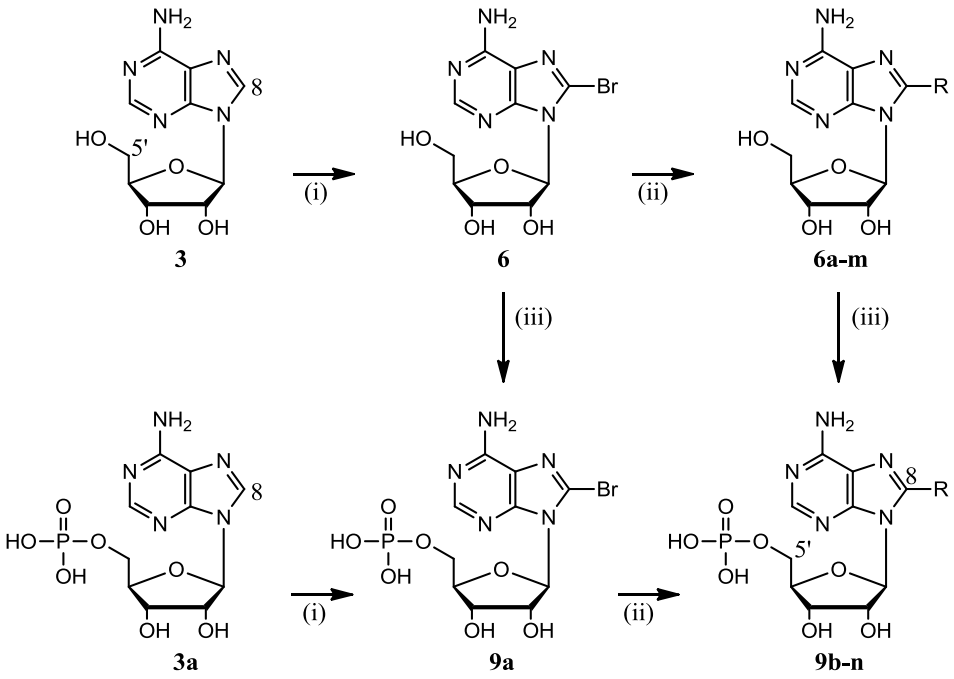

Scheme 2.13 Synthetic route to 8-aryl/heteroaryl AMP derivatives. (i) Bromination on C-8; (ii) Suzuki-Miyaura cross-coupling; (iii) phosphorylation of 5′-OH (R is an aryl/heteroaryl group).

2.5.1 Bromination of C-8 of adenosine and adenosine monophosphate

The bromination on C-8 of adenosine (**3**) has been performed by adding saturated bromine water to the adenosine solution in sodium acetate buffer (pH 4). The buffered conditions are fundamental to avoid the pH dropping down dramatically because of the release of HBr from the reaction, with consequent depurination. Under these conditions, the product **6** crashed out from the reaction mixture as a solid in 80% yield.[155, 156]

The bromination on C-8 of adenosine monophosphate (**3a**) described in the literature requires the same conditions as for the bromination of adenosine,[155, 156] starting from its sodium salt. Slight modifications were performed in this study to simplify this procedure, using neat bromine instead of saturated bromine water. Since the formation of side-products was observed during the reaction in sodium acetate buffer, the solvent was substituted with a 0.25 M KH_2PO_4 solution (pH 4). An almost complete conversion of **3a** to **9a** was obtained with 50-60% yield after ion-pair chromatography purification (Scheme 2.14).

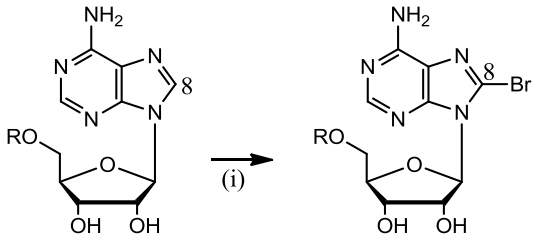

3: R = H
3a: R = P_i

6: R = H (method 1)
9a: R = P_i (method 2)

Scheme 2.14 Bromination on C-8 of adenosine, **3**, and AMP, **3a**. Method 1: **3**, saturated bromine water, 1 M NaOAc buffer (pH 4), rt, 24 h, 80%. Method 2: **3a**, neat bromine, 0.25 M KH_2PO_4 (pH 4), rt, 24 h, 50-60%.

2.5.2 Suzuki-Miyaura cross-coupling on C-8 of 8-bromo adenosine monophosphate to 8-aryl/heteroaryl AMP derivatives

The Suzuki-Miyaura cross-coupling on C-8 of purine nucleosides/nucleotides has been investigated in detail and successful conditions are well established in the literature, using Na_2PdCl_4, TPPTS and K_2CO_3 in water as the optimal catalytic system.[144, 150-152, 157-160]

This project was aimed in particular at the challenging synthesis of *N*-heteroaryl or amino-aryl substituted AMP derivatives. Indeed, the cross-coupling reactions with free amino moieties are generally complicated by the inhibition of the catalytic center by *N*-coordination, or polymerization, in addition to the low reactivity of electron-deficient *N*-heteroaryl boronic acids.[142, 143, 161, 162] Therefore, an accurate optimization of the reaction conditions was required to successfully afford the desired products.

A small library of 8-aryl/heteroaryl AMP derivatives (**9b**-**n**) (Table 2.1, Scheme 2.15) was generated and their conformational and spectroscopic properties investigated in Chapter 3. A range of aryl, electron-poor and electron-rich substituents was introduced in position 8 of the adenine ring. The Suzuki-Miyaura cross-coupling conditions were optimized to obtain decent yields even for the most difficult substitutions with electron-deficient *N*-heteroaryl groups.

cmpd	*R (substituent on C-8)*	*Yield (%)*[a]
9b	Phenyl	80-90
9c	3-(*N*-Boc-aminomethyl)phenyl	78
9d	3-(Aminomethyl)phenyl	85
9e	Pyridin-3-yl	70
9f	Pyridin-4-yl	80
9g	2,4-*DMT*-pyrimidin-5-yl	75
9h	Pyrrol-2-yl	57
9i	Furan-2-yl	67
9j	1*H*-Pyrazol-4-yl	57
9k	5-Formyl-thien-2-yl	52
9l	5-Bromo-thien-2-yl	17
9m	Indol-2-yl	83
9n	Benzofuran-2-yl	10

[a]Yield of isolated products

Table 2.1 Synthesis of the 8-aryl/heteroaryl AMP derivatives (**9b**-**n**).

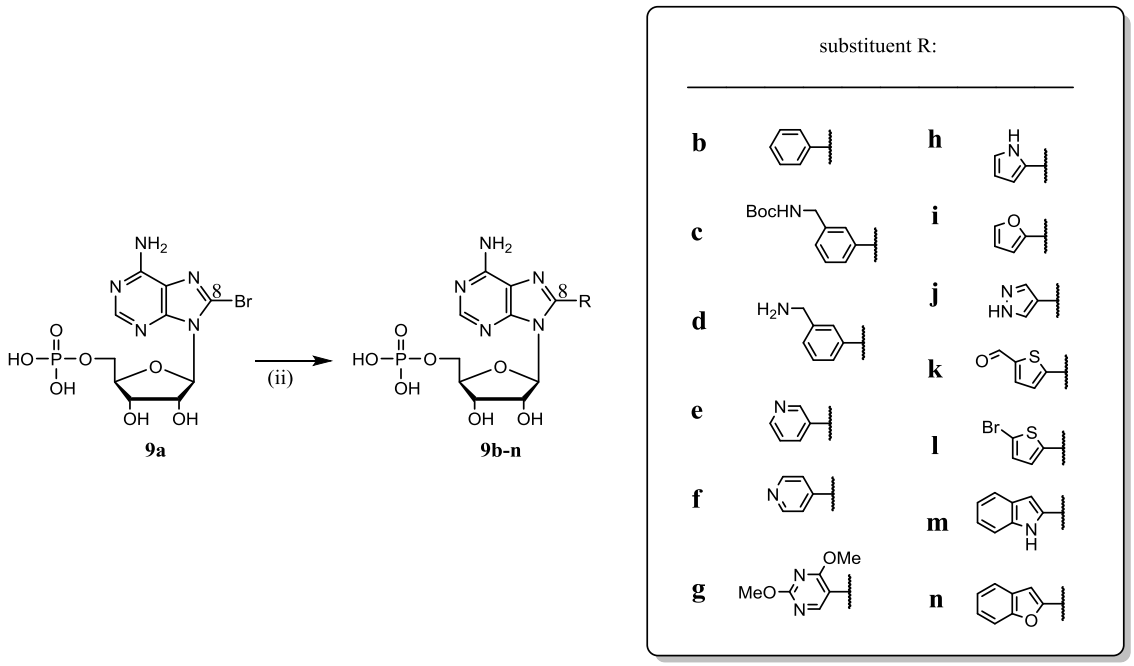

Scheme 2.15 Suzuki-Miyaura cross-coupling on C-8 of 8-bromo AMP, **9a**. (ii) Aryl/heteroaryl boronic acid, Na_2PdCl_4, TPPTS, K_2CO_3 in water, Δ, 1 – 24 h, 10-90%.

Generally, the Suzuki-Miyaura cross-couplings with simple aryl boronic acids can be performed at low temperature using small amounts of base and palladium/ligand catalyst. For example, **9b** and **9c** could be synthesized at only 40 °C using the right catalytic system. In contrast, the Suzuki-Miyaura cross-couplings with electron-poor boronic acids generally require stronger reaction conditions, using very high temperature and more equivalents of base and palladium/ligand catalyst to react in the transmetallation step.

In this study, the pyridinyl group was the most electron-poor in the range of selected substituents to introduce on the position 8 of the adenine ring. Due to the electron-poor nature of the pyridine ring, the boron in the 3-pyridinyl boronic acid has a pronounced Lewis acid behavior, which makes it poorly reactive. However, in water the 3-pyridinyl boronic acid is normally present as a zwitterion, with a positive charge on the pyridine basic nitrogen and a negative charge on the boron (Figure 2.2). Therefore, the aqueous conditions increase the reactivity of the boron and block the pyridine basic nitrogen from inhibiting the catalytic palladium centre.[162, 163]

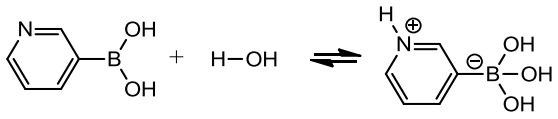

Figure 2.2 Ionization equilibrium of the 3-pyridinyl boronic acid in water.

Due to its poor reactivity, the Suzuki-Miyaura cross-coupling of **9a** with the 3-pyridinyl boronic acid to obtain **9e**, required high temperature (100 °C) and a Pd/ligand ratio 1:3. A screening of base equivalents, ranging from 1.5 to 10, showed a slow conversion with 1.5 equiv., fast with 3 and 5, but no conversion with 10 equiv. of base. The application of micellar-catalyzed Suzuki-Miyaura cross-coupling was considered to perform the reaction at lower temperature in water and in absence of co-solvent. Indeed, the formation of micelles should improve the solubility of the boronic acid in water accelerating the reaction.[164-166] In particular, the use of surfactants, such as PTS (polyoxyethanyl α-tocopheryl sebacate, a nonionic amphiphile) and TBAF, was investigated, performing parallel reactions between **9a** and the 3-pyridinyl boronic acid at 40 °C for 2 days to obtain **9e**. While the reactions did not work with the standard amounts of Pd catalyst (2 – 2.5 mol%), adding more (10 mol%), a conversion was observed, higher in the reactions performed with PTS (> 60%) than those with TBAF (≤ 40%).

Several interesting observations were made during the synthesis of **9c** and **9d**. When the Suzuki-Miyaura cross-coupling was performed with the 3-(*N*-Boc-aminomethyl)phenyl boronic acid at 80 °C in 1 h, no *Boc*-deprotection occurred in the basic reaction conditions. By contrast, when the same reaction was performed at 40 °C over two days, an almost complete deprotection occurred, affording **9d**. To obtain the unprotected **9d**, two different synthetic routes were used (Scheme 2.16). In the first istance, the deprotection of the cross-coupled **9c** was carried out by refluxing with TFA in methanol until the disappearance of the starting material was observed. In the second route, the deprotection of the 3-(*N*-Boc-aminomethyl)phenyl boronic acid with TFA in CH_2Cl_2 at room temperature was performed to use the unprotected boronic acid in the subsequent Suzuki-Miyaura cross-coupling with **9a** to afford **9d**.

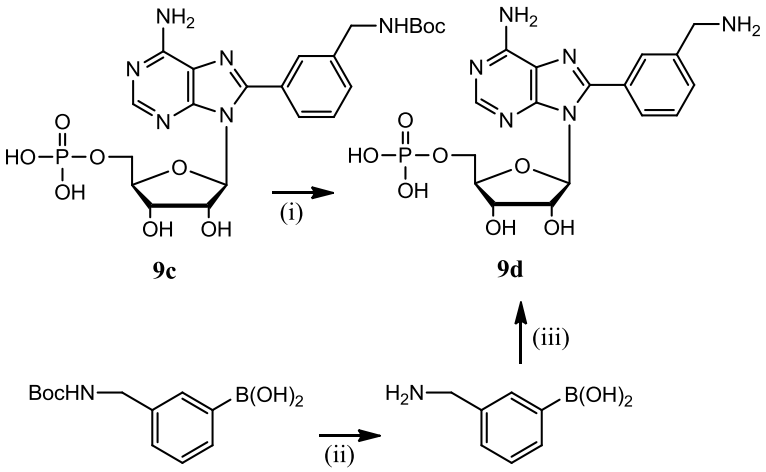

Scheme 2.16 Synthesis of **9d**. (i) TFA, MeOH, reflux; (ii) TFA, CH_2Cl_2, rt, 1 h, quantitative yield; (iii) Suzuki-Miyaura cross-coupling: **9a**, Na_2PdCl_4, TPPTS, K_2CO_3 in water, 80 °C, 2 h.

With the first strategy, after the disappearance of the starting material **9c**, two new spots could be observed by TLC (thin layer chromatography), one very polar and one less polar than the starting **9c**. Probably, a mixture of the differently protonated forms of **9d**, in equilibrium with each other during the TLC run in iPA/H_2O/NH_4OH (6:3:1), was observed. After purification by ion-pair chromatography, **9d** was recovered as a single product corresponding to the most polar spot in TLC.

A titration of the obtained **9d** was performed with NaOH and HCl to investigate its different protonation states. At pH < 1, **9d** should be completely protonated on the phosphate group, the amino group on the substituent and N-1.[167] Increasing the pH, the phosphate would lose the first proton (pK_1 $P_i \approx 0.9$),[167] followed by N-1 (pK_a N-1 ≈ 3.4), the second proton on the phosphate (pK_2 $P_i \approx 6.6$) and, finally, the primary amine on the substituent (pK_a $NH_2 \approx 9.2$) (Figure 2.3). These pK_a values are comparable with those in the literature for the related groups.[167]

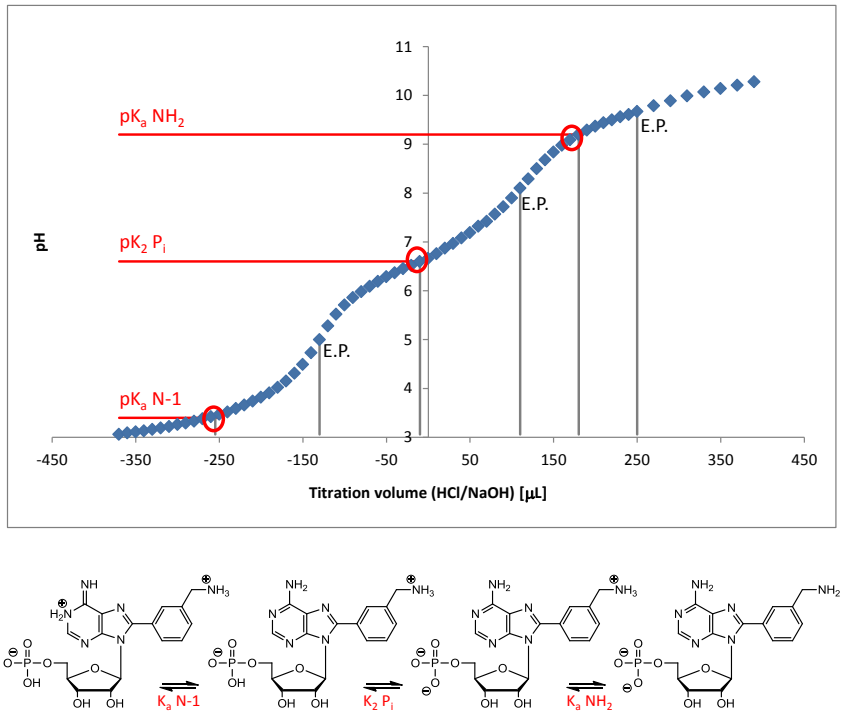

Figure 2.3 Acid-base titration of 3-(aminomethyl)phenyl AMP (**9d**) using a pH meter. To a solution of **9d** in water (pH 6.7), 370 µL of 0.1 N HCl (left) and 390 µL of 0.1 N NaOH (right) were added respectively in portions of 10 µL each. The pH was read and recorded after each addition. The equivalence point (E.P.) volumes were found plotting the first derivative [ΔpH/ΔmL] as a function of the titration volume [µL]: each maximum in the first derivative corresponded to the equivalence point volume. The pK$_a$ values were calculated in correspondence of each half-equivalence point (red circles), where pH = pK$_a$.

When **9d** was synthesized by Suzuki-Miyaura cross-coupling of **9a** with 3-(aminomethyl)phenyl boronic acid (Scheme 2.16), two different new spots could be observed by TLC during the cross-coupling reaction. In this case, it was possible to isolate by ion-pair purification the two corresponding different products, and investigate their nature by ^{1}H NMR and HR-MS. Both techniques confirmed the same identity for both products as **9d**; however, differences in the ^{1}H NMR spectra, in particular in the phenyl and *CH*$_2$NH$_2$ regions, suggested their forms as two possible distinct conformers (Figure 2.4). Examining the *CH*$_2$NH$_2$ peaks, the enantiotopic protons appeared as a singlet in the possible conformer **a**, where the aminomethyl substituent heads far from the phosphate; indeed, in this case these protons would be too similar to be distinguished. By contrast, in the other possible conformer **b**, stabilized by salt formation between the 5′-phosphate on the adenosine and the amino group on the substituent, the enantiotopic protons would have a very different electronic environment and, therefore, appear as a doublet.

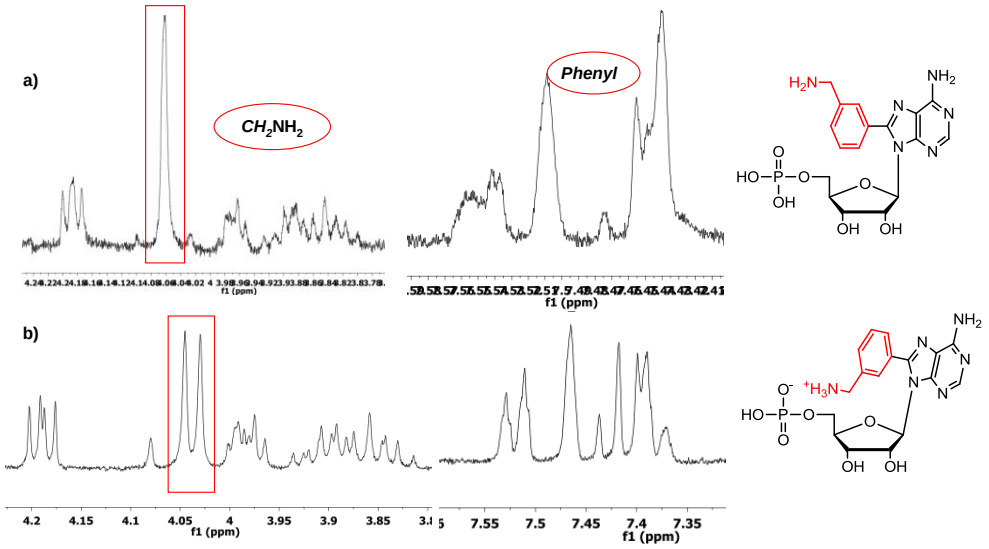

Figure 2.4 ^{1}H NMR spectra of the two isolated conformers, **a** and **b**, for **9d**.

To support this hypothesis, it was observed that **9d(a)** had 1.3 mol TEA as a counter ion, while **9d(b)** had only 0.5 mol TEA because of the involvement of the phosphate group in a salt formation with the amino group of the substituent. Hence, it was suggested that, when **9d** was synthesized by deprotection of **9c**, only the kinetically favoured conformer **9d(a)** was obtained. Indeed, in **9c** the hindered substituent containing the *Boc* group would assume the conformation where it heads far from the phosphate; since the deprotection occurred rapidly, the product **9d** would preferentially remain in the conformation assumed by its precursor. In contrast, when **9d** was synthesized by Suzuki-Miyaura cross-coupling with the unprotected boronic acid, the substituted phenyl ring was able to rotate and to assume both the different positions compared to the phosphate group, leading to the formation of both kinetically and thermodynamically favoured conformers. An useful experiment to prove the existence of the two different conformers would be to increase the temperature during the ^{1}H NMR experiment; indeed, the energy provided would allow the phenyl substituent to rotate freely around its bond with C-8 of the adenine ring, avoiding the stabilization of the two different conformers and giving an average NMR signal for phenyl and CH_2NH_2 peaks.

2.6 Synthesis of aryl/heteroaryl adenine-modified NAD$^+$ derivatives (pathway a)

2.6.1 AMP activation *via* phosphoromorpholidate intermediate

The formation of the pyrophosphate bond between the aryl/heteroaryl adenine-modified AMP derivatives and *β*-NMN to generate the final aryl/heteroaryl adenine-modified NAD$^+$ derivatives, requires the activation of either phosphate group of the reactants. The Khorana-Moffatt procedure, involving the coupling between a nucleotide and a nucleotide phosphoromorpholidate, was chosen in our project to perform the pyrophosphate bond formation. Indeed, the nucleotide phosphoromorpholidate intermediates are reactive enough phosphate derivatives, but also sufficiently stable to be handled and stored.[168, 169]

Because of the fragility of *β*-NMN due to its labile nicotinamide *N*-glycosidic bond, it was chosen to synthesize the phosphoromorpholidate intermediates of the aryl/heteroaryl adenine-modified AMP derivatives, to subsequently couple them with *β*-NMN. The synthesis of the phosphoromorpholidate intermediates was performed by an oxidation-reduction condensation under the Mukaiyama's conditions,[170, 171] which had already been successfully used for the preparation of different pyrophosphate bonds.[112, 151] A complete conversion occurred from all the starting materials and the obtained products were usually precipitated as sodium salts and used in the next step without any further purification (Scheme 2.17).

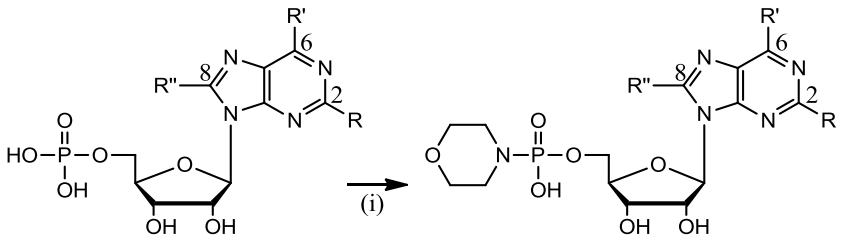

7a-b: R = X, R' = NH_2, R" = H
8a-b: R = H, R' = X, R" = H
9b,**c**,**e**,**g**,**h**: R = H, R' = NH_2, R" = H

10a-b: R = X, R' = NH_2, R" = H
11a-b: R = H, R' = X, R" = H
12b,**c**,**e**,**g**,**h**: R = H, R' = NH_2, R" = H

Scheme 2.17 Synthesis of aryl/heteroaryl adenine-modified AMP-morpholidate derivatives. (i) Morpholine, 2,2′-dithiopyridine, PPh_3, anhydrous DMSO, rt, 1 h, 70-97% (X is an aryl/heteroaryl group, see Scheme 2.18, Table 2.2).

2.6.2 Coupling with β-NMN

Once the aryl/heteroaryl adenine-modified AMP-morpholidate derivatives were synthesized, it was possible to proceed to their coupling with β-NMN to obtain the final aryl/heteroaryl adenine-modified NAD^+ derivatives. As described in the literature,[110] the Khorana-Moffatt coupling for the synthesis of β-NAD^+ needs the presence of Lewis acid additives to make the morpholidates more reactive. Indeed, β-NMN in the reaction conditions (pH 7) is probably an inner salt, with a poorly nucleophilic phosphate and, therefore, unable to efficiently attack the activated phosphoromorpholidates. A $MnCl_2$ solution in formamide has been used for this purpose.[110-112, 172] A fundamental requirement for the success of the reaction is the dryness of the system; indeed, because of its nucleophilicity, the water could hydrolyse the phosphoromorpholidates or the newly formed pyrophosphate bond, decreasing the final yields. Therefore, the $MnCl_2$ solution in formamide needs to be dried over molecular sieves for several days prior its use. Furthermore, anhydrous $MgSO_4$ is added to the reaction mixture to capture any excess water.

The literature conditions report the use of 1.1 equiv. of β-NMN to the morpholidate. However, because of the high value of β-NMN, the use of its excess was reconsidered in our procedure. In contrast, where possible, an excess of morpholidate was used to improve the reaction yields (Scheme 2.18, Table 2.2). The aryl/heteroaryl adenine-modified NAD^+ derivatives, **13a-b**, **14a-b**, **15b**, **c**, **e**, **g**, **h**, were obtained with yields ranging from 24 to 87%. The same variability along the reaction yields was noticed in the literature, where the Khorana-Moffatt coupling gave the NAD^+ derivatives with yields between 30 and 70%.[110-112]

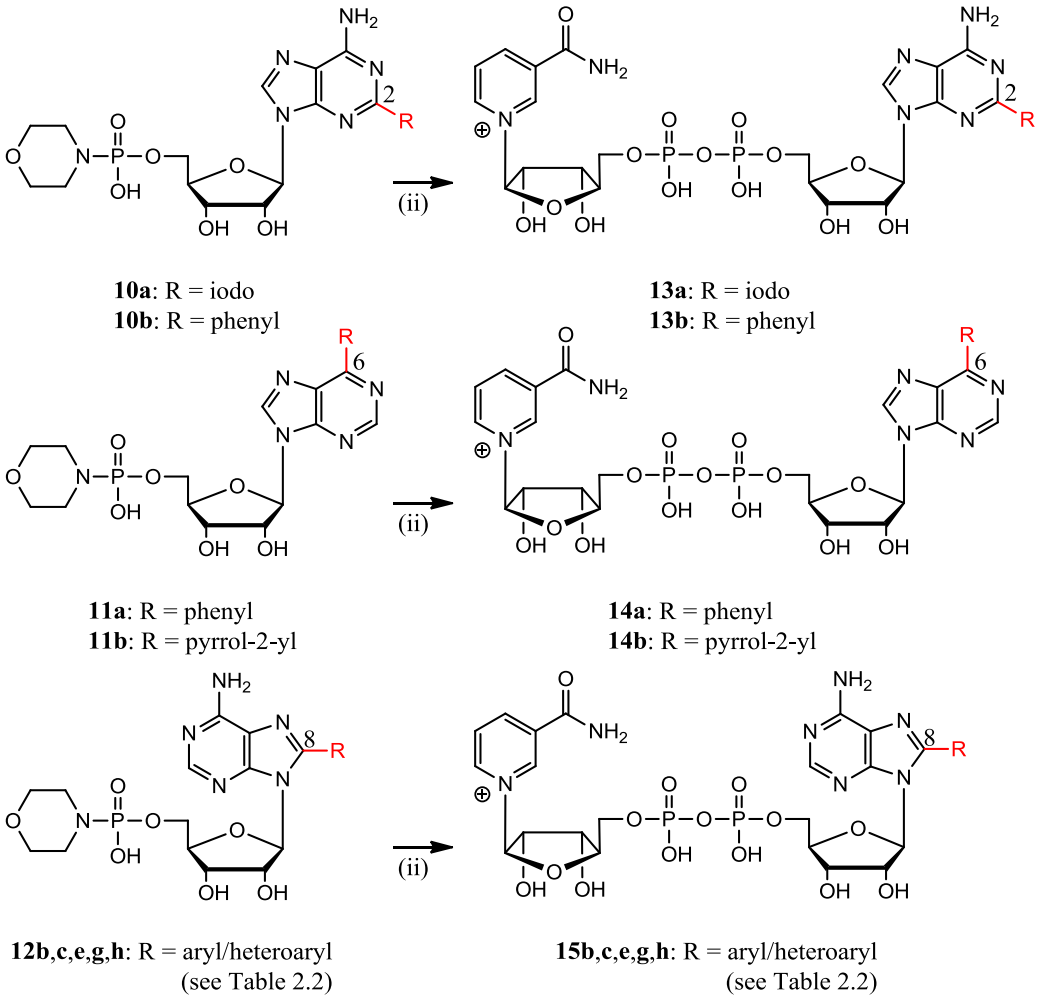

Scheme 2.18 Synthesis of aryl/heteroaryl adenine-modified NAD^+ derivatives. (ii) *β*-NMN, anhydrous $MgSO_4$, 0.2 M $MnCl_2$ in formamide, rt, 12 h, 24-87% (R is an aryl/heteroaryl group, see Table 2.2).

compd	*Position of substitution*	*R (substituent)*	*Yield (%)*[a]
13a	2	Iodo	53
13b	2	Phenyl	28
14a	6	Phenyl	56
14b	6	Pyrrol-2-yl	87
15b	8	Phenyl	41
15c	8	3-(*N*-Boc-aminomethyl)phenyl	61
15e	8	Pyridin-3-yl	24
15g	8	2,4-*DMT*-pyrimidin-5-yl	43
15h	8	Pyrrol-2-yl	30

[a]Yield of isolated products

Table 2.2 Synthesis of the aryl/heteroaryl adenine-modified NAD^+ derivatives **13a-b**, **14a-b**, **15b**,**c**,**e**,**g**,**h**.

β-NAD^+ and its derivatives are relatively fragile compounds and need to be handled extremely carefully to prevent their decomposition. As discussed in 1.1, the nicotinamide *N*-glycosidic bond is sensitive to basic conditions, since the hydroxyde can act as a nucleophile and substitute the nicotinamide ring to give the corresponding ADPR derivative. During the acquisition of ^{31}P NMR spectra, the addition of triethylamine to the samples in D_2O is required to sharpen the peaks and show the coupling constants, $J_{P,P}$, between the two phosphorus of the pyrophosphate bond. Therefore, the acquisition of these spectra is particularly tricky for the NAD^+ derivatives, since the smallest quantity of TEA has to be added to the cold samples to avoid their immediate degradation, detected by a sudden change in the colour of the solution from colourless to orange.

2.7 Alternative synthetic strategies to aryl/heteroaryl adenine-modified NAD^+ derivatives

2.7.1 Aryl/heteroaryl adenine-modified NAD^+ derivatives *via* phosphoramidite method (pathway b)

One of the approaches to shorten the synthesis of the NAD^+ derivatives is the phosphoramidite method. The phosphoramidite chemistry is commonly used for the solid-phase synthesis of oligonucleotides, where a 3′-phosphoramidite nucleoside intermediate reacts with the 5′-OH of a nucleoside to form the 3′,5′-phosphodiester bond. The phosphoramidite intermediate is very reactive, allowing successful couplings with almost quantitative yields, a fundamental requirement for the synthesis of long oligonucleotide sequences.[173-175] In the case of the formation of the pyrophosphate bond in dinucleotides, this method allows the coupling between a phosphoramidite nucleoside intermediate and the phosphate group of a nucleotide.[113]

For the synthesis of aryl/heteroaryl adenine-modified NAD^+ derivatives, the substitution of the adenosine with aryl/heteroaryl groups in the favourite position is followed by the preparation of the corresponding reactive phosphoramidite intermediate, ready to undergo the coupling with β-NMN (Scheme 2.19). Therefore, the phosphorylation and activation of the phosphate occur in a single step and with the purification of a single intermediate compared to the multistep synthesis (pathway a).

In this project, the pathway b was tested starting from the 2′,3′-*O*-isopropylidene-2-phenyl adenosine (**4b**), forming its corresponding phosphoramidite intermediate and attempting its coupling with *β*-NMN under the conditions described in the literature.[113] However, the coupling turned out to be unsuccessful despite the high reactivity of the phosphoramidite intermediate. The reason could be due, as in the Khorana-Moffatt procedure, to the poor nucleophilicity of the phosphate of *β*-NMN in the reaction conditions. In addition, the insolubility of *β*-NMN in the reaction solvent (acetonitrile) could negatively influence the effectiveness of the reaction. The addition of small DMF/DMSO percentages in the reaction media was tried to improve the solubility of *β*-NMN; however, the reaction did not proceed. Further investigations and optimizations studies should be performed to exploit the potential of this synthetic pathway.

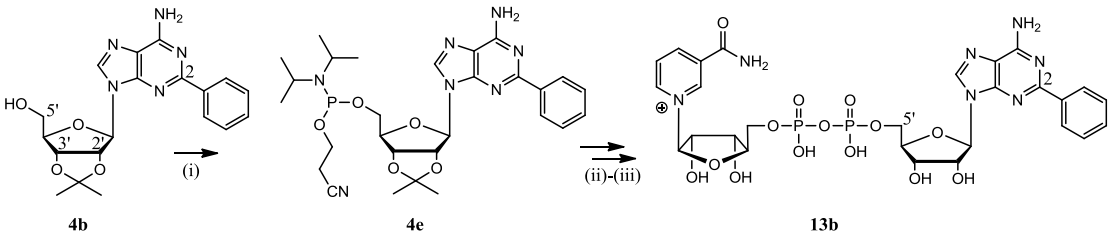

Scheme 2.19 Synthesis of **13b** *via* phosphoramidite method (pathway b). (i) Phosphoramidite synthesis: 2-cyanoethyl *N*,*N*-diisopropylchlorophosphoramidite, DIPEA, anhydrous CH_2Cl_2, rt, 1 h; (ii) coupling with *β*-NMN: *β*-NMN, DCI, anhydrous acetonitrile, rt, 1 – 2 h; then, 5.0 – 6.0 M ^{t}BuOOH in nonane, rt, 1 h; NH_4OH, rt, 3 h; (iii) 2′,3′-*O*-isopropylidene deprotection: Dowex 88 (H^+), rt, 12 h.

2.7.2 Aryl/heteroaryl adenine-modified NAD^+ derivatives *via* one-pot, two-step procedure (pathway c)

β-NAD^+ is a very sensitive molecule, difficult to handle and to work with because of the labile bonds present in its structure. Its derivatives are rarely synthesized directly from the natural *β*-NAD^+ because of its easy degradation even under mild reaction conditions. For this reason, the most common pathway to synthesize NAD^+ derivatives is the multistep synthesis (pathway a, Scheme 2.1).

The direct introduction of aryl/heteroaryl substituents on the *β*-NAD^+ scaffold by Suzuki-Miyaura cross-coupling has been an open challenge, since *β*-NAD^+ is susceptible to the required basic reaction conditions. The first step for the substitution of

the adenine ring of β-NAD^+ by Suzuki-Miyaura cross-coupling is its halogenation in the favoured position. References for the halogenation of β-NAD^+ have been found in the literature,[107, 108] using neat bromine to brominate the reactive C-8 of the adenine ring at room temperature in 30 min. Unfortunately, the halogenation of the adenine ring in other positions is not as straightforward as that on C-8 and, therefore, this pathway can exclusively be applied to the synthesis of 8-aryl/heteroaryl NAD^+ derivatives.

The subsequent Suzuki-Miyaura cross-coupling on C-8 requires an accurate optimization of every reaction parameters, such as the catalyst, the amount of base, the temperature and the reaction time, to guarantee the occurrence of the cross-coupling before the beginning of the degradation of the starting material at basic pH.[70] As already shown in the Wagner group, the combination of Na_2PdCl_4 with the electron-rich phosphine, TXPTS, allowed fast Suzuki-Miyaura cross-couplings at 40 °C on 8-bromo NAD^+, using aryl/heteroaryl, electron-rich and electron-poor substituents (Scheme 2.20).[70]

To further shorten this synthesis, a one-pot, two-step procedure was set up, where, immediately after the bromination, the aqueous solution was extracted with $CHCl_3$ to remove the bromine excess, and the residue evaporated to dryness. The crude material was directly used in the Suzuki-Miyaura cross-coupling, adding more equivalents of base to bring the pH 4 to the optimum pH 9. The yields obtained with this method were comparable to those obtained with the multistep synthesis.[70]

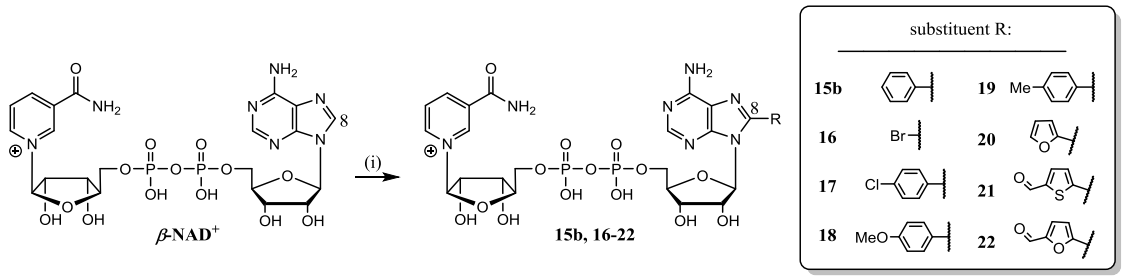

Scheme 2.20 Synthesis of 8-aryl/heteroaryl adenine-modified NAD^+ derivatives *via* one-pot, two-step procedure (pathway c). (i) Bromination: neat bromine, 1 M NaOAc buffer (pH 4), rt, 30 min; then, Suzuki-Miyaura cross-coupling: aryl/heteroaryl boronic acid, Na_2PdCl_4, TXPTS, K_2CO_3 in water, 40 °C, 20 – 30 min, 36-64% (experimental procedures in reference 70).

Although this method works for a large range of boronic acids, including aryl/heteroaryl and electron-rich/electron-poor ones, the Suzuki-Miyaura cross-couplings with pyridinyl and pyrrolyl boronic acids required a too basic pH and high temperature to be applied to the β-NAD^+ without any decomposition. The use of surfactants, discussed in 2.5.2, to perform the couplings with electron-poor boronic acids at low temperature was attempted during the one-pot, two-step procedure with β-NAD^+ without any positive result. Therefore, for certain classes of boronic acids, this pathway still remains unsuccessful and needs further investigations.

2.8 Conclusions

Owing to the importance of β-NAD^+ as a substrate for many different enzymes involved in major biological processes, the interest toward the synthesis of NAD^+ derivatives as biochemical tools has become more and more relevant, making necessary the development of efficient, rapid and robust synthetic routes.

After the optimization of the already known multistep synthesis (pathway a), which allows us to synthesize any NAD^+ derivatives starting from the nucleoside precursors, new routes were explored to improve and shorten the synthesis of NAD^+ derivatives. The phosphoramidite strategy (pathway b) failed but, because of its attractive potential in remarkably shortening the synthesis, still deserves further investigations. The one-pot, two-step synthesis (pathway c), although useful exclusively for the synthesis of 8-aryl/heteroaryl NAD^+ derivatives, has successfully allowed the synthesis of several NAD^+ derivatives in a very short time.

Therefore, a small library of NAD^+ derivatives substituted on C-2, C-6 or C-8 of the adenine ring with aryl/heteroaryl groups was generated, to be tested on different NAD^+-consuming enzymes as inhibitors for drug discovery or NNSs as biochemical tools.

3 CONFORMATIONAL AND SPECTROSCOPIC ANALYSIS OF ARYL/HETEROARYL ADENINE-MODIFIED AMP AND NAD+ DERIVATIVES

The NAD^+ derivatives synthesized in Chapter 2 were designed for their biological application as inhibitors and/or NNSs toward NAD^+-consuming enzymes. To perform their functions, the compounds have to interact with the enzymes and their active sites, consequently requiring particular conformations that are adaptable to the enzyme recognition. A certain degree of flexibility in the molecule is required for enzyme recognition. In particular, in the case of nucleosides/nucleotides, a fundamental feature is the orientation of the nucleobase in relation to the ribose. Of course, the presence of additional groups on the adenine-modified NAD^+ derivatives, able to change the natural nucleobase orientation and the normal H-bonding or hydrophobic interactions of the natural β-NAD^+ within the enzyme active sites, influences the recognition and its strength, and it is responsible for the compounds activity as inhibitors and/or NNSs.

In view of the potential activity of aryl/heteroaryl adenine-modified NAD^+ derivatives as NNSs for NAD^+-consuming enzymes, their spectroscopic features could lead to their application as biochemical probes for the development of sensitive assays based on spectroscopic techniques, such as UV/Vis absorption or fluorescence emission spectroscopies. For example, it is known, as will be discussed in 3.3.2, that adenine rings, substituted in position 8 with aryl/heteroaryl groups, belong to the class of emissive nucleobases.

Therefore, this chapter will first describe the conformational properties of the natural AMP and β-NAD^+, and their derivatives synthesized in Chapter 2, to help later correlate structures with the bio-activities observed. Then, their spectroscopic features will be described to explore the suitability of aryl/heteroaryl NAD^+ derivatives as biochemical probes for NAD^+-consuming enzymes.

3.1 Conformational analysis of nucleosides and nucleotides

Nucleosides and nucleotides are characterized by free or restricted rotation around several bonds, which allows them to assume different conformations in solution. The topology of a nucleoside in solution is determined by interdependent conformational equilibria involving the most flexible bonds in the structure. The nucleobase is oriented perpendicularly to the plane of the ribose ring and can mainly assume two different conformations, *syn* and *anti*, by rotation around the *N*-glycosidic bond. The torsion angle around this bond, χ, determines which conformation is favoured (Figure 3.1).[176]

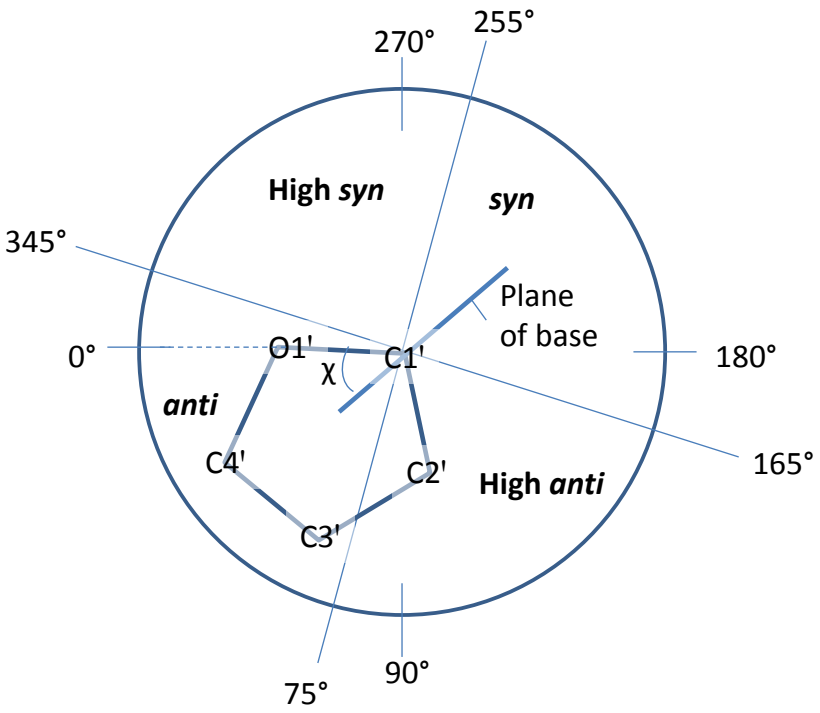

Figure 3.1 Glycosidic conformational ranges of nucleosides and nucleotides.

The rotation around the *N*-glycosidic bond is not free, due to the steric hindrance between the nucleobase and the ribose. For this reason, the *anti* conformation, in which the nucleobase is pointing away from the ribose, is generally favoured by nucleosides/nucleotides compared to the *syn* conformation, which has a higher energy (Figure 3.2).

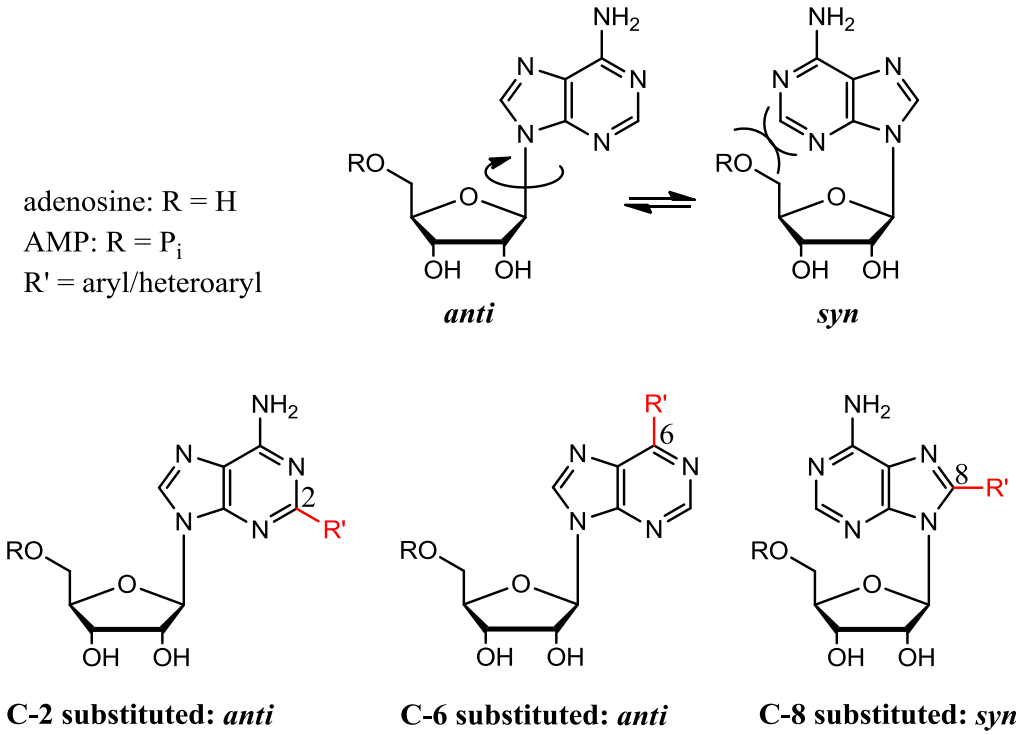

Figure 3.2 Adenine conformations in the natural adenosine/AMP and the aryl/heteroaryl adenine-modified adenosine/AMP derivatives.

The *syn*/*anti* equilibrium largely influences the ribose conformation: indeed, the ribose can pucker its structure, assuming the North (N, or C3′-*endo*) or South (S, or C2′-*endo*) conformation (Figure 3.3), in equilibrium to each other. The general ratio between N and S conformations for *β*-D-ribonucleosides is 1:1, but because the N-conformation is more hindered than the S-conformation, nucleosides/nucleotides with the nucleobase in the *syn* orientation will prefer the S to the N conformation.[167, 177]

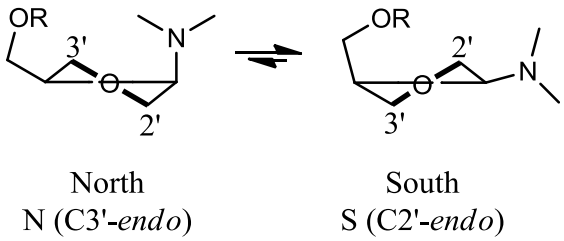

Figure 3.3 Ribose conformations of nucleosides (R = H) and nucleotides (R = P_i).

3.1.1 Conformation of aryl/heteroaryl adenine-modified AMP derivatives

A conformational analysis was performed on the various substituted AMP derivatives synthesized in Chapter 2 (Table 3.1). The natural AMP exists predominantly with the adenine in *anti* conformation, while the less hindered S-conformation is slightly favoured by the ribose.[178] To determine the preference of the adenine between *syn* and *anti* conformation in the AMP derivatives, it is possible to observe the difference in chemical shift of H-2′ between the natural AMP and the different derivatives (ΔH-2′). In particular, a downfield shift for H-2′ compared to its chemical shift in AMP indicates a deshielding due to the adenine assuming a *syn* conformation and, consequently, the ribose favouring an S-conformation. The coupling constant, $J_{1',2'}$, is related to the percentage of the ribose population in S conformation.[179, 180]

cmpd	*Position of substitution*	*R (substituent)*	*S-type conformer (%) ($10J_{1',2'}$)*	*H-2′ (ppm)*	*ΔH-2′ (ppm)*[a]	*syn/anti*
AMP		H	52	4.75	–	*anti*
7a	2	Iodo	57	4.72	-0.03	*anti*
7b	2	Phenyl	49	4.68	-0.07	*anti*
8a	6	Phenyl	53	4.68	-0.07	*anti*
8b	6	Pyrrol-2-yl	55	4.75	0	*anti*
9a	8	Bromo	60	5.19	0.44	*syn*
9b	8	Phenyl	62	5.21	0.46	*syn*
9c	8	3-(*N*-Boc-aminomethyl)phenyl[b]	58	5.51	–	*syn*
9d	8	3-(Aminomethyl)phenyl	62 **a)**; 64 **b)**	5.17	0.42	*syn*
9e	8	Pyridin-3-y	–	5.22	0.47	*syn*
9f	8	Pyridin-4-yl	51	5.27	0.52	*syn*
9g	8	2,4-*DMT*-pyrimidin-5-yl	62	5.19	0.44	*syn*
9h	8	Pyrrol-2-yl	62	5.19	0.44	*syn*
9i	8	Furan-2-yl	57	5.31	0.56	*syn*
9j	8	1*H*-Pyrazol-4-yl	62	5.25	0.50	*syn*
9k	8	5-Formyl-thien-2-yl	–	5.30	0.55	*syn*
9l	8	5-Bromo-thien-2-yl	61	5.42	0.67	*syn*
9m	8	Indol-2-yl	57	5.42	0.67	*syn*
9n	8	Benzofuran-2-yl	53	5.39	0.64	*syn*

[a] ΔH-2′ has been calculated as the difference between the chemical shift of H-2′ of the aryl/heteroaryl adenine-modified AMP derivatives and H-2′ of AMP (4.75 ppm) in D_2O (referenced for D_2O, $\delta = 4.79$ ppm). [b] ^1H NMR spectrum for **9c** recorded in CD_3OD.

Table 3.1 Conformational analysis of the various aryl/heteroaryl adenine-modified AMP derivatives synthesized in this study.

As shown in Table 3.1, a clear trend amongst the various substituted AMP derivatives could be observed. In particular, AMP derivatives substituted on C-2 and C-6 adopted a favoured *anti* conformation and an S-type conformer percentage ≥ 50. In contrast, AMP derivatives substituted on C-8 preferred a *syn* conformation with an S-type conformer percentage > 50. Looking at the molecular structures of the several AMP derivatives (Figure 3.2), these were the expected behaviours. Indeed, AMP derivatives substituted on C-2 were very hindered on the pyrimidine ring and, therefore, they could not afford a *syn* conformation which would bring a huge steric hindrance with the ribose. Regarding the AMP derivatives substituted on C-6, that have the substituent heading in the opposite direction compared to the ribose, they could assume the same *anti* conformation as the natural AMP. Finally, AMP derivatives substituted on C-8 preferred to place the substituents far from the ribose, assuming therefore a *syn* conformation, in which the pyrimidine ring steric hindrance was less strong than that deriving from the substituents.

3.1.2 Conformation of aryl/heteroaryl adenine-modified NAD^+ derivatives

The conformations of the NAD^+ derivatives followed approximatively the same trend described for the corresponding AMP derivatives. Therefore, the NAD^+ derivatives substituted on C-2 had the adenine in *anti* conformation, slightly turning into *syn* conformation compared to the favoured *anti* conformation in the AMP derivatives. The NAD^+ derivatives substituted on C-8 generally preferred the adenine in *syn* conformation and the ribose in S (Table 3.2).[70] Slight differences of S-type conformer percentage and ΔH-2′ in the NAD^+ derivatives compared to the AMP derivatives, were due to a different arrangement of the riboses and the adenine ring within the β-NAD^+ structure. Indeed, β-NAD^+ is a very flexible molecule because of a variety of rotatable bonds and many different functional groups, which are able to interact in several ways with each other, with the solvent and/or with the amino acids of the enzymatic pockets where β-NAD^+ is the substrate.

cmpd	*Position of substitution*	*R (substituent)*	*S-type conformer (%) ($10J_{1',2'}$)*	*H-2′ (ppm)*	*ΔH-2′ (ppm)*[a]	*syn/anti*
***β*-NAD$^+$**	-	H	55	4.71	–	*anti*
13a	2	Iodo	53	4.74	0.03	*anti*
13b	2	Phenyl	–	4.84	0.13	*anti*
15b	8	Phenyl	59	5.14	0.43	*syn*
15c	8	3-(*N*-Boc-aminomethyl)phenyl	–	5.16	0.45	*syn*
15e	8	Pyridin-3-yl	57	5.24	0.53	*syn*
15g	8	2,4-*DMT*-pyrimidin-5-yl	55	5.08	0.37	*syn*
15h	8	Pyrrol-2-yl	48	5.33	0.62	*syn*

[a]ΔH-2′ has been calculated as the difference between the chemical shift of H-2′ of the aryl/heteroaryl adenine-modified NAD$^+$ derivatives and H-2′ of *β*-NAD$^+$ (4.71 ppm) in D_2O (referenced for D_2O, δ = 4.79 ppm).

Table 3.2 Conformational analysis of the various aryl/heteroaryl adenine-modified NAD$^+$ derivatives synthesized in this study.

3.2 Nucleobases and their photochemical properties

Absorption and emission spectroscopies are based respectively on the measurement of light absorbed or emitted by molecules. Depending on the energy of the absorbed light, different phenomena can occur in the molecules and, consequently, different techniques have been developed to explore them.

UV/Vis absorption spectroscopy looks at the absorption by the molecules of UV/Vis light, which promotes the electrons in the external shell from the ground state, S_0, to an electronically excited state, S_1. Then, the excited electrons decay back to the S_0 dissipating the energy by different processes, non radiative in the form of heat, or radiative by emission of photons. The last process is called photoluminescence.

Photoluminescence processes can be divided into fluorescence (F) and phosphorescence (P) (Figure 3.4). The former occurs when excited and ground states have the same spin multiplicities ($S_1 \rightarrow S_0$); by contrast, the latter occurs when they have different spin multiplicities ($T_1 \rightarrow S_0$). The quantum yield (Φ) is a relative fluorescence measurement of the compounds, indicating the fraction of excited molecules that decay back by fluorescence emission.[181-183]

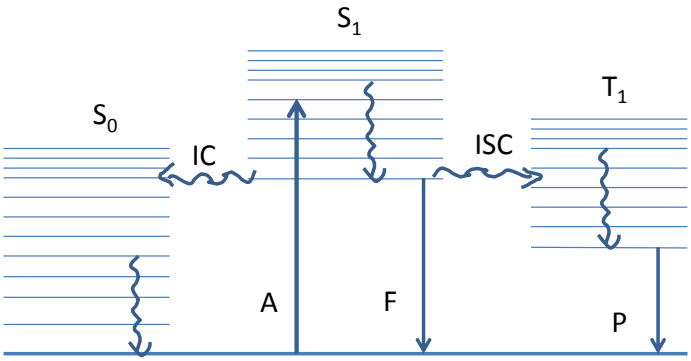

Figure 3.4 Physical processes occurring when a molecule absorbs UV/Vis light. S_0 is the electronic ground state of the molecule; S_1 and T_1 are respectively the excited singlet and triplet states at lower energy. The straight arrows indicate radiative processes with emission of photons, while the curly ones the non radiative processes to dissipate energy. **A** (Absorption), **F** (Fluorescence), **P** (Phosphorescence), **IC** (Internal Conversion), **ISC** (Inter System Crossing).

Fluorescence spectroscopy is a very sensitive technique, largely used in biochemistry to investigate and understand many major biochemical topics (*e.g.* structure, binding, recognition). Intrinsically fluorescent biological molecules are present in nature and act as natural biochemical probes (*e.g.* β-NADH, tryptophan, phenylalanine and tyrosine).[85] In the case of nucleic acids, the most common nucleobases, such as purines and pyrimidines, are generally not emissive in neutral aqueous conditions. However, rare exceptions of naturally occurring emissive nucleobases can be found in nature and used as "built-in" probes.[47, 184, 185]

In particular, adenine and its corresponding nucleoside, adenosine, can be considered not emissive, since their quantum yields are very low (respectively 3×10^{-4} and 5×10^{-5}) and the excited-state lifetimes of the order of picoseconds. In adenine, the decay to the ground state occurs by internal conversion, adopted by the nucleobases as a natural defence to protect the nucleic acids from the photodecomposition. Surprisingly, the adenine isomer, 2-amino purine (2-AP), where the NH_2 is in position 2 instead of 6 on the purine ring, is strongly emissive (Φ = 0.66, and 0.68 for the ribonucleoside) with a long excited-state lifetime. In this case, the electronic stabilization of the C-2 surrounded by three nitrogens would decrease the energy of the excited state, minimizing the internal conversion of the excited molecules to the ground state. This is just an example of how small changes in the nucleobase structure can modify completely its photochemical properties.[186-189]

Owing to the importance of the nucleic acids and their crucial role in life, a deep knowledge about their structure and the biological processes in which they are involved, such as DNA replication, repair, and recombination, transcription and translation, and many others, are some of the most attractive, challenging and always relevant source of scientific interest. In addition, nucleosides, nucleotides and their derivatives are involved as substrates or signalling molecules in many cellular processes. Therefore, the study of their activities and binding to the proteins is important to understand fundamental biological processes. For this reason, major efforts have been undertaken to synthesize emissive nucleobases that, introduced in nucleosides and their derivatives, allow their study by fluorescence spectroscopy.

3.3 Design of emissive nucleosides

3.3.1 Fluorophore features

For the design of emissive nucleosides, many factors influencing the fluorescence properties have to be taken in consideration. The main features that characterize a good fluorophore are summarised below:

- Extended *electron delocalization*; the more extended the delocalization, the more stable and at lower energy (red shift) is the excited state, minimising the photodecomposition of the molecule.

- *Rigidity* of the fluorophore; too many rotational and vibrational levels in the excited state can cause the decay to the ground state *via* vibrational relaxation, decreasing the fluorescence emission.

- *Quantum yield* of the fluorophore (Φ_f) is the ratio of photons absorbed to photons emitted by fluorescence; the maximum value for Φ_f is 1. The higher the quantum yield, the stronger is the fluorescence of the fluorophore and, consequently, the sensitivity of the fluorescence detection, even at low concentrations of the fluorophore.

- *Solvatochromism*, or fluorescence changes of the molecules depending on the surrounding environment, such as the polarity and the H-bonding ability of the solvent. The solvent molecules that solvate the fluorophore assist the stabilization of its excited state by solvent relaxation. The stronger the solvation, the higher is the solvent relaxation; hence, the more stable and at lower energy (red shift) is the excited state and the larger is the distance between λ_{ex} and λ_{em} (Stokes shift).

- *Quenching*, or any process which decreases the fluorescence of a molecule. It can be caused by quenchers present in the sample, such as O_2, or by the same fluorophore, if present in too high concentrations (*self-quenching*). The quenching can be due to intra/intermolecular collisions (*dynamic quenching*); or to the formation of not emissive fluorophore-quencher complexes (*static quenching*).[181-183]

Keeping in mind all these factors influencing the fluorescence, it is possible to design fluorophores with suitable features to their use.

3.3.2 Families of existing nucleobase-modified emissive nucleosides

Several approaches have been followed to obtain emissive nucleosides, such as the modification on the nucleobase or the ribose.[47, 185] Herein, the attention has been focused on the main families of emissive nucleosides modified on the nucleobase.[184, 190]

Figure 3.5 shows the emissive nucleosides obtained by the replacement of the nucleobases with well known fluorophores, as polycyclic aromatic hydrocarbons (PAH), or natural heterocycles, as pteridines; or by the introduction on the nucleobases of fluorophores not directly conjugated with them. This family of emissive nucleosides is characterized by the fluorescent properties of the attached fluorophores.[191]

Since the fluorescence is due to an extended delocalization of π-electrons, it is possible to obtain emissive nucleosides extending the electronic delocalization of the natural nucleobases. From this approach, the so-called *expanded* and *extended nucleobases* have been generated (Figure 3.6).

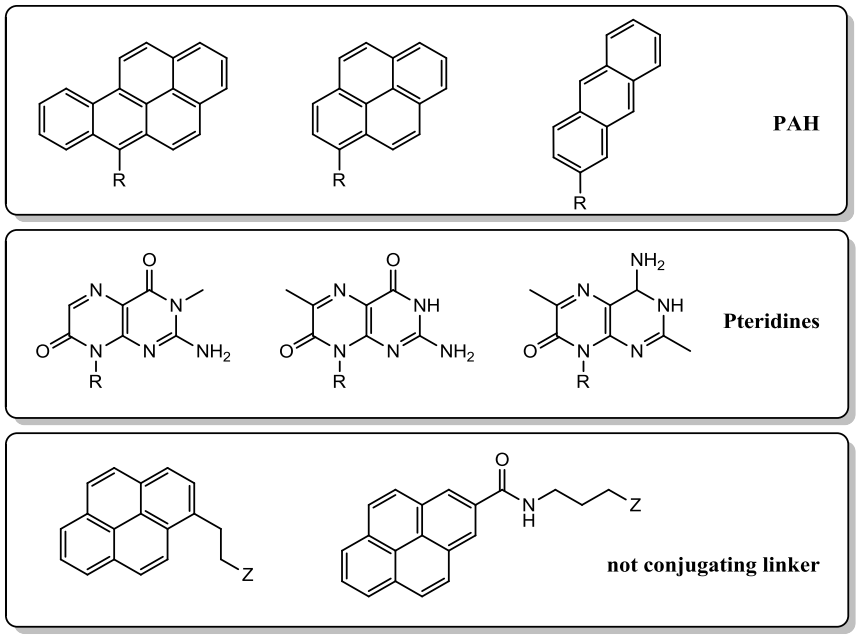

R = ribose or 2'-deoxyribose
Z = nucleobase

Figure 3.5 Emissive nucleosides obtained by replacement of the nucleobases or introduction on their skeleton of known fluorophores.

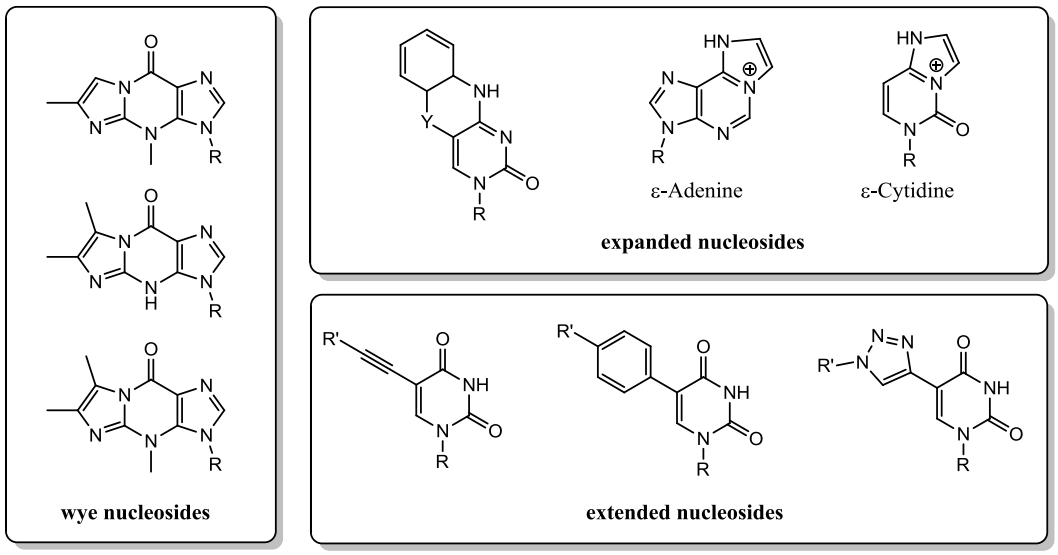

R = ribose or 2'-deoxyribose
R' = alkyl, aryl
Y = O, S

Figure 3.6 Expanded and extended nucleosides, obtained by extension of the π-electrons delocalization of the nucleobases.

The expanded nucleobases have additional aromatic rings fused to the natural nucleobases to extend their electronic conjugation (inspired by the rare natural wye nucleosides found in *t*RNA[192, 193]).[83, 194-196] In contrast, the extended nucleobases have known fluorophores connected *via* electronically conjugated linkers.[130, 197-200] The emissive nucleosides belonging to these families are characterized by peculiar fluorescent properties, since all the conjugated groups of the molecule are an integral part of fluorophore.

Finally, the *isomorphic nucleobases* are heterocycles resembling the natural nucleobases in size and H-bonding patterns, but with characteristic fluorescent features (Figure 3.7).[151, 152, 172, 200-203]

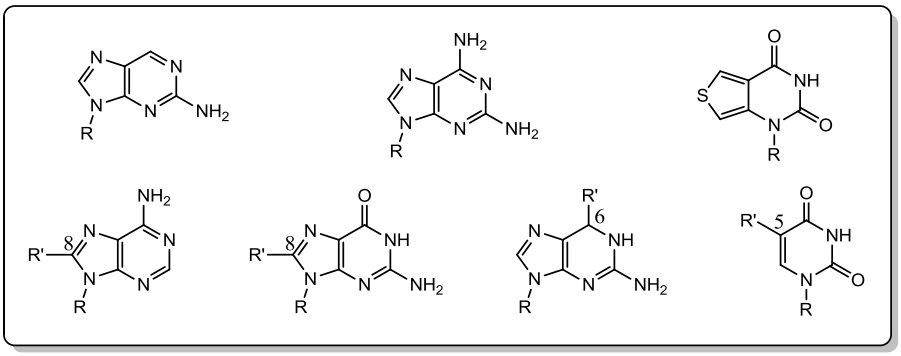

Figure 3.7 Emissive isomorphic nucleosides.

Many of them contain aryl/heteroaryl groups as substituents on the purine and pyrimidine skeleton. It has already been reported that adenosines substituted on C-8 of the adenine ring with aryl/heteroaryl groups belong to the class of emissive isomorphic nucleosides,[130, 200, 202] while those substituted on C-2 and C-6 are weakly emissive, as experimental evidence will suggest in this study.

In this chapter, the spectroscopic analysis of aryl/heteroaryl adenine-modified AMP and corresponding NAD^+ derivatives, synthesized in Chapter 2, will be performed in view of their possible biochemical applications.

3.4 Measurements of quantum yield for aryl/heteroaryl adenine-modified AMP and NAD^+ derivatives

The most common method to measure the unknown quantum yield of a fluorophore, Φ_x, is the comparative method,[204, 205] which involves the use of standards with known Φ_{st} values. Indeed, assuming that solutions of standard and sample at the same λ_{ex} absorb the same number of photons, the ratio between the integrated fluorescence intensities of the two solutions will be the ratio of their Φ values, from which Φ_x can be easily calculated.

In practice, the quantum yield measurements can be affected by many factors that influence the experimental results. The choice of the standards, which must have similar λ_{ex} and, possibly, also λ_{em} to the compound with unknown Φ_x, is critical. The cross-calibration of two standards with each other is crucial for robust and reliable results, since the Φ_{st} is used to calculate Φ_x. Only when the cross-calibration gives Φ_{st} values in agreement with those in the literature, it is possible to proceed to the measurement of Φ_x with a certain level of confidence. In addition, the choice of a proper range of concentrations to guarantee a linear response in the absorbance and fluorescence measurements is fundamental to correctly measure Φ_x. Indeed, at high concentrations the self-quenching phenomena are quite common due to intermolecular collisional energy transfers.

For the Φ_x measurement, absorbance and fluorescence spectra of sample and standard at different dilutions are recorded and their integrated area plotted, fluorescence *versus* absorbance. The gradient of the two extrapolated lines ($Grad_x$ and $Grad_{st}$) can be substituted in the following equation [1] and corrected for the refractive indexes of sample and standard solutions (η_x and η_{st}), allowing the calculation of Φ_x:

$$\Phi_x = \Phi_{st} \times \left(\frac{Grad_x}{Grad_{st}}\right)\left(\frac{\eta_x^2}{\eta_{st}^2}\right) \qquad [1]$$

Φ values were calculated for different AMP and NAD^+ derivatives synthesized in Chapter 2, using 2-amino pyridine and tryptophan as standards, previously cross-calibrated to each other. AMP and NAD^+ derivatives substituted respectively in 2 and 6 position on the adenine ring turned out to be poorly emissive. A simple evaluation of

their fluorescence was performed by visualization under UV light (254/365 nm) of their spots in TLC, showing no trace of fluorescence; Φ values were calculated only for the 6-(pyrrol-2-yl) AMP (**8b**) and the corresponding NAD^+ derivative (**14b**), which showed in these conditions to be slightly more fluorescent than the others. In contrast, 8-substituted AMP and NAD^+ derivatives were good fluorophores and, therefore, Φ values were calculated for many of them.

3.5 Spectroscopic analysis of aryl/heteroaryl adenine-modified AMP derivatives

Table 3.3 summarises the spectroscopic analysis for aryl/heteroaryl adenine-modified AMP derivatives synthesized in Chapter 2. Different trends in λ_{ex}, λ_{em}, Stokes shift and Φ values were observed in the series of fluorescent 8-aryl/heteroaryl AMP derivatives depending on the nature of the substituent; the values followed approximately the same trends in water and methanol.

cmpd	*Position of substitution*	*R (substituent)*	*solvent*	λ_{ex}/*nm*	λ_{em}/*nm*	*Stokes shift*[a]/cm^{-1}	*Φ*
AMP	–	H	Water	260	380	12146	–
7b	2	Phenyl	Water	270	374	10299	–
8a	6	Phenyl	Water	288	387	8882	–
8b	6	Pyrrol-2-yl	Water	340	382	3234	0.0041
9b	8	Phenyl	Water	274	381	10250	0.669
			MeOH	281	376	8991	0.225
9c	8	3-(*N*-Boc-aminomethyl)phenyl	Water	274	383	10387	0.888
			MeOH	281	378	9132	0.639
9e	8	Pyridin-3-yl	Water	277	401	11163	0.0034
			MeOH	287	406	10213	0.021
9f	8	Pyridin-4-yl	Water	284	421	11458	0.032
			MeOH	293	422	10433	0.044
9g	8	2,4-*DMT*-pyrimidin-5-yl	Water	270	410	12647	0.021
			MeOH	272	404	12012	0.147
9h	8	Pyrrol-2-yl	Water	306	374	5942	0.231
			MeOH	306	376	6084	0.272
9i	8	Furan-2-yl	Water	302	378	6658	0.538
			MeOH	300	375	6667	0.638
9k	8	5-Formyl-thien-2-yl	Water	334	436	7004	0.084

[a] Stokes shift = $(1/\lambda_{ex} - 1/\lambda_{em})$.

Table 3.3 Spectroscopic analysis in water and methanol of natural AMP and aryl-heteroaryl adenine-modified AMP derivatives synthesized in this study.

Firstly, the absorbance spectra of 8-aryl/heteroaryl AMP derivatives were studied. They presented two absorbance bands due to different electronic transitions, that at longer wavelengths (lowest energy) diagnostic for the substituents introduced on the adenine ring and, therefore, for larger π-electron delocalizations. In Figure 3.8, the absorbance spectra of phenyl (**9b**), pyridin-3-yl (**9e**) and pyrrol-2-yl (**9h**) AMP derivatives are shown to compare the effect of phenyl, electron-poor and electron-rich substituents on the λ_{ex} maxima. Analysing the shift of λ_{ex} with the substituents, a red shift (bathochromic effect) occurred moving from the phenyl, through the electron-poor, to the electron-rich substituted adenine rings (Figure 3.8, Figure 3.9). Indeed, 2,4-*DMT*-pyrimidine has the excited state with the highest energy because of the partial aromatic delocalization due to its tautomeric form. To follow, the phenyl ring with an equal π-electron delocalization. Then, the pyridine with the energetic difference between the ground (HOMO) and the excited state (LUMO) smaller than benzene, because of the non-bonding orbitals containing the nitrogen lone pair (HOMO) at higher energy. Finally, the electron-rich heterocycles, better π-donors than the six-membered rings, with the smaller difference between HOMO and LUMO due to the large π-electron delocalization.

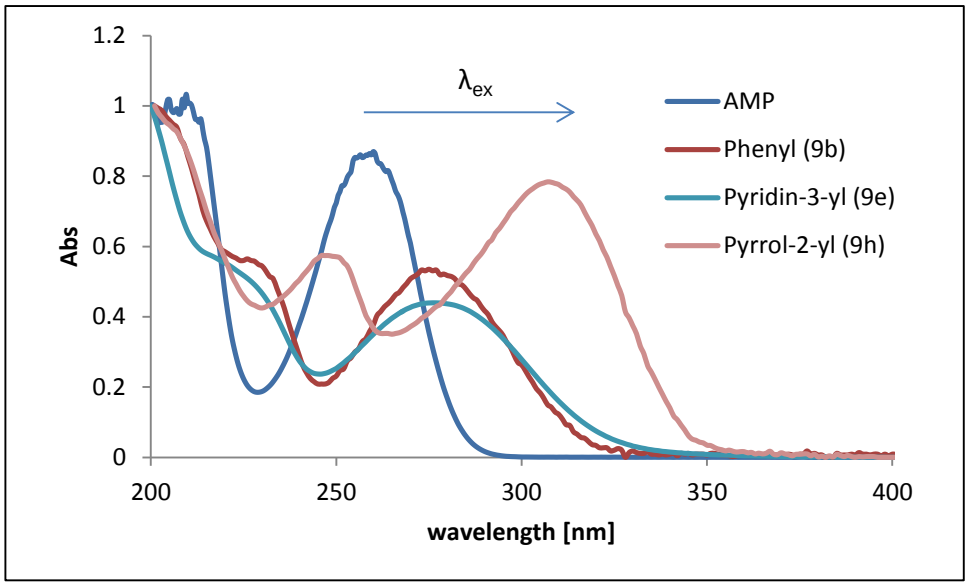

Figure 3.8 Absorbance spectra of AMP and **9b**,**e**,**h** in water.

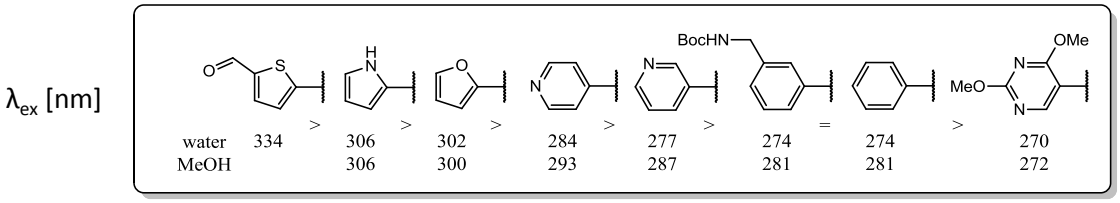

Figure 3.9 Variations of λ_{ex} with the different substituents in water and methanol for the 8-aryl/heteroaryl adenine-modified AMP derivatives synthesized in this study.

The fluorescence spectra of 8-aryl/heteroaryl AMP derivatives showed a main emission band between 370 and 440 nm, typical for the emission of the substituted adenine rings. A less intense band between 650 and 900 nm could be due to Pd(II) impurities, deriving from the Suzuki-Miyaura cross-coupling. Indeed, Pd(II) can form Pd(II)-adenine complexes with the exocyclic NH_2 and N-7, or N-1 (Figure 3.10).[206, 207]

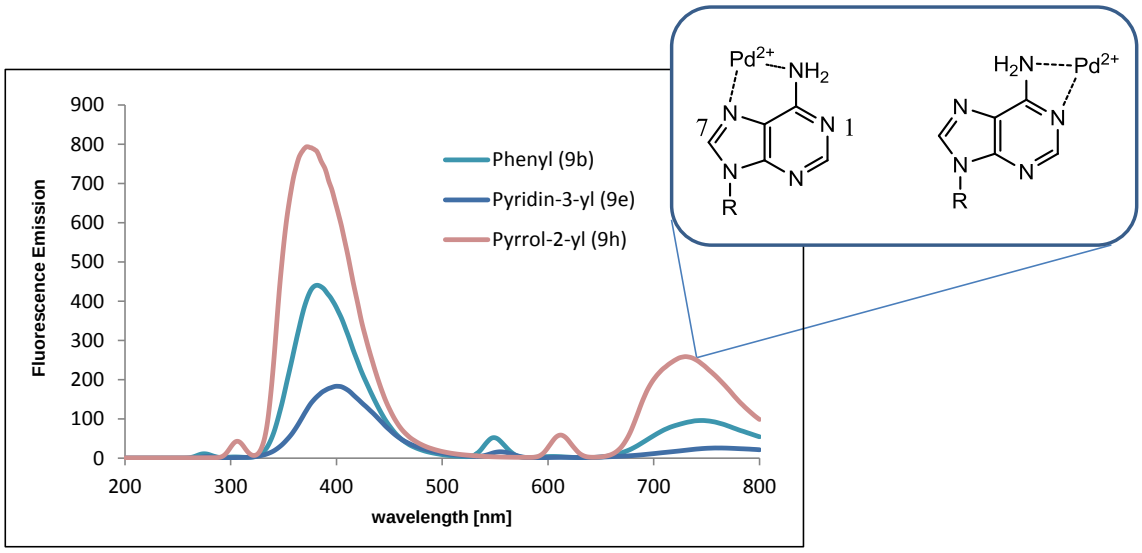

Figure 3.10 Fluorescence emission spectra of **9b**,**e**,**h** in water at λ_{ex} maxima (see Table 3.3).

The λ_{em} for the 8-aryl/heteroaryl AMP derivatives followed a less clear trend compared to λ_{ex} along the different substituents. However, with few exceptions, the trend for λ_{em} was the same followed by the Stokes shift values, that clearly increased from the electron-rich, through the phenyl, to the electron-poor substituted adenine rings (Figure 3.11). The λ_{em} and Stokes shift depend on vibrational and solvent relaxation; the stronger these two effects, the larger is the Stokes shift and the longer is the λ_{em}.

Electron-rich substituted adenine rings, having a large π-electron delocalization, are more rigid and planar than those phenyl and electron-poor substituted, having minor π-electron distribution. Consequently, λ_{em} and Stokes shift, depending on vibrational relaxation, were larger for electron-poor and phenyl substituted adenine rings, having many vibrational energetic levels in the excited state, than those that were electron-rich substituted (Figure 3.11). In addition, electron-poor substituted adenine rings had longer λ_{em} and larger Stokes shift than those phenyl substituted because of a higher solvent relaxation, due to their H-bonding ability and large dipole moment in the excited state. The Stokes shift values were generally larger in water than in methanol because of more H-bonds, which caused a higher solvent relaxation. However, electron-rich substituted adenine rings appeared unaffected by the solvent change, with their Stokes shift values unchanged between water and methanol. Therefore, these substituents could be insensitive to the surrounding environment, as confirmed later from their unchanged Φ values.

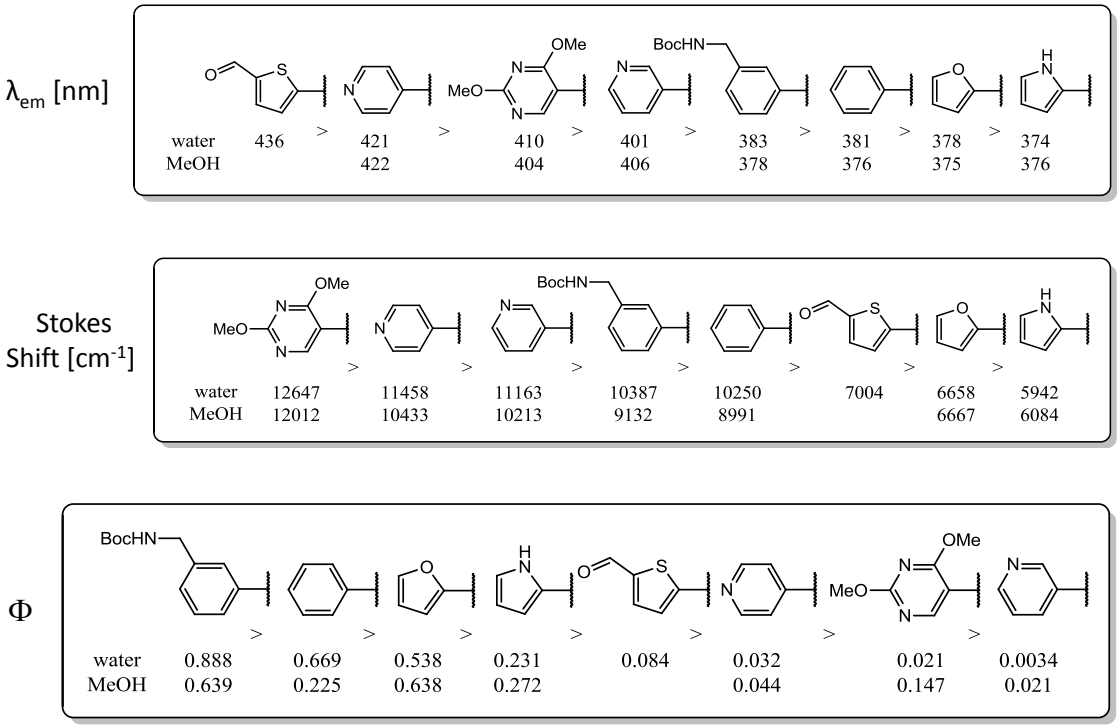

Figure 3.11 Variations of λ_{em}, Stokes shift and quantum yield (Φ) values with the different substituents in water and methanol for the 8-aryl/heteroaryl adenine-modified AMP derivatives synthesized in this study.

The Φ values for the substituted adenine rings seemed to follow a precise trend along the introduced substituents, as well as λ_{ex}, λ_{em} and Stokes shift. In particular, they increased moving from the electron-poor, through the electron-rich, to the phenyl substituted adenine rings (Figure 3.11). The trend was similar between water and methanol. From the previous considerations, electron-rich substituted adenine rings would be expected to be the most fluorescent in the series because of a larger π-electron delocalization, rigidity and planarity, and limited sensitivity to the solvent effect. However, a new factor, the dynamic/static quenching, could influence Φ values. Indeed, the strong planarity of electron-rich substituted adenine rings would favour the intermolecular base stacking interactions with consequent fluorescence decrease.

The Φ values should increase in methanol compared to water because of a minor solvent relaxation. This effect was observed for electron-poor substituted adenine rings; in contrast, Φ values decreased for those phenyl substituted, and remained approximately the same for electron-rich substituted adenine rings. In the first case, the strongly emissive phenyl substituted adenine rings could undergo a dynamic/static fluorescence quenching, decreasing overall their Φ values. Regarding the electron-rich substituted adenine rings, the unchanged Φ values could be due to their insensitivity to the solvent, already observed in the Stokes shift values.

The spectral properties of AMP derivatives with the same substituent but in different positions were analysed (Table 3.4, Figure 3.12). Moving from the AMP derivatives substituted on C-6 to those substituted on C-2 and C-8, λ_{ex}, even more than λ_{em}, underwent a substantial blue shift (hypsochromic effect), responsible for an increase of Stokes shift. In addition, in the case of 8-substituted AMP derivatives, a significant increase in Φ was observed. Therefore, it was suggested that the substitution of the exocyclic amino group in position 6 on the adenine ring with aryl/heteroaryl groups helped stabilize the electronic configuration of the 6-substituted adenine rings, decreasing the gap between HOMO and LUMO, larger otherwise in 2 and 8-substituted adenine rings. In addition, the removal of the exocyclic amino group would decrease the H-bonding ability of 6-substituted AMP derivatives and, consequently, their Stokes shift values.

Phenyl substituent						*Pyrrol-2-yl substituent*					
cmpd	*C*	λ_{ex}/nm	λ_{em}/nm	*Stokes shift*[a]/cm^{-1}	*Φ*	*cmpd*	*C*	λ_{ex}/nm	λ_{em}/nm	*Stokes shift*[a]/cm^{-1}	*Φ*
7b	2	270	374	10299	–	–	–	–	–	–	–
8a	6	288	387	8882	–	**8b**	6	340	382	3234	0.0041
9b	8	274	381	10250	0.669	**9h**	8	306	374	5942	0.231

[a] Stokes shift = $(1/\lambda_{ex} - 1/\lambda_{em})$.

Table 3.4 Comparative spectroscopic analysis of adenine-modified AMP derivatives with the same substituent (phenyl and pyrrol-2-yl) in different positions.

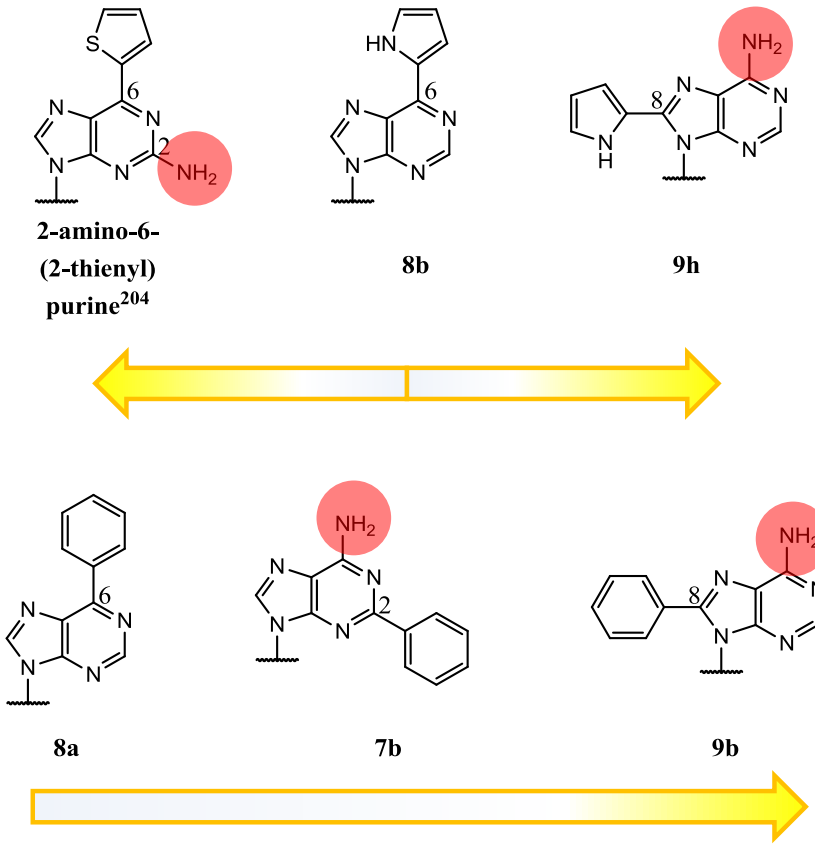

Figure 3.12 Comparison of fluorescence of adenine-modified AMP derivatives with the same/similar aryl/heteroaryl substituent in different positions. To notice the influence of the position of the exocyclic amino group on the fluorescence. The direction of the arrow indicates an increase in fluorescence.

It is important to notice the change in fluorescence related to the position of the substituent and the exocyclic amino group on the purine ring (Table 3.4, Figure 3.12). As discussed in 3.2, 2-AP is more fluorescent than adenine because of the presence of the exocyclic amino group on C-2 instead of C-6. This relatively simple change of

position of the substituent decreases the internal conversion of the excited molecules to the ground state and, consequently, increases their fluorescence. In the same way, looking in Figure 3.12 at the differently substituted adenine rings, it can be observed that, when the substituent is on the pyrimidine ring, as in 2-amino-6-(2-thienyl) purine,[203] **8a**, **8b** and **7b**, the presence of the exocyclic amino group in the specific position 2 is fundamental to generate the fluorescence, more than its absence/presence in generic positions. In contrast, its presence in position 6 does generate fluorescence only if the substituent is on the imidazole ring. Therefore, energetic differences in excited states of adenine rings substituted in different positions are responsible for their quantum yield changes.

3.6 Spectroscopic analysis of aryl/heteroaryl adenine-modified NAD$^+$ derivatives

Table 3.5 summarises the spectroscopic analysis for aryl/heteroaryl adenine-modified NAD$^+$ derivatives synthesized in this study. As for the AMP derivatives, different trends in λ_{ex}, λ_{em}, Stokes shift and Φ values were observed in the series of fluorescent 8-aryl/heteroaryl NAD$^+$ derivatives depending on the nature of the substituents.

cmpd	*Position of substitution*	*R (substituent)*	*solvent*	λ_{ex}/*nm*	λ_{em}/*nm*	*Stokes shift*[a]/*cm*$^{-1}$	*Φ*
***β*-NAD$^+$**	–	H	Water	259	380	12294	–
13b	2	Phenyl	Water	268	380	10998	–
14a	6	Phenyl	Water	289	400	9602	–
14b	6	Pyrrol-2-yl	Water	344	388	3297	0.0012
15b	8	Phenyl	Water	272	381	10518	0.2067
			MeOH	274	378	10041	0.080
15c	8	3-(*N*-Boc-aminomethyl)phenyl	Water	274	383	10387	0.150
			MeOH	273	379	10245	0.148
15e	8	Pyridin-3-yl	Water	273	401	11692	0.0035
			MeOH	276	399	11169	0.016
15g	8	2,4-*DMT*-pyrimidin-5-yl	Water	268	412	13042	0.0026
			MeOH	267	411	13122	0.0054
15h	8	Pyrrol-2-yl	Water	309	374	5624	0.0053
			MeOH	307	371	5619	0.055

[a] Stokes shift = $(1/\lambda_{ex} - 1/\lambda_{em})$.

Table 3.5 Spectroscopic analysis in water and methanol of natural *β*-NAD$^+$ and aryl-heteroaryl adenine-modified NAD$^+$ derivatives synthesized in this study.

The trends along the series of the NAD^+ derivatives were generally similar to those observed for the AMP derivatives. In contrast to the AMP derivatives, the Stokes shift values for the NAD^+ derivatives were approximately the same in water and methanol (Table 3.5). This suggested that the NAD^+ derivatives were generally less influenced by the solvatochromism effect than the corresponding AMP derivatives. In addition, Φ values remained generally the same, or increased in methanol compared to water. This trend, not apparently due to the solvatochromism effect, was attributed to a new factor occurring in the NAD^+ derivatives, such as a dynamic/static fluorescence quenching due to the intramolecular stacking interactions, or close proximity between the nicotinamide and the substituted adenine rings. These interactions could be disrupted by methanol or less polar solvents, which would help β-NAD^+ passing from a folded to an extended conformation. This phenomenon and other evidence for its occurrence will be largely discussed in 3.7.

Looking carefully at the absorbance spectra of the NAD^+ derivatives, it was observed that the lowest energy band was the result of overlapping bands, due to the substituted adenine and the nicotinamide ring (Figure 3.13).

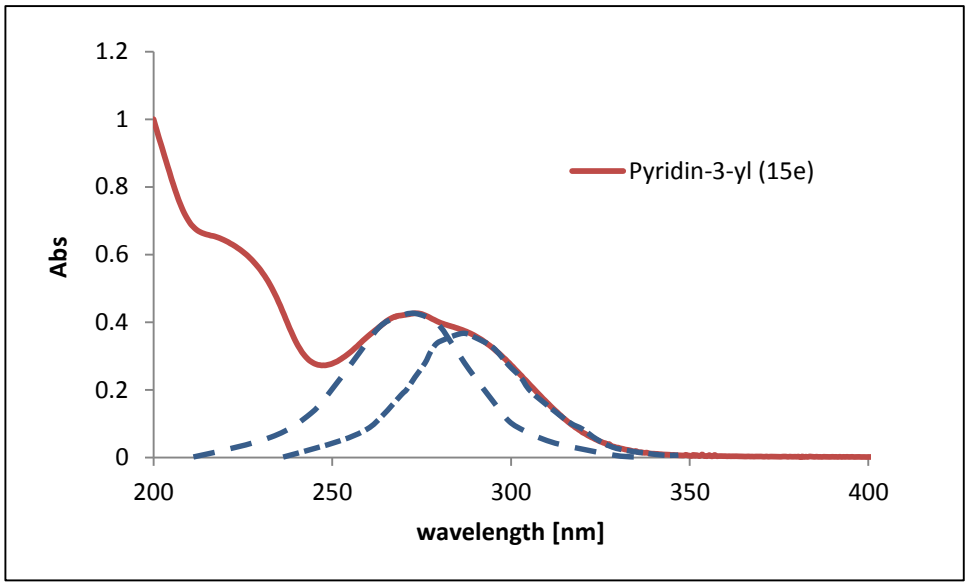

Figure 3.13 Absorbance spectrum of **15e** in water. The absorbance spectrum is the pink line; the broken lines (blue) indicate the overlap for the bands related to the substituted adenine and nicotinamide rings.

The fluorescence emission spectra of 8-aryl/heteroaryl NAD^+ derivatives, shown in Figure 3.14, again presented the two typical bands observed for the AMP derivatives.

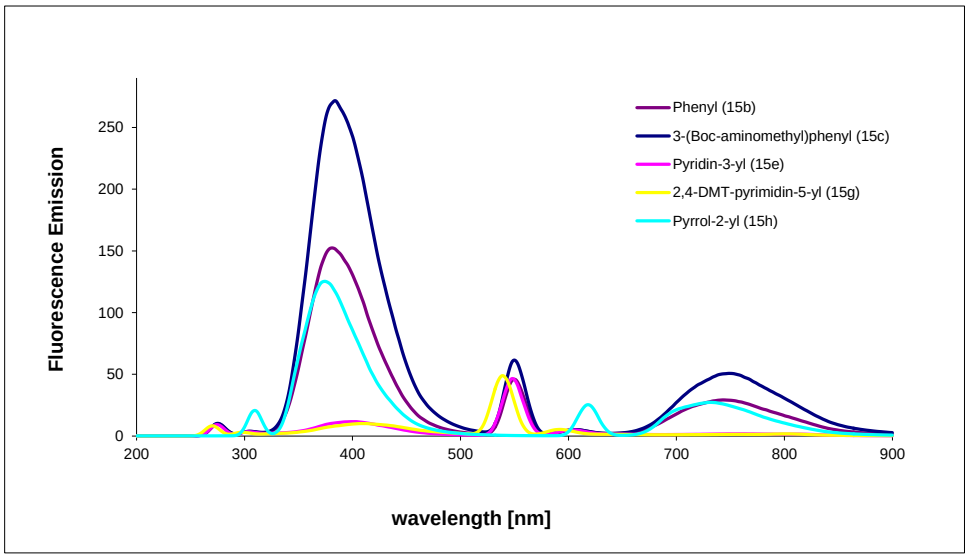

Figure 3.14 Fluorescence emission spectra for **15b**,**c**,**e**,**g**,**h** (0.8 μM in water) at λ_{ex} maxima (see Table 3.5).

Further spectroscopic analyses were performed on 8-aryl/heteroaryl NAD^+ derivatives. In particular, the fluorescence changes with the pH were investigated. Indeed, the fluorescence can be strongly influenced by the pH, since different protonation states can generate in the fluorophore different π-electron delocalization and distribution. In the case of the 8-aryl/heteroaryl NAD^+ derivatives, the fluorophore examined was the substituted adenine ring, which could be protonated on the basic N-1 (Figure 3.15).

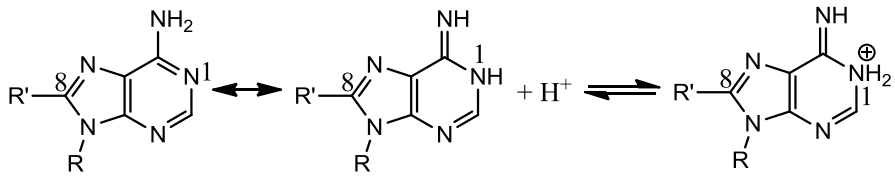

R = nicotinamide diphosphate ribose
R' = H (β-NAD^+)
R' = aryl/heteroaryl (**15b**,**c**,**e**,**g**,**h**)

Figure 3.15 Protonation of N-1 of 8-aryl/heteroaryl adenine-modified NAD^+ derivatives.

At acidic pH, the positive charge on the protonated N-1 destabilized the π-electron delocalization on the adenine ring decreasing its fluorescence (hypochromic effect). By contrast, at basic pH, the aromaticity of the adenine ring was re-established and the fluorescence increased (hyperchromic effect).

This behaviour was observed for all 8-aryl/heteroaryl NAD^+ derivatives, with the exception of **15g**, where fluorescence decreased as the pH increased (Figure 3.16). Indeed, at acidic pH, the nitrogens on the 2,4-*DMT*-pyrimidine would be protonated with two partial positive charges; therefore, they would be able to form an extended network of H-bonds, making the substituted adenine ring more rigid and, consequently, more fluorescent than at basic pH (Figure 3.17). Plotting the fluorescence *versus* the pH, it was possible to extrapolate the pK_a values for N-1 of 8-aryl/heteroaryl NAD^+ derivatives (Figure 3.16).[172]

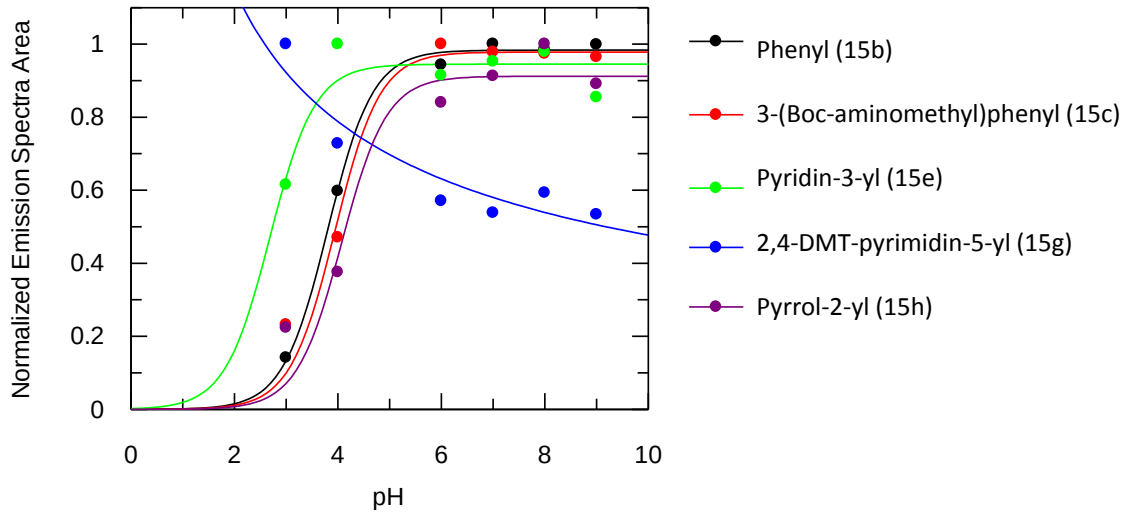

Figure 3.16 Fluorescence emission at different pH for **15b**,**c**,**e**,**g**,**h**. *Conditions*: NaOAc/AcOH buffer (50 mM) was used for pH 3 and 4; KH_2PO_4/NaOH buffer (50 mM) was used for pH 6; Tris/HCl buffer (50 mM) was used for pH 7, 8 and 9. The compound concentrations were respectively: 1.01 µM for **15b**, 3.9 µM for **15c**, 3.6 µM for **15e**, 3.5 µM for **15g**, 0.81 µM for **15h**. Fluorescence emission spectra were recorded at λ_{ex} maxima (see Table 3.5), rt. Emission spectra areas were normalized to the highest value for each compound and the values were fitted to the pK_a single equation using GraFit5 (except for **15g**, fitted to a single exponential equation).

The pK_a calculated by potentiometric titration for β-NAD^+ is 3.88 ± 0.02.[186, 208] As shown in Table 3.6, the pK_a values obtained for 8-aryl/heteroaryl NAD^+ derivatives were close to that of the natural β-NAD^+, although following a certain trend depending on the nature of the substituent, which influenced the basicity of N-1.

cmpd	*R (substituent on C-8)*	*pK_a*
β-NAD^+ [208]	H	3.88 ± 0.02
15b	Phenyl	3.81 ± 0.04
15c	3-(*N*-Boc-aminomethyl)phenyl	3.95 ± 0.14
15e	Pyridin-3-yl	2.69 ± 0.18
15h	Pyrrol-2-yl	4.07 ± 0.21

Table 3.6 pK_a values for the natural β-NAD^+ and **15b**,**c**,**e**,**h**.

The phenyl substituents in **15b** and **15c** did not change substantially the π-electron delocalization of the adenine ring, which had very similar pK_a values to β-NAD^+. The electron-poor substituents, withdrawing electrons from the adenine ring, decreased the pK_a of N-1; in particular, the pyridine ring in **15e** at acidic pH would be present as the pyridinium ion, a very strong electron-withdrawing group. The electron-rich substituents, as the pyrrole in **15h**, donated electrons to the adenine ring increasing the basicity of N-1 and, therefore, its pK_a. A red shift (bathochromic effect) in λ_{em} was observed for **15e** and **15g** as the pH increased. This effect could be due to a stronger vibrational relaxation occurring at basic pH, because of the lack of H-bonds occurring at acidic pH (Table 3.7, Figure 3.17). In contrast, λ_{em} for the other substituted adenine rings did not undergo any substantial shift with the pH (Table 3.7).

		λ_{em}/nm					
cmpd	*R (substituent on C-8)*	*pH 3*	*pH 4*	*pH 6*	*pH 7*	*pH 8*	*pH 9*
15b	Phenyl	385	382	383	383	383	383
15c	3-(*N*-Boc-aminomethyl)phenyl	383	383	383	384	384	384
15e	Pyridin-3-yl	374	390	404	404	406	406
15g	2,4-*DMT*-pyrimidin-5-yl	380	387	413	413	413	415
15h	Pyrrol-2-yl	375	375	375	375	375	375

Table 3.7 λ_{em} maxima of **15b**,**c**,**e**,**g**,**h** at different pH. *Conditions*: NaOAc/AcOH buffer (50 mM) was used for pH 3 and 4; KH_2PO_4/NaOH buffer (50 mM) was used for pH 6; Tris/HCl buffer (50 mM) was used for pH 7, 8 and 9. Fluorescence emission spectra at λ_{ex} maxima (see Table 3.5), rt.

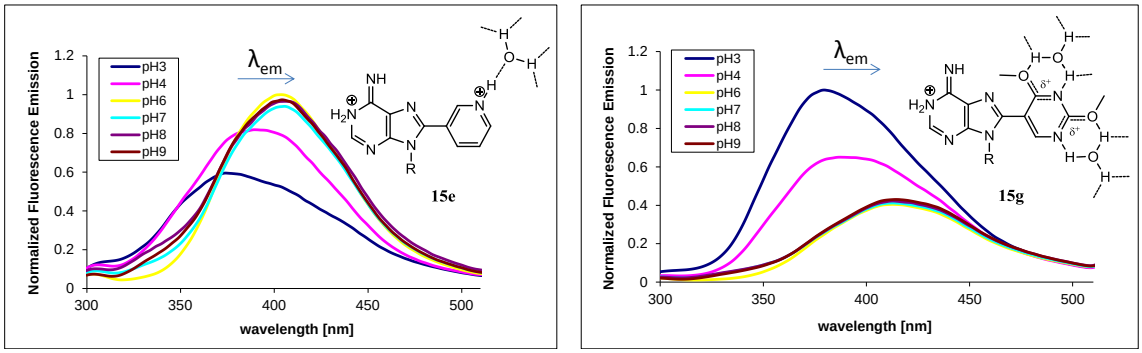

Figure 3.17 Network of H-bonds around **15e** and **15g**, responsible for the red shift of λ_{em} in **15e** and **15g** with the increase of the pH, and the hypochromic effect at basic pH in **15g**. *Conditions*: NaOAc/AcOH buffer (50 mM) was used for pH 3 and 4; KH_2PO_4/NaOH buffer (50 mM) was used for pH 6; Tris/HCl buffer (50 mM) was used for pH 7, 8 and 9. The compound concentrations were respectively: 3.6 μM for **15e** and 3.5 μM for **15g**. Fluorescence emission spectra were recorded at λ_{ex} maxima (see Table 3.5), rt. Emission spectra areas were normalized to the highest value for each compound.

3.7 Fluorescence quenching in 8-aryl/heteroaryl NAD$^+$ derivatives

3.7.1 Fluorescence basis for internal quenching in NAD$^+$ derivatives

As mentioned in 3.6, clues for a dynamic/static fluorescence quenching due to the intramolecular interactions between the nicotinamide and the 8-aryl/heteroaryl adenine rings of the corresponding NAD$^+$ derivatives were found comparing Φ values in water and methanol. Indeed, the values suggested a fluorescence quenching occurring in water, where the *β*-NAD$^+$ scaffold would assume a folded conformation with the hydrophobic aromatic rings in close proximity with each other. Methanol would disrupt these interactions solvating the aromatic rings and allowing the passage of *β*-NAD$^+$ from a folded to an extended conformation with re-establishment of the fluorescence.[64, 209]

A thorough investigation was undertaken to explore this phenomenon in the series of 8-aryl/heteroaryl NAD$^+$ derivatives synthesized in this project. Similar studies have been previously undertaken with another important fluorescent NAD$^+$ derivative, ε-NAD$^+$,[87] already introduced in Chapter 1 (Figure 3.18). This compound and its derivatives (ε-AMP, ε-ADP, ε-ATP, ε-ADPR, *c*εADPR) have been extensively studied since the early 1970s, and have found wide applications as fluorescent probes for several enzymes, due to their characteristic fluorescent features.[83, 210] Indeed, etheno-derivatives are

characterized by λ_{ex} and λ_{em} not interfering with those of biological systems (Table 3.8). Moreover, their high Φ values make them very good fluorescent probes.

cmpd	λ_{ex}/*nm*	λ_{em}/*nm*	*Stokes shift*[a]/*cm*$^{-1}$	*Φ*
ε-NAD$^+$ [83]	306	410	8289	0.028
ε-AMP	306	400	7680	0.56
Tryptophan[181]	295	353	5570	0.13
Tyrosine[181]	275	304	3469	0.14
Phenylalanine[181]	260	282	3000	0.02

[a] Stokes shift = $(1/\lambda_{ex} - 1/\lambda_{em})$.

Table 3.8 Spectroscopic properties of ε-NAD$^+$ and fluorescent amino acids.

In the case of ε-NAD$^+$, a low quantum yield value is due to a strong internal fluorescence quenching occurring between the stacked ε-adenine and nicotinamide rings in the ε-NAD$^+$ structure. These stacking interactions can be disrupted by chemical or enzymatic removal of the nicotinamide ring with consequent fluorescence increase. Indeed, the quantum yield value of ε-AMP is ~ 20 fold greater than the corresponding ε-NAD$^+$ (Table 3.8, Figure 3.18).[83, 87, 88] The internal quenching occurring in the intact ε-NAD$^+$ compared to the ε-adenine moiety is the basis for the development of fluorescence-based assays for NAD$^+$-consuming enzymes,[7] that use *β*-NAD$^+$ as a substrate, cleaving the high-energy bonds present in its structure (*i.e.* the pyrophosphate and *N*-glycosidic bond). A short review of the main assays for NAD$^+$-consuming enzymes based on the fluorescence changes of ε-NAD$^+$ has been presented in 1.4.2.

The fluorescence quenching in ε-NAD$^+$ is due to a mixed dynamic/static quenching. The dynamic quenching is mainly due to intramolecular collisional interactions of the excited molecule and, therefore, it affects the quantum yield and the fluorescence lifetime. In contrast, the static quenching is due to the formation of dark, not emissive complexes between the stacked bases in the ground state and, therefore, it affects the quantum yield but not the fluorescence lifetime. It is possible by measurement of fluorescence lifetimes to distinguish the two type of quenching and their contributions; it has been shown that ε-NAD$^+$ is subjected to both, with prevalence of the static quenching. Moreover, it has been calculated that ε-NAD$^+$ at 25 °C in water is present in a 45 ± 5% stacked conformation.[88]

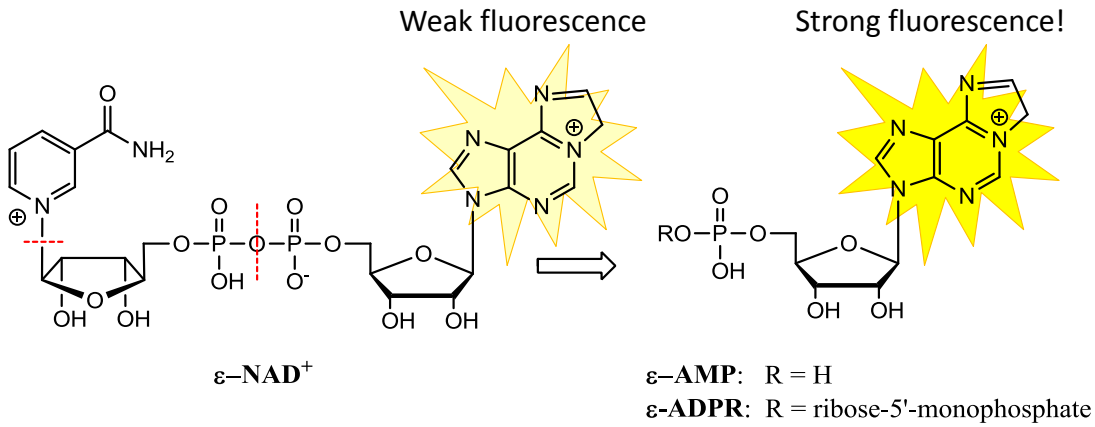

Figure 3.18 ε-NAD^+ and its fluorescence internal quenching.

Different studies were undertaken to prove the existence of an intramolecular fluorescence quenching in the series of fluorescent 8-aryl/heteroaryl NAD^+ derivatives. Interesting information could be deducted from the comparison of quantum yield values between AMP and NAD^+ derivatives (Table 3.9). The quantum yield values of 8-aryl/heteroaryl AMP derivatives were higher than the corresponding NAD^+ derivatives, with the only exception of 8-(pyridin-3-yl) AMP (**9e**) and its corresponding NAD^+ derivative (**15e**).[172] As for ε-NAD^+, these differences in quantum yield could occur because of an intramolecular fluorescence quenching due to stacking and collisional interactions between the fluorophore and the nicotinamide ring. The larger the Φ differences, the stronger would be the interactions between the two aromatic rings. 8-(Pyrrol-2-yl) AMP (**9h**) and its corresponding NAD^+ derivative (**15h**) showed the largest Φ difference in water amongst the NAD^+ derivatives synthesized. This effect could be due to a stronger planarity of the 8-(pyrrol-2-yl) adenine ring, which facilitated the stacking interactions with the nicotinamide ring. When Φ values for this couple were measured in methanol, Φ difference decreased since the organic solvent helped the solvation and the separation of the hydrophobic aromatic rings in **15h** with re-establisment of the fluorescence. In contrast, 8-(pyridin-3-yl) AMP (**9e**) and its corresponding NAD^+ derivative (**15e**) did not show any Φ difference either in water or methanol, indicating a possible lack of planarity in the 8-(pyridin-3-yl) adenine ring and, consequently, poor stacking interactions with the nicotinamide ring.

cmpd	*scaffold*	*Position of substitution*	*R (substituent)*	*solvent*	Φ_{AMP}	Φ_{NAD}	$\Phi_{AMP/NAD}$
εNAD$^+$ [83]	NAD	*n.a.*	*n.a.*	Water	0.56	0.028	20
εAMP[83]	AMP						
14b	NAD	6	Pyrrol-2-yl	Water	0.0041	0.0012	3.42
8b	AMP						
15b	NAD	8	Phenyl	Water	0.669	0.2067	3.24
9b	AMP			MeOH	0.225	0.080	2.81
15c	NAD	8	3-(*N*-Boc-aminomethyl)phenyl	Water	0.888	0.150	5.92
9c	AMP			MeOH	0.639	0.148	4.32
15e	NAD	8	Pyridin-3-yl	Water	0.0034	0.0035	0.97
9e	AMP			MeOH	0.021	0.016	1.31
15g	NAD	8	2,4-*DMT*-pyrimidin-5-yl	Water	0.021	0.0026	8.08
9g	AMP			MeOH	0.147	0.0054	27.22
15h	NAD	8	Pyrrol-2-yl	Water	0.231	0.0053	43.58
9h	AMP			MeOH	0.272	0.055	4.94

n.a. not applicable.

Table 3.9 Comparison of Φ values in water and methanol for ε-AMP/ε-NAD$^+$, and aryl/heteroaryl adenine-modified AMP/NAD$^+$ derivatives synthesized in this study.

To further prove the existence of the internal quenching in 8-aryl/heteroaryl NAD$^+$ derivatives and its decrease passing from water to an organic solvent, a methanol titration of aqueous solutions of 8-aryl/heteroaryl NAD$^+$ derivatives was performed (Figure 3.19). In fact, even if the trends did not completely agree with Φ values calculated in methanol for the different compounds, a general fluorescence increase was observed with the increase of methanol percentage, as expected from the disruption of the internal quenching in organic solvent.[211] In addition, a blue shift in λ_{em} maxima for the different NAD$^+$ derivatives was observed with the increase of the methanol percentage because of a lower solvent relaxation occurring in methanol compared to water (Table 3.10). However, the shift was so small that it did not substantially modify the Stokes shift values, as observed in 3.6, making the NAD$^+$ derivatives quite insensitive to slight environmental changes.

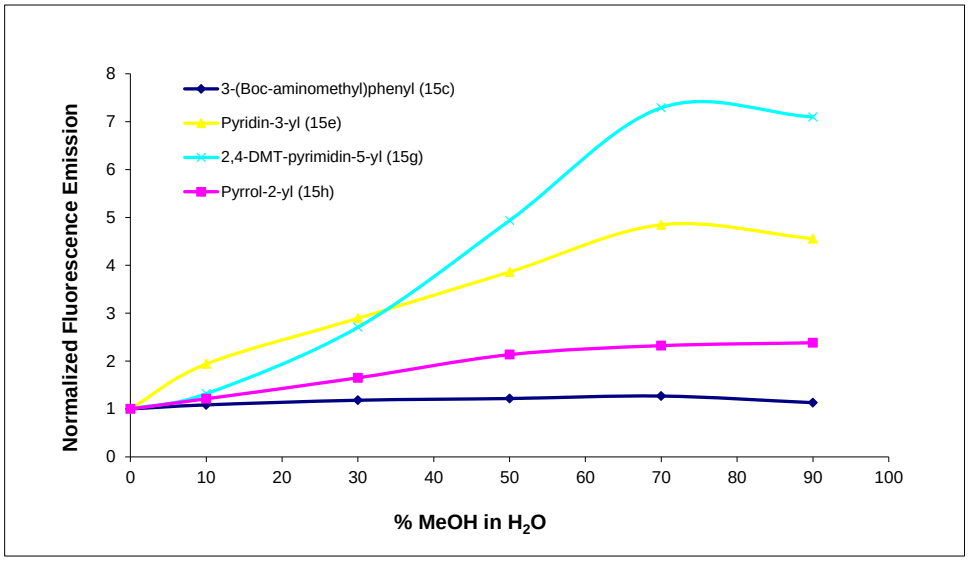

Figure 3.19 MeOH titration of **15c**,**e**,**g**,**h**. *Conditions*: aqueous solutions of the different NAD^+ derivatives with several MeOH percentage (ranging from 10 to 90% MeOH with an interval of 20%) were prepared and their fluorescence emission spectra recorded at λ_{ex} maxima (see Table 3.5), rt. The fluorescence emission values at λ_{em} maxima for the spectra at different MeOH percentage were normalized for those at λ_{em} maxima in H_2O for each compound; then, the normalized values were plotted as function of the solvent composition.

		λ_{em}/nm at different MeOH/H_2O (%)					
cmpd	*R (substituent on C-8)*	*0*	*10*	*30*	*50*	*70*	*90*
15c	3-(*N*-Boc-aminomethyl)phenyl	384	382	382	382	379	380
15e	Pyridin-3-yl	406	415	405	401	399	407
15g	2,4-*DMT*-pyrimidin-5-yl	411	414	410	410	409	409
15h	Pyrrol-2-yl	375	374	373	373	372	370

Table 3.10 λ_{em} maxima of **15b**,**d**,**f**,**g** at different MeOH percentage. *Conditions*: aqueous solutions of the different NAD^+ derivatives with several MeOH percentage (ranging from 10 to 90% MeOH with an interval of 20%) were prepared and their fluorescence emission spectra recorded at λ_{ex} maxima (see Table 3.5), rt.

Finally, a chemical hydrolysis of the fluorescent 8-aryl/heteroaryl NAD^+ derivatives was performed to give conclusive evidence of the internal fluorescence quenching due to the intramolecular interactions between the fluorescent substituted adenine and nicotinamide rings. As discussed in 1.1, the nicotinamide *N*-glycosidic bond can be hydrolysed in 0.1 – 1 N NaOH with a first order reaction in hydroxide.[8, 9, 11] The removal of NaM in 8-aryl/heteroaryl NAD^+ derivatives would result in the formation of the corresponding 8-aryl/heteroaryl ADPR derivatives, with re-establishment of the fluorescence of the substituted adenine rings.

The chemical hydrolysis for all 8-aryl/heteroaryl NAD^+ derivatives was followed by fluorescence (Figure 3.20) and, in the case of 8-(pyrrol-2-yl) NAD^+ (**15h**), also by HPLC (Figure A1).[172] As expected, a fluorescence increase was observed during the hydrolysis of all NAD^+ derivatives examined. However, the fluorescence increase was higher for **15h**, which showed the strongest fluorescence internal quenching amongst the NAD^+ derivatives synthesized. The HPLC time-course for the basic hydrolysis of **15h** confirmed the formation of NaM and the corresponding ADPR derivative, **23**.

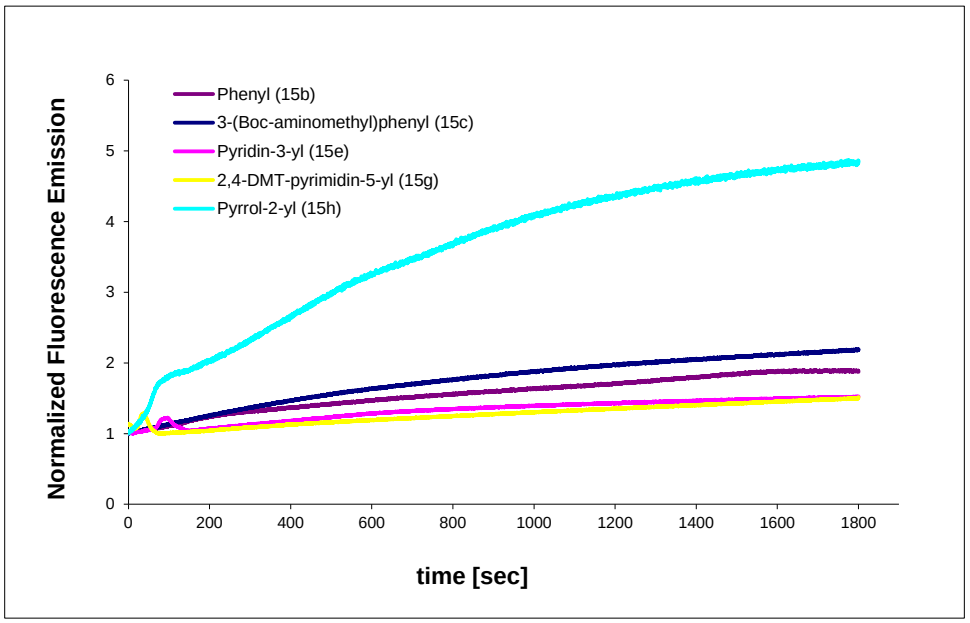

Figure 3.20 Fluorescence time-course for the basic hydrolysis of NAD^+ derivatives **15b**,**c**,**e**,**g**,**h**. *Conditions*: 0.8 μM in 0.1 N NaOH, rt; for λ_{ex} and λ_{em} maxima, see Table 3.5.

3.7.2 NMR basis for internal quenching in NAD^+ derivatives

To investigate if dynamic/static quenching was occurring in aryl/heteroaryl adenine-modified NAD^+ derivatives, NMR studies were undertaken. Indeed, the occurrence of π-stacking interactions between aromatic rings can influence the chemical shifts of their protons because of a "shielding-increasing" ring current. Therefore, an upfield shift should be observed with the increase of π-stacking interactions, which shield the aromatic protons; and *viceversa*, a downfield shift should occur when the π-stacking interactions decrease and the protons are deshielded.

This phenomenon has been largely studied on nucleosides and nucleotides which self-associate by intermolecular π-stacking interactions depending on their concentration in aqueous solution.[212, 213] The more diluted the solution, the less self-association is observed between the nucleobases. In the case of β-NAD^+ and NAD^+ derivatives, the prevalent intramolecular π-stacking interactions are concentration-independent; only at high concentrations, also intermolecular associations start to occur.[214-218] Consequently, to show the occurrence of intramolecular π-stacking interactions in diluted aqueous solutions, a titration experiment monitored by ^{1}H NMR was set up to observe the effect of increasing percentages of acetonitrile on the protons of the natural β-NAD^+ and 8-(pyrrol-2-yl) NAD^+ (**15h**). Changes in the chemical shifts of the protons of the two molecules should show the passage of the β-NAD^+ scaffold from a folded to an open conformation. This experiment was the analogue of the methanol titration performed on 8-aryl/heteroaryl NAD^+ derivatives and monitored by fluorescence in Figure 3.19. As expected, a downfield shift in the aromatic protons occurred with the increase of acetonitrile in both the natural β-NAD^+ and **15h**, with a stronger effect in the case of **15h**. Indeed, the 8-(pyrrol-2-yl) adenine ring could be able to establish stronger π-stacking interactions than the adenine itself with the nicotinamide ring because of a more extended ring current and strong planarity.

Following the titration of β-NAD^+, 2_N-H and 2-H showed a significant downfield shift with the increase of acetonitrile in solution, compared to a smaller shift for 4_N-H and 5_N-H. In contrast, 6_N-H and 8-H showed an upfield shift (Figure 3.21). Strong interactions between the pyrimidine part of the adenine ring and the nicotinamide would occur in water more than in acetonitrile, facilitated by the formation of H-bonds; the result would be the substantial shielding of 2_N-H and 2-H. Conversely, 6_N-H and 8-H, because of their positions on the aromatic rings, would be only partially involved in the shielding interactions occurring between the six-membered rings; this would result in a deshielding effect stronger in water than in acetonitrile.

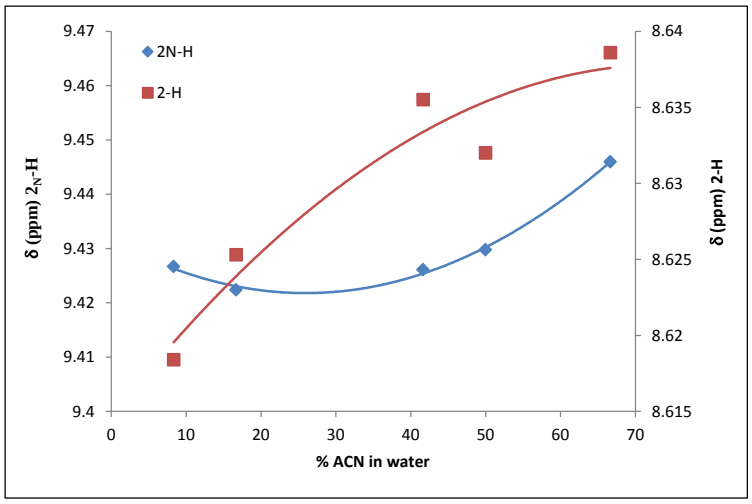

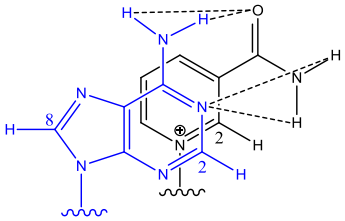

Aromatic proton	Δδ (ppb)
2_N-H	19.3
6_N-H	-9.8
4_N-H	4.3
2-H	20.2
8-H	-22.6
5_N-H	11.4

Figure 3.21 ^{1}H NMR analysis of aromatic protons in *β*-NAD$^+$ with increasing percentage of ACN. Δδ indicates the difference in chemical shift between the highest and the lowest ACN percentage: values are given in ppb (part per billion: 1000 ppb = 1 ppm). *Conditions*: solutions in D_2O of *β*-NAD$^+$ (0.0025 M) with several ACN percentage (ranging from 10 to 60% anhydrous ACN with an interval of 10%) were prepared and their ^{1}H NMR spectra recorded at rt. The spectra were referenced to the protons of CH_3 in ACN (δ_H 2.06).

Since the solvation of the aromatic rings in organic solvents promotes the passage of *β*-NAD$^+$ from a folded to an open conformation, a change in the conformation of the riboses and, consequently, in the chemical shifts and *J* coupling constants of their protons (Figure 3.22, Figure 3.23) should be observed.

The chemical shifts and *J* coupling constants of 1′-H and 1″-H were analysed. 1′-H and its $J_{1',2'}$ did not undergo any substantial change with the solvent composition. On the other hand, 1″-H did undergo an upfield shift, or a shielding effect, with increasing percentage of acetonitrile. This effect could be due to a change in the conformation of the nicotinamide ribose, which would bring 1″-H far apart from the positively charged nicotinamide ring. In addition, $J_{1'',2''}$ decreased with increasing acetonitrile percentage, indicating the preference of the nicotinamide ribose toward a N-conformation in the *β*-NAD$^+$ extended conformation (see 3.1).

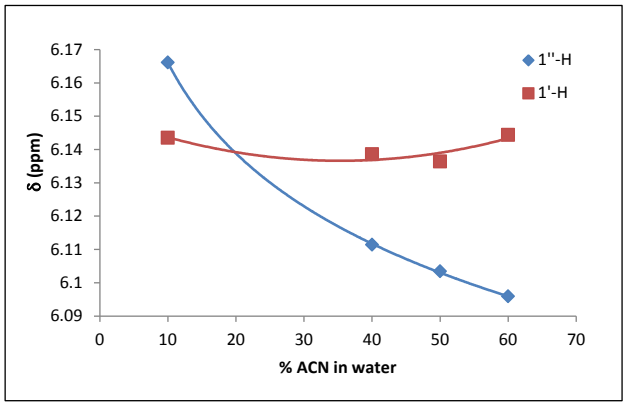

Sugar protons	Δδ (ppb)
1'-H	0.9
1''-H	-70.2

J coupling	Δ*J* (Hz)
$J_{1',2'}$	0.16
$J_{1'',2''}$	-0.44

Figure 3.22 ^{1}H NMR analysis of 1′-H and 1″-H in β-NAD^{+} with increasing percentage of ACN. Δδ indicates the difference in chemical shift between the highest and the lowest ACN percentage: values are given in ppb (part per billion: 1000 ppb = 1 ppm). *Conditions*: solutions in D_2O of β-NAD^{+} (0.0025 M) with several ACN percentage (ranging from 10 to 60% anhydrous ACN with an interval of 10%) were prepared and their ^{1}H NMR spectra recorded at rt. The spectra were referenced to the protons of CH_3 in ACN (δ_H 2.06).

In Figure 3.23, the NMR peaks for 1′-H and 1″-H are shown at different acetonitrile percentage. 1″-H showed a substantial upfield shift compared to 1′-H with increasing acetonitrile percentage. The 1″-H peak, during its upfield shift, overlapped the 1′-H peak at 20% of acetonitrile.

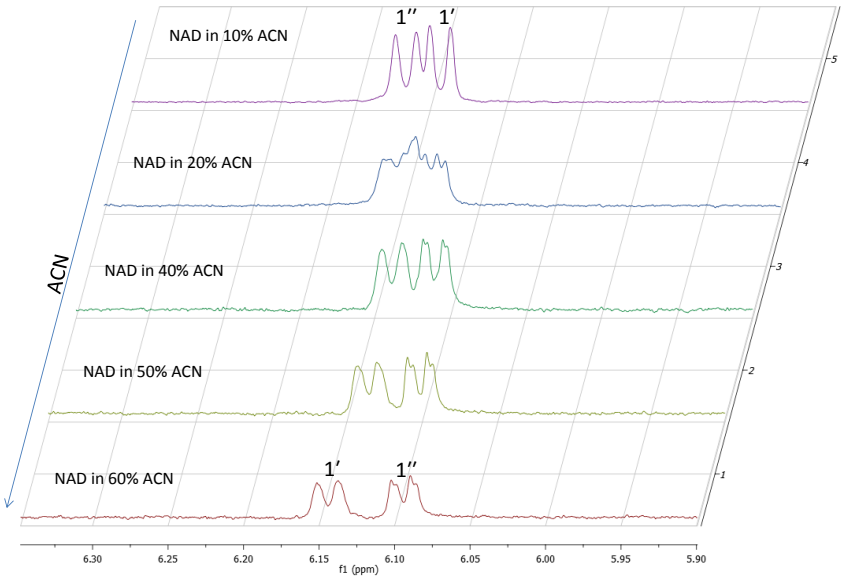

Figure 3.23 ^{1}H NMR peaks of 1′-H and 1″-H in β-NAD^{+} with increasing percentages of ACN. *Conditions*: solutions in D_2O of β-NAD^{+} (0.0025 M) with several ACN percentage (ranging from 10 to 60% anhydrous ACN with an interval of 10%) were prepared and their ^{1}H NMR spectra recorded at rt. The spectra were referenced to the protons of CH_3 in ACN (δ_H 2.06).

In **15h**, a downfield shift with increasing acetonitrile percentage occurred for all aromatic signals with stronger or weaker intensity, indicating an extended "shielding-increasing" ring current involving all aromatic protons (Figure 3.24). However, 2-H, which in β-NAD$^+$ was undergoing a strong downfield shift, in **15h** showed only a very weak shift. This effect could be due to the deshielding effect played by the close phosphate group, since the adenine ring assumed in **15h** a *syn* conformation (Figure 3.25).

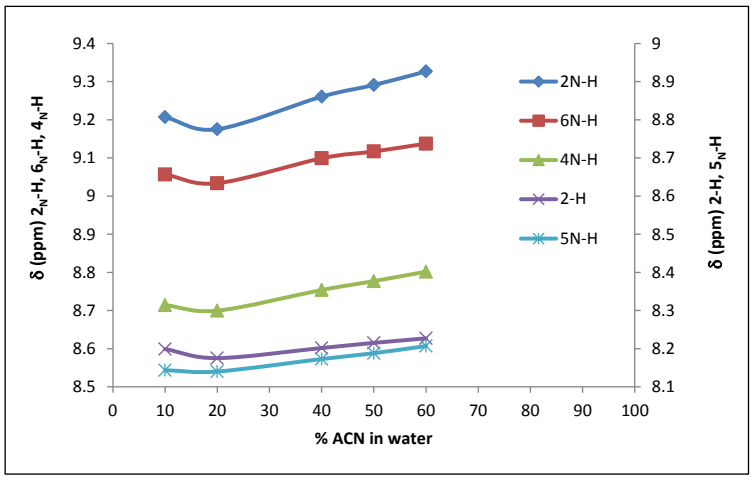

Aromatic proton	Δδ (ppb)
2_N-H	119.9
6_N-H	81
4_N-H	87.7
2-H	28.1
5_N-H	63.3
5_{py}-H	11.8
3_{py}-H	60.9
4_{py}-H	9.9

Figure 3.24 ^{1}H NMR analysis of aromatic protons in **15h** with increasing percentage of ACN. Δδ indicates the difference in chemical shift between the highest and the lowest ACN percentage: values are given in ppb (part per billion: 1000 ppb = 1 ppm). *Conditions*: solutions in D_2O of **15h** (0.0025 M) with several ACN percentage (ranging from 10 to 60% anhydrous ACN with an interval of 10%) were prepared and their ^{1}H NMR spectra recorded at rt. The spectra were referenced to the protons of CH_3 in ACN (δ_H 2.06).

In **15h**, 1′-H and 1″-H, conversely to their behaviour in β-NAD$^+$, showed a downfield shift, or a deshielding effect, with increasing acetonitrile percentage (Figure 3.26). This effect could indicate the involvement of these protons in the "shielding-increasing" ring current, stronger in **15h** than in β-NAD$^+$. In addition, $J_{1',2'}$ and $J_{1'',2''}$ decreased with increasing acetonitrile percentage. Therefore, during the passage of **15h** from a folded to an open conformation, both riboses puckered toward a N-conformation (see 3.1), especially the nicotinamide ribose.

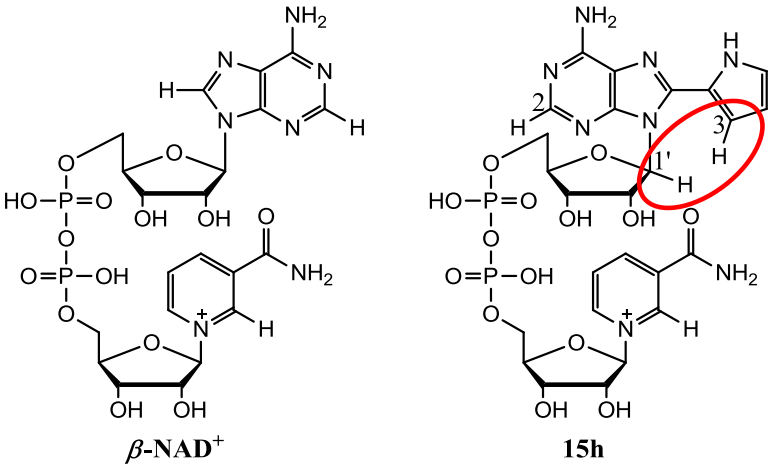

Figure 3.25 β-NAD$^+$ and **15h** folded conformations.

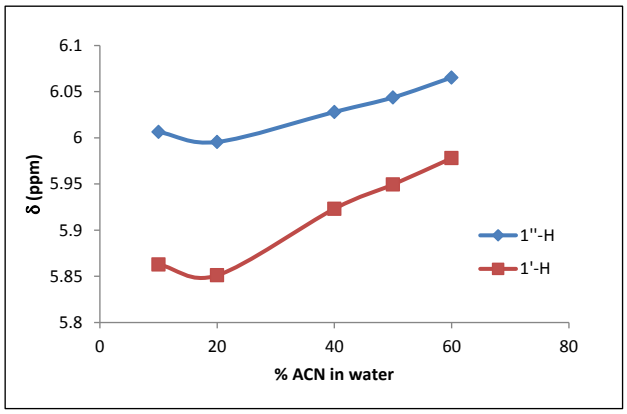

Sugar protons	Δδ (ppb)
1'-H	115.1
1''-H	58.9

J coupling	Δ*J* (Hz)
$J_{1',2'}$	-80
$J_{1'',2''}$	-200

Figure 3.26 ^{1}H NMR analysis of 1′-H and 1″-H in **15h** with increasing percentage of ACN. Δδ indicates the difference in chemical shift between the highest and the lowest ACN percentage: values are given in ppb (part per billion: 1000 ppb = 1 ppm). *Conditions*: solutions in D_2O of **15h** (0.0025 M) with several ACN percentage (ranging from 10 to 60% anhydrous ACN with an interval of 10%) were prepared and their ^{1}H NMR spectra recorded at rt. The spectra were referenced to the protons of CH_3 in ACN (δ_H 2.06).

From the 2D NOESY experiment on **15h**, no particular NOE signals were observed, with the exception of that correlating 1′-H and 3*pyrrole* -H, as expected because of the *syn* conformation of the adenine and the consequent proximity of the two protons (Figure 3.25). Unfortunately, the molecular weight of **15h** is in the range where the NOE signal should be theoretically zero; consequently, the 2D NOESY experiment did not allow observation of any interaction between the aromatic bases.

Of course, it is difficult to predict only from the ^{1}H NMR experiments the presence of β-NAD^{+} and its derivatives in solution in a folded or open conformation. Many studies have been undertaken to find a univocal solution using different techniques; however, contrasting opinions have been often reached.[64, 214-216] Surely, intramolecular interactions between the aromatic bases are present in aqueous solutions of β-NAD^{+}, due to stacking or just proximity effects. However, it is not possible to exclude the presence of intermolecular stacking interactions depending on the concentration. In addition, the interactions between the nucleobases could occur in many different ways, depending on the orientation of the aromatic faces.[214] The results shown here seem at least to confirm the presence of interactions between the aromatic bases in aqueous solutions and, in particular, a stronger effect occurring in **15h** compared to β-NAD^{+}. This is in agreement with what we would expect from a more extended π-electron delocalization occurring in the 8-(pyrrol-2-yl) adenine, which increases the eventual π-stacking interactions with the nicotinamide ring.

3.8 Conclusions

In contrast to the non-emissive adenine derivatives modified in position 2 or 6 with aryl/heteroaryl substituents, the fluorescence features of 8-aryl/heteroaryl adenine derivatives make them interesting compounds from the perspective of the applicability as biochemical tools to investigate enzymatic structures, bindings and activities. Indeed, since the development of the ε-adenine derivatives and their versatile biological applications, not many other isomorphic fluorescent adenine derivatives have been developed with the same purpose of fluorescent probes. However, in this series of isomorphic emissive 8-aryl/heteroaryl adenine derivatives a new fluorophore class can be identified with tunable fluorescent properties and, in some cases, as will be shown later, unique behaviours toward certain types of enzymes. A comparison between ε-adenine and 8-aryl/heteroaryl adenine derivatives is shown in Table 3.11 and Figure 3.27.

ε-adenine derivatives	*8-aryl/heteroaryl adenine derivatives*
Fixed modification (etheno bridge)	Variable modification (aryl/heteroaryl substituent)
N-1 and NH_2 blocked	N-1 and NH_2 free for H-bonds
Adenine in *anti* conformation	Adenine in *syn* conformation
λ_{ex} = 306 nm; λ_{em} = 410 nm (ε-NAD^+)	λ_{ex} = 309 nm; λ_{em} = 374 nm (**15h**)
$\Phi_{AMP/NAD}$ = 20 (ε-NAD^+)	$\Phi_{AMP/NAD}$ = 44 (**15h**)

Table 3.11 Comparison between ε-adenine and 8-aryl/heteroaryl adenine derivatives.

A characteristic feature of 8-aryl/heteroaryl adenine derivatives is their highly variable structure, due to the large range of substituents that can be introduced on C-8 of the adenine ring by Suzuki-Miyaura cross-coupling. As shown later in the chapter, by changing the substituent, it is possible to modulate the fluorescent properties of the compounds. Therefore, it would be theoretically possible to predict the fluorescent properties depending on the nature of the introduced substituents. This structural variability is not applicable to the ε-adenine, where the etheno bridge, extending the aromaticity of the modified adenine ring, is responsible for the fluorescent properties of the compounds. No substantial modifications can be performed on its structure to change or tune the fluorescent features of this fluorophore class, resulting therefore in a big disadvantage compared to emissive 8-aryl/heteroaryl adenine derivatives.

In addition to the fact that ε-adenine structure cannot be modified to increase fluorescence, the introduction of the etheno bridge between the exocyclic amino group and N-1 on the pyrimidine ring blocks two important moieties responsible for enzyme recognition and binding. Conversely, the new fluorophore class leaves the adenine structure unaltered making the compounds more similar to the natural substrate and, therefore, more likely to interact with the enzymes.

The two fluorophore classes differ also in the orientation of the modified adenine rings related to their riboses; indeed, ε-adenine prefers an *anti* conformation, while 8-aryl/heteroaryl adenine a *syn* conformation. This difference could have separate influences on their biological activities toward NAD^+-consuming enzymes, as will be discussed in Chapter 4 and 5.

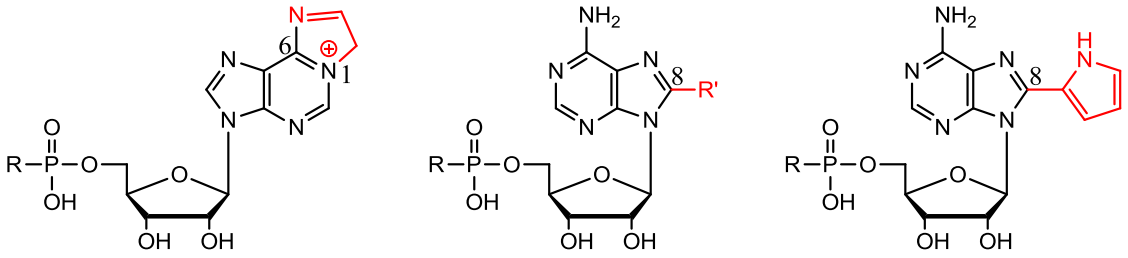

AMP derivatives: R = OH
NAD^+ derivatives: R = β-NMN
R' = aryl/heteroaryl

Figure 3.27 Structures for ε-adenine and 8-aryl/heteroaryl adenine derivatives.

A common feature between the two fluorophore classes is represented by the internal fluorescence quenching occurring in the NAD^+ derivatives. Based on the example of ε-NAD^+ and depending on its ability to act as a NNS for NAD^+-consuming enzymes, 8-(pyrrol-2-yl) NAD^+ (**15h**), the most promising fluorescent 8-aryl/heteroaryl NAD^+ derivative synthesized in Chapter 2, will be used to set up fluorescence-based assays for NAD^+-consuming enzymes. Indeed, this compound, as seen with ε-NAD^+, is characterized by λ_{ex} and λ_{em} not interfering with the protein fluorescence; in addition, its fluorescence quenching, ~ 2 fold stronger than ε-NAD^+, could allow an increase in sensitivity of the fluorescence-based assays.

4 EVALUATION OF 8-ARYL/HETEROARYL NAD+ DERIVATIVES AS FLUORESCENT PROBES FOR NAD+-CONSUMING ENZYMES

As mentioned in Chapter 1, NAD^+-consuming enzymes are fundamental in all organisms as they are involved in many major biological processes. These enzymes use β-NAD^+ as a substrate/co-substrate, cleaving the high energy bonds present in its structure; then, the energy released can be used for the synthesis of signalling molecules or transferred to other acceptors to catalyze further reactions. Several different types of NAD^+-consuming enzymes are present in cells and have a variety of functions, often related to each other. The knowledge of their activities is therefore crucial to understand many biological processes and their pathological implications.

This chapter will review activities and reaction mechanisms of some representatives of major classes of NAD^+-consuming enzymes, in particular those belonging to the ecto-enzymes class, such as NPPs, ADPRCs and NADases, responsible for the extracellular β-NAD^+ homeostasis. Since β-NAD^+ is the only substrate involved in their catalytic reactions, they will be used as a model for the proof of concept of the use of NAD^+ derivatives as biochemical tools.

In particular, the biological evaluation of **15h** as a fluorescent NNS for the selected NAD^+-consuming enzymes will be provided, and its use for the development of fluorescence-based assays for their monitoring will be assessed. Indeed, this compound, amongst all NAD^+ derivatives synthesized in Chapter 2, has shown the best fluorescent features to compete with ε-NAD^+ as an alternative biochemical probe for the monitoring of the NAD^+-consuming enzyme activities. Its fluorescence stability between pH 6 and 9, the pH working range for several NAD^+-consuming enzymes, and its λ_{ex} and λ_{em} not overlapping with those of biological systems, make it a good fluorophore for biological applications. In addition, the internal fluorescence quenching occurring in **15h** is ~ 2 fold bigger than that occurring in ε-NAD^+, possibly making it a more sensitive probe in fluorescence-based assays. Moreover, the intact adenine structure in **15h** could be an advantage compared to ε-NAD^+ in terms of interactions and recognition by NAD^+-consuming enzymes.

4.1 Nucleotide pyrophosphatases (NPPs)

Nucleotide pyrophosphatases/phosphodiesterases (NPPs) belong to the same class of enzymes, able to catalyze the hydrolysis of pyrophosphate or phosphodiester bonds of a variety of nucleotides to give nucleoside 5′-monophosphates.[16] A broad range of possible substrates are accepted by NPPs.

Mammalian NPPs are also called ecto-NPPs (ENPPs) since most of them are ecto-enzymes, or enzymes situated on the outer membrane of the cell and characterized by having their catalytic site in the extracellular space. The activity of these enzymes in the extracellular space seems to be fundamental to regulate the extracellular balance between nucleotides and nucleosides connected to a variety of events, such as nucleotide/nucleoside signalling (purinergic modulation signalling), the salvage pathway of many nucleotides, bone and cartilage mineralization, and insulin signalling.[16, 17, 219, 220] Because of these activities, an increased interest toward mammalian ENPPs has developed to fully characterize and define their structure, active site and reaction mechanism.

ENPPs share the same reaction mechanism already identified for snake venom phosphodiesterases:[48] it is a two-step mechanism, involving a covalent enzyme-nucleotidylate intermediate by a threonine catalytic residue (Scheme 4.1).[221] The ENPPs catalytic site contains two divalent cations, coordinating the phosphate group of pyrophosphate or phosphodiester bonds of the incoming nucleotides, B*pp*B′ and B*p*B′ respectively. A nucleophilic residue, such as threonine (T256) in human NPP1, attacks the phosphate with consequent release of a leaving group, such as a nucleotide B′*p* or a nucleoside B′, and formation of a covalent enzyme-nucleotidylate intermediate (**I**). Therefore, a molecule of water, activated by coordination to the cation, would attack the phosphate, regenerating the catalytic threonine and releasing the product, a nucleoside 5′-monophosphate, B*p*.[16, 222]

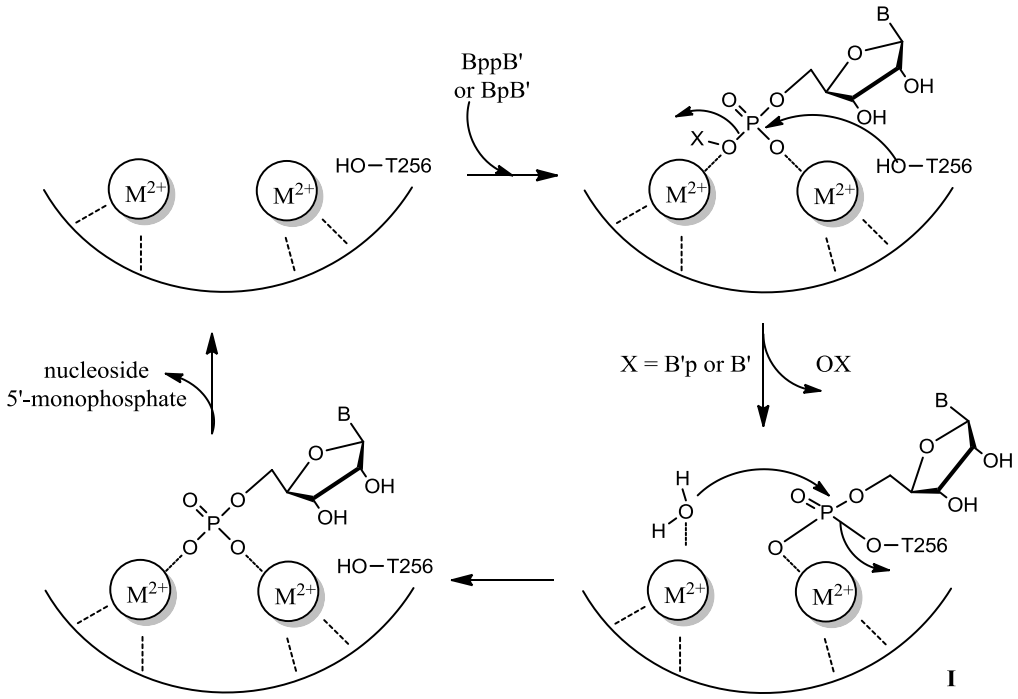

Scheme 4.1 Catalytic mechanism of ENPPs.

The observed dependence of the efficiency of the pyrophosphatase reactions on divalent cations in the reaction buffer can be explained by the necessary presence in the active site of two cations to catalyze the reaction.[223, 224] In addition, the optimum basic pH for the pyrophosphatase reaction helps to speed the second reaction step, where a more nucleophilic hydroxide, instead of a neutral molecule of water, would attack the phosphate group.

In contrast to the several studies performed on snake venom phosphodiesterases and ENPPs, little information is known about the commercially available nucleotide pyrophosphatase from *Crotalus adamanteus* venom. This enzyme has wide application in the chemo-enzymatic synthesis of nucleotide derivatives with quite good yields[225] but has not been fully characterized. Here, its activity as a nucleotide pyrophosphatase, its properties and reaction mechanism will be discussed in accordance with its assumed similarity to other well described nucleotide pyrophosphatases/phosphodiesterases.

4.1.1 Fluorescence-based assay for nucleotide pyrophosphatase

Compound **15h** was tested as a NNS of the commercially available nucleotide pyrophosphatase (NPP) from *Crotalus adamanteus* venom. This enzyme catalyzes the cleavage of *β*-NAD$^+$ on the pyrophosphate bond to produce AMP and *β*-NMN.

The enzymatic reaction was monitored by HPLC to check the suitability of **15h** as a substrate for NPP; in fact, the enzyme recognised the NNS and catalyzed its hydrolysis on the pyrophosphate bond generating *β*-NMN and **9h**,[172] as confirmed by the use of standards for the two reaction products (Figure 4.1).

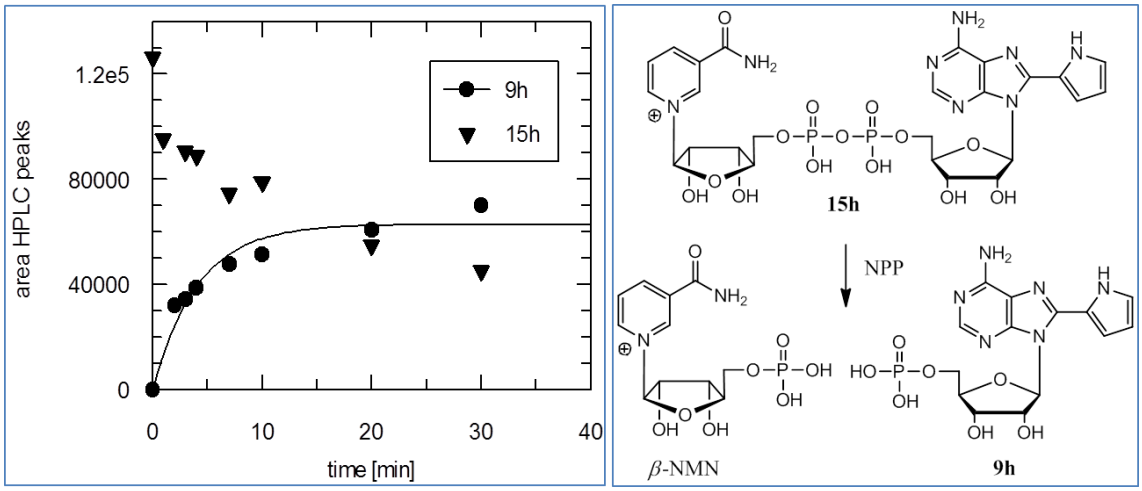

Figure 4.1 HPLC time-course of the enzymatic reaction of NPP from *Crotalus adamanteus* venom and **15h**. *Conditions*: NPP (0.01 U/mL), **15h** (24.74 μM), $MgCl_2$ (10 mM), Tris/HCl buffer (50 mM, pH 8), 30 °C; all concentrations are final concentrations. Data from single experiment, peak area *vs* time [min], data plotting to a 1st order rate equation with Grafit5.

Since NPP was able to recognise and convert **15h** into **9h**, the opportunity for monitoring the enzymatic reaction by fluorescence was investigated. Owing to the fluorescence internal quenching occurring in **15h** compared to **9h** (Chapter 3, see 3.7.1), a fluorescence increase due to the production of **9h** from the cleavage of **15h** was observed with the progress of the enzymatic reaction (Figure 4.2), proving the possibility to prepare fluorescence-based assays to monitor NPP activity, similar to those developed with ε-NAD$^+$.[87, 89]

Kinetic experiments for the estimation of kinetic parameters, as K_m and V_{max}, for NPP toward the new substrate **15h** were set up. After confirming the linearity of the fluorescence response across a range of concentrations for both **15h** and its enzymatic product **9h**, initial reaction velocities were measured as a function of NPP concentration at a fixed **15h** concentration to explore the rate changes with NPP concentration (Appendix 8, Figure A2). Initial velocities were found to be proportional at low NPP concentration, before the substrate **15h** became the limiting factor. A suitable enzyme/substrate ratio was established to have smooth enzymatic reaction rates from which to calculate linear initial velocities. Afterwards, the substrate concentration was varied to generate a saturation curve for the determination of the value of K_m.

At this stage, the experiment set-up required a considerable optimization to establish the appropriate conditions to reduce and control the variability affecting the results and attributed to several factors influencing the fluorescence signal. Major issues identified were the temperature changes within the wells of the microplate, due to the addition of the cold enzyme solution at the beginning of the reaction, and the instability of the fluorescence signal. To address these problems, a few precautions were taken, such as the addition of all components of the reaction into the microplate at room temperature and always in the same order; a fluorescence stabilization period was allowed before starting the reaction; shaking of the microplate occurred before each cycle of measurement; use of 120 µL total volume in the wells (100 – 250 µL is the volume range suggested for the NUNC 96 plate). The introduction of positive and negative controls into the microplate was useful to check the variability sources in the experiments. The buffer alone was used as a negative control, while the reaction product, **9h**, at a fixed concentration was used as a positive control. Their variability was checked across the plate after the fluorescence signal stabilization and during the reaction time to guarantee a uniform fluorescence signal. No particular fluorescence trends were noticed across the plate, indicating the suitability of NUNC 96 plate for these experiments.

All experiments were run at least in duplicate. The raw data showed time-courses of fluorescence intensity, expressed in RFU [relative fluorescence unit], *versus* time [sec]. The fluorescence difference between the positive control (**9h** at a fixed concentration) and the negative control (buffer) allowed conversion of the fluorescence intensity into **9h** concentration [μM], necessary to estimate V_{max} (Figure 4.2).

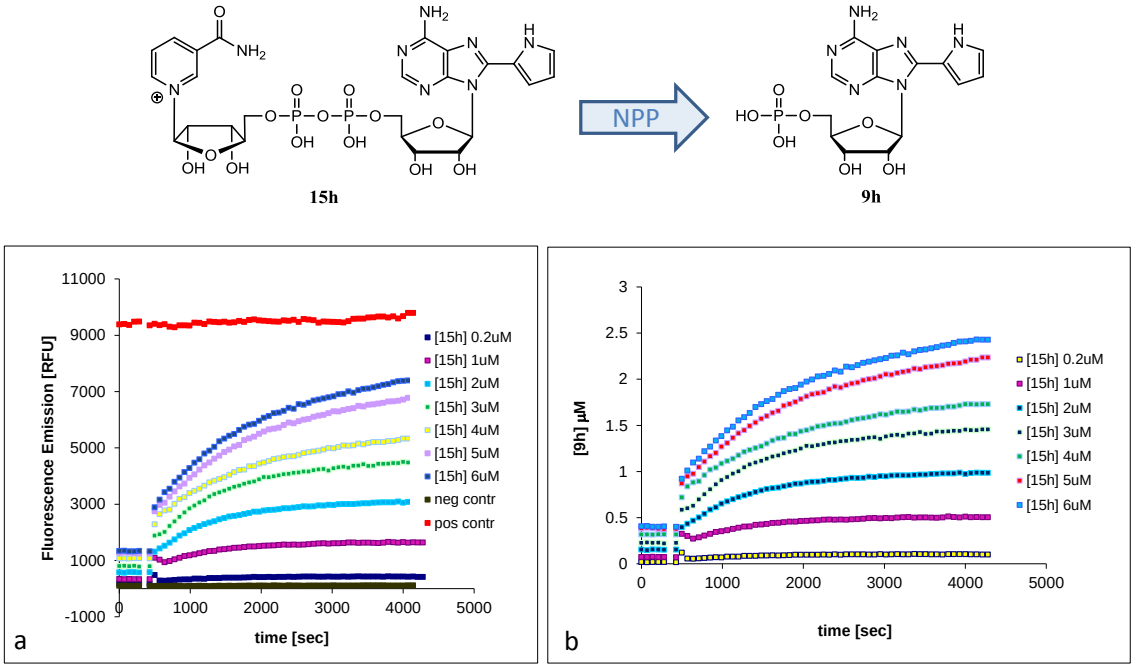

Figure 4.2 Fluorimetric assay of NPP from *Crotalus adamanteus* venom and **15h**. **a)** fluorescence time-course as fluorescence emission [RFU] *vs* time [sec]; **b)** fluorescence time-course as **9h** concentration [μM] *vs* time [sec]. *Conditions*: NPP (0.007 U/mL), **15h** (0.2 – 6 μM), $MgCl_2$ (10 mM), Tris/HCl buffer (50 mM, pH 8), 30 ºC, λ_{ex} = 300 nm, λ_{em} = 410 nm, gain 15%. Enzyme addition at 420 sec. Positive control: **9h** (3 μM). Negative control: buffer; all the concentrations are final concentrations. Each data point is the mean of experiments run in duplicate, data plotting with Excel.

Variation of initial velocity with **15h** concentration was well described by the Michaelis-Menten equation (Figure 4.3), and Lineweaver-Burk and Hanes-Woolf plots (Appendix 8, Figure A3).[172] Values for K_m and V_{max} of NPP related to **15h** were determined by non-linear regression analysis of the Michaelis-Menten plot, resulting in an average K_m value of 1.5 ± 0.4 μM and V_{max} of 0.001 ± 0.0001 μmol·min^{-1}·mg^{-1}.

The presence of Mg^{2+} in the buffer was required to stimulate the enzymatic reaction;[223, 224] indeed, V_{max} showed a drop of ~ 3.5 fold when the reaction was carried out in absence of $MgCl_2$ (data not shown).

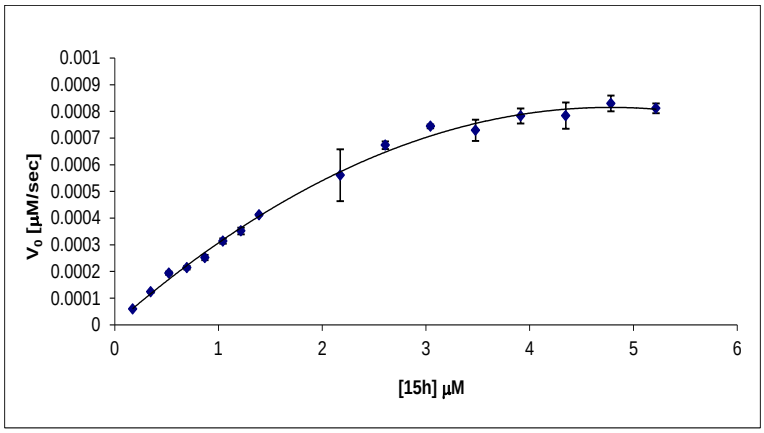

Figure 4.3 Michaelis-Menten plot of NPP from *Crotalus adamanteus* venom with **15h**. *Conditions*: NPP (0.007 U/mL), **15h** (0.2 – 5.2 µM), $MgCl_2$ (10 mM), Tris/HCl buffer (50 mM, pH 8), 30 ºC, λ_{ex} = 300 nm, λ_{em} = 410 nm, gain 15%; all concentrations are final concentrations. Initial velocity values (V_0) were calculated from the corresponding time-courses measuring the fluorescence signals generated when 10% product was formed. Each data point is the mean (± SD) of experiments run in duplicate, data plotting with Excel.

To assess the NPP site of **15h** binding and transformation, experiments were performed to evaluate the impact of *β*-NAD^+, AMP and *β*-NMN on the rate of hydrolysis for **15h** by NPP. Competition experiments with *β*-NAD^+ showed a decrease of NPP activity related to **15h** for increasing quantity of *β*-NAD^+ in solution: at concentrations of *β*-NAD^+ above *ca* 250 µM, there was no significant indication of catalysis. An IC_{50} value of 12.8 ± 3.8 µM was estimated for *β*-NAD^+ (Figure 4.4).

For greater insight into the mode of inhibition exhibited by *β*-NAD^+ toward the activity of NPP related to **15h**, kinetic analysis was performed for a range of *β*-NAD^+ concentrations (Figure 4.5, Appendix 8, Figure A4). From the data analysis, *β*-NAD^+ turned to be a competitive inhibitor of **15h**; indeed, V_{max} did not change with increasing *β*-NAD^+ concentrations, while the K_m value of **15h** related to NPP increased because of a lower affinity for the binding site.

This was in agreement with what observed in the IC_{50} experiment. In addition, a K_i value for β-NAD^+ of 7.4 ± 1.7 µM was estimated from the Dixon plot (Figure 4.5).

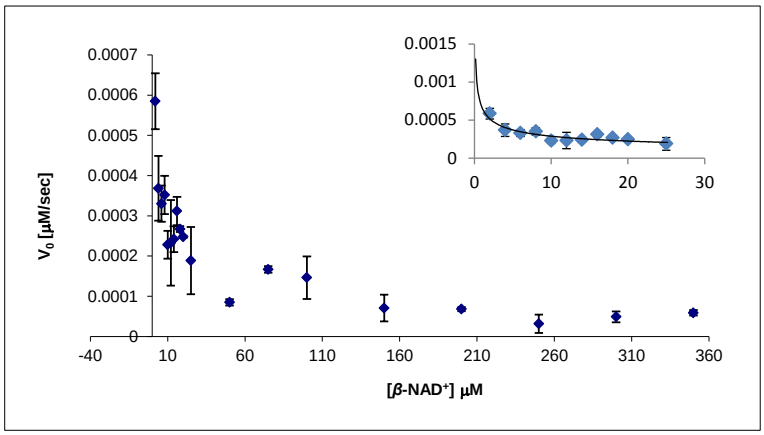

Figure 4.4 IC_{50} estimation for β-NAD^+ toward the activity of NPP from *Crotalus adamanteus* venom and **15h**. *Conditions*: NPP (0.007 U/mL), **15h** (4.4 µM), β-NAD^+ (0 – 350 µM), $MgCl_2$ (10 mM), Tris/HCl buffer (50 mM, pH 8), 30 ºC, λ_{ex} = 300 nm, λ_{em} = 410 nm, gain 15%; all concentrations are final concentrations. Initial velocity values (V_0) were calculated from the corresponding time-courses measuring the fluorescence signals generated when 10% product was formed. The insert shows the range of β-NAD^+ (0 – 25 µM) where the NPP activity drastically decreases. Each data point is the mean (± SD) of experiments run in duplicate, data plotting with Excel.

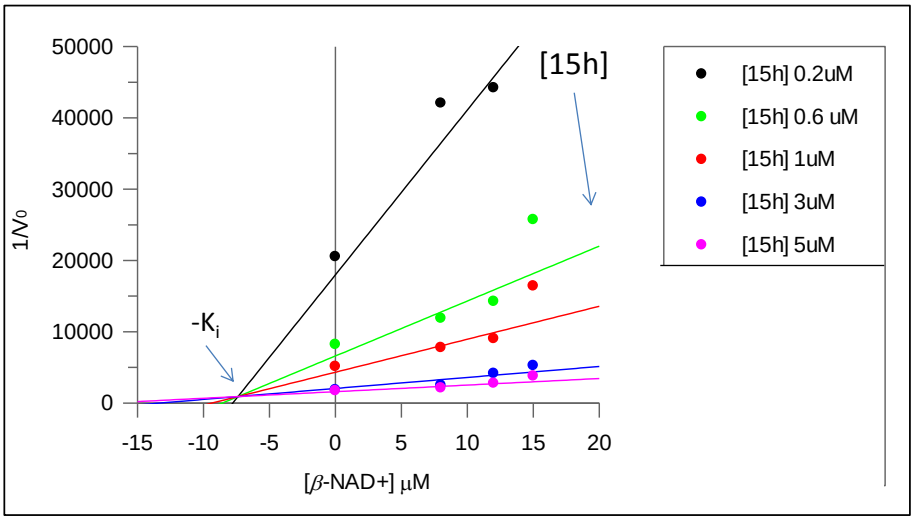

Figure 4.5 Dixon plot for β-NAD^+ inhibition toward the activity of NPP from *Crotalus adamanteus* venom and **15h**. *Conditions*: NPP (0.007 U/mL), **15h** (0.2 – 5 µM), β-NAD^+ (8 – 15 µM), $MgCl_2$ (10 mM), Tris/HCl buffer (50 mM, pH 8), 30 ºC, λ_{ex} = 300 nm, λ_{em} = 410 nm, gain 15%; all concentrations are final concentrations. Initial velocity values (V_0) were calculated from the corresponding time-courses measuring the fluorescence signals generated when 10% product was formed. Each data point is the mean (± SD) of experiments run in duplicate, data plotting with Grafit5. The *x* value for the lines intersection is equal to $-K_i$; the *y* value for the lines intersection is equal to $1/V_{max}$.

To understand the influence of AMP and *β*-NMN on the NPP activity and their possible mode of inhibition related to **15h**, kinetic analyses were performed for a range of AMP (Figure 4.6) and *β*-NMN concentrations.

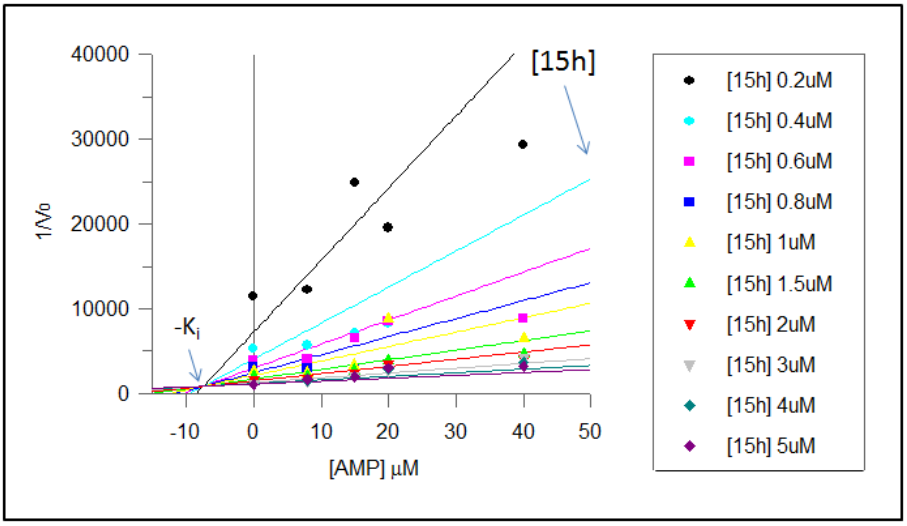

Figure 4.6 Dixon plot for AMP inhibition toward the activity of NPP from *Crotalus adamanteus* venom and **15h**. *Conditions*: NPP (0.007 U/mL), **15h** (0.2 – 5 µM), AMP (8 – 40 µM), $MgCl_2$ (10 mM), Tris/HCl buffer (50 mM, pH 8), 30 °C, λ_{ex} = 300 nm, λ_{em} = 410 nm, gain 15%; all concentrations are final concentrations. Initial velocity values (V_0) were calculated from the corresponding time-courses measuring the fluorescence signals generated when 10% product was formed. Each data point is the mean (± SD) of experiments run in duplicate, data plotting with Grafit5. The *x* value for the lines intersection is equal to $-K_i$; the *y* value for the lines intersection is equal to $1/V_{max}$.

From the data analysis, AMP turned to be a competitive inhibitor of **15h**; indeed, V_{max} did not change, while the K_m value for **15h** increased with increasing *β*-NAD^+ concentrations. The estimated K_i for AMP from the Dixon plot was 7.5 ± 1.6 µM.

Oppositely to AMP, *β*-NMN turned to not compete with **15h** for NPP binding site in our experimental conditions; indeed, both K_m and V_{max} for **15h** toward the NPP activity remained approximately the same with increasing *β*-NAD^+ concentrations (data not shown).

4.1.2 Kinetic analysis of NPP activity

The K_m and V_{max} values obtained for **15h** related to the activity of NPP from *Crotalus adamanteus* venom were compared to those found in the literature for *β*-NAD^+ and other fluorescent derivatives (ε-NAD^+, ε-$PdAD^+$ and ε-hy^4$PdAD^+$) related to several pyrophosphatases (Table 4.1).[89, 223, 226-230] NPPs are generally characterized by a wide substrate specificity, with the enzyme recognition requiring mainly the presence of a pyrophosphate bond. However, in detailed studies of some NPPs, particular trends in the substrate affinities were observed. In particular, a nucleotide pyrophosphatase isolated from *Haemophilus influenzae* showed different substrate affinities for the binding site depending on the aromatic rings of the analysed dinucleotides. It was found that the enzyme recognition was strongly influenced by the adenine ring and its modifications, more than by the presence of the nicotinamide ring and its derivatives. The poor substrate activity of ε-NAD^+ appeared to be due more to the steric hindrance of the modified adenine ring in the active site than to the loss of the exocyclic amino group and, consequently, H-bonding ability.[226]

Organism	*β-NAD$^+$*		*ε-NAD$^+$[a] or ε-PdAD$^+$[b]*		***15h***	
	K_m (mM)	*V_{max} (μmol· min^{-1}·mg^{-1})*	*K_m (mM)*	*V_{max} (μmol· min^{-1}·mg^{-1})*	*K_m (mM)*	*V_{max} (μmol· min^{-1}·mg^{-1})*
Haemophilus parasuis[227]	0.0041	13.5	0.144[a]	2.5[a]	n.a.	n.a.
Haemophilus influenzae[226]	0.0054	2.7	0.632[a]	3.6[a]	n.a.	n.a.
Yeast[228]	0.17	0.09	*n.a.*[c]	*n.a.*	*n.a.*	*n.a.*
Potato[229, 230]	0.05	*n.a.*	0.013[a]	*n.a.*	*n.a.*	*n.a.*
Rat liver[223]	0.028	*n.a.*	*n.a.*	*n.a.*	*n.a.*	*n.a.*
Mouse splenocytes[89]	*n.a.*	*n.a.*	0.29 – 0.33[b]	*n.a.*	*n.a.*	*n.a.*
Crotalus adamanteus	*n.a.*	*n.a.*	*n.a.*	*n.a.*	0.0015	0.001

[a]ε-NAD^+; [b]ε-$PdAD^+$; [c]not available.

Table 4.1 Enzymological properties for *β*-NAD^+, ε-NAD^+ and the related dinucleotide ε-$PdAD^+$, and **15h** with different nucleotide pyrophosphatases.

Compound **15h** was found to have a very low K_m value related to the NPP from *Crotalus adamanteus* venom, much closer to that of the natural *β*-NAD^+ than those of etheno-derivatives for other NPPs. This result suggested a strong affinity of **15h** for the enzyme active site, due to the similarity of 8-(pyrrol-2-yl) adenine to adenine of the natural *β*-NAD^+. However, the low V_{max} indicated that the substitution in position 8 on the adenine ring, although tolerated by NPP during the binding of **15h** in the active site, was strongly influencing its catalytic mechanism.

From the IC_{50} determination and the kinetic analyses performed to understand the *β*-NAD^+ mode of inhibition, *β*-NAD^+ was confirmed to be a competitive inhibitor related to **15h**, indicating their binding on the same ligand site.

Regarding AMP and *β*-NMN, it would be expected that both, as reaction products, are competitive inhibitors related to *β*-NAD^+ for the NPP activity. In fact, although AMP was found to be a strong competitive inhibitor for several NPPs (Table 4.2), *β*-NMN had no relevant activity, indicating again a stronger affinity of NPPs for the adenine moiety of the dinucleotides.[226, 227, 230] In accordance with the literature, in this study AMP turned to be a competitive inhibitor related to **15h**, with a K_i value similar to that of *β*-NAD^+, indicating the strong affinity of NPPs for the adenine moiety of dinucleotides. In contrast, *β*-NMN did not exert any inhibition toward NPP from *Crotalus adamanteus* venom.

Organism	*AMP*	*β-NMN*
	K_i (mM)	*K_i (mM)*
Haemophilus parasuis[227]	0.0366	inactive
Haemophilus influenzae[226]	0.0151	inactive
Potato[230]	0.145	inactive
Crotalus adamanteus	0.0075	inactive

Table 4.2 Competitive inhibition of AMP and *β*-NMN toward different nucleotide pyrophosphatases.

In addition, kinetic experiments were performed with the other 8-aryl/heteroaryl NAD^+ derivatives synthesized in Chapter 2, to confirm the reasonable choice of **15h** as a fluorescent probe for the development of fluorescence-based assays. **15b** and **15c** acted both as NNSs toward NPP from *Crotalus adamanteus* venom, as confirmed by a

fluorescence increase occurring during the enzymatic reaction with NPP (Appendix 8, Figure A5, Figure A6). However, the fluorescence difference generated along the reaction course was smaller than that occurring with **15h**, because of a smaller fluorescence internal quenching in **15b** and **15c** compared to **15h**. By contrast, **15e** and **15g** did not show any fluorescence increase during the progress of the enzymatic reaction. Assuming their activity as NNSs of NPP because of their belonging to the class of 8-substituted NAD^+ derivatives, this result was predictable for **15e**, since no fluorescence internal quenching was observed compared to its corresponding AMP derivative, **9e**. However, this result was surprising for **15g**, since it had shown a large fluorescence internal quenching compared to its corresponding AMP derivative, **9g**. Probably, because of their extremely low Φ values, the fluorescence assay was not sensitive enough to detect the fluorescence changes.

4.2 NAD^+-glycohydrolases (NADases) and ADP-ribosyl cyclases (ADPRCs)

Ca^{2+} is a secondary messenger involved in cellular signalling and several intracellular controlled events.[231] The Ca^{2+} concentration inside the cells is ~ 10 – 100 nM and it is kept constant by the presence of Ca^{2+} channels, that actively pump Ca^{2+} from the cytosol to the extracellular space or into the endoplasmic reticulum in which it is stored. Sudden increases in the intracellular Ca^{2+} concentration, due to its release from the endoplasmic reticulum, are mediated by different Ca^{2+}-release pathways. The best characterized is the IP_3 (Inositol triphosphate)-mediated pathway, where IP_3 binds and opens Ca^{2+} channels on the endoplasmic reticulum, allowing Ca^{2+} release in the cytosol. Another less understood pathway is that of Ca^{2+}-induced Ca^{2+}-release (CICR), where an intracellular Ca^{2+} increase, due to influx from the extracellular space or to the IP_3-pathway, generates a further Ca^{2+} release from the endoplasmic reticulum *via* ryanodine receptors, another type of internal Ca^{2+} channel, completely independent from the IP_3 channel.

Cyclic ADPR, *c*ADPR, has been found to be an endogenous regulator of the CICR pathway, effective as much as IP_3 in the IP_3-pathway.[232, 233] *c*ADPR is formed by the removal of NaM from *β*-NAD^+, and cyclization of the remaining ADPR between N-1 of the adenine ring and C-1″ of the "northern" ribose (the one linked to NaM in the whole

β-NAD^+) in the β-configuration.[234, 235] *c*ADPR metabolism is controlled by different enzymes, its formation being catalyzed by ADP-ribosyl cyclases, while its degradation to ADPR catalyzed by *c*ADPR-hydrolases.

ADP-ribosyl cyclase (ADPRC) was first isolated from sea urchin eggs as a membrane-bound protein, but was then found in higher quantity on the *Aplysia* invertebrates as a soluble protein.[236] This enzyme initially showed only cyclase activity, catalyzing the consumption of β-NAD^+ to *c*ADPR. In contrast, *c*ADPR-hydrolases were found prevalently in brain extracts as membrane-bound proteins.[237] Homology studies underlined the similarity of the ADPRC sequence with that of the human antigen CD38, supporting the idea of them belonging to the same class of enzymes. Nevertheless, a differentiation in preferential activities has occurred during the evolution of these enzymes: ADPRC has preferentially developed the cyclase activity, while CD38 shows prevalently NAD^+-glycohydrolase (NADase) activity.[56, 63] Later, ADPRC was shown to have *c*ADPR-hydrolase activity[238] and NADase activity[71] when stressed in particular conditions. Likewise, CD38 was shown to have cyclase activity in conditions that do not favour the hydrolysis of β-NAD^+ to ADPR.[232, 239] Moreover, *c*ADPR-hydrolases found in brain extracts as membrane-bound proteins,[237] showed in turn cyclase and NADase activity,[240] as well as proclaimed NADases showed cyclase activity.[241]

These enzymes are therefore multifunctional and, depending on the substrate or the reaction conditions, show preferential activities. A unifying mechanism for *Aplysia* ADPRC, CD38 and NADases has been proposed to explain the activity differentiation between these multifunctional enzymes belonging to the same class (Scheme 4.2). A partitioning mechanism would be involved, rather than a sequential one, in which a common oxocarbenium ion would be formed from β-NAD^+ after the removal of NaM; the oxocarbenium ion would then evolve preferentially to *c*ADPR or ADPR by competitive pathways.[238] As will be discussed in 4.2.3, the *c*ADPR-hydrolase activity of *Aplysia* ADPRC is an example of a limiting form of the partitioning mechanism, in which the enzyme sequentially forms *c*ADPR, then hydrolysing it to ADPR in presence of high enzyme concentrations.

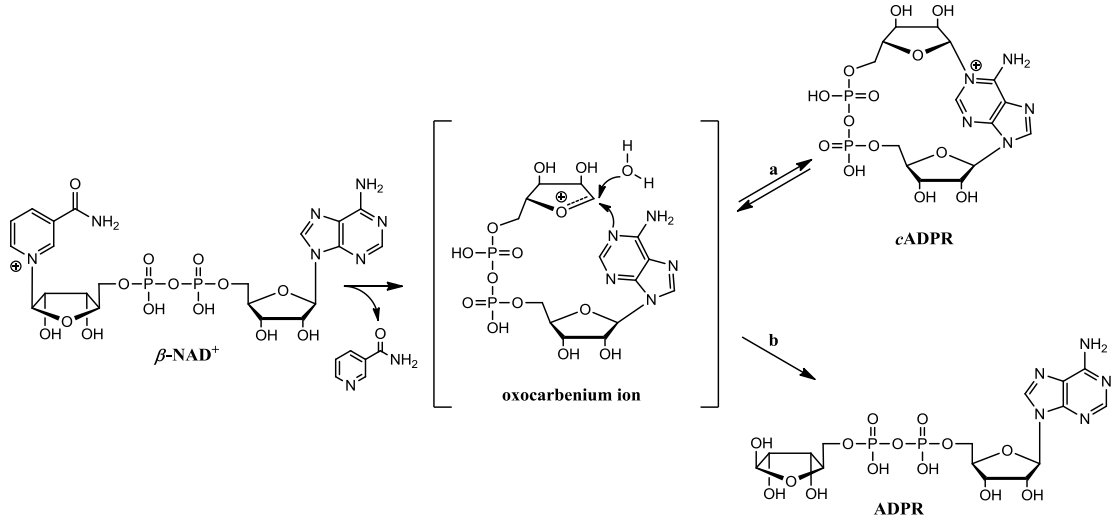

Scheme 4.2 Partitioning mechanism for *Aplysia* ADPRC, CD38 and NADases.

4.2.1 Fluorescence-based assay for NAD^+-glycohydrolase

Compound **15h** was tested as a NNS of the commercially available NAD^+-glycohydrolase (NADase) from porcine brain. This enzyme catalyzes the cleavage of the nicotinamide *N*-glycosidic bond of β-NAD^+ to produce NaM and ADPR.

The enzymatic reaction was monitored by HPLC to check the suitability of **15h** as an NADase substrate. In fact, the enzyme recognised the NNS and consumed it catalyzing its hydrolysis at the nicotinamide *N*-glycosidic bond to generate the ADPR derivative, **23**, and NaM (Figure 4.7).[172] The reaction product, **23**, was identified by ^{1}H NMR.

Once it was established that **15h** was used as a NNS by NADase, the monitoring of the NADase activity by fluorescence was attempted. However, NADase is a membrane-bound enzyme and, consequently, completely insoluble in the reaction buffer. This problem made it difficult to carry out the enzymatic reaction on a microplate reader, unless a soluble form of the enzyme was used,[87, 91, 242, 243] or samplings during the experiments were performed.[243, 244]

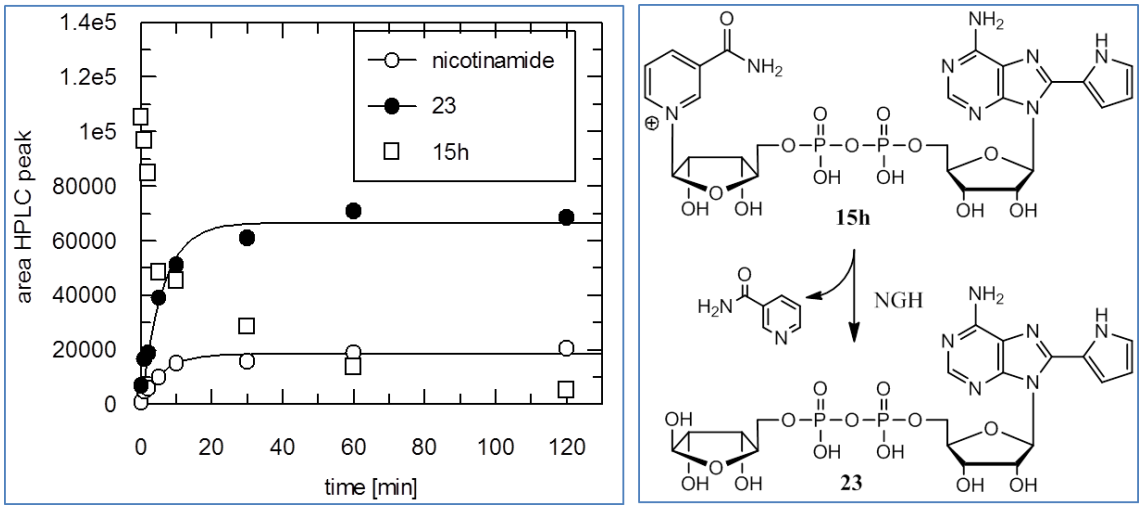

Figure 4.7 HPLC time-course of the enzymatic reaction of NADase from porcine brain and **15h**. *Conditions*: NADase (0.009 U/mL), **15h** (24.74 µM), Tris/HCl buffer (50 mM, pH 8), 37 ºC; all concentrations are final concentrations. Data from single experiment, peak area *vs* time [min], data plotting to a 1st order rate equation with Grafit5.

Since the purpose of the experiments was not to develop a fluorescence-based assay for NADase, but to show the applicability of **15h** as a biochemical tool to monitor several enzymatic reactions, we did not attempt the solubilization of the NADase. Instead, the fluorescence monitoring of the enzymatic reaction was performed in a cuvette to find out the suitability of **15h** for such applications. Unfortunately, no fluorescence increase was observed. This result was ascribed to the turbidity of the reaction mixture and the scattering due to the enzyme in suspension, which did not allow any measurement of fluorescence changes.

The only alternative to prove a fluorescence change during the progress of the enzymatic reaction was to sample the reaction mixture and read its fluorescence using the microplate reader. After filtering, diluting and reading the fluorescence of the samples, a fluorescence increase was finally observed and a time-course obtained (Figure 4.8), supporting once again the idea of using **15h** as a fluorescent probe for the monitoring of NAD^+-consuming enzyme activities. These results suggested that it is likely that a continuous fluorimetric assay could be set up with **15h** using a solubilized form of the NADase enzyme.

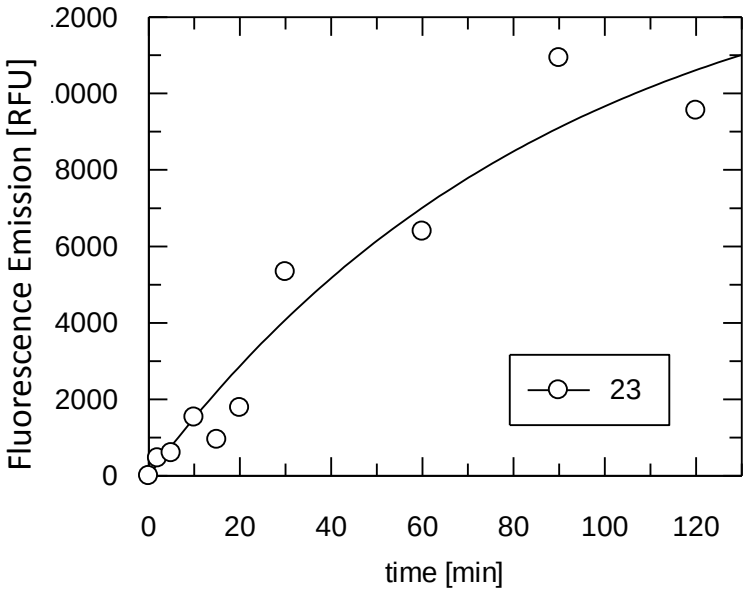

Figure 4.8 Fluorimetric assay of NADase from porcine brain and **15h**. Fluorescence time-course as fluorescence emission [RFU] *vs* time [min]. *Conditions*: NADase (0.0075 U/mL), **15h** (5.25 μM), Tris/HCl buffer (50 mM, pH 8), 37 ºC, λ_{ex} = 300 nm, λ_{em} = 410 nm, gain 15%; all concentrations are final concentrations. Data from single experiment, data plotting to a 1st order rate equation with Grafit5.

4.2.2 Fluorescence-based assay for ADP-ribosyl cyclase

Compound **15h** was tested as a NNS of the commercially available ADP-ribosyl cyclase (ADPRC) from *Aplysia californica*. This enzyme catalyzes the cyclization of *β*-NAD$^+$ to *c*ADPR with removal of NaM.

It is known from the literature that 8-substituted NAD$^+$ derivatives are recognised by this enzyme and used as NNSs to give 8-substituted *c*ADPR derivatives.[112] The enzymatic reaction was monitored by HPLC to check the suitability of **15h** as an ADPRC substrate. In fact, the enzyme recognised the NNS and consumed it, catalyzing the removal of NaM and cyclization of the remaining ADPR intermediate to the *c*ADPR derivative, **24** (Figure 4.9).[172] The reaction product, **24**, was identified by ^{1}H NMR.

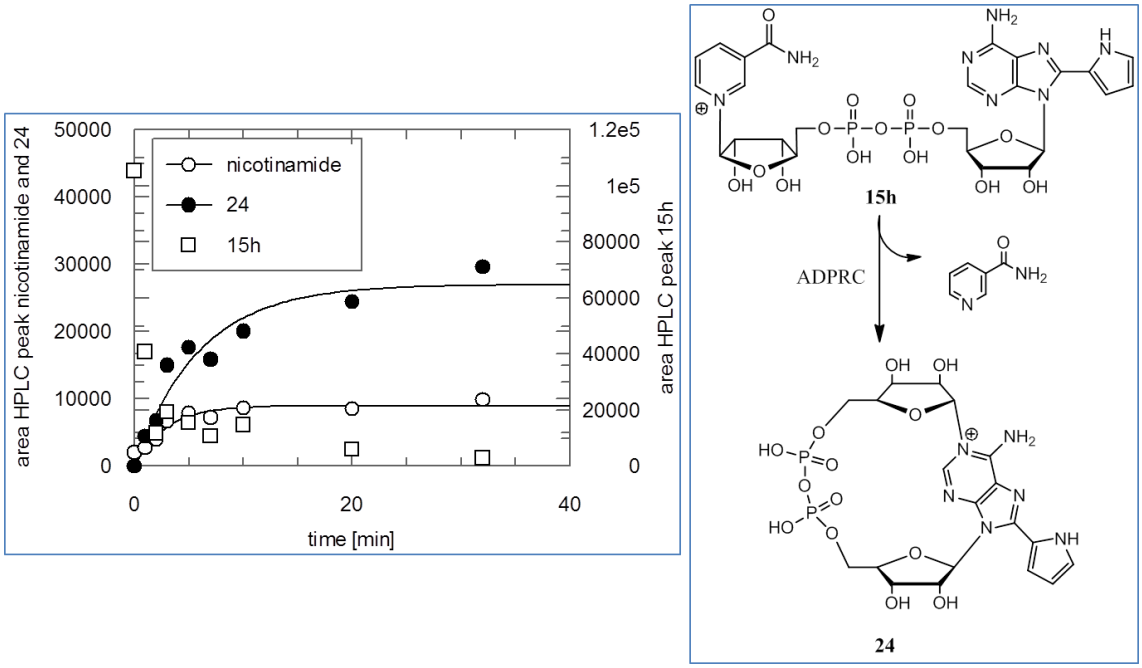

Figure 4.9 HPLC time-course of the enzymatic reaction of ADPRC from *Aplysia californica* and **15h**. *Conditions*: ADPRC (0.05 U/mL), **15h** (12.37 µM), HEPES buffer (50 mM, pH 7.4), 25 °C; all concentrations are final concentrations. Data from single experiment, peak area *vs* time [min], data plotting to a 1st order rate equation with Grafit5.

The possibility to develop a fluorescence-based assay to monitor the ADPRC activity using **15h** as a fluorescent probe was explored. A fluorescence increase during the enzymatic reaction due to the loss of NaM was expected, by analogy with the behavior shown with NPP and NADase. However, it was not clear whether a fluorescence increase or decrease would occur following the cyclization of the ADPR intermediate to the *c*ADPR derivative, **24**.

Several attempts were made in a cuvette to find the right substrate/enzyme ratio which allowed a fluorescence change to be observed during the progress of the enzymatic reaction. The results allowed us to visualize the mechanism suggested in the literature for the enzymatic reaction.[26] Indeed, as shown in Figure 4.10, moving to more diluted enzyme concentrations and increasing the substrate/enzyme ratio (as indicated in the brackets), the enzymatic reaction became increasingly slower highlighting the existence of two or more reaction steps.

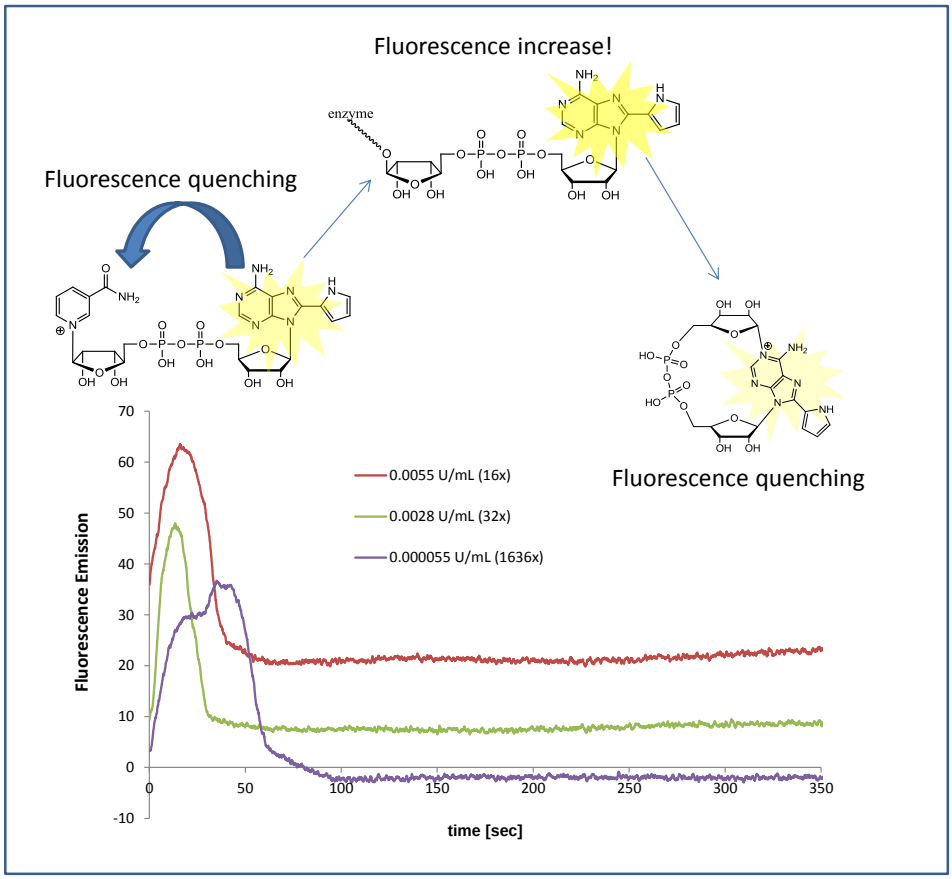

Figure 4.10 Fluorescence changes observed during the enzymatic reaction between ADPRC from *Aplysia californica* and **15h**. *Conditions*: ADPRC (0.000055 – 0.0055 U/mL), **15h** (0.09 μM), HEPES buffer (50 mM, pH 7.4), 25 °C, λ_{ex} = 300 nm, λ_{em} = 410 nm; all concentrations are final concentrations. Data plotting with Excel.

At the moment of enzyme addition to start the reaction, a sudden fluorescence increase was observed, probably due to the removal of NaM and, consequently, the disruption of the internal quenching in **15h**, now transformed into the more fluorescent ADPR intermediate. Then, the latter, bound to the enzyme, would start folding to cyclize into **24**. This cyclization would cause a change in the electronic delocalization on the substituted adenine ring, resulting in a final drop of fluorescence with the release of the product by the enzyme.

A further confirmation to this two-step reaction, consisting in the removal of NaM and following cyclization of the ADPR intermediate to *c*ADPR, was given by the HPLC assay. First, it was observed that the rate constant for the formation of NaM, k_{NaM}, was twice that for the formation of **24**, k_{24} (k_{NaM} 0.3525 min^{-1}; k_{24} 0.1700 min^{-1}), indicating that the formation of the two products was not simultaneous. Moreover, no trace of the

ADPR intermediate appeared in the chromatogram, suggesting the binding of the intermediate to the enzyme with subsequent release of the cyclized product.

To be able to kinetically characterize **15h** related to ADPRC from *Aplysia californica*, we used high enzyme concentrations allowing us to monitor the decrease in fluorescence due to the release of **24**. An enzyme concentration range between 0.025 and 2.5 U/mL was investigated to find the appropriate enzyme/substrate ratio that allowed the calculation of linear initial velocities (Figure 4.11).

Surprisingly, at the highest enzyme concentrations (1.25 – 2.5 U/mL), after the initial fluorescence drop due to the formation of **24**, a fluorescence increase was observed.[172] In the literature it is known that ADPRC from *Aplysia californica* shows a *c*ADPR-hydrolase activity unmasked only at high enzyme concentration, revealing this enzyme to be multifunctional in respect of its apparent unique ADPRC activity.[238] Using **15h** and its exclusive fluorescent properties, we were able to monitor this secondary activity of the enzyme transforming the newly formed **24** into the ADPR derivative, **23**.[172]

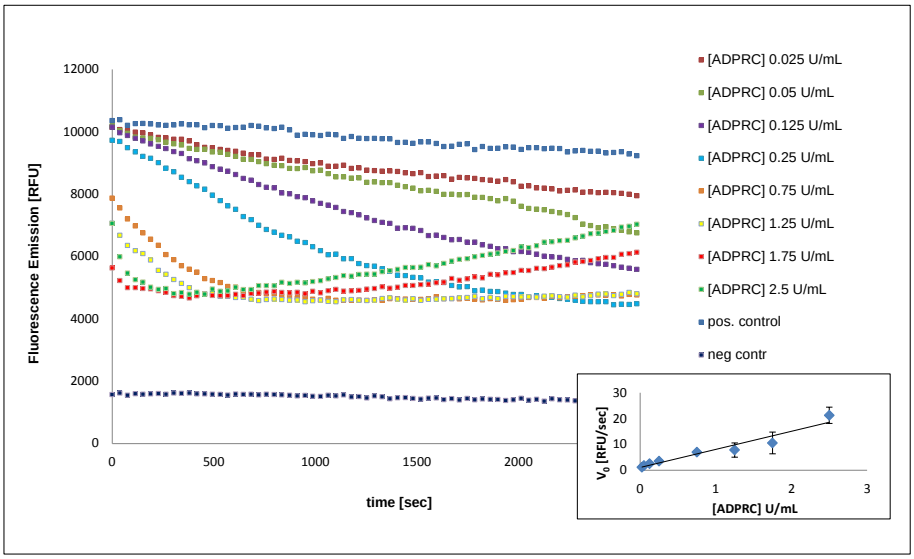

Figure 4.11 Fluorimetric assay of ADPRC from *Aplysia californica* and **15h**: initial velocity (V_0) as function of ADPRC concentration. Fluorescence time-course as fluorescence emission [RFU] *vs* time [sec]. *Conditions*: ADPRC (0.025 – 2.5 U/mL), **15h** (9.6 µM), HEPES buffer (50 mM, pH 7.4), 25 °C, λ_{ex} = 300 nm, λ_{em} = 410 nm, gain 15%. Positive control: **15h** (9.6 µM); negative control: buffer; all concentrations are final concentrations. Initial velocity values (V_0) were calculated from the reaction time measuring the fluorescence signals generated when 10% product was formed. Initial velocity values were fitted to a linear equation (insert) with Excel: y = 7.0142x+1.0531, r^2 = 0.9348. Each data point is the mean (± SD) of experiments run in duplicate.

To estimate K_m and V_{max} of **15h** related to the ADPR-cyclase activity of ADPRC from *Aplysia californica*, the substrate concentration was varied to generate a saturation curve (Appendix 8, Figure A7). Unfortunately, the small range of **15h** concentration with a linear fluorescence response was not enough to generate a saturation curve that could be used by Michaelis-Menten equation to determine accurately the enzymatic parameters related to **15h**. Therefore, a $K_m > 34$ μM (concentration limit with a linear fluorescence response for **15h**) and K_m/V_{max} of 3.7 min·mg·L^{-1}, extrapolated by Hanes-Woolf plot, could be estimated for **15h** (Appendix 8, Figure A8).[172]

Then, the estimation of K_m and V_{max} of **15h** related to the *c*ADPR-hydrolase activity of ADPRC from *Aplysia californica* was attempted. However, also in this case, the small range of **15h** concentration with a linear fluorescence response was not enough to generate a saturation curve that could be used by Michaelis-Menten equation (Appendix 8, Figure A9). This indicated quite high K_m for the *c*ADPR-hydrolase activity of ADPRC from *Aplysia californica* when using **15h**, as confirmed in the literature by HPLC studies revealing a K_m for the natural *c*ADPR of 1.04 ± 0.15 mM and a V_{max} of 3.34 ± 1.15 μmol·min^{-1}·mg^{-1}.[238]

4.2.3 Mechanistic aspects of ADPRC activity

In the literature the reaction mechanism of the ADPRC from *Aplysia californica* is well described and consistent with the results reported here, obtained by the fluorimetric and HPLC experiments, that suggest a two-step reaction (Figure 4.12).[26] The enzymatic reaction proceeds *via* binding of *β*-NAD^+ in the catalytic site; there, E179 interacts by H-bonding with 2″, 3″-OH of the nicotinamide ribose, destabilizing the nicotinamide *N*-glycosidic bond and favouring the formation of the oxocarbenium intermediate following the release of NaM.[30] In the catalytic site, the oxocarbenium intermediate is stabilized on the nicotinamide ribose and the diphosphate group by an extended network of H-bonds; slowly, the intermediate undergoes minor movements bringing the adenine ring, previously in *anti* conformation and stacked with Y81, into a *syn* conformation with the adenine ring stacked with W140. At this stage, N-1 of the adenine ring, more nucleophilic than N-7, points to the electrophilic C-1″, where the cyclization takes place.

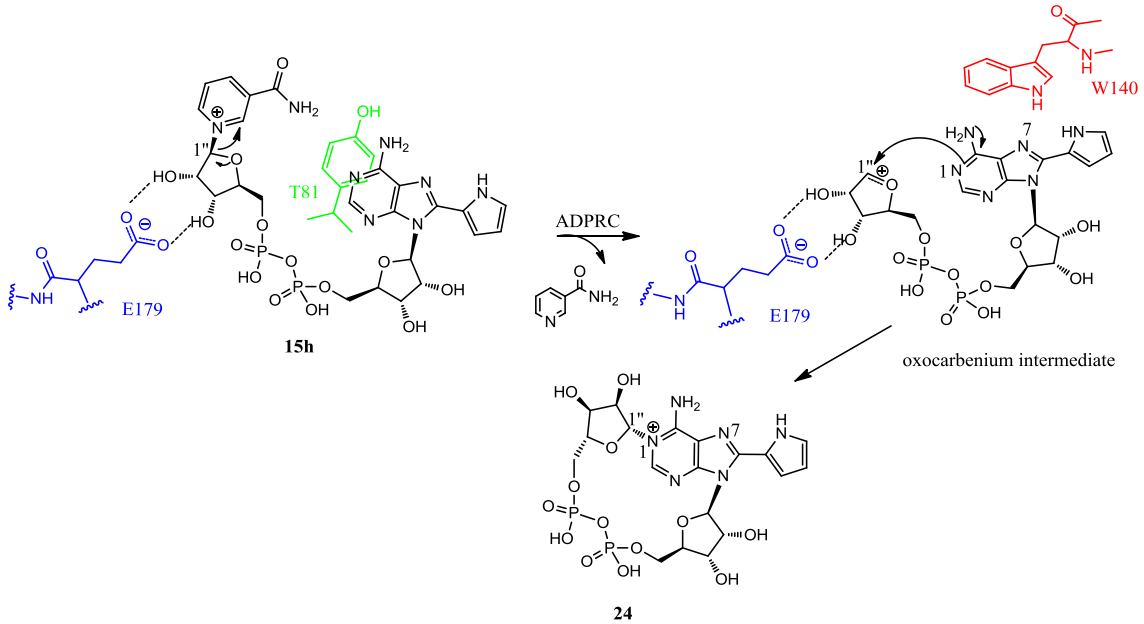

Figure 4.12 Reaction mechanism for N-1 cyclization of **15h** with ADPRC from *Aplysia californica*.

This mechanism is in agreement with that suggested by the HPLC assay, where the immediate release of NaM would be followed by a slower release of the product, since an intermediate is formed which rearranges to give the final *c*ADPR.

As shown in 3.1.2, 8-aryl/heteroaryl substituted NAD^+ derivatives, in particular **15h**, have the adenine ring in *syn* conformation because of the steric hindrance caused by the substituent in position 8.[70] Consequently, if at the moment of binding, **15h** has the adenine in a *syn* conformation in contrast to the *anti* in the natural *β*-NAD^+, then, at the moment of cyclization, **15h** already has the right *syn* conformation with N-1 pointing in the direction of C-1″. Since the rate-limiting step in the reaction mechanism seems to be the cyclization, the comparable K_m values for **15h** and *β*-NAD^+ related to ADPRC from *Aplysia californica* could be explained by their similarities in the cyclization position (Table 4.3).[172]

Fluorescence-based assays to study the activity of ADPRC from *Aplysia californica* were already present in the literature and based on the fluorescence changes of the well known ε-NAD^+, or other dinucleotides, such as NGD^+, NHD^+ and NXD^+ (see 1.4.3).[69, 90, 232, 239, 245] Conversely from **15h**, all these compounds showed an increase of fluorescence with the progress of the enzymatic reaction. In particular, NGD^+, NHD^+

and NXD^+ became fluorescent only after their cyclization to *c*GDPR, *c*IDPR and *c*XDPR. All these dinucleotides were characterized by the cyclization position on N-7, due to the lack of availability of N-1, as in the case of ε-NAD^+, or to the weak nucleophilicity of the amidic/imidic N-1 compared to N-7 in the case of NGD^+, NHD^+ and NXD^+ (Figure 4.13). Studies on the fluorescent properties of adenine rings substituted on N-1 and N-7 suggested that, while the substitution on N-1 did not cause any fluorescence, substitution on N-7 generated fluorescence;[69] this would explain the reduced fluorescence of **24** compared to **15h**, and the strong fluorescence of *c*GDPR, *c*IDPR and *c*XDPR compared to NGD^+, NHD^+ and NXD^+.

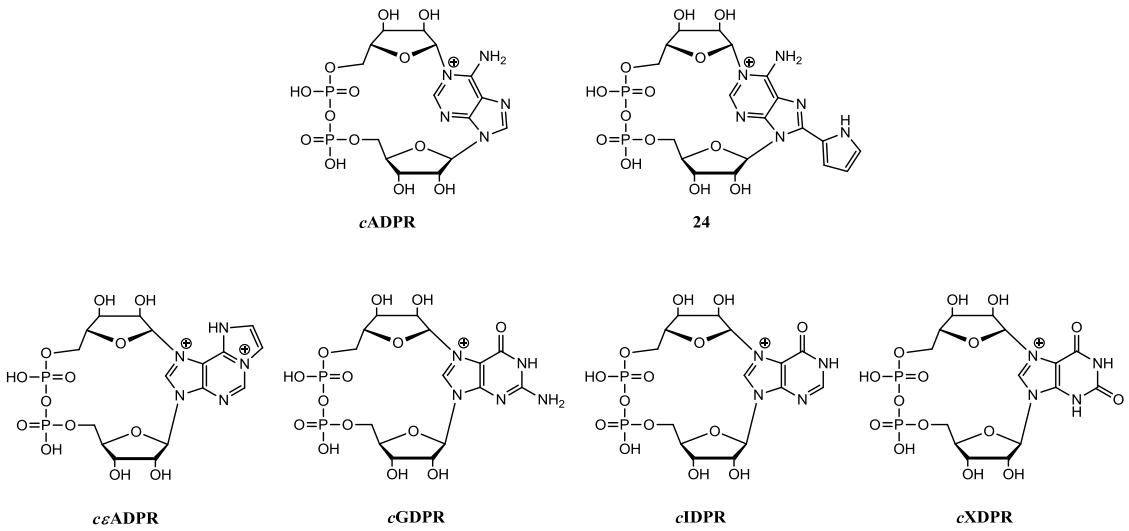

Figure 4.13 Cyclic ADP-ribose derivatives obtained by cyclization on N-1 or N-7 with ADPRC from *Aplysia californica*.

	β-NAD$^+$	***15h***	*ε-NAD*$^+$	*NGD*$^+$	*NHD*$^+$	*NXD*$^+$
K_m [μM]	39[69], 135[58]	> 34	6.2[69]	1.7[69], 15.5[58]	0.5[69], 8.8[58]	6.2[69]
V_{max} [μmol·min^{-1}·mg^{-1}]	500[69]	~ 20	94.4[69]	36.3[69]	4.6[69]	50[69]

Table 4.3 Enzymological properties for *β*-NAD^+, **15h**, ε-NAD^+ and other dinucleotide substrates of ADPRC from *Aplysia californica*.

All the dinucleotides cyclizing in N-7 of the adenine ring turned out to have extremely low K_m values compared to those of β-NAD^+ and **15h** (Table 4.3), showing stronger affinities for ADPRC from *Aplysia californica* than the natural substrate itself. This behaviour could be explained with the favourable *anti* conformation of the purine rings having N-7 pointing in the direction of C-1″, ready for the cyclization without the need to rotate as in the case of adenine in β-NAD^+.[69]

As already mentioned in 4.2, *Aplysia* ADPRC, characterized at a first investigation only by the cyclase activity,[236] turned out to be a *c*ADPR-hydrolase[238] as well as a NADase.[63, 71] These activities show up only in particular conditions in which the enzyme is forced to follow a different from the preferred mechanism. A partitioning mechanism, more than a sequential mechanism, is responsible for the choice of the reactions performed by CD38, NADases and ADPRC belonging to the same family (see 4.2, Scheme 4.2).

In the case of the NADase activity of ADPRC, unless the cyclization is completely blocked by the use of some NAD^+ derivatives,[71] the rate for the cyclization is so fast compared to the solvolysis that the enzyme would follow a macroscopic sequential mechanism, where β-NAD^+ is first converted to *c*ADPR (cyclase activity), which then undergoes hydrolysis to give ADPR (*c*ADPR-hydrolase activity). This sequential reaction mechanism can be clearly visualized in the experiments performed using **15h** as a fluorescent NNS for ADPRC,[172] where an initial fluorescence drop, indicating the formation of **24**, changes into a fluorescence increase due to the formation of **23** (Figure 4.11).

In other respects, with ε-NAD^+ it would not be possible to distinguish between cyclase and *c*ADPR-hydrolase activities of ADPRC from *Aplysia californica*, since its fluorescence would increase after the formation of both *c*εADPR and ε-ADPR. Moreover, *c*εADPR is quite resistant to the hydrolysis[90] and, therefore, it would not probably be susceptible to the *c*ADPR-hydrolase activity.

In principle, the continuous monitoring of the sequential reaction mechanism for the formation of ADPR from β-NAD^+ *via* *c*ADPR would be possible using NGD^+, NHD^+ and NXD^+. Indeed, these compounds should show a fluorescence increase with the

formation of the cyclic product (cyclase activity), followed by a fluorescence decrease with the formation of the corresponding nucleotide diphosphoribose derivatives (*c*ADPR-hydrolase activity). Only NHD^+ is actually used to fluorimetrically monitor the *c*ADPR-hydrolase activity,[69, 245] since its cyclic derivative, *c*IDPR, is less hydrolytically stable than *c*GDPR[69, 232, 239] and *c*XDPR. Nevertheless, no application of *c*IDPR for the monitoring of the recently discovered *c*ADPR-hydrolase activity of ADPRC from *Aplysia californica* has been found in the literature.

The study and understanding of ADPRC from *Aplysia californica* is important from a biological perspective since this enzyme belongs to the same family of human CD38, that is involved in the *β*-NAD^+ regulation and Ca^{2+} signalling. In addition, it is used for the chemo-enzymatic synthesis of well known or novel *c*ADPR derivatives, useful as biochemical tools or potential inhibitors of the Ca^{2+}-signalling pathway. Hence, it is essential to know more about this enzyme, its reaction mechanism and its specifity.

The previous results, showing on analytical scale the occurrence of the cyclization by ADPRC of **15h** into the less fluorescent product, **24**, were subsequently confirmed by the preparation of **24** on a synthetic scale allowing its spectroscopic analysis.[246] ADPRC from *Aplysia californica* was used to cyclize **15h** into **24** on a synthetic scale; the reaction progress was monitored by HPLC and the reaction mixture purified by anion-exchange chromatography to give the desired product with a 96% yield (Scheme 4.3).[246]

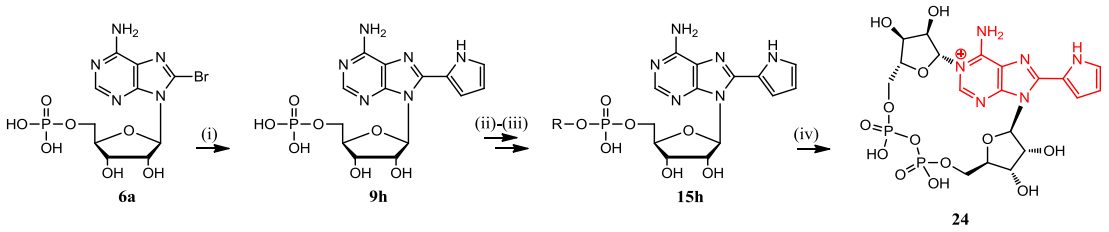

Scheme 4.3 Synthetic pathway to 8-(pyrrol-2-yl) *c*ADPR, **24**. (i) Suzuki-Miyaura cross-coupling; (ii) morpholidate formation; (iii) coupling with *β*-NMN (R); (iv) cyclization with ADPRC from *Aplysia californica*.

In the literature it has been reported that *c*ADPR is quite stable in basic conditions;[234] indeed, the N^1-ribosyl bond does not undergo any hydrolysis or rearrangement at pH 10, and the pyrophosphate bond is hydrolysed only under strong basic condition. However, *c*ADPR is slightly acid-labile, its half-life for spontaneous hydrolysis at 37 °C is 24 h, and it can be easily hydrolysed by NADases or ADPRC with *c*ADPR-hydrolase activity, but not by NPPs.[234, 235] Compounds **15h** and **24** were subjected to similar hydrolytic conditions (0.1 N NaOH and HCl) to identify the chemical stability of **24** compared to **15h** (Appendix 8, Figure A10).

Spectroscopic and ^{1}H NMR analyses for **24** were performed and compared to **15h**; the results are summarised in Table 4.4 and Table 4.5.[246] Compound **24** showed a substantial red shift in λ_{ex} compared to **15h**, with consequent decrease in Stoke shift, which indicated a minor vibrational relaxation due to the constrained conformation of the adenine ring cyclized in N-1 position. The Φ value of **24**, as expected from the fluorescence-based assay for ADPRC, was less than **15h**, probably due to the change of the electron delocalization along the adenine ring, now positively charged.

The ^{1}H NMR spectrum clearly showed the cyclization product. Indeed, the nicotinamide signals disappeared, while a considerable downfield shift was noticed for 2-H on the adenine ring and, consequently, for 1′-H and 1″-H, deshielded because of the newly formed N^1-ribosyl bond and the positively charged adenine ring.

cmpd	λ_{ex}/*nm*	λ_{em}/*nm*	*Stoke shift*[a]/cm^{-1}	*Φ*
15h	309	374	5624	0.0053
24	316	378	5190	0.004

[a] Stokes shift = $(1/\lambda_{ex} - 1/\lambda_{em})$.

Table 4.4 Spectroscopic analysis and Φ values of **15h** and **24** in water.

cmpd	*2-H (ppm)*	*1′-H (ppm)*	*1″-H (ppm)*
15h	8.09	5.73	5.91
24	8.98	6.42	6.16

All the spectra are referenced for D_2O (δ = 4.79 ppm).

Table 4.5 ^{1}H NMR analysis for **15h** and **24**. Comparison of chemical shift (ppm) for 2-H, 1′-H and 1″-H.

5 EVALUATION OF ARYL/HETEROARYL ADENINE-MODIFIED NAD+ DERIVATIVES AS INHIBITORS AND NON-NATURAL SUBSTRATES FOR NAD+-CONSUMING ENZYMES

In Chapter 4, **15h**, the most promising fluorescent NAD^+ derivative belonging to the class of those 8-aryl/heteroaryl substituted, was evaluated as a biochemical probe for NAD^+-consuming enzymes; in particular, its role as a NNS was analysed. Of course, the activity of **15h** as a NNS for NAD^+-consuming enzymes implies a competitive inhibition with the natural substrate β-NAD^+, which was only superficially explored in the previous enzymatic evaluation of **15h**.

Herein, greater attention will be given to the inhibitory effects of the aryl/heteroaryl adenine-modified NAD^+ derivatives toward NAD^+-consuming enzymes. It will be stressed how competitive inhibition does not necessarily correlate with substrate activity, as was the case with the enzymes analysed in Chapter 4. Instead, for complex enzymes that involve more than one substrate in their reactions, the situation can change due to the more complicated catalytic mechanisms and active sites, requiring elaborate and discriminating factors in the recognition and use of their substrates. NAD^+-dependent DNA ligases and sirtuins have been chosen in this project as complex NAD^+-consuming enzymes to evaluate the biological activities of the differently substituted NAD^+ derivatives as inhibitors and/or NNSs. These enzymes require β-NAD^+ as a co-substrate in their reactions and have in their structures specific adenine binding domains, which reflect on the different activities exerted by the adenine-modified NAD^+ derivatives as inhibitors and/or NNSs.

5.1 NAD^+-dependent DNA ligases

DNA is continuously exposed to damage and lesions deriving from the physiological processes in which it is involved, for instance, mismatches during DNA replication, or DNA strand breaks due to aborted topoisomerase activity. However, DNA damage is mostly due to processes unrelated to its biological roles, like the attack from ROS and environmental factors, such as ultraviolet light, radioactive exposure or tobacco products.

To defend themselves, living cells have developed complicated and efficient systems to detect DNA damage and repair it; the DNA-damage response (DDR) implies an intricate cascade of signalling processes and enzymatic activities that are not yet fully understood, but are continuously under study.[247] DNA polymerases, ligases, methyltransferases, helicases, endonucleases, PARPs and many other enzymes are fundamental components of the DDR. Defects in DDR are associated with the development of many diseases, such as heritable neurodegenerative diseases and cancer. In the latter case, there is a strong connection between cancer and DDR, since defects in DDR cause genome instability and, therefore, mutations and malignancies; however, DDR is also responsible for cancer-therapy resistance. Consequently, DDR inhibitors can in some cases be used for anticancer therapy.

DNA ligases are essential enzymes found in all living cells, involved in DNA replication, repair and recombination;[15, 248, 249] their activity consists of sealing DNA single-strand breaks between 5′-phosphate and 3′-hydroxyl termini. DNA ligases have been differentiated into two classes depending on their co-substrate specificity; eukaryotic DNA ligases are ATP-dependent, while bacterial and some viral DNA ligases are NAD^+-dependent. In fact, ATP-dependent DNA ligase sequences have been found in bacteria in addition to the NAD^+-dependent ones, even though they are expressed only in particular conditions;[250] in contrast, NAD^+-dependent DNA ligases have never been found in eukaryotic organisms.

The restricted distribution in bacteria, the necessary requirement for bacteria viability and the absolute co-substrate uniqueness make NAD^+-dependent DNA ligases a possible target for the development of antibacterial drugs. NAD^+-dependent DNA ligases from different bacteria have been structurally characterized to better understand their activities and reaction mechanism, and to develop possible inhibitors. High homologies have been found between sequences of several bacterial DNA ligases, showing highly conserved motifs and the same modular architecture. The sequence similarity with ATP-dependent DNA ligases is quite poor, as expected because of the different co-substrate; however, NAD^+-dependent and ATP-dependent DNA ligases share exactly the same reaction mechanism (Scheme 5.1).[249]

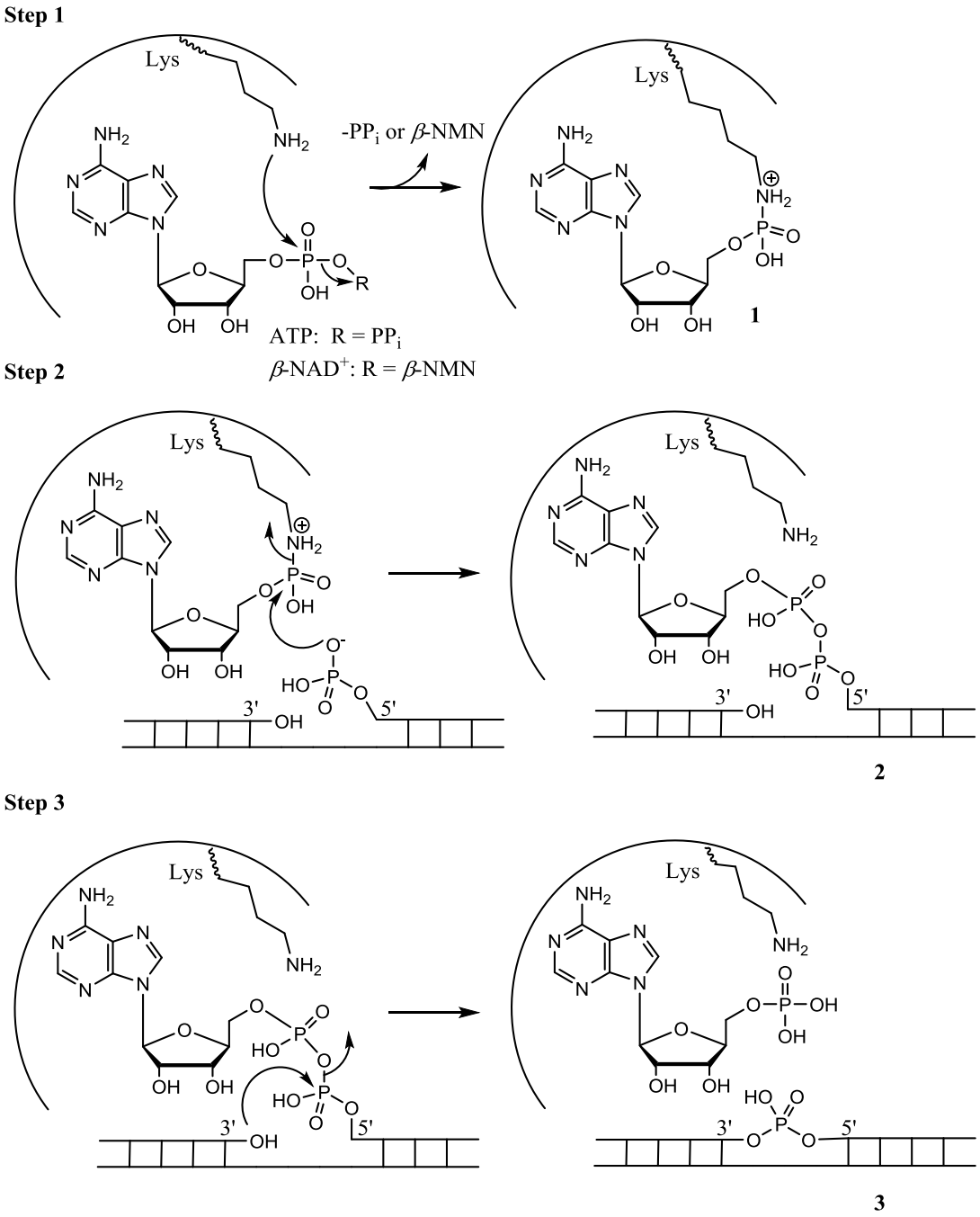

Scheme 5.1 Reaction mechanism for DNA ligation by ATP and NAD^+-dependent DNA ligases.

The ligation of DNA occurs in three steps. In the first step, ATP or β-NAD^+ binds to the active site of the enzyme; there, a nucleophilic lysine residue attacks the phosphate of the adenosine in the co-substrate with subsequent release of the leaving group, respectively pyrophosphate (PP_i) and β-NMN, and formation of adenylated-ligase intermediate (**1**). In the second step, after the positioning of the DNA nick in the

proximity of the adenylated-ligase intermediate (**1**), the nucleophilic phosphate in the 5′ position attacks the phosphoramidate bond in **1** to form an adenylated-DNA intermediate (**2**). In the third and final step, the nucleophilic hydroxyl group in the 3′ position attacks the new pyrophosphate bond with formation of a phosphodiester bond between the 5′ and 3′ positions of the DNA (**3**), and release of AMP.

The NAD^+-dependent DNA ligases have a modular architecture consisting of four main domains linked by single chains (Figure 5.1). Domain 1 is formed by two subdomains; subdomain **1a**, at the N-terminus, binds the β-NMN moiety of β-NAD^+, while subdomain **1b** is the adenylation domain, or the nucleotidyltransferase domain (NTase), since it binds the AMP moiety of β-NAD^+. Domain 2 is the oligonucleotide binding site (**OB**). Domain 3 consists of subdomain **3a**, a Cys_4-type zinc finger, and subdomain **3b**, containing a helix-hairpin-helix motif (HhH). Domain 4, at the C-terminus, is a **BRCT** domain (Breast cancer Carboxy-Terminal). The catalytic core of DNA ligase consists of subdomain **1b** and **OB**, flanked by N and C-terminal domains arranged in a C-shape that clamps the double-stranded DNA.[251]

Subdomain **1a** has been shown to interact with the β-NMN moiety of β-NAD^+, indeed it is not present in ATP-dependent DNA ligases.[252] Its presence is fundamental to initiate the ligation reaction, but not essential in the case of preadenylated-enzyme and its interaction with DNA; this means that subdomain 1a is required for the β-NAD^+ binding and the adenylation step. From crystallographic studies, it was possible to identify an "open" enzyme conformation, in which β-NAD^+ was bound to the solvent exposed NTase domain. Therefore, the closure of subdomain 1a to bury β-NAD^+ and interact closely with β-NMN puts the latter in an apical position as a leaving group during the nucleophilic attack of the lysine residue on the adenosine phosphate; the subdomain 1a has to swivel by almost 180° to switch from the "open" to the "closed" conformation.[253]

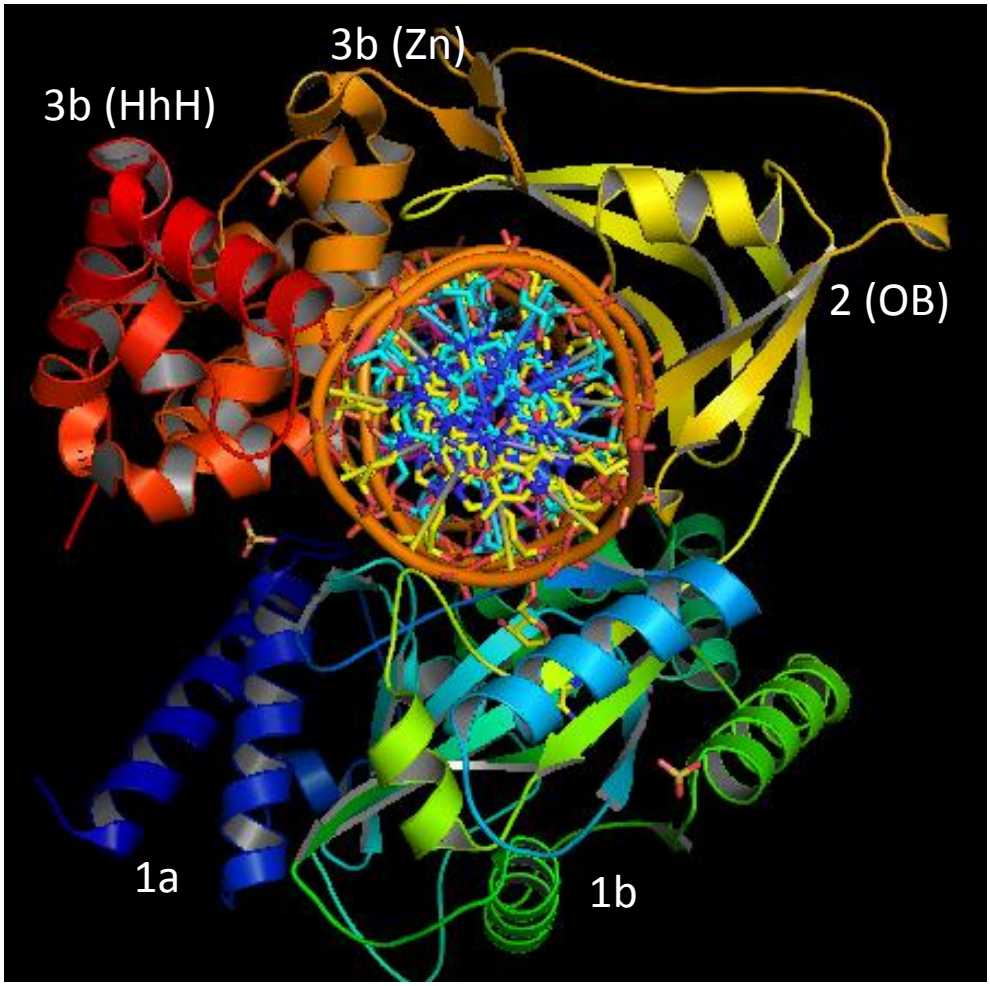

Figure 5.1 Structure of DNA ligase from *E. coli* (EcLigA) (PDB 2OWO) in complex with nicked DNA. Visualization by PyMol software. Subdomain **1a** (light blue), subdomain **1b** (green), **OB** domain (yellow), subdomain **3a** (orange), subdomain **3b** (red).

Subdomain **1b** is the adenylation domain, or the core of the DNA ligase. Several residues have been found to be fundamental in the NTase for the enzyme activity, their modifications bringing a considerable rate decrease or inactivation of the enzyme. The main residues in NTase, their interactions and their roles are summarised in Table 5.1.[252, 254]

The **OB** domain is involved in the oligonucleotide binding, as it contacts the double-strand DNA covering the nick and help in positioning it into the NTase domain. Its action is supported by subdomain **3b**, HhH, which binds both DNA strands in a non-specific sequence manner across the minor groove. OB, NTase and HhH clamp the double-strand DNA along 19 bp.[255]

Residue	*Pos.*	*Interaction*	*Role*
Lysine	**115**	Part of KXDG conserved motif; nucleophilic attack to adenosine phosphate of β-NAD^+	Formation of adenylated-ligase intermediate (**1**)
Aspartate	**117**	Part of KXDG conserved motif	Stabilization active site
Glycine	**118**	Part of KXDG conserved motif	Stabilization active site
Glutamate	**173**	Coordination of O-2′ of the adenosine ribose in β-NAD^+ and AMP	Involvement in step 1 and 3
Lysine	**290**	H-bonding with N-1 on adenine ring	Stabilization of adenine conformation
Lysine	**314**	H-bonding with the adenosine phosphate and O-2′ of the nicotinamide ribose in β-NAD^+	Involvement in step 1 and 3
Arginine	**136**	H-bonding with β-NAD^+ pyrophosphate and 5′-phosphate side of the nick	Involvement in step 1 and 2
Arginine	**200**	Interaction with subdomain 1a in closed conformation of adenylation domain; interactions with 3′-OH side of nick and DNA minor groove	Involvement in step 1 and 3
Arginine	**208**		
Arginine	**218**	Interaction with 3′-OH side of the nick	Involvement in step 2 and 3
Arginine	**277**	H-bonding with Ile284	Stabilization active site
Aspartate	**285**	Interaction with Mg^{2+}	Metal binding
Arginine	**308**	Interaction with 5′-phosphate side of the nick	Involvement in step 2 and 3

Table 5.1 Essential residues in the NTase domain of EcLigA and their roles.

Subdomain **3a**, the Cys_4-type zinc finger, seems to hold OB and HhH during DNA binding, showing therefore a structural role.[251, 255, 256] Finally, the C-terminal domain 4, **BRCT**, has a controversial role in DNA ligases; indeed, from the crystal structures of different enzymes, BRCT appears as a very flexible unit, with a structure that cannot to be properly resolved, and it is apparently not involved in the adenylation step. Indeed, DNA ligase proteins not including BRCT in their modular structures are still able to perform their ligation reaction, despite a lower rate. Moreover, DNA binding was shown to be tighter for a DNA ligase with BRCT domain compared to DNA ligase not containing it. Therefore, the BRCT domain could stabilize the DNA binding on DNA ligases, even though it does not interact directly with DNA.[251, 255-257] Another possible

function as a signal transducer of the DNA-damage response could be assigned to BRCT; indeed, other well known proteins use this domain for protein-protein interactions to transmit signalling responses.[251] Overall, the modular structure of NAD^+-dependent DNA ligase allows it to catalyze the ligation reaction involving considerable movements of the different domains.

The first DNA ligase inhibitors were found by screening libraries of classes of compounds, including alkaloids, flavonoids, pyridochromanones, quinoline and quinacrine derivatives, and many others.[248, 258-260] The scaffolds of the compounds showing inhibitory activity were subsequently optimized on the basis of computational studies to improve activity, selectivity, specificity, solubility, and many other factors.[73, 74, 261, 262] However, a deeper knowledge of the structure of NAD^+-dependent DNA ligases allowed the design of more specific inhibitors. At the outset of this project, the crystal structures of several NAD^+-dependent DNA ligases were resolved and published, showing the existence of a hydrophobic tunnel between the outside and the adenylation domain next to N-1, C-2 and N-3 of the adenine ring of β-NAD^+; in particular, C-2 pointed exactly in the direction of the tunnel (Figure 5.2).[15, 255]

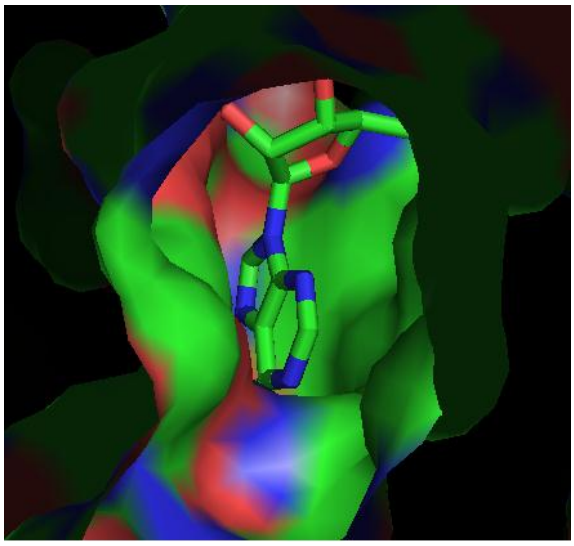

Figure 5.2 Hydrophobic tunnel on NTase domain of DNA ligase from *Enterococcus faecalis* (PDB 1TAE). C-2 of the adenine ring points in the direction of the tunnel. Visualization by PyMol software.

Many known inhibitors were docked into the active site and shown to fit into this tunnel.[15] This observation initiated the discovery of NAD^+-dependent DNA ligase inhibitors based on mimics of the adenine/adenosine structure substituted in position 2,[261, 262] which can compete for β-NAD^+ binding. Indeed, ATP-dependent DNA ligases do not have this tunnel in their structure, providing the possibility that such inhibitors may act specifically against NAD^+-dependent DNA ligases.

Until now, different adenosine/ADP/ATP derivatives substituted in position 2 with alkyl or cycloalkyl substituents have been tested *in vitro*/*in vivo* as antibacterial agents with promising results (Figure 5.3).[73, 74, 263] However, to the best of our knowledge no AMP or NAD^+ derivatives have been reported as inhibitors of NAD^+-dependent DNA ligases. It is likely that the difficult synthesis of NAD^+ derivatives, their hydrophilicity, their flexible/multifunctional structure making β-NAD^+ binding quite unspecific, together with their potential NNS activity interfering with that as inhibitors, have been the reasons why such compounds have not been described yet.

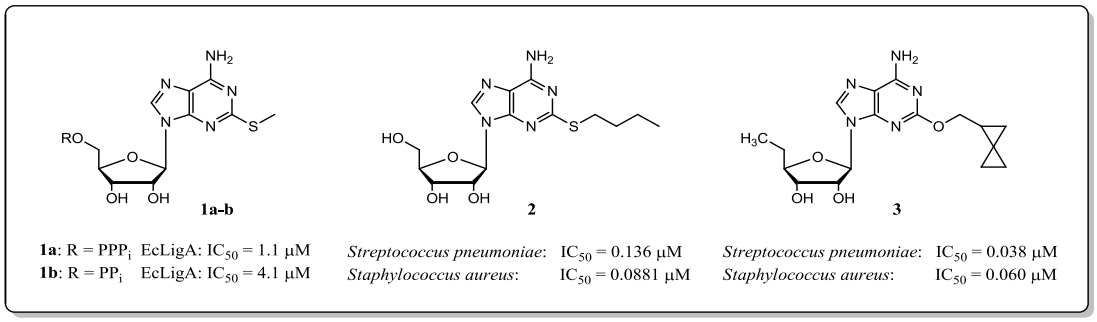

Figure 5.3 C-2 adenine-modified adenosine derivatives and their efficacies as NAD^+-dependent DNA ligases inhibitors.[73, 74, 263]

In this project, the biological activity of the NAD^+ derivatives and some of their corresponding AMP and AMP-morpholidate derivatives, modified in position 2, 6 or 8 of the adenine ring, as inhibitors and/or NNSs was assessed toward EcLigA, one of the best characterized NAD^+-dependent DNA ligases. In particular, the whole β-NAD^+ scaffold, differently from adenosine or AMP scaffolds that could bind also to ATP-dependent DNA ligases, should provide selectivity toward NAD^+-dependent DNA ligases, as well as the introduction of substituents in position 2 on the adenine ring. In

addition, the introduction of aryl/heteroaryl substituents in position 2, 6 or 8 of the adenine ring and the biological activities of the corresponding derivatives would improve understanding of the enzyme active site and the essential interactions for the *β*-NAD^+ binding.

5.1.1 Expression, purification and activity of *Escherichia coli* DNA ligase

Escherichia coli DNA ligase (EcLigA) is a protein consisting of 671 amino acids, with a molecular weight of 74 kDa. The protocol for the overexpression and purification of a recombinant form of EcLigA, containing a 10-His-tag at the N-terminus of the protein that allows its straightforward purification, is well established in the literature[257] and it was followed with minor changes to obtain highly pure EcLigA with 24 μM concentration (Figure 5.4).

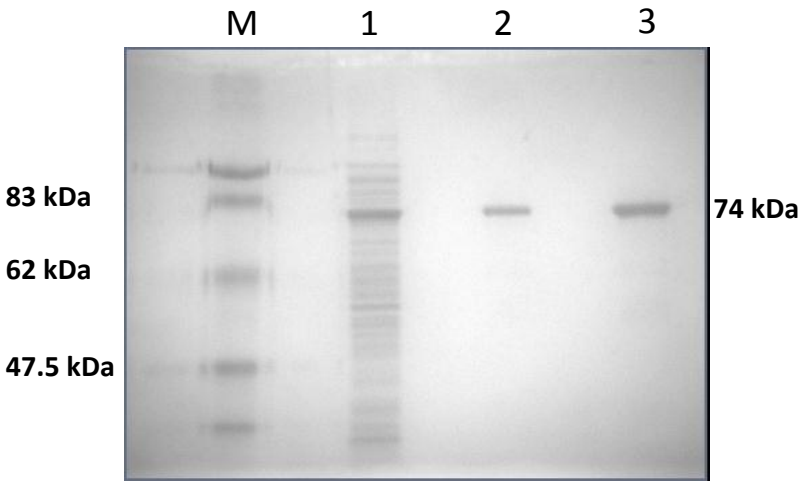

Figure 5.4 Purification of EcLigA. Lane M: marker of protein molecular weights; lane 1: crude extract of overexpressed proteins in the soluble fraction; lane 2: 10 x dilution of purified protein; lane 3: purified protein. Visualization of SDS-PAGE gel by Coomassie blue staining.

The activity of EcLigA was tested by a gel electrophoresis assay of the ligation of nicked DNA (Figure 5.5 **a**). The DNA substrate was prepared by annealing of a 40-mer strand (LigSub1+2) with two complementary 18-mer (LigSub1) and 22-mer (LigSub2) strands forming a nick between the 18th and 19th bases of one strand; LigSub1 and LigSub2 were characterized by the addition of fluorescein (F) and a phosphate group (P) in their 5′ positions respectively. For the preparation of this substrate, the

appropriate ratio between the different strands and salt concentration were established to obtain complete annealing (Appendix 8, Figure A11). The ligation reaction was monitored by formation of a fluorescent 40-mer strand, migrating less than the fluorescent 18-mer strand on a denaturing gel, which separates DNA strands based on their molecular size (Figure 5.5 **b**).

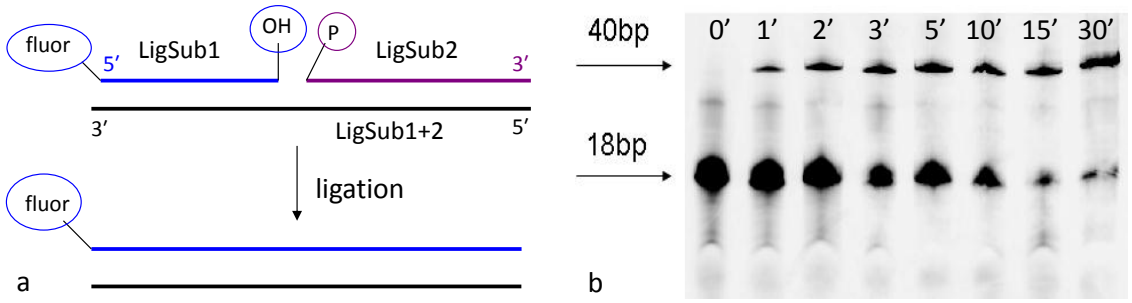

Figure 5.5 Ligation assay with fluorescent annealed nicked substrate. **a)** Scheme of ligation assay with fluorescent annealed nicked substrate; **b)** denaturing PAGE for time-course of ligation reaction with fluorescent annealed nicked substrate. *Conditions*: DNA substrate (0.125 µM), EcLigA (0.1 µM), *β*-NAD^+ (26 µM) in 1 x buffer (30 mM Tris/HCl pH 8, 4 mM $MgCl_2$, 1 mM DTT, 50 µg/mL BSA); all concentrations are final concentrations. Reactions incubated at 30 °C under shaking; samplings at 0, 1, 2, 3, 5, 10, 15 and 30 min. Gel visualization by fluorescence imaging.

Preliminary experiments were carried out to establish the conditions for the ligation reaction during the inhibition and NNS activity studies. Indeed, it is important to choose the right enzyme concentration and, consequently, the time sampling, to have 40 – 50% ligation in the control reaction without inhibitor. These conditions, varying from batch to batch of enzyme, allow clear detection of inhibition and activation of the enzyme activity in the same set of experiments, since the ligation is still not complete and not influenced by displacement of the inhibitors by the natural *β*-NAD^+. Therefore, the following studies investigated the reaction in an initial state, not influenced by reversible reactions, inhibition by products or enzyme deactivation.

For the NNS activity test, the reactions in some cases were maintained for longer to allow the NNS to be recognised and metabolized by the enzyme. Therefore, the enzyme activity and the substrate stability were checked over time to be sure they would not negatively influence the ligation reactions. EcLigA retained full activity after 90 min at

30 °C; however, the activity dropped dramatically after 3.5 h at 30 °C. The annealed substrate was shown to be stable over 1 h (data not shown).

To validate the gel electrophoresis assay and its application in the inhibition studies, quinacrine, a well characterized inhibitor of EcLigA, was tested at different concentrations and its IC_{50} estimated and compared with the value in the literature (Appendix 8, Figure A12). The obtained value, 3.9 ± 1.5 μM, was close to that in the literature, 1.5 ± 0.2 μM,[260] indicating the suitability of the method in studying inhibitors.

At this stage, it was possible to proceed with the biological testing of the synthesized compounds. The series of NAD^+ derivatives substituted on either C-2, C-6 or C-8 and some of their corresponding AMP and AMP-morpholidate derivatives were successively tested as NNSs and inhibitors of EcLigA.

5.1.2 Biological testing of 2-substituted AMP and NAD^+ derivatives

Firstly, 2-substituted AMP and NAD^+ derivatives, respectively **7a-b** and **13a-b**, were tested as NNSs of EcLigA at 250 μM in the absence of β-NAD^+ (Figure 5.6); this concentration, 10 fold larger than that used for the assay with the natural β-NAD^+, was chosen to ensure detection of any substrate activity. From these experiments, a NNS activity was observed for both the NAD^+ derivatives, **13a** and **13b**, but not for the AMP derivatives, **7a** and **7b**. This was expected because the AMP derivatives have a phosphate that is not reactive enough to be attacked by the nucleophilic lysine residue in the active site (see 5.1, Scheme 5.1).

When the NNS activity for **13a** and **13b** was tested at different substrate concentrations between 50 and 250 μM, **13a** showed the same or a lower activity than the natural β-NAD^+ at 26 μM (Figure 5.7 **a**), while **13b** showed the same or slightly higher activity than the natural β-NAD^+ at 26 μM (Figure 5.7 **b**).

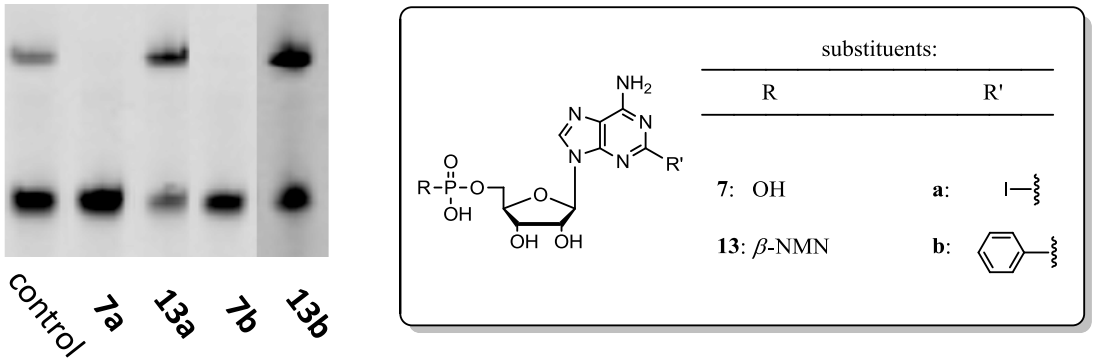

Figure 5.6 Denaturing PAGE for the NNS activity of 2-substituted AMP and NAD^+ derivatives at 250 µM. *Conditions*: DNA substrate (0.5 µM), EcLigA (0.05 µM), 2-substituted derivative (250 µM) in 1 x buffer (30 mM Tris/HCl pH 8, 4 mM $MgCl_2$, 1 mM DTT, 50 µg/mL BSA); all concentrations are final concentrations. Reactions incubated at 30 °C under shaking and sampled at 15 min. Control reaction at the same conditions with β-NAD^+ (26 µM) without any 2-substituted derivative. Gel visualization by fluorescence imaging.

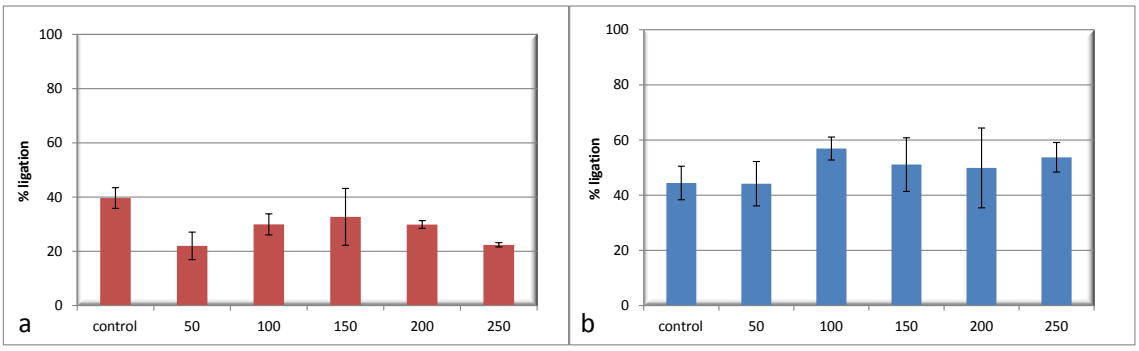

Figure 5.7 NNS activity of 2-substituted NAD^+ derivatives at concentrations between 50 and 250 µM. *Conditions*: DNA substrate (0.5 µM), EcLigA (0.05 µM), **13a** (**a**) (50 – 250 µM), **13b** (**b**) (50 – 250 µM) in 1 x buffer (30 mM Tris/HCl pH 8, 4 mM $MgCl_2$, 1 mM DTT, 50 µg/mL BSA); all concentrations are final concentrations. Reactions incubated at 30 °C under shaking and sampled at 5 min. Control reaction at the same conditions with β-NAD^+ (26 µM) without any 2-substituted derivative. Analysis of assay run on denaturing PAGE and gel visualized by fluorescence imaging. Data analysed using ImageJ. Each data point is the mean (± SD) of a set of experiments run in triplicate; data plotting with Excel.

Next, inhibition studies were undertaken testing 2-substituted AMP/AMP-morpholidate/NAD^+ derivatives, respectively **7a-b**, **10b**, and **13a-b**, at 200 µM with β-NAD^+ at 26 µM; the samplings were performed at 5 and 15 min (Figure 5.8 and Appendix 8, Figure A13). A clear inhibition was observed for the 2-iodo AMP and NAD^+ derivatives, respectively **7a** and **13a**, which showed around 80% inhibition at 200 µM at 5 min. Regarding the 2-phenyl derivatives, a clear inhibition under the experimental conditions was observed only for the AMP-morpholidate derivative, **10b**,

showing around 70% inhibition, while AMP and NAD^+ derivatives, respectively **7b** and **13b**, showed no inhibition. At 15 min, the ligation for all reactions reached the level of the control reaction. IC_{50} values were measured for **7a** and **13a** (Appendix 8, Figure A14), and are summarised in Table 5.2.

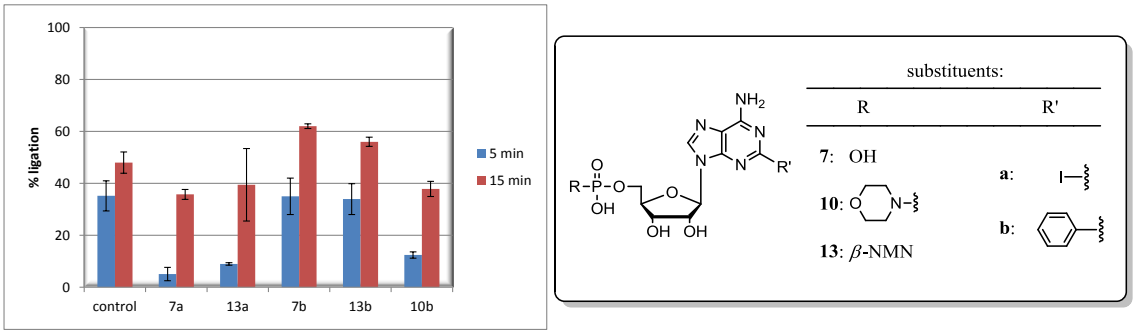

Figure 5.8 Inhibition of 2-substituted AMP/AMP-morpholidate/NAD^+ derivatives at 200 µM. *Conditions*: DNA substrate (0.5 µM), EcLigA (0.05 µM), *β*-NAD^+ (26 µM), 2-substituted derivative (200 µM) in 1 x buffer (30 mM Tris/HCl pH 8, 4 mM $MgCl_2$, 1 mM DTT, 50 µg/mL BSA); all concentrations are final concentrations. Reactions incubated at 30 °C under shaking and sampled at 5 and 15 min. Control reaction at the same conditions without any 2-substituted derivative. Analysis of assay run on denaturing PAGE and gel visualized by fluorescence imaging. Data analysed using ImageJ. Each data point is the mean (± SD) of a set of experiments run in triplicate; data plotting with Excel.

cmpd	*scaffold*	*Position of substitution*	*R (substituent)*	*IC_{50} (µM)*
7a	AMP	2	Iodo	119.9 ± 23.4
13a	NAD	2	Iodo	137.6 ± 17.8
2-MeSADP[263]	ADP	2	Methyl	4.1 ± 0.5
2-MeSATP[263]	ATP	2	Methyl	1.1 ± 0.4

Table 5.2 IC_{50} values ± SD for **7a** and **13a** toward EcLigA.

An activity comparison between 2-iodo and 2-phenyl substituted derivatives was undertaken to investigate the influence of the substituents on the different biological activities observed for the compounds. EcLigA was inhibited by 2-iodo NAD^+, **13a** (Figure 5.8); however, due to its NNS activity (Figure 5.7 **a**), it actively competed with *β*-NAD^+ for the same active site and catalytic reaction. Since in the inhibition study **13a** was used in a large excess (200 µM) compared to *β*-NAD^+ (26 µM), EcLigA (0.05 µM) would have bound in its active site more **13a** than *β*-NAD^+, independently from the different affinities (K_m) of the compounds (Figure 5.9). The fact that the resulting

ligation was much slower than the control reaction with only β-NAD$^+$ and gave at 5 min an inhibition overall, indicated that **13a** was used preferentially as substrate because of its excess in the reaction media, but it had a very slow turnover (low k_{cat}) along the different reaction steps compared to β-NAD$^+$. Indeed, at 15 min the ligation reached the same level of the control reaction, strongly suggesting a kinetic difference between the reaction steps involving **13a** and β-NAD$^+$.

In contrast to **13a**, 2-phenyl NAD$^+$, **13b**, seemed to have no inhibitory activity toward EcLigA (Figure 5.8); however, its NNS activity (Figure 5.7 **b**) implied a competition of **13b** with β-NAD$^+$ for the same active site. Also in this case, **13b** was used in a large excess (200 μM) compared to β-NAD$^+$ (26 μM); therefore, EcLigA (0.05 μM) would have bound in its active site more **13b** than β-NAD$^+$, independently from the different affinities (K_m) of the compounds (Figure 5.9). The fact that the resulting ligation at 5 min was the same as that for the control reaction, suggested that **13b** had a very similar turnover compared to β-NAD$^+$, hence EcLigA could perform its ligation at a similar rate than with β-NAD$^+$.

The 2-substituted AMP derivatives, **7a** and **7b**, as well as the corresponding NAD$^+$ derivatives, **13a** and **13b**, showed a distinct activity depending on the substituent introduced in position 2 on the adenine ring. Owing to the lack of the NNS activity due to the AMP scaffold, **7a** and **7b** provided some clues about the different affinities of the compounds, generated by the different substituents, toward the active site of EcLigA. The 2-iodo AMP, **7a**, acted as an inhibitor of EcLigA in the presence of β-NAD$^+$ at 5 min (Figure 5.8); because of its analogy with **13a**, **7a** would presumably bind in the same β-NAD$^+$ binding site, and the inhibitor activity would indicate its good affinity for EcLigA. The increased ligation at 15 min would be due to the displacement of **7a** by β-NAD$^+$ with the re-establishment of the normal enzyme activity. In contrast to **7a**, the 2-phenyl AMP, **7b**, showed no inhibition (Figure 5.8). This effect could be due to a low affinity of **7b** toward EcLigA; hence, **7b** would not bind, or just weakly, to EcLigA and could be easily displaced by β-NAD$^+$, giving no substantial inhibition overall.

Finally, the inhibitor activity of the 2-phenyl AMP-morpholidate, **10b**, (Figure 5.8) would be due to its modification on the phosphate, since its corresponding AMP derivative, **7b**, showed no inhibitor activity at all.

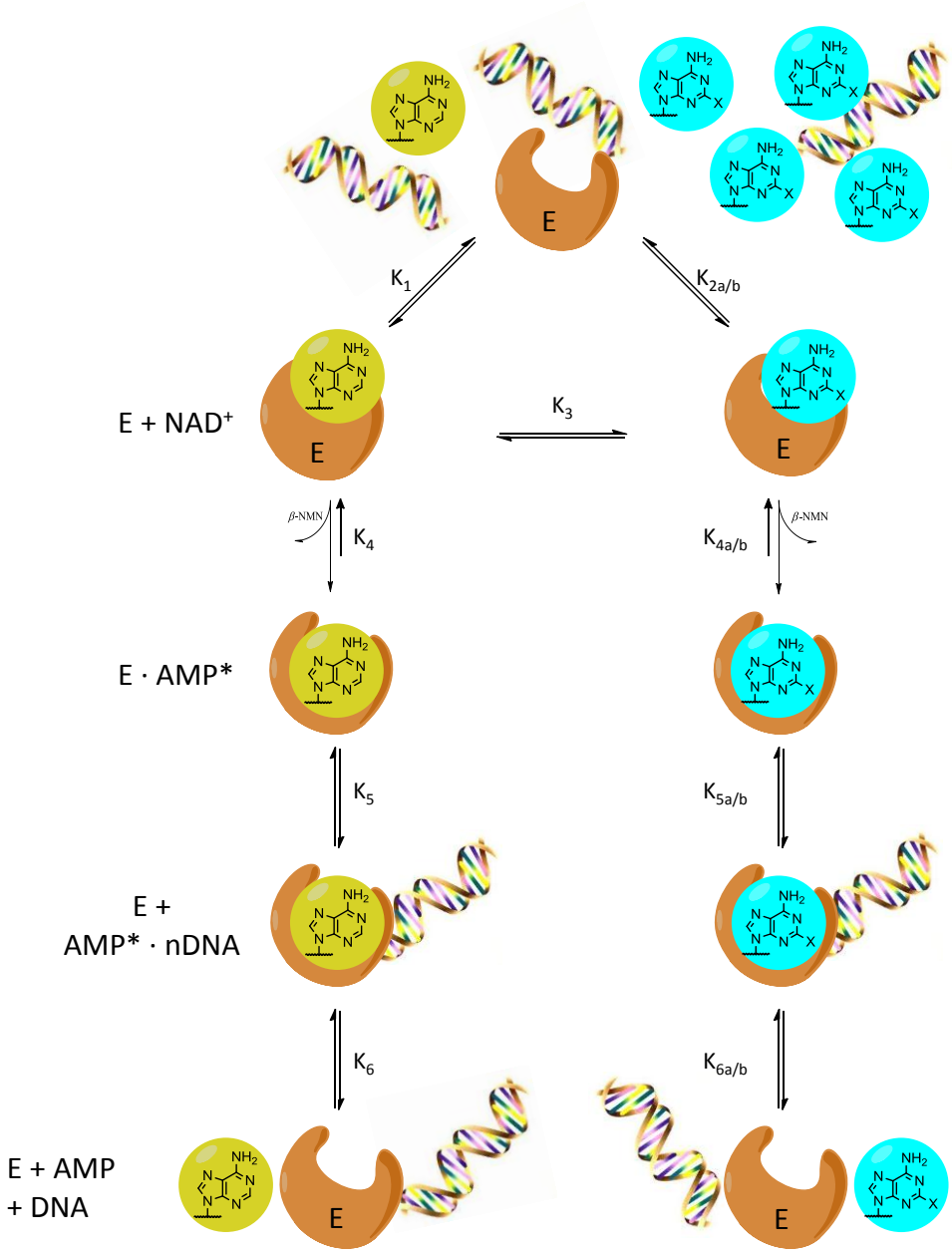

Figure 5.9 Competition of 2-substituted NAD^+ derivatives, **13a-b** (light blue), with β-NAD^+ (green) for EcLigA (E, brown). k_1 is the binding constant of β-NAD^+ to EcLigA; k_{2a} and k_{2b} are the binding constants respectively of **13a** and **13b** to EcLigA; k_3 is the rate constant for the displacement reaction; k_4 and $k_{4a/b}$ are the rate constants for the enzyme adenylation ($E{\cdot}AMP^*$) respectively with β-NAD^+, **13a** and **13b**; k_5 and $k_{5a/b}$ are the rate constants for the nicked DNA adenylation ($E + AMP^*{\cdot}nDNA$) respectively with β-NAD^+, **13a** and **13b**; k_6 and $k_{6a/b}$ are the rate constants for the ligation (E + AMP + DNA) respectively with β-NAD^+, **13a** and **13b**. In the inhibition experiments, where the excess of **13a-b** shifts the equilibria toward the binding of **13a-b** compared to β-NAD^+, the resulting ligation is due to differences in the rate of any of the steps involved in the metabolism of β-NAD^+ and **13a-b**.

5.1.2.1 Biological activities of 2-substituted AMP and NAD^+ derivatives

In agreement with the already developed inhibitors based on modifications of C-2 on the adenine ring of adenosine, ADP or ATP structures (see 5.1, Figure 5.3),[73, 74, 263] 2-substituted AMP/AMP-morpholidate/NAD^+ derivatives were found to be biologically active as inhibitors and/or NNSs of EcLigA, suggesting the validity of the introduction of substituents in position 2 on the adenine ring.

Interesting observations came out of the screening of the activities of the different compounds. As suggested by the combined observations of NNS and inhibitor activities, 2-iodo NAD^+, **13a**, was a NNS for EcLigA with a slow turnover compared to β-NAD^+, causing an inhibitory effect overall. In addition, 2-iodo AMP, **7a**, not a NNS because of its AMP scaffold, showed inhibitor activity and, therefore, a certain affinity for EcLigA. The activities for 2-phenyl NAD^+, **13b**, and 2-phenyl AMP, **7b**, were less clear. At first glance, the results showing no inhibition could be easily interpreted as no or weak binding to EcLigA; however, the NNS activity of **13b** suggested a similar binding and turnover compared to β-NAD^+, hence justifying the same extent of ligation as the control reaction. In contrast, **7b**, due to the AMP scaffold, could not be a NNS for EcLigA, but neither did it not show any inhibitory activity, therefore suggesting that **7b** could indeed have no activity.

The reasons for the different activities could be clearly ascribed to the different nature of the substituents. Size, conformational and electronic differences explained the different behaviors. Looking at the AMP derivatives activities, not complicated by the presence of NNS activity, it was evident that iodine imparted to **7a** a certain affinity for the enzyme active site, hence its ability to act as an inhibitor; in contrast, the phenyl group in **7b** did not generate any inhibition, indicating a low affinity/binding to the enzyme. These effects are likely to be due to the different size of the substituents and, therefore, to their ability to fit into the hydrophobic tunnel of the enzyme in correspondence to the C-2 of the adenine ring. Indeed, iodine and phenyl groups have a substantially different van der Waals volume (V_w), respectively 19.64 and 45.84 $cm^3 \cdot mol^{-1}$;[264] therefore, they would have a different occupancy in the hydrophobic tunnel of NAD^+-dependent DNA ligases. The phenyl substituent, larger than iodine,

could not fit properly into the tunnel, disfavouring the stabilization of **7b** in the active site; this would justify its low binding to EcLigA and, therefore, its absent inhibitor activity. Instead, iodine could fit more easily into the tunnel, causing the higher affinity of **7a** for EcLigA and, therefore, its activity as inhibitor.

The conformation of iodine and phenyl substituted adenine related to the ribose has to be considered when comparing the different activities. In 3.1.1, an adopted *anti* conformation in solution for the 2-substituted AMP derivatives was confirmed by ^{1}H NMR analysis, which tended toward a *syn* conformation for the 2-substituted NAD^{+} derivatives (see 3.1.2), in particular for the 2-phenyl NAD^{+}, **13b**. In the active site of NAD^{+}-dependent DNA ligases, the adenine of the natural *β*-NAD^{+} assumes a high *syn* conformation (Figure 5.10 **a**); in fact, in the literature it is known that often nucleosides/nucleotides with high *syn* or high *anti* conformations have high biological activities.[176, 265] Therefore, 2-substituted NAD^{+} derivatives should be able to assume a high *syn* conformation in the active site, where the substituents point far from the ribose avoiding any steric hindrance (Figure 5.10 **b**). A more pronounced high *syn* conformation for 2-phenyl NAD^{+}, **13b**, due to the larger volume occupied by the phenyl substituent, could be responsible for its higher similarity to the natural *β*-NAD^{+}, leading to its high substrate activity.

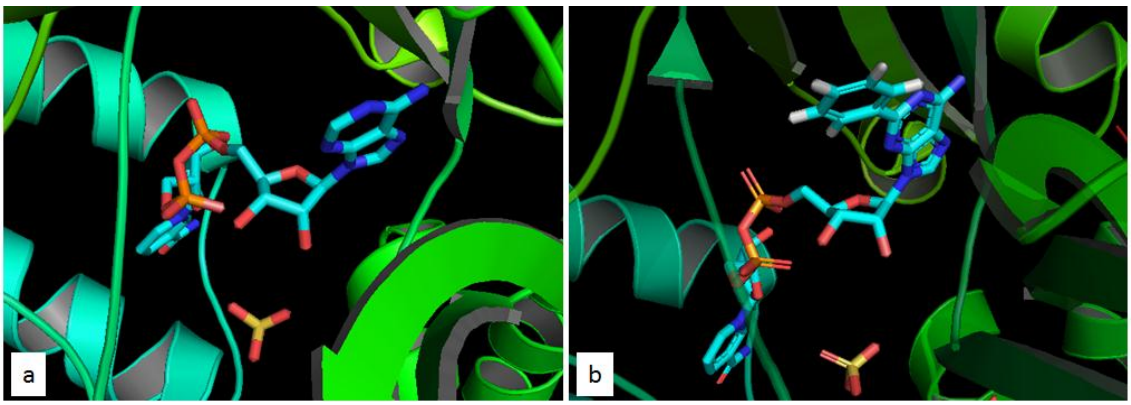

Figure 5.10 *β*-NAD^{+} (**a**) and **13b** (**b**) in the active site of DNA ligase from *E. faecalis* (PDB 1TAE). **13b** is built on the *β*-NAD^{+} structure. The high *syn* conformation of the adenine ring related to the ribose tolerates the introduction of substituents in position 2 without interfering with the binding in the active site. Visualization by PyMol software.

Examining the activities of **13a** and **13b**, both iodine and phenyl substituted NAD^+ derivatives had NNS activities; this indicated the essential nature of the β-NAD^+ scaffold in stabilizing in the active site the 2-phenyl AMP moiety, which alone did not bind properly to the enzyme. The different turnover of the two NAD^+ derivatives used as NNSs by EcLigA could be explained as due to electronic differences between the iodine and phenyl substituted adenine rings. Indeed, iodine is more electron-withdrawing than the phenyl group and, consequently, it can influence the electronic properties of the closest atoms in the aromatic ring.[176, 265] Then, N-1 and N-3 on the 2-iodo adenine could undergo a reduction of electron density reflecting on their H-bonding ability and, therefore, on the conformation assumed by the adenine ring related to the ribose. As mentioned in 5.1, an essential residue in the active site of EcLigA is Lys 290,[254] which is involved in H-bonding with N-1 on the adenine ring during all the three catalytic steps. Its presence is fundamental for making contacts with the adenine ring to keep it in the right position in the active site; its modification in mutants makes the enzyme almost inactive, suggesting its essential nature. In the case of 2-iodo NAD^+, **13a**, the reduced electron density on N-1 would negatively influence its ability to form H-bonds with Lys 290, explaining the hypothesized slow turnover of **13a** compared to β-NAD^+ and, therefore, its resulting inhibitory activity. Conversely, 2-phenyl NAD^+, **13b**, would keep intact the ability of N-1 to interact with Lys 290; indeed, the phenyl group would increase the electronic density on N-1, making the H-bonding even stronger than in the natural β-NAD^+. This effect would explain the similarity and competition of **13b** with β-NAD^+, and the resulting lack of ligation inhibition overall.

5.1.3 Biological testing of 6-substituted AMP and NAD^+ derivatives

The activity of 6-substituted AMP, AMP-morpholidate and NAD^+ derivatives was tested toward EcLigA. Firstly, 6-substituted NAD^+ derivatives, **14a** and **14b**, were tested as NNSs of EcLigA in the absence of natural β-NAD^+ at 250 μM, choosing this high concentration to ensure detection of any eventual NNS activity. Both compounds showed no activity as NNSs of EcLigA (data not shown).

Next, 6-substituted AMP/AMP-morpholidate/NAD^+ derivatives, respectively **8a**-**b**, **11a**, and **14a**-**b**, were tested as inhibitors of EcLigA. Inhibition studies were performed

testing the compounds at 250 µM, 10 fold higher than the natural β-NAD$^+$, with sampling at 7 and 15 min (Figure 5.11). From inhibition experiments, the compounds showed no activity as inhibitors of EcLigA, with the exception of the 6-phenyl AMP-morpholidate, **11a**, which showed 60% inhibition at 250 µM at 7 min. At 15 min, the ligation for the reaction containing **11a** increased to the level of the control reaction. The estimated IC_{50} value for **11a** was 172.7 ± 4.1 µM (Appendix 8, Figure A15).

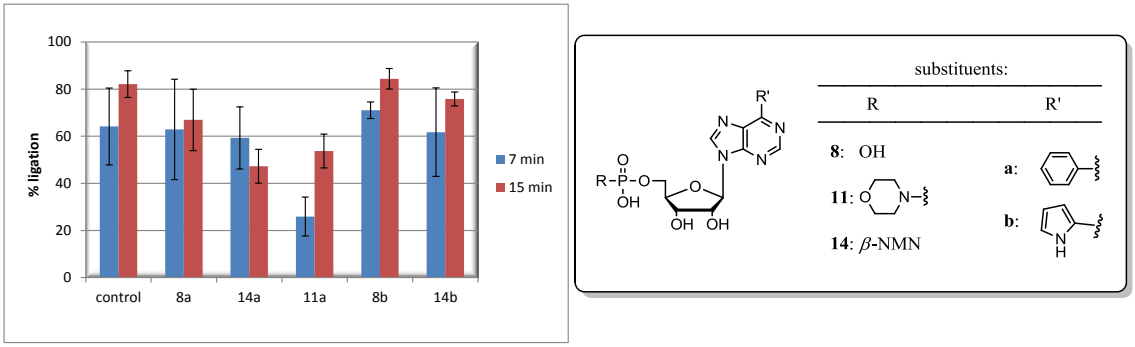

Figure 5.11 Inhibition of 6-substituted AMP/AMP-morpholidate/NAD$^+$ derivatives at 250 µM. *Conditions*: DNA substrate (0.5 µM), EcLigA (0.05 µM), β-NAD$^+$ (26 µM), 6-substituted derivative (250 µM) in 1 x buffer (30 mM Tris/HCl pH 8, 4 mM $MgCl_2$, 1 mM DTT, 50 µg/mL BSA); all concentrations are final concentrations. Reactions incubated at 30 °C under shaking and sampled at 7 and 15 min. Control reaction at the same conditions without any 6-substituted derivative. Analysis of assay run on denaturing PAGE and gel visualized by fluorescence imaging. Data analysed using ImageJ. Each data point is the mean (± SD) of a set of experiments run in triplicate; data plotting with Excel.

5.1.3.1 Biological activities of 6-substituted AMP and NAD$^+$ derivatives

From activity tests of 6-substituted AMP/AMP-morpholidate/NAD$^+$ derivatives, it was clear that the series of 6-substituted adenine derivatives was inactive toward EcLigA as inhibitors and NNSs, independent of the nature of the introduced substituent. Indeed, both phenyl and pyrrolyl substituents failed to show any kind of activity.

Looking at the crystal structure of β-NAD$^+$-bound DNA ligase from *E. faecalis* (PDB 1TAE), there exists a small polar cavity that would be able to accommodate the exocyclic amino group in position 6 on the adenine ring, but which would probably be too narrow to accommodate a phenyl or a pyrrolyl substituent. In addition, since there are no essential residues in the active site that interact with the amino group in position 6, its modification should not cause any effect on the activity of the enzyme. Therefore,

the lack of inhibitory activity of 6-substituted adenine derivatives could be due to their inability to strongly interact with the enzyme active site, consequently allowing an easier displacement by the natural β-NAD^+. In addition, the lack of NNS activity could be due to some distortion of the adenine ring in the active site to accommodate the introduced substituent, which would not fit into the cavity for the exocyclic amino group.

5.1.4 Biological testing of 8-substituted NAD^+ derivatives

NAD^+ derivatives substituted in position 8, **15b**,**c**,**e**,**g**,**h**, were tested as NNSs and inhibitors of EcLigA. For the NNS activity, the compounds were tested at 250 μM in the absence of β-NAD^+; this concentration, 10 fold larger than that used for the assay with the natural β-NAD^+, was chosen to ensure detection of any substrate activity. All compounds belonging to this series appeared inactive as NNSs, even after long reaction times. Indeed, in the attempt to assess their substrate activity, pre-incubation studies of 8-substituted NAD^+ derivatives with EcLigA were performed at different temperatures and reaction times starting the reaction with addition of DNA; nevertheless, none of these experiments showed any ligation activity (data not shown). In addition, when natural β-NAD^+ was added to the unsuccessful reactions, the ligation immediately went to completion (Figure 5.12), indicating the enzyme retained full activity and, therefore, confirming its inability to use 8-substituted NAD^+ derivatives as NNSs.

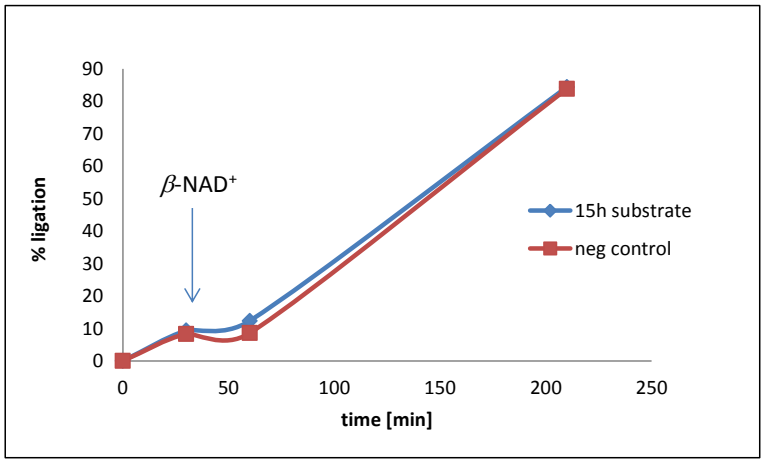

Figure 5.12 NNS activity test of **15h**. *Conditions*: DNA substrate (0.125 µM), EcLigA (0.1 µM), **15h** (250 µM) in 1 x buffer (30 mM Tris/HCl pH 8, 4 mM $MgCl_2$, 1 mM DTT, 50 µg/mL BSA); all concentrations are final concentrations. Negative control at the same conditions without **15h**. Reaction incubated at 30 °C under shaking for 1 h; then, addition of β-NAD^+ (26 µM), and reaction stopped and analysed by denaturing PAGE after 2.5 h. Gel visualization by fluorescence imaging, data analysis by ImageJ, and data plotting with Excel.

Inhibition studies were performed by testing the compounds at 250 µM in the presence of β-NAD^+ at 26 µM. From these experiments, 8-substituted NAD^+ derivatives showed weak or no activity at all as inhibitors of EcLigA at 250 µM (Figure 5.13); only **15e** and **15h** inhibited EcLigA around 40% at 250 µM.

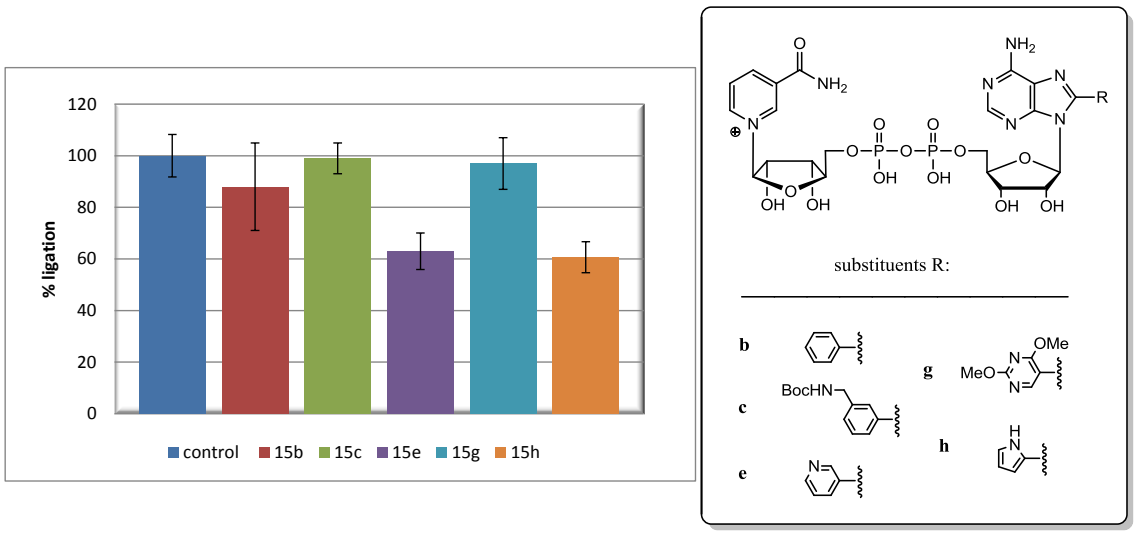

Figure 5.13 Inhibition of 8-substituted NAD^+ derivatives at 250 µM. *Conditions*: DNA substrate (0.125 µM), EcLigA (0.1 µM), β-NAD^+ (26 µM), 8-substituted NAD^+ derivative (250 µM) in 1 x buffer (30 mM Tris/HCl pH 8, 4 mM $MgCl_2$, 1 mM DTT, 50 µg/mL BSA); all concentrations are final concentrations. Reactions incubated for 10 min at 30 °C under shaking. Control reaction at the same conditions without any 8-substituted NAD^+ derivative. Analysis of assay run on denaturing PAGE and gel visualized by fluorescence imaging. Data analysed using ImageJ. Each data point is the mean (± SD) of a set of experiments run in triplicate; data plotting with Excel.

5.1.4.1 Biological activities of 8-substituted NAD^+ derivatives

From activity tests of 8-substituted NAD^+ derivatives, it was clear that this series was practically inactive toward EcLigA as inhibitors and NNSs, independent of the nature of the introduced substituent. To explain the inactivity of 8-substituted NAD^+ derivatives, a deeper investigation of the enzyme active site was performed.

Looking at the β-NAD^+-bound DNA ligase from *E. faecalis* (PDB 1TAE), a clear steric hindrance between the position 8 on the adenine of β-NAD^+ and a close loop delimiting the active site can be seen (Figure 5.14 **a**); consequently, the introduction of a substituent in position 8 on the adenine ring would cause an unavoidable clash with the loop (Figure 5.14 **b**).

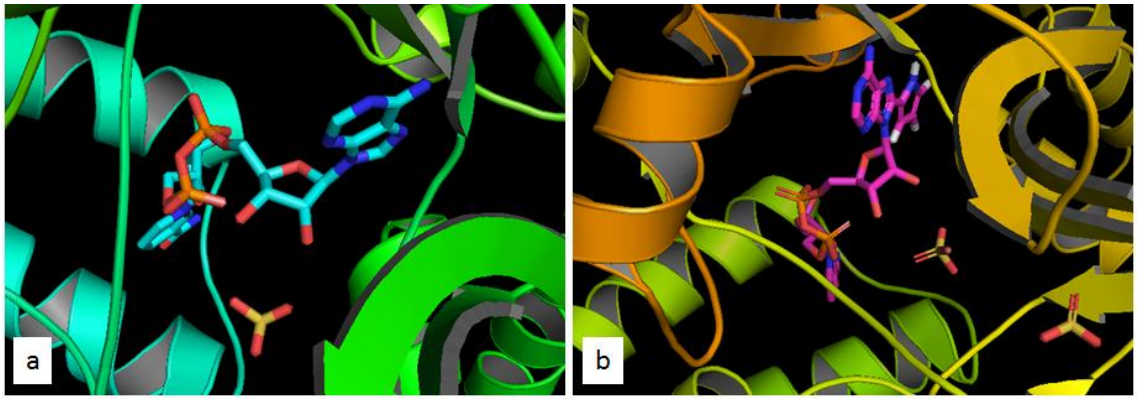

Figure 5.14 β-NAD^+ (**a**) and **15h** (**b**) in the active site of DNA ligase from *E. faecalis* (PDB 1TAE). **15h** is built on the β-NAD^+ structure. The introduction of substituents in position 8 on the adenine ring would interfere with the binding in the active site. Visualization by PyMol software.

As discussed in 3.1.2, 8-substituted NAD^+ derivatives are characterized by a pronounced *syn* conformation of the adenine ring, where the substituent in position 8 points far from the ribose. Therefore, 8-substituted NAD^+ derivatives would already have the appropriate *syn* conformation to fit in the active site of DNA ligase with the same binding mode of β-NAD^+; however, the steric clash with the loop would prevent their initial accommodation into the active site.

This observation raises the question as to whether 8-substituted NAD^+ derivatives would be able to bind in the enzyme active site at all. In an attempt to answer this

question, the docking of a representative compound from the series of 8-substituted NAD^+ derivatives, **15h**, into the crystal structure of DNA ligase from *E.faecalis* (PDB 1TAE) was performed and the resulting structures with the best scores were compared with the structure of the natural β-NAD^+. The best docked structures showed **15h** respectively in *anti* (**a**), *syn* (**b**) and high *syn* (**c**) conformation (Figure 5.15).

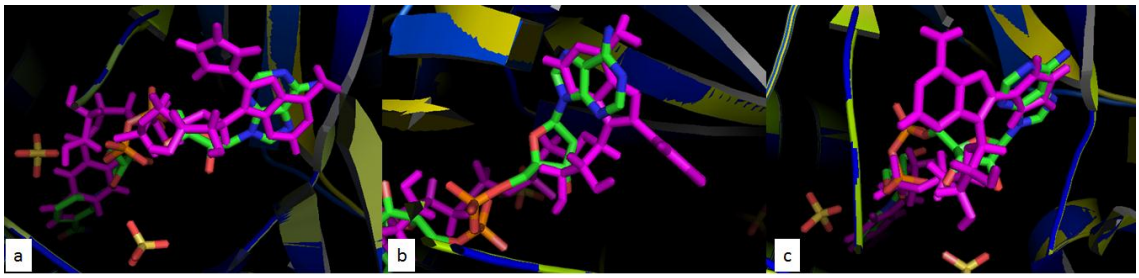

Figure 5.15 Docking of **15h** (pink) and superimposition with β-NAD^+ (green) in the active site of DNA ligase from *E. faecalis* (PDB 1TAE). **a)** Docked **15h** in *anti* conformation; **b)** docked **15h** in *syn* conformation; **c)** docked **15h** in high *syn* conformation. Visualization by PyMol software.

In an attempt to avoid the steric clash between the substituent in position 8 and the loop, the docking software flipped the adenine of 180° around the *N*-glycosidic bond, keeping the ribose fixed in case **a)** to obtain an *anti* conformation; or flipped the adenine of 180° around the *N*-glycosidic bond and also rotated the ribose in case **b)** to allow the adenine to remain in the favoured *syn* conformation; or in case **c)**, the adenine kept the high *syn* conformation without any torsion around the *N*-glycosidic bond moving back compared to its position in β-NAD^+ to avoid the steric clash of the substituent with the loop.

The assumption of an *anti* conformation by **15h** in case **a)** would require a large conformational change and distortion of the nucleobase related to the ribose, representing an unrealistic situation. Instead, the maintenance of a *syn* conformation in case **b)** owing to the ribose rotation around the *N*-glycosidic bond is more likely to occur because of the ribose flexibility, as well as the maintenance of high *syn* conformation in case **c)**, due to the backwards movement of the adenosine moiety to avoid the steric clash with the loop.

Another interesting observation among the different docked structures was that, by flipping the adenine of 180° around the *N*-glycosidic bond, C-8 and its substituent pointed into the hydrophobic tunnel, instead of C-2, as is the case of the natural *β*-NAD^+. Therefore, both the potential *anti* and *syn* (Figure 5.15 **a** and **b** respectively) conformations of the docked **15h** would accommodate the pyrrolyl substituent inside the hydrophobic tunnel, stabilizing their position in the active site.

These reasonable structures assumed by **15h** in the active site of DNA ligase from *E. faecalis* show the possibility of the compound fitting in the active site. However, in all these potential structures the contacts with the essential catalytic residues in the binding site (Table 5.1) are destroyed. This effect could be fatal in terms of any possible binding and consequent activity as inhibitors and/or NNSs of 8-substituted NAD^+ derivatives on the DNA ligases.

5.1.5 Summary

Summarising all the results obtained by the screening of AMP/AMP-morpholidate/NAD^+ derivatives substituted on C-2, C-6 or C-8 of the adenine ring, it was possible to conclude that only the series of the 2-substituted adenine derivatives showed biological activity toward EcLigA as inhibitors and/or NNSs, depending on the introduced substituent and its interactions within the active site. Indeed, both the presence of the hydrophobic tunnel in the enzyme structure in which the substituent in position 2 can be accommodated, and the high *syn* conformation of the adenine base related to the ribose, resembling the natural *β*-NAD^+, allowed the stabilization of the 2-substituted adenine derivatives in the active site and, therefore, their ability to interfere with the enzyme activity. In contrast, compounds belonging to the series of adenine derivatives substituted on C-6 and C-8 could not actively interact within the active site, consequently showing no activity.

To create new antibacterial drugs acting on the activity of NAD^+-dependent DNA ligases, the appropriate choice of substituents introduced in position 2 of the adenine ring has to be considered. As shown previously in the literature, the introduction of long alkyl chains that fit into the hydrophobic tunnel blocking the compounds in the active

site allows the development of efficient inhibitors of NAD^+-dependent DNA ligases.[73, 74] From our studies, it emerged that the insertion of small electron-withdrawing groups in position 2 of the adenine ring, that are able to substantially change the H-bonding ability of the adenine ring could be important for developing good inhibitors. Moreover, the size of the substituents would be crucial in generating inhibitory activity; indeed, from our analysis it was suggested that a phenyl group was already too large to properly fit into the hydrophobic tunnel. This could be a limit to the application of the Suzuki-Miyaura cross-coupling in modifying the C-2 position on the adenine ring, since only aryl groups smaller than the phenyl could be possibly inserted in the adenine ring to generate inhibitors. In addition, as expected because of their inactivity as NNSs, AMP derivatives would be more suitable backbones than NAD^+ derivatives as inhibitors, since no side substrate activity could interfere in their influence on the enzyme activity.

AMP-morpholidates, **10b** and **11a**, showed inhibitor activities toward EcLigA regardless of the introduced substitution and its position on the adenine ring. At the outset of this project, it was expected that AMP-morpholidates would either act as NNSs or inhibit the enzyme by covalent modification. Indeed, their phosphate, activated compared to that in the AMP derivatives, could undergo the nucleophilic attack by the lysine residue into the active site to form the adenylated-enzyme; then, the latter could be active and evolve in the next ligation steps, or be inactive and block the ligation. However, AMP-morpholidates did not show any NNS activity. Moreover, in the inhibition experiments the ligation increased at later times in the reaction with both **10b** and **11a** (Figure 5.8, Figure 5.11); therefore, the inhibition could not be due to covalent modification of the enzyme, but it is more likely to be due to reversible binding of the derivatives in the active site. The fact that 2-phenyl AMP-morpholidate, **10b**, was active as an inhibitor in contrast to 2-phenyl AMP, **7b**, and that 6-phenyl AMP-morpholidate, **11a**, was active as an inhibitor in contrast to all other derivatives belonging to its series, showed that the modification on the phosphate, and not those on the adenine ring, was responsible for the inhibition by AMP-morpholidates.

Looking at the perspective for generating biochemical tools for biochemical investigations, the development of 2-substituted NAD^+ derivatives as NNSs for NAD^+-dependent DNA ligases has been a useful achievement in this project. Indeed, the

different activities of the differently substituted NAD^+ derivatives can be related to structural and mechanistic details of the enzyme, providing a deeper understanding and, therefore, a more strategic development of inhibitors.

5.2 Sirtuins

Protein acetylation/deacetylation is a fundamental process to regulate protein activity, localization, interaction, stability and degradation. Consequently, it contributes to cellular regulation of processes such as transcription, proliferation, apoptosis and differentiation, occurring in response to signalling pathways. As is the case for the phosphorylation performed by kinases with a broad substrate specificity, acetylation/deacetylation seems to involve many biological targets in answer to particular intracellular and extracellular signals.[266]

The main and best known targets for acetylation modification are the histones, proteins found in all eukaryotic cells, involved in the packaging of DNA into chromatin and, therefore, responsible for gene regulation. Histones contain many basic lysine residues that can undergo acetylation/deacetylation modification by acetylases/deacetylases. When histones are acetylated on relevant lysine residues, the resulting charge on these amino acids becomes neutral overall and, therefore, histones do not interact so well with the negatively charged DNA; the latter can then be more easily unwound and transcribed or replicated by RNA or DNA polymerases. In contrast, when histones are deacetylated on relevant lysine residues, the resulting positive charge on these amino acids allows them to interact with the negatively charged DNA, winding it more tightly and avoiding its transcription or replication. The acetylation/deacetylation process is therefore part of the epigenetic changes in gene expression that occur without modifying the DNA sequence; thus, acetylases/deacetylases can regulate gene transcription and modulate gene silencing and transcriptional repression.

Acetylases/deacetylases are better known as histone acetyltransferases (HATs) and histone deacetylases (HDACs), despite acting on a variety of substrates. HDACs, first isolated in yeast from *Saccharomyces cerevisiae*, are divided into four classes: I, II and IV classes formed by zinc-dependent deacetylases, while III class by NAD^+-dependent

deacetylases. The latter class is responsible for gene silencing, from which its name, Sir, stands for "silent information regulator".[267]

In humans, seven NAD^+-dependent HDACs have been isolated and, because of their homology with the yeast Sir family, these are called sirtuins. An increased interest in sirtuins has developed in the past years because of their involvement in a variety of biological processes. The transcriptional gene regulation and the implication of sirtuins in DNA repair are the main processes in which they are involved, together with cellular stress resistance, therefore ageing control and life span increase; metabolic regulation, as they influence glucose, fat and insulin metabolism; and apoptosis regulation, thus their possible implication as anticancer targets. All these processes have been connected since the discovery that enzymes, such as sirtuins, appear to be involved in the regulation of them all.[268-270]

Sir2 from *Saccharomyces cerevisiae*, belonging to class III of NAD^+-dependent HDACs, has been structurally characterized. The protein consists of a large domain containing a Rossmann-fold structure, with two small domains inserted; one of them is a zinc-binding module, not involved in the catalytic cycle (Figure 5.16 **a**). The β-NAD^+-binding pocket is characterized by three regions, A for the adenosine binding, B for the nicotinamide ribonucleoside binding and C, a deep region in the catalytic pocket involved in the nicotinamide cleavage (Figure 5.16 **b**). When β-NAD^+ binds to the enzyme, NaM would fit in the B region but, in the presence of acetyl lysine, the enzyme would undergo a conformational change bringing NaM into the C region, where the *N*-glycosidic bond is cleaved.

As mentioned in 1.2.1, it is not certain if sirtuins cleave the nicotinamide *N*-glycosidic bond by an S_N1 mechanism, *via* formation of the oxocarbenium ion intermediate, or by an S_N2 mechanism, with nucleophilic attack by the oxygen of the acetyl lysine on C-1″ and simultaneous release of NaM. However, the reaction products are the deacetylated lysine and the 2′-OAc-ADPR, in equilibrium with the 3′-OAc-ADPR.[31, 267, 269]

As described in Chapter 1, inhibition or activation of sirtuins activity can regulate different biological processes and provide understanding of their mode of action. NaM, one of the sirtuins reaction products, is a non-competitive inhibitor for sirtuins. It seems

to bind in the C region of the catalytic pocket, more than in the B one, causing the regeneration of β-NAD$^+$ by transglycosidation.[31] Consequently, many sirtuins inhibitors based on mimicking NaM have been developed, together with others mimicking the adenosine[72] and NAD$^+$ structure (see 1.3.1).[31, 70, 267]

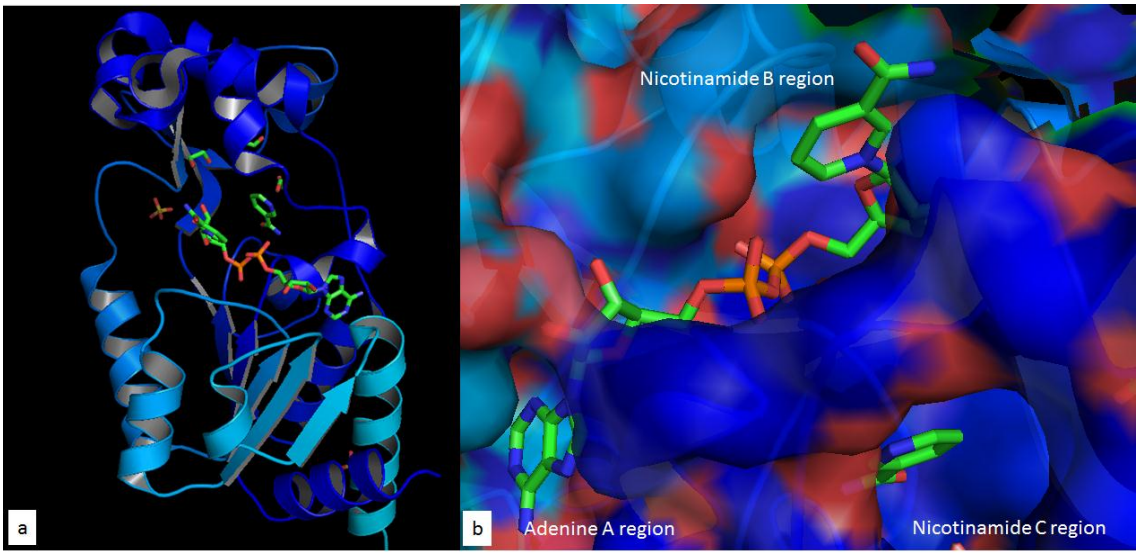

Figure 5.16 **a)** Structure of archaeal Sir2-Af2 with β-NAD$^+$ bound; **b)** β-NAD$^+$-binding pocket (PDB 1YC2). Visualization by PyMol software.

Since several biological processes, such as life span increase, seem to be linked to an activation of the sirtuins activity, the discovery of sirtuins activators has become more important. A class of polyphenols, resveratrol being the most known and representative, has shown activator activity toward sirtuins; this effect seems to be connected with the binding of activators in the C region, where otherwise free NaM released from the reaction would bind and inhibit the sirtuins activity.[271]

5.2.1 Biological testing of 8-substituted NAD$^+$ derivatives

As mentioned in Chapter 1, NAD$^+$ derivatives can be effective inhibitors or NNSs of sirtuins depending on the substitutions performed to modify the structure of the natural substrate.[31] It has been shown that carba-NAD$^+$ (Figure 1.15), where the β-D-ribose of the nicotinamide ribonucleoside has been replaced with a 2,3-dihydroxycyclopentane

ring, is not a hydrolysable NAD^+ derivative and, therefore, acts as an inhibitor of sirtuins. This compound has been a useful biochemical tool to investigate and understand the structure of the active site and the sirtuins reaction mechanism.[31]

8-aryl/heteroaryl NAD^+ derivatives, **15b**, **15h**[246], **16-22**, synthesized in Chapter 2 (see 2.7.2, Scheme 2.20 and Figure 5.17), were tested as inhibitors and/or NNSs of human SIRT1-2[70] in collaboration with Prof. M. Jung and co-workers. The assay described in Chapter 1 (see 1.4.7), using Z-MAL as a non-natural peptide substrate for sirtuins, was used to evaluate the activities of the tested compounds.

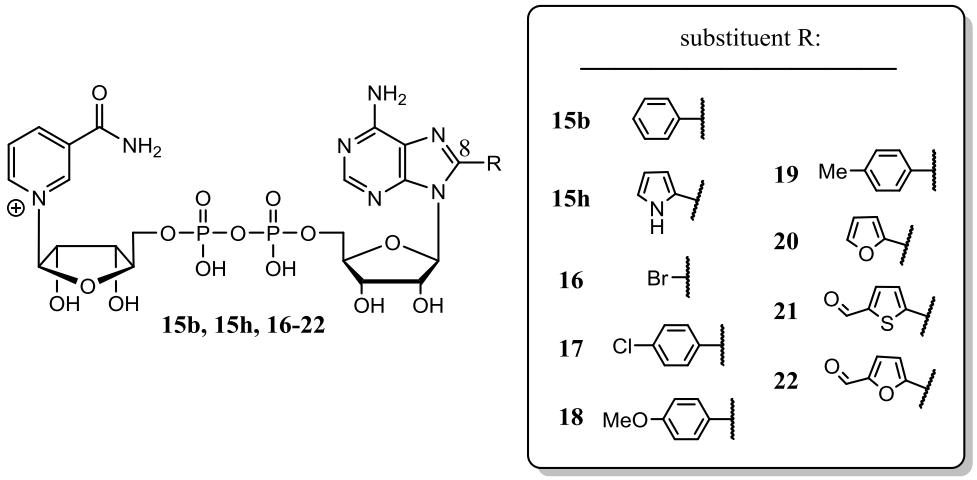

Figure 5.17 8-aryl/heteroaryl NAD^+ derivatives, **15b**, **15h**, **16-22**, tested as inhibitors and/or NNSs of human SIRT1-2.[70]

From the inhibition experiments with 8-aryl/heteroaryl NAD^+ derivatives and a few of the corresponding adenosine and AMP derivatives at 50 μM, it emerged that, with the exception of **15h**[246] and **20**, all 8-aryl/heteroaryl NAD^+ derivatives exerted preferentially an inhibitory activity toward SIRT2 compared to SIRT1. For those compounds showing an inhibitory activity ≥ 50% at 50 μM on either sirtuins isoforms, IC_{50} values were estimated and found to be in the order of low micromolar concentration.[70] In addition to the 8-aryl/heteroaryl NAD^+ derivatives, the inhibitory activity was tested for the corresponding adenosine and AMP derivatives with bromo and phenyl substituents. With the exception of 8-phenyl AMP, all other derivatives showed no activity toward either SIRT1 nor SIRT2, indicating the necessity to have the

whole β-NAD^+ scaffold to be effective inhibitors.[70] With the hypothesis that 8-aryl/heteroaryl NAD^+ derivatives could act as NNSs for sirtuins and, consequently, influence the inhibition results, their substrate activity was also tested. With the exception of **15b**, which showed a minor substrate activity, all other derivatives did not have any.[70]

5.2.2 Biological activities of 8-substituted NAD^+ derivatives

Investigations using computational studies were undertaken to provide a better understanding of the mode of inhibition of 8-aryl/heteroaryl NAD^+ derivatives and their apparent selectivity toward the different isoforms of human sirtuins. The alignment of sequences for SIRT1 and SIRT2 was used to analyse the similarities between the different isoforms; effectively, only a 44% identity was observed between the two enzymes.[70]

Examining the crystal structures available for human SIRT2 (PDB 1J8F) and SIRT3 (PDB 3GLT), a flexible loop with a high level of sequence conservation has been reported to be involved in the β-NAD^+ binding and NaM release.[31] However, in the different isoforms the loop seems to assume completely different conformations. Therefore, interferences between the substituents in position 8 and the flexible loop could be responsible for the selectivity of 8-aryl/heteroaryl NAD^+ derivatives toward the different isoforms of human sirtuins and for their lack of substrate activity.[70]

The few available crystal structures for different sirtuins isoforms containing β-NAD^+ or ADPR show an adenine in *anti* conformation compared to the ribose. However, as discussed in 3.1.2, all 8-aryl/heteroaryl NAD^+ derivatives have the adenine ring in a more or less definite *syn* conformation because of the steric hindrance between the substituent in position 8 and the ribose.[70] From the docking of a representative 8-substituted NAD^+ derivative (**17** in Figure 5.17) within SIRT2 (PDB 1J8F) and superimposition with β-NAD^+ in the archaeal enzyme Sir2-Af2 (PDB 1YC2), the same *anti* conformation was observed for adenine in **17** and β-NAD^+, suggesting that 8-aryl/heteroaryl NAD^+ derivatives could undergo conformational changes during their binding to the enzyme. Sirtuins themselves could be able to induce these conformational

changes with a different ability depending on the isoform involved, consequently influencing the inhibition selectivity of 8-aryl/heteroaryl NAD^+ derivatives toward the different sirtuins isoforms. In support of this hypothesis, it was observed that **15h**[246] and **20**, characterized by a strong *syn* conformation (Table 3.2), had no inhibitor and substrate activities,[70] presumably because sirtuins would not be able to overcome such definite conformations of the molecule.

6 CONCLUSIONS AND FUTURE WORK

NAD^+-consuming enzymes play a crucial role in important biological processes; hence, it is fundamental to require a better understanding of their biological activities, how they are modulated and how they influence each other and the activities of other important enzymes in cells. The development of NAD^+ derivatives as biochemical tools for the study of this class of enzymes has been, and is still, one of the most challenging biochemical topics.

Reviewing the substitutions performed on the existing NAD^+ derivatives and their influences on the enzyme activities, the modification of the adenine ring appeared as the most suitable to confer selective biological activities as inhibitors and/or NNSs to the novel NAD^+ derivatives toward a selected range of enzymes. Due to the recent and impressive advances in the application of palladium-mediated cross-couplings to the nucleosides/nucleotides modifications, the choice of using the Suzuki-Miyaura cross-coupling to substitute the adenine ring made possible the development of aryl/heteroaryl adenine-modified NAD^+ derivatives. In particular, positions 2, 6 and 8 were modified with phenyl, and, where possible, pyrrolyl groups to explore the different properties of the compounds and their activities generated by the introduction of hydrophobic and H-bond making groups.

The successful synthesis of aryl/heteroaryl NAD^+ derivatives substituted on C-2, C-6 or C-8 of the adenine ring was accomplished following the optimization of the known multistep synthesis to generate the new classes of compounds. However, two additional strategies, requiring further studies, were investigated to accelerate the synthesis of the NAD^+ derivatives. The pathway *via* phosphoramidite nucleoside intermediate was unsuccessful presumably because of the low nucleophilicity and insolubility of *β*-NMN in acetonitrile. Therefore, beyond a screening of polar aprotic solvents (*e.g.* DMSO, DMF, acetone) to improve the solubility of *β*-NMN, the replacement of DCI with other phosphoramidite activators (*e.g.* tetrazole, HOBt) during the coupling with *β*-NMN could bring the reaction to success. On the other hand, the pathway *via* *β*-NAD^+ bromination/Suzuki-Miyaura cross-coupling in a one-pot, two-step procedure allowed

the successfull synthesis of different 8-aryl/heteroaryl NAD^+ derivatives, although it did fail in the coupling with very electron poor boronic acids.

The synthesized compounds were analysed from the spectroscopic and conformational perspective, showing interesting properties. In particular, 8-aryl/heteroaryl adenine derivatives showed fluorescent properties that could be modulated depending on the nature of the substituent introduced. In addition, as shown from our studies and previous data about the conformational properties of β-NAD^+ and its well known derivative, ε-NAD^+, all of the synthesized NAD^+ derivatives were characterized by a folded conformation in aqueous solution, due to the interactions between the hydrophobic aromatic rings in the molecule. This folded conformation could be released by solvation in organic solvents, bringing the opening of the β-NAD^+ scaffold to an extended conformation. These conformational properties, combined with the fluorescence of 8-aryl/heteroaryl NAD^+ derivatives, were the basis of their use as fluorescent probes to monitor the activities of NAD^+-consuming enzymes. Indeed, the folded conformation of the compounds caused a fluorescence quenching that could be disrupted by the separation of the modified adenine ring, the fluorophore under discussion, and the nicotinamide moiety with consequent fluorescence re-establishment. The enzymatic cleavage of the β-NAD^+ scaffold on the pyrophosphate or the nicotinamide *N*-glycosidic bonds, catalyzed by NAD^+-consuming enzymes, was therefore responsible for a fluorescence increase allowing monitoring of the enzymatic reactions.

The use of fluorescent 8-substituted NAD^+ derivatives as NNSs by NAD^+-consuming enzymes made them useful biochemical probes to investigate enzymatic structures, activities and kinetics in more detail by monitoring their fluorescence changes. Therefore, fluorescence-based assays were successfully developed for selected NAD^+-consuming enzymes, giving interesting mechanistic information.

The fluorescence principle of the assays using 8-aryl/heteroaryl NAD^+ derivatives is essentially the same as those developed with the well known ε-NAD^+. However, the use of our best fluorophore, **15h**, containing a pyrrolyl group in position 8 on the adenine ring, increased the sensitivity of the assays compared to those using ε-NAD^+ because of a stronger fluorescence increase during the enzymatic reaction. Moreover, the

application of **15h** for the monitoring of enzymes for which ε-NAD^+ failed in the development of continuous fluorescence-based assays could be investigated. For instance, as discussed in Chapter 1, ε-NAD^+ was not a good substrate for PARPs and a continuous fluorescence-based assay could not be developed. Therefore, it would be worth testing **15h** on PARPs activity to assess whether there were positive differences compared to ε-NAD^+.

In contrast to the 8-aryl/heteroaryl NAD^+ derivatives, those substituted in position 2 and 6 showed weak, or no fluorescence at all; therefore, they could not be used as fluorescent biochemical probes. Nevertheless, they were still useful tools to investigate enzymatic structures and mechanisms. In particular, the biological activities of 2-substituted NAD^+ derivatives toward DNA ligases gave clues to fundamental interactions between the *β*-NAD^+ scaffold and its binding site.

It was shown that 2-iodo and 2-phenyl NAD^+ derivatives, both non-fluorescent, were NNSs of EcLigA. Therefore, an idea for developing fluorescent NNSs came from the considerations of their activities. Since a substituent in position 2 on the adenine ring is crucial to confer to the NAD^+ derivatives the ability to bind in the active site by positioning the substituent into the hydrophobic tunnel, as well as to assume a high *syn* conformation resembling that of the natural *β*-NAD^+, the substitution of the adenine ring with 2-amino purine (**1**) or 2,6-diamino purine (**2**)[190] (Figure 6.1), both isomorphic fluorescent nucleobases (Chapter 3, see 3.3.2), may confer to the corresponding NAD^+ derivatives their fluorescence properties.

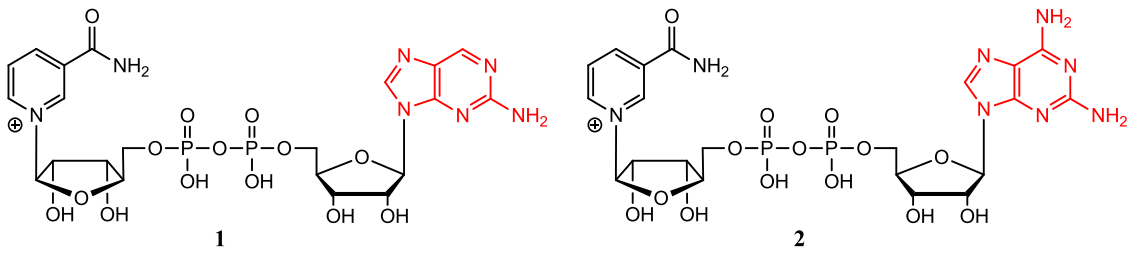

Figure 6.1 Two possible fluorescent NNSs of NAD^+-dependent DNA ligases: nicotinamide 2-amino purine dinucleotide (**1**) and nicotinamide 2,6-diamino purine dinucleotide (**2**).

These compounds could potentially be exploited for binding and kinetic/mechanistic studies. The binding studies could rely on the fluorescence enhancement of the NNSs following their passage from a folded quenched conformation in solution to an extended conformation in the active site. On the other hand, the DNA ligase activity could be monitored by the fluorescence increase due to the formation of the AMP derivative from the cleavage of the quenched NAD^+ derivative (the same principle on which the monitoring of NPPs is based). In addition, kinetic and mechanistic details could come from the fluorescence changes occurring in the fluorescent adenine derivatives following their interactions with Lys 290 in the active site along the three different reaction steps. Indeed, the formation of the H-bond between N-1 and Lys 290 would change the electronic delocalization along the adenine-modified rings; hence, the formation of a partial positive charge on N-1 could bring a fluorescence quenching similar to that occurring in the N^1-*c*ADPR derivatives analysed in Chapter 4.

Of course, these modifications could have some limitations. Firstly, the introduced amino group in position 2 is polar, so it is unlikely to properly interact with the hydrophobic tunnel of the DNA ligase, and could be unable to stabilize the NAD^+ derivatives in the active site. Secondly, 2-AP would lack the exocyclic amino group of the adenine ring, which could cause a decreased binding in the active site for this compound. However, since no fluorescent NAD^+ derivatives have been reported as NNSs for NAD^+-dependent DNA ligases (ε-NAD^+ and 8-aryl/heteroaryl NAD^+ derivatives did not show any activity), it would be worth exploring the activity of these two compounds in order to create fluorescent probes for NAD^+-dependent DNA ligases.

A comparison of activities exerted by 8-aryl/heteroaryl NAD^+ derivatives against all of the enzymes examined in this project was undertaken to investigate their selectivity and, therefore, their potential application for *in vitro*/*in vivo* studies. A summary of the biological evaluation of the 8-substituted NAD^+ derivatives against the different NAD^+-consuming enzymes is shown in Table 6.1.

	Activity	
Enzyme	*Inhibitor*	*Substrate*
NPP (*Crotalus adamanteus* venom)	✓	✓
NADase (porcine brain)	✓	✓
ADPRC (*Aplysia californica*)	✓	✓
Human SIRT1-2	✓	–
DNA ligase (EcLigA)	–	–

Table 6.1 Activities of 8-aryl/heteroaryl NAD^+ derivatives toward different NAD^+-consuming enzymes. The tick ✓ indicates that the compounds showed the specified activity toward the selected enzyme; the line – indicates that the compounds did not show the specified activity toward the selected enzyme.

A certain selectivity exerted by 8-aryl/heteroaryl NAD^+ derivatives against the different enzymes was observed. Indeed, with the exception of NADase and ADPRC sharing the same unifying catalytic mechanism (Chapter 4, see 4.2), the enzymes examined, though sharing the same substrate/co-substrate, have different active sites and modes of *β*-NAD^+ binding, which are responsible for their different catalytic reactions and, therefore, for the different activities shown by 8-substituted NAD^+ derivatives. To underline the intrinsic structural differences that distinguish these enzymes and their activities, the available crystal structures for *β*-NAD^+-bound ADPRC from *Aplysia californica* (**a**), archaeal Sir2-Af2 (**b**) and DNA ligase from *E. faecalis* (**c**) were examined and their active sites were compared (Figure 6.2).

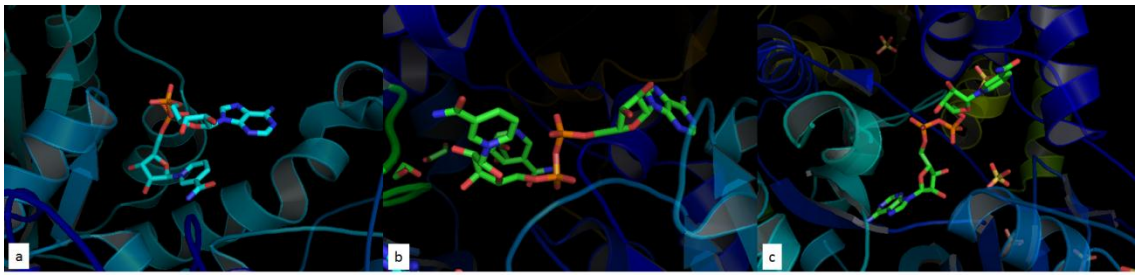

Figure 6.2 *β*-NAD^+ in the active site of ADPRC from *Aplysia californica* (PDB 3ZWM) (**a**), archaeal Sir2-Af2 (PDB 1YC2) (**b**), DNA ligase from *E. faecalis* (PDB 1TAE) (**c**). Visualization by PyMol software.

In ADPRC (Figure 6.2 **a**), the *β*-NAD^+ binding site is completely exposed to the solvent and *β*-NAD^+ is bound in a folded conformation, since the enzyme catalyzes its cyclization to *c*ADPR. The adenine ring, free from any interaction with the enzyme and originally in an *anti* conformation related to the ribose, during the catalytic cycle will

orient in a *syn* conformation to facilitate the cyclization on N-1 (Table 6.2). Due to the lack of interactions of the adenine ring with the enzyme, the substitution in position 8 in the synthesized NAD^+ derivatives could be tolerated by the enzyme and the compounds could fit in the active site already in a *syn* conformation, which facilitates the cyclization.

In the archaeal Sir2-Af2 (Figure 6.2 **b**), the β-NAD^+ binding site is quite exposed to the solvent and β-NAD^+ is bound in an extended conformation. The adenine ring, in *anti* conformation related to the ribose (Table 6.2), interacts strongly with the active site residues though not directly involved in the catalytic reaction. Therefore, its modification interferes with the enzyme activity, making 8-substituted NAD^+ derivatives inhibitors of sirtuins.

Finally, in DNA ligase (Figure 6.2 **c**), the β-NAD^+ binding site is exposed to the solvent at the moment of the binding and β-NAD^+ is bound in an extended conformation. The adenine ring, directly involved in the catalytic reaction (see 5.1), interacts with the active site residues. Its initial high *syn* conformation in β-NAD^+ will turn into *anti* in the adenylated-enzyme intermediate (**1**) (Scheme 5.1), to finally return to high *syn* in the adenylated-DNA intermediate (**2**) (Scheme 5.1, Table 6.2). Hence, in the DNA ligase catalytic mechanism the adenine moiety is key for the enzymatic reaction and the β-NAD^+ binding is so specific that substitutions on the adenine ring, unless the adenine orientation in β-NAD^+ is left unchanged, do not allow any enzymatic activity. Indeed, NAD^+ derivatives substituted on C-6 and C-8 of the adenine ring, in which the substituents change the position/orientation of the adenine in the active site, did not exert any effect on the activity of EcLigA because they could not bind in any active way to the enzyme.

Just from this simple visual analysis of the active site and β-NAD^+ binding mode, it is possible to suggest a structural and, therefore, biological diversity between the three examined enzymes, justifying the different biological activity exerted by 8-substituted NAD^+ derivatives.

Enzyme	*Adenine conformation changes during the catalytic cycle*
ADPRC (*Aplysia californica*)	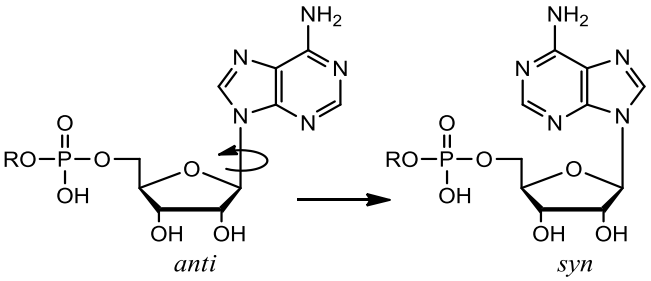 R = β-NMN
Human SIRT1-2	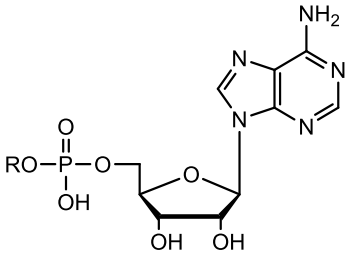 R = β-NMN
DNA ligase (EcLigA)	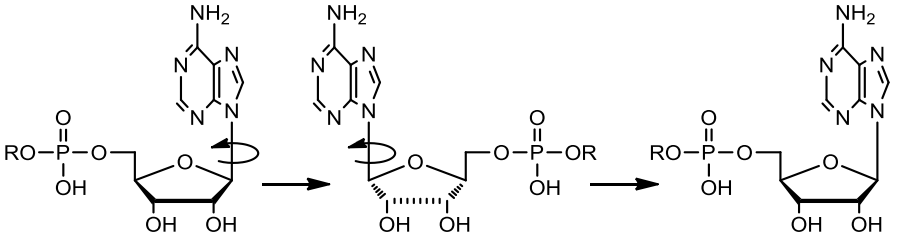 R = β-NMN **1**; R = enzyme **2**; R = DNA

Table 6.2 Changes in the adenine conformation during the catalytic cycle in ADPRC, SIRT1-2 and DNA ligase.

For the examined structures of ADPRC from *Aplysia californica*, archaeal Sir2-Af2 and DNA ligase from *E. faecalis*, a sequence alignment was performed, showing only 0.9% of identity. Therefore, structure similarities were estimated pairwise by comparing the results obtained with rigid and flexible structure alignments (Appendix 8, Table A1).[272, 273] The latter method allows consideration of proteins as flexible bodies, as they are in reality; hence, the program, instead of just answering how large is the similar part that two proteins share, as happens in the rigid structure alignment, it also estimates how much a protein can rearrange itself to be more similar to another one. All these analyses were in agreement with a deep structural diversity of the enzymes examined, confirming once again their different biological roles, though sharing the same substrate/co-

substrate, β-NAD^+. This structural diversity definitively reflected on the various activities exerted by 8-substituted NAD^+ derivatives toward these enzymes.

Summarising the results obtained in this project, it is possible to conclude that aryl/heteroaryl substitutions on different positions on the adenine ring can generate novel NAD^+ derivatives with biological activities toward NAD^+-consuming enzymes. The preferential action of aryl/heteroaryl adenine-modified NAD^+ derivatives as inhibitors and/or NNSs toward specific NAD^+-consuming enzymes offers the prospective of their use for *in vitro*/*in vivo* studies. Of course, such a step forward in their biological evaluation means considering many factors that until now have not been an issue. For instance, in the case of their activity on intracellular enzymes, such as sirtuins or DNA ligases, their resistance to the degradation exerted by ecto NAD^+-consuming enzymes or intracellular nucleases should be considered. Therefore, chemical modifications on the β-NAD^+ scaffold or alternative delivering methods should be developed related to the use for which they are designed. However, the validity of their use as biochemical probes is already a great pace to widen the knowledge of fundamental biological processes involving NAD^+-consuming enzymes.

7 EXPERIMENTAL

7.1 General

7.1.1 Synthesis and characterization

All synthetic reagents were obtained commercially and used as received, including anhydrous solvents over molecular sieves, unless otherwise stated. Milli-Q water was used for the preparation of aqueous solutions and as solvent in the reactions. For the synthesis of phosphoramidites, CH_2Cl_2 was distilled over calcium hydride, and DIPEA was dried over molecular sieves (4 Å) for four days before the use. For the preparation of dinucleotides, $MnCl_2$ solution in formamide was dried over molecular sieves (4 Å) and stored under nitrogen atmosphere. All reagents and solvents used for analytical applications were of analytical quality. TLC was performed on precoated slides of Silica Gel 60 F_{254} (Merck). Spots were visualized under UV light (254/365 nm). Reaction products were characterized by high-resolution mass spectrometry (HR-MS), ^{1}H, ^{13}C and ^{31}P NMR spectroscopy, and HPLC. ^{1}H NMR spectra were recorded at 298 K on a Varian VXR 400 S spectrometer at 400 MHz, or on a Bruker Avance DPX-300 spectrometer at 300 MHz, or on a Bruker BioSpin GmbH at 400 MHz. ^{13}C NMR spectra were recorded at 300 K on a Bruker BioSpin GmbH at 150.90 MHz and at 101 MHz. ^{31}P NMR spectra were recorded at 298 K on a Varian VXR 400 S spectrometer at 161.98 MHz, or on a Bruker BioSpin GmbH at 161.98 MHz. Chemical shifts (δ) are reported in ppm (parts per million) and referenced to D_2O, CD_3OD or $CDCl_3$ (respectively, δ_H 4.79, 3.31, 7.26) for ^{1}H NMR, and to CH_3 of TEA, CD_3OD or $CDCl_3$ (respectively, δ_C 9.07, 49.00, 77.16) for ^{13}C NMR. Coupling constants (*J*) are reported in Hz. Accurate electrospray ionization mass spectra were obtained on a Finnigan MAT 900 XLT mass spectrometer at the EPSRC National Mass Spectrometry Service Centre, Swansea. Ion-pair and ion-exchange chromatography was performed on a Biologic LP chromatography system equipped with a peristaltic pump and a 254 nm UV Optics Module. For detailed conditions, see 7.1.2. High performance liquid chromatography (HPLC) was performed on a Perkin Elmer series 200 equipped with a Supelcosil LC-18T column (25 cm x 4.6 mm, particle size 5 μm), a diode array detector (detection wavelengths: 254/280 nm) and a column oven (temperature: 30 ºC). For

detailed conditions, see 7.1.2. Absorbance spectra were recorded on a PerkinElmer Lambda 25 UV/Vis spectrometer at room temperature in FarUV quartz cells (path length 1.0 cm). Fluorescence spectra were recorded on a PerkinElmer LS-45 spectrometer at room temperature in a quartz fluorescence cell (path length 1.0 cm).

7.1.2 Chromatography conditions

Preparative chromatography – purification method 1: Ion-pair chromatography was performed using Lichroprep RP-18 resin and a variable gradient of methanol against 0.05 M TEAB (triethylammonium bicarbonate buffer). Product containing fractions were combined and reduced to dryness. The residue was co-evaporated repeatedly with methanol to remove residual TEAB.

Preparative chromatography – purification method 2: Anion-exchange chromatography was performed using Bioscale™ Mini Macro-Prep High Q cartridges and a gradient of 0-100% 1 M TEAB (pH 7.3) against Milli-Q H_2O. Product containing fractions were combined and reduced to dryness. The residue was co-evaporated repeatedly with methanol to remove residual TEAB.

High performance liquid chromatography (HPLC): samples (injection volume: 20 μL) were analysed using a mobile phase composed of 0.05 M triethylammonium phosphate buffer at pH 8 (solvent A) and methanol (solvent B), according to the gradient steps in Table 7.1 (flow rate: 1.5 mL/min).

Step	*Minutes (min)*	*Gradient*
1	0 – 2	90% A – 10% B
2	2 – 17	10 – 50% B
3	17 – 19	50% B
4	19 – 21	50 – 10% B
5	21 – 25	90% A – 10% B

Table 7.1 Gradient steps for HPLC analysis of the NAD^+ derivatives.

7.1.3 Enzymology

All reagents used for biological application were of analytical quality and solutions prepared with Milli-Q water. NPP from *Crotalus adamanteus* venom, NADase from porcine brain and ADPRC from *Aplysia californica* were purchased from Sigma. Human SIRT1-2 were expressed and purified as described[70, 274] with minor modifications. EcLigA from *E. coli* was expressed and purified as described[250] with minor modifications (see 7.7.1). pET-16b vector, His-tag binding column (IDA-based His-Bind Resin Ni^{2+} precharged) and its buffer kit were purchased from Novagen. Protein desalting was performed using a PD-10 Column (Sephadex G-25 Medium) and its buffer (20 mM Tris, 200 mM NaCl, pH 7.5). To quantify the protein concentration according to the Bradford method, the Bio-Rad Protein Assay, consisting of a protein dye reagent (Coomassie Brilliant Blue G-250 in acidic solution), was purchased from Bio-Rad (absorbance reading at 595 nm). The oligonucleotides for the ligation assay were supplied by Eurogentec. For fluorescence imaging, Molecular Dynamics Storm Phosphorimager was used. Fluorescence assays were performed in NUNC 96 plates on a BMG labtech PolarStar microplate reader equipped with suitable absorbance and emission filters.

7.2 Synthesis

7.2.1 General synthetic procedures

A Iodination of C-2 by diazotization-iodine substitution[134]

Isoamyl nitrite (3.1 equiv.) was added to a mixture of respectively **1a** and **1c** (1 equiv.) with I_2 (1 equiv.), CH_2I_2 (10.4 equiv.) and CuI (1 equiv.) in the given volume of THF. The mixture was refluxed for the given time and then, cooled down at room temperature. Inorganic salts were removed by filtration, and the filtrate was evaporated to dryness *in vacuo.* The crude product was purified by silica gel chromatography, as indicated for each compound.

B1 Suzuki-Miyaura cross-coupling on C-6[158]

6-chloro purine nucleoside (**5**) (1 equiv.), Na_2PdCl_4 (0.03 equiv.), TPPTS (2.5 equiv. to Pd), K_2CO_3 (2 equiv.) and aryl/heteroaryl boronic acid (1.2 equiv.) were placed in a flask and purged with nitrogen for 15 min. Degassed water was added by syringe to the reaction vessel and the mixture was stirred at 100 °C under nitrogen for the given time. When the reaction was complete, the mixture was evaporated *in vacuo*, and the crude product purified as indicated for each compound.

B2 Suzuki-Miyaura cross-coupling on C-8[172]

8-Br-AMP (**9a**) (1 equiv.) and the appropriate amounts of Na_2PdCl_4, TPPTS, K_2CO_3 or K_3PO_4, and aryl/heteroaryl boronic acid were placed in a flask and purged with nitrogen for 15 min. Degassed water was added by syringe to the reaction vessel and the mixture was stirred at the appropriate temperature under nitrogen for the given time. When the reaction was complete, the mixture was evaporated *in vacuo*, and the crude product purified by chromatography, as indicated for each compound.

C 2′,3′-*O*-isopropylidene protection[141]

The respective nucleoside (1 equiv.) was suspended in acetone and 70% $HClO_4$ (2.5 equiv.) was added to the mixture. The reaction was stirred at room temperature for 1.5 h. Then, NH_4OH 25% (5.6 equiv.) was added to the reaction, and the solution stirred for 3 h. The mixture was diluted with EtOAc and extracted with brine (3x). Then, the organic phase was dried over anhydrous $MgSO_4$ and evaporated to dryness *in vacuo.* The crude product was purified as indicated for each compound.

D1 Phosphorylation of 5′-OH by $POCl_3$ (method 1)[136, 144]

The respective 2′,3′-*O*-isopropylidene protected nucleoside (1 equiv.) was dissolved in the given solvent with optional proton sponge, and the solution cooled down to 2 °C in ice-bath. Then, the appropriate amount of $POCl_3$ was added drop-wise to the reaction mixture, that was kept at 4 °C for 12 h. The reaction was quenched adding drop-wise 1 M TEAB buffer. If proton sponge was present, the mixture was diluted with EtOAc and

extracted (3x). Then, the aqueous solution was evaporated to dryness *in vacuo* and the crude product purified by purification method 2, as indicated for each compound.

D2 Phosphorylation of 5′-OH *via* phosphoramidite (method 2)[113]

The respective 2′,3′-*O*-isopropylidene protected nucleoside (1 equiv.) was dissolved in anhydrous CH_2Cl_2 and co-evaporated twice to dryness. Then, it was dissolved again in anhydrous CH_2Cl_2, and DIPEA (2.5 equiv.) and the given quantity of 2-cyanoethyl *N*,*N*-diisopropyl chlorophosphoramidite were added *via* syringe. The reaction was stirred under nitrogen at room temperature for the given time. Then, 5.0 – 6.0 M ^{t}BuOOH in nonane solution (4 equiv.) was added to the reaction and stirred for the given time. The mixture was diluted with EtOAc and extracted with a saturated sodium bicarbonate solution (2x) and brine (1x). The organic phase was dried over anhydrous $MgSO_4$ and evaporated to dryness *in vacuo*; then, the residue was suspended in NH_4OH 25% (30 equiv.) under stirring at room temperature overnight. The solution was evaporated to dryness *in vacuo*, and the crude product used for the next step (see procedure E).

E 2′,3′-O-isopropylidene deprotection[136]

The respective 2′,3′-*O*-isopropylidene protected nucleotide was dissolved in water and stirred with Dowex 88 (H^+) (*ca* 0.1 g) overnight. After filtration, the solution was evaporated to dryness *in vacuo* and the crude product purified by purification method 1, as indicated for each compound.

F Synthesis of AMP-morpholidate derivatives[112, 172]

The respective nucleotide (1 equiv.) was dissolved in DMSO, and then co-evaporated with DMF (3x). The residue was dissolved in anhydrous DMSO and morpholine (6 equiv.) was added. After 5 min, 2,2′-dithiopyridine (3 equiv.) was added and, subsequently, triphenylphosphine (3 equiv.). The yellow solution was stirred at room temperature under nitrogen until TLC showed complete conversion. The product was isolated by purification method 1, or by precipitation as sodium salt with NaI in acetone (0.1 M), as indicated for each compound. The NaI solution was added drop-wise to the reaction mixture until a solid precipitate formed; then, the precipitate was washed

repeatedly with acetone until the solution was colourless. The crude product was dried and used in the next reaction step without further purification.

G Synthesis of NAD^+ derivatives[112, 172]

The appropriate amounts of AMP-morpholidate and *β*-NMN were co-evaporated with pyridine (3x). The flask with the residual solid was purged with nitrogen for 15 min. Anhydrous $MgSO_4$ (2 equiv.) and $MnCl_2$ (0.2M in formamide, 1.5 equiv.) were added and the reaction was stirred at room temperature under nitrogen until TLC showed complete conversion. The reaction was stopped by drop-wise addition of acetonitrile until a white precipitate formed. The supernatant was removed and the solid dissolved in water and evaporated to dryness *in vacuo*. The crude product was purified by chromatography, as indicated for each compound.

7.2.2 Preparation of 2-substituted AMP derivatives (**7a-c**)

2-Amino-6-chloro-9*β*-(2′,3′,5′-tri-*O*-acetyl-D-ribofuranosyl)-purine (1a)[134]

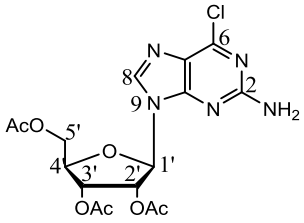

1a

Triethylamine (8.7 equiv.), DMAP (12 equiv.) and acetic anhydride (10.7 equiv.) were added to a suspension of the commercially available **1c** (0.4465 g, 1 equiv.) in acetonitrile (30 mL). The clear mixture was stirred at room temperature for 1 h, then quenched with MeOH and evaporated to dryness *in vacuo*. The crude product was extracted with EtOAc/water (2x) and the organic phase was dried over anhydrous $MgSO_4$. After concentration to dryness *in vacuo*, the residue was crystallized from MeOH to give **1a** as white crystals (0.5635 g, 89% yield). ^{1}H NMR (400 MHz; $CDCl_3$) δ: 7.87 (1H, s, 8-H), 6.00 (1H, d, $J_{1',2'}$ = 4.9 Hz, 1′-H), 5.95 (1H, apparent t, 2′-H), 5.74 (1H, apparent t, 3′-H), 4.51 – 4.31 (3H, m, 4′-H, 5′-H_2), 2.14 (3H, s, *Ac*), 2.10 (3H, s,

Ac), 2.09 (3H, s, *Ac*); ^{13}C NMR (101 MHz; $CDCl_3$) δ: 170.66, 169.73, 169.50, 164.16, 159.20, 152.09, 140.82, 86.75, 80.14, 72.86, 70.61, 63.06, 51.05, 20.87, 20.70, 20.58.

2-Iodo-6-chloro-9*β*-(2′,3′,5′-tri-*O*-acetyl-D-ribofuranosyl)-purine (1b)[134]

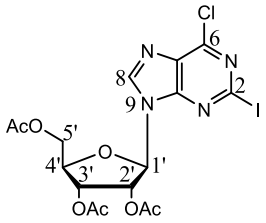

1b

The title compound was prepared according to the general synthetic procedure A, from **1a** (0.1257 g, 1 equiv.), isoamyl nitrite, I_2, CH_2I_2 and CuI in THF (1.5 mL). The mixture was refluxed for 12 h and then, cooled down at room temperature. The crude product was purified by silica gel chromatography, washing the column with CH_2Cl_2 to remove the iodine, then with an eluent 98:2 CH_2Cl_2/MeOH. **1b** was obtained as white crystals (0.1349 g, 85% yield). ^{1}H NMR (400 MHz; $CDCl_3$) δ: 8.20 (1H, s, 8-H), 6.18 (1H, d, $J_{1',2'}$ = 5.4 Hz, 1′-H), 5.76 (1H, apparent t, 2′-H), 5.57 (1H, m, 3′-H), 4.59 – 4.22 (3H, m, 4′-H, 5′-H_2), 2.15 (3H, s, *Ac*), 2.11 (3H, s, *Ac*), 2.08 (3H, s, *Ac*); ^{13}C NMR (101 MHz; $CDCl_3$) δ: 170.29, 169.64, 169.48, 152.02, 151.02, 143.28, 132.29, 117.06, 86.72, 80.88, 73.41, 70.61, 62.99, 20.94, 20.64, 20.50.

2-Iodo-6-chloro-9*β*-D-ribofuranosyl-purine (1d)

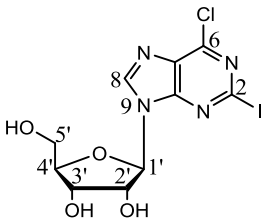

1d

The title compound was prepared according to the general synthetic procedure A, from the commercially available **1c** (0.5544 g, 1 equiv.), isoamyl nitrite, I_2, CH_2I_2 and CuI in THF (40 mL). The mixture was refluxed for 4 h and then, cooled down at room temperature. The crude product was purified by silica gel chromatography, washing the

column with CH_2Cl_2 to remove the iodine, then with an eluent 90:10 CH_2Cl_2/MeOH. **1d** was obtained as a colourless oil (0.382 g, 51% yield). ^{1}H NMR (400 MHz; CD_3OD) δ: 8.77 (1H, s, 8-H), 6.09 (1H, d, J = 5.0 Hz, 1′-H), 4.65 (1H, apparent t, 2′-H), 4.36 (1H, apparent t, 3′-H), 4.15 (1H, m, 4′-H), 3.90 (1H, dd, $J_{5'a,4'}$ = 3.1 Hz, $J_{5'a,b}$ = 12.3 Hz, 5′a-H), 3.79 (1H, dd, $J_{5'b,4'}$ = 3.5 Hz, $J_{5'b,a}$ = 12.3 Hz, 5′b-H). 6-Chloro-9*β*-D-ribofuranosyl-purine was eluted later as a side-product of the reaction. ^{1}H NMR (400 MHz; CD_3OD) δ: 8.86 (1H, s, 2-H), 8.75 (1H, s, 8-H), 6.16 (1H, d, J = 5.2 Hz, 1′-H), 4.71 (1H, apparent t, 2′-H), 4.38 (1H, apparent t, 3′-H), 4.16 (1H, m, 4′-H), 3.90 (1H, dd, $J_{5'a,4'}$ = 3.0 Hz, $J_{5'a,b}$ = 12.3 Hz, 5′a-H), 3.79 (1H, dd, $J_{5'b,4'}$ = 3.3 Hz, $J_{5'a,b}$ = 12.3 Hz, 5′b-H).

2-Iodo-9*β*-D-ribofuranosyl-adenine (4)[134]

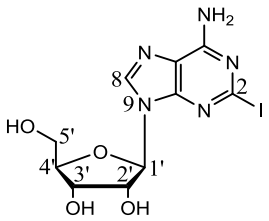

4

1b (0.1304 g, 1 equiv.) and **1d** (0.382 g, 1 equiv.) were respectively dissolved in 7 N methanolic ammonia and heated at 60 °C for 12 h in a sealed tube. After degassing the solution, the latter was evaporated to dryness *in vacuo*; then, the residue was crystallized from water to give **4** as white crystals (0.0381 g, 40% yield from **1b**, 0.1111 g, 30% yield from **1d**). ^{1}H NMR (400 MHz; CD_3OD) δ: 8.21 (1H, s, 8-H), 5.91 (1H, d, $J_{1',2'}$ = 6.1 Hz, 1′-H), 4.67 (1H, apparent t, 2′-H), 4.32 (1H, m, 3′-H), 4.15 (1H, m, 4′-H), 3.89 (1H, dd, $J_{5'a,4'}$ = 2.7 Hz, $J_{5'a,b}$ = 12.5 Hz, 5′a-H), 3.75 (1H, dd, $J_{5'b,4'}$ = 3.0 Hz, $J_{5'b,a}$ = 12.5 Hz, 5′b-H); ^{13}C NMR (101 MHz; CD_3OD) δ: 157.17, 150.57, 141.59, 120.74, 120.45, 90.96, 87.84, 75.42, 72.40, 63.26.

2-Iodo-9*β*-(2′,3′-*O*-isopropylidene-D-ribofuranosyl)-adenine (4a)[135]

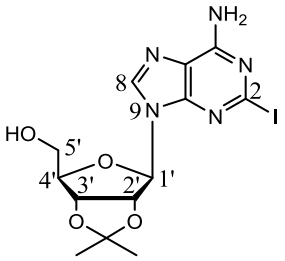

4a

The title compound was prepared according to the general synthetic procedure C, from a suspension of **4** (0.148 g, 1 equiv.) in acetone (10 mL), adding 70% $HClO_4$ (82 µL) and NH_4OH (82 µL). The crude product was purified by silica gel chromatography with an eluent 98:2 CH_2Cl_2/MeOH. **4a** was obtained as a colourless oil (0.160 g, 98% yield). ^{1}H NMR (400 MHz; CD_3OD) δ: 8.20 (1H, s, 8-H), 6.10 (1H, d, $J_{1',2'}$ = 3.2 Hz, 1′-H), 5.24 (1H, m, 2′-H), 5.01 (1H, m, 3′-H), 4.34 (1H, m, 4′-H), 3.79 (1H, dd, $J_{5'a,4'}$ = 3.7 Hz, $J_{5'a,b}$ = 12.0 Hz, 5′a-H), 3.72 (1H, dd, $J_{5'b,4'}$ = 4.5 Hz, $J_{5'b,a}$ = 12.0 Hz, 5′b-H), 1.61 (3H, s, *isoprop.*), 1.38 (3H, s, *isoprop.*); m/z (ESI) 432.0167 $[M-H]^-$, $C_{13}H_{15}IN_5O_4^-$ requires 432.0174.

2-Phenyl-9*β*-(2′,3′-*O*-isopropylidene-D-ribofuranosyl)-adenine (4b)[136]

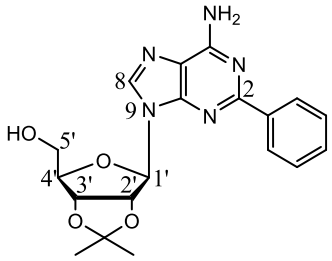

4b

4a (0.083 g, 1 equiv.), phenyl boronic acid (1.7 equiv.), $Pd(OAc)_2$ (0.12 equiv.), (2-biphenyl)dicyclohexylphosphine (0.16 equiv.) and K_3PO_4 (2.2 equiv.) were added in a sealed tube and purged with nitrogen for 10 min; after addition of anhydrous 1,4-dioxane (3 mL), the tube was sealed and heated at 100 °C for 24 h. The reaction mixture was evaporated to dryness *in vacuo* and the crude product was purified by silica gel chromatography with a gradient 0-6% MeOH/CH_2Cl_2. **4b** was obtained as white

crystals (0.0318 g, 43% yield). ^{1}H NMR (400 MHz; $CDCl_3$) δ: 8.33 – 8.08 (2H, m, *Ph*), 7.83 (1H, s, 8-H), 7.46 (3H, m, *Ph*), 5.90 (1H, d, $J_{1',2'}$ = 4.6 Hz, 1′-H), 5.64 – 5.41 (1H, m, 2′-H), 5.19 (1H, m, 3′-H), 4.48 (1H, m, 4′-H), 3.81 (2H, m, 5′-H_2), 1.66 (3H, s, *isoprop.*), 1.41 (3H, s, *isoprop.*); ^{13}C NMR (101 MHz; $CDCl_3$) δ: 160.95, 155.71, 150.15, 140.86, 138.12, 130.27, 128.64, 128.47, 119.71, 114.30, 93.45, 85.92, 82.60, 81.71, 63.34, 27.76, 25.48; m/z (ESI) 384.1670 $[M+H]^+$, $C_{19}H_{22}N_5O_4^+$ requires 384.1666.

2-(*N*-Me-Pyrrol-2-yl)-9*β*-(2′,3′-*O*-isopropylidene-D-ribofuranosyl)-adenine (4c)

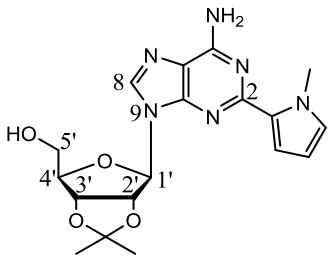

4c

4a (0.083 g, 1 equiv.), tributyl-(*N*-Me-pyrrol-2-yl) stannane (5 equiv.), optional anhydrous LiCl (1.2 equiv.), $PdCl_2(PPh_3)_2$ (0.06 equiv.) were added in a sealed tube and purged with nitrogen for 10 min; after addition of anhydrous 1,4-dioxane (2.5 mL), the tube was sealed and heated at 90 °C for 48 h. The reaction mixture was evaporated to dryness *in vacuo* and the crude product was purified by silica gel chromatography with an eluent 98:2 CH_2Cl_2/MeOH. **4c** was never isolated pure, but in a mixture with the starting material **4a** and stannane contamination; the ^{1}H NMR showed 43-50% conversion. ^{1}H NMR (400 MHz; CD_3OD) δ: 8.30 (1H, s, 8-H), 6.97 (1H, br s, 5-H *pyrrole*), 6.86 (1H, br s, 3-H *pyrrole*), 6.20 (1H, d, $J_{1',2'}$ = 2.9 Hz, 1′-H), 6.16 – 6.11 (1H, m, 4-H *pyrrole*), 5.39 (1H, m, 2′-H), 5.02 – 5.00 (1H, m, 3′-H), 4.09 (3H, s, *N*-CH_3), 4.38 (1H, m, 4′-H), 3.87 – 3.67 (2H, m, 5′-H_2), 1.7 – 1.3 (6H, 2s, 2 *isoprop.*).

Phosphoric acid mono-5′-[2-iodo-9*β*-(2′,3′-*O*-isopropylidene-D-ribofuranosyl)-adenine] (4g)[136]

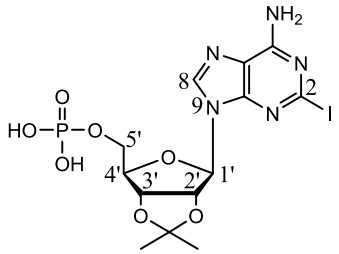

4g

The title compound was prepared according to the general synthetic procedure D1, from **4a** (0.0753 g, 1 equiv.) and $POCl_3$ (0.1 mL, 6.2 equiv.) in anhydrous acetonitrile (2.5 mL). The crude product was purified by purification method 1 (0-60% MeOH against 0.05 M TEAB buffer over 350 mL, then isocratic 60% over 50 mL, flow: 3 mL/min, fraction size: 5 mL), to give **4g** as a colourless oil (0.0102 g, 1.45 equiv. TEA, 9% yield). ^{1}H NMR (400 MHz; D_2O) δ: 8.35 (1H, s, 8-H), 6.19 (1H, d, $J_{1',2'}$ = 3.2 Hz, 1′-H), 5.36 (1H, m, 2′-H), 5.17 (1H, m, 3′-H), 4.62 (1H, br s, 4′-H), 3.99 (3H, m, 5′-H_2), 3.18 (8.7H, q, *J* = 7.3 Hz, CH_2 TEA), 1.66 (3H, s, *isoprop.*), 1.43 (3H, s, *isoprop.*), 1.25 (13.2H, t, *J* = 7.3 Hz, CH_3 TEA); ^{31}P NMR (162 MHz; D_2O) δ: 1.54.

Phosphoric acid mono-5′-[2-phenyl-9*β*-(2′,3′-*O*-isopropylidene-D-ribofuranosyl)-adenine] (4h)[136]

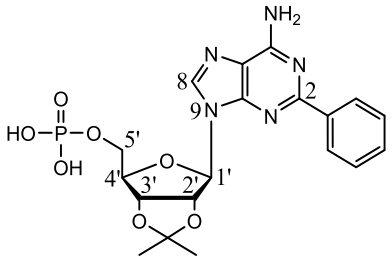

4h

The title compound was prepared according to the general synthetic procedure D1, from **4b** (0.0155 g, 1 equiv.), proton sponge (6 equiv.) and $POCl_3$ (25 µL, 6 equiv.) in triethylphosphate (4 mL). The crude product was purified by purification method 2 (0-100% 1 M TEAB buffer against H_2O over 300 mL, flow: 2 mL/min, fraction size: 5 mL), to give **4h** as a colourless oil (yield not calculated because the product was full of TEA salts). ^{1}H NMR (400 MHz; D_2O) δ: 8.33 (1H, s, 8-H), 8.06 (2H, m, *Ph*), 7.49 (3H,

m, *Ph*), 6.32 (1H, br s, 1′-H), 5.44 (1H, s, 2′-H), 5.21 (1H, s, 3′-H), 4.61 (1H, s, 4′-H), 4.01 (2H, m, 5′-H_2), 3.35 (85.7H, q, *J* = 7.3 Hz, *CH_2* TEA), 1.68 (3H, s, *isoprop.*), 1.45 (3H, s, *isoprop.*), 1.25 (88.7H, t, *J* = 7.2 Hz, *CH_3* TEA); ^{31}P NMR (162 MHz; D_2O) δ: 0.23.

Phosphoric acid mono-5′-[2-iodo-9*β*-D-ribofuranosyl-adenine] (7a)

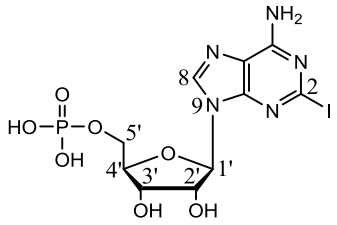

7a

The title compound was prepared according to the general synthetic procedure E, from **4g** (0.0102 g, 1 equiv.). The crude product was purified by purification method 1 (0-50% MeOH against 0.05 M TEAB buffer over 300 mL, then isocratic 50% over 50 mL, flow: 3 mL/min, fraction size: 5 mL), to obtain **7a** as a colourless oil (0.0037 g, 1.86 equiv. TEA, 36% yield).

The title compound was prepared according to the general synthetic procedures D2 and E. A mixture of **4a** and **4c** (0.0308 g, 1 equiv., 43% of **4c** by ^{1}H NMR estimation) was dissolved in anhydrous CH_2Cl_2 (2 mL) and DIPEA (2.5 equiv.) and 2-cyanoethyl *N*,*N*-diisopropyl chlorophosphoramidite (1 equiv.) were added *via* syringe. The reaction was stirred under nitrogen at room temperature for 2 h. Then, 5.0 – 6.0 M ^{t}BuOOH in nonane solution was added to the reaction and stirred for 1 h. After extractions, the organic phase was evaporated to dryness *in vacuo* and the residue was suspended in NH_4OH under stirring at room temperature overnight. The solution was evaporated to dryness *in vacuo*, suspended in water and stirred with Dowex 88 (H^+) overnight. The crude product was purified by purification method 1 (0-50% MeOH against 0.05 M TEAB buffer over 350 mL, then isocratic 50% over 50 mL, flow: 3 mL/min, fraction size: 5 mL), to obtain **7a** as a colourless oil (0.005 g, 1.68 equiv. TEA, 19% yield).

^{1}H NMR (400 MHz; D_2O) δ: 8.47 (1H, s, 8-H), 6.02 (1H, d, $J_{1',2'}$ = 5.7 Hz, 1′-H), 4.72 (1H, apparent t, 2′-H), 4.50 – 4.44 (1H, m, 3′-H), 4.34 (1H, m, 4′-H), 4.07 – 3.89 (2H, m, 5′-H_2), 3.17 (10.1H, q, *J* = 7.3 Hz, CH_2 TEA), 1.25 (15.1H, t, *J* = 7.3 Hz, CH_3 TEA); ^{13}C NMR (101 MHz; D_2O) δ: 156.10, 150.29, 145.45, 140.40, 120.35, 87.93, 85.06, 75.49, 71.26, 64.78, 47.49, 9.07; ^{31}P NMR (162 MHz; D_2O) δ: 1.65; m/z (ESI) 473.9666 $[M+H]^+$, $C_{10}H_{14}IN_5O_7P^+$ requires 473.9670.

Phosphoric acid mono-5′-[2-phenyl-9*β*-D-ribofuranosyl-adenine] (7b)

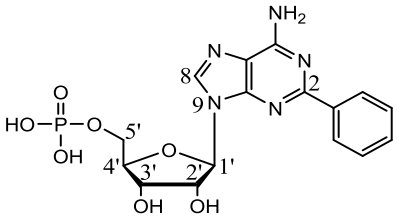

7b

The title compound was prepared according to the general synthetic procedures D2 and E. **4b** (0.032 g, 1 equiv.) was dissolved in anhydrous CH_2Cl_2 (2.5 mL) and DIPEA (2.5 equiv.) and 2-cyanoethyl *N*,*N*-diisopropyl chlorophosphoramidite (2 equiv.) were added *via* syringe. The reaction was stirred under nitrogen at room temperature for 2 h. The intermediate **4e** was isolated as a mixture of diastereomers by silica gel chromatography, with an eluent 80:20 CH_2Cl_2/EtOAc with 3% TEA. ^{1}H NMR (400 MHz; $CDCl_3$) δ: 8.42 – 8.34 (2H, m, *Ph*), 7.98 (1H, s, 8-H), 7.49 – 7.41 (3H, m, *Ph*), 6.23 (0.5H, d, $J_{1',2'}$ = 2.1 Hz, 1′-H), 6.20 (0.5H, d, $J_{1',2'}$ = 2.1 Hz, 1′-H), 5.58 (0.5H, dd, *J* = 6.2, 2.1 Hz, 2′-H), 5.55 (0.5H, dd, *J* = 6.2, 2.1 Hz, 2′-H), 5.21 – 5.15 (1H, m, 3′-H), 4.50 – 4.45 (1H, m, 4′-H), 3.96 – 3.66 (4H, m, 5′-H_2, *P-O-*CH_2), 3.51 (2H, m, *N-CH*), 2.66 (2H, m, CH_2-CN), 1.65 (3H, s, *isoprop.*), 1.42 (3H, s, *isoprop.*), 1.14 – 1.05 (6H, m, *N-isoprop.*); ^{31}P NMR (162 MHz; $CDCl_3$) δ: 148.98. Then, 5.0 – 6.0 M ^{t}BuOOH in nonane solution was added to the reaction and stirred for 1 h. After extractions, the organic phase was evaporated to dryness *in vacuo* and the residue was suspended in NH_4OH under stirring at room temperature overnight. The solution was evaporated to dryness *in vacuo*, suspended in water and stirred with Dowex 88 (H^+) overnight. The crude product was purified by purification method 1 (0-50% MeOH against 0.05 M TEAB buffer over 350 mL, then isocratic 60% over 50 mL, flow: 3 mL/min, fraction

size: 5 mL), to obtain **7b** as a colourless oil (0.0075 g, 0.92 equiv. TEA, 17% yield). ^{1}H NMR (400 MHz; D_2O) δ: 8.35 (1H, s, 8-H), 7.90 (2H, d, *J* = 7.0 Hz, *Ph*), 7.40 (3H, m, *Ph*), 6.11 (1H, d, $J_{1',2'}$ = 5.2 Hz, 1′-H), 4.68 (1H, apparent t, 2′-H), 4.48 (1H, m, 3′-H), 4.32 (1H, br s, 4′-H), 4.17 – 3.98 (2H, m, 5′-H_2), 3.13 (5.5H, q, *J* = 7.3 Hz, CH_2 TEA), 1.22 (9.6H, t, *J* = 7.3 Hz, CH_3 TEA); ^{13}C NMR (101 MHz; D_2O) δ: 156.37, 152.78, 152.38, 145.28, 134.60, 132.37, 131.31, 130.25, 129.66, 99.29, 88.30, 84.94, 75.33, 71.21, 65.19, 59.67, 47.51, 9.07; ^{31}P NMR (162 MHz; D_2O) δ: 0.94; m/z (ESI) 422.0870 $[M-H]^-$, $C_{16}H_{17}N_5O_7P^-$ requires 422.0871.

Phosphoric acid mono-5′-[2-(*N*-Me-pyrrol-2-yl)-9*β*-D-ribofuranosyl-adenine] (7c)

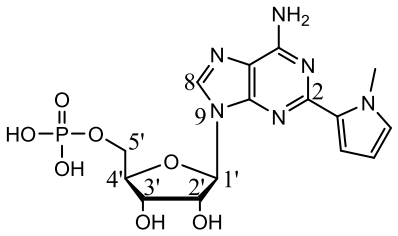

7c

The title compound was prepared according to the general synthetic procedures D2 and E. A mixture of **4a** and **4c** (0.0308 g, 1 equiv., 43% of **4c** by ^{1}H NMR estimation) was dissolved in anhydrous CH_2Cl_2 (2 mL) and DIPEA (2.5 equiv.) and 2-cyanoethyl *N*,*N*-diisopropyl chlorophosphoramidite (1 equiv.) were added *via* syringe. The reaction was stirred under nitrogen at room temperature for 2 h. Then, 5.0 – 6.0 M ^{t}BuOOH in nonane solution was added to the reaction and stirred for 1 h. After extractions, the organic phase was evaporated to dryness *in vacuo* and the residue was suspended in NH_4OH under stirring at room temperature overnight. The solution was evaporated to dryness *in vacuo*, suspended in water and stirred with Dowex 88 (H^+) overnight. The crude product was purified by purification method 1 (0-50% MeOH against 0.05 M TEAB buffer over 350 mL, then isocratic 50% over 50 mL, flow: 3 mL/min, fraction size: 5 mL), to obtain **7c** as a yellow oil (0.0067 g, yield not calculated because of stannane impurities still present in the product). ^{1}H NMR (400 MHz; D_2O) δ: 8.91 (1H, s, 8-H), 8.21 (1H, d, *J* = 1.7 Hz, 5-H *pyrrole*), 7.62 (2H, d, 3-H *pyrrole*, 4-H *pyrrole*), 6.28 (1H, d, $J_{1',2'}$ = 5.4 Hz, 1′-H), 4.81 (1H, m, 2′-H), 4.55 – 4.48 (1H, m, 3′-H), 4.40

(1H, br s, 4′-H), 4.14 (2H, m, 5′-H_2), 3.98 – 3.86 (3H, m, *N*-CH_3), 3.17 (5.2H, q, *J* = 7.3 Hz, CH_2 TEA); ^{31}P NMR (162 MHz; D_2O) δ: 0.54.

7.2.3 Preparation of 6-substituted AMP derivatives (**8a**-**b**)

6-Phenyl-9*β*-D-ribofuranosyl-purine (5a)[147]

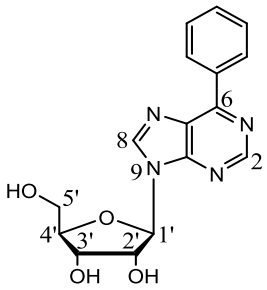

5a

The title compound was prepared according to the general synthetic procedure B1, from **5** (0.2 g, 1 equiv.), using Na_2PdCl_4, TPPTS, phenyl boronic acid and K_2CO_3 in water (6 mL) at 100 ºC. After 1 h, the reaction was cooled down and extracted with EtOAc; the organic phase was dried over anhydrous $MgSO_4$ and evaporated to dryness *in vacuo* to obtain **5a** as a white powder (0.1136 g, 50% yield). ^{1}H NMR (400 MHz; DMSO-d_6) δ: 9.02 (1H, s, 2-H), 8.93 (1H, s, 8-H), 8.84 (2H, d, *J* = 8.0 Hz, *Ph*), 7.55 – 7.65 (3H, m, *Ph*), 6.11 (1H, d, $J_{1',2'}$ = 5.5 Hz, 1′-H), 5.56 (1H, d, *J* = 5.7 Hz, 2′-*OH*), 5.25 (1H, d, *J* = 5.0 Hz, 3′-*OH*), 5.13 (1H, t, *J* = 5.4 Hz, 5′-*OH*), 4.67 (1H, m, 2′-H), 4.23 (1H, m, 3′-H), 4.02 (1H, m, 4′-H), 3.76 – 3.59 (2H, m, 5′-H_2).

6-(Pyrrol-2-yl)-9*β*-D-ribofuranosyl-purine (5b)

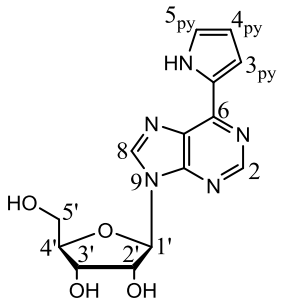

5b

The title compound was prepared according to the general synthetic procedure B1, from **5** (0.2 g, 1 equiv.), using Na_2PdCl_4, TPPTS, *N*-Boc-2-pyrrole boronic acid and K_2CO_3 in water (6 mL) at 100 ºC. After 24 h, the reaction was cooled down and evaporated to dryness *in vacuo*. The crude product was purified by purification method 1 (0-50% MeOH against 0.05 M TEAB buffer over 350 mL, then isocratic 60% over 50 mL, flow: 2 mL/min, fraction size: 5 mL) to obtain **5b** as a yellow oil (0.0825 g, 37% yield). ^{1}H NMR (400 MHz; CD_3OD) δ: 8.69 (1H, s, 2-H), 8.59 (1H, s, 8-H), 7.51 (1H, dd, $J_{5,4}$ = 3.8 Hz, $J_{5,3}$ = 1.4 Hz, 5-H *pyrrole*), 7.16 (1H, dd, $J_{3,4}$ = 2.5 Hz, $J_{3,5}$ = 1.4 Hz, 3-H *pyrrole*), 6.36 (1H, dd, $J_{4,5}$ = 3.7 Hz, $J_{4,3}$ = 2.6 Hz, 4-H *pyrrole*), 6.09 (1H, d, $J_{1',2'}$ = 6.0 Hz, 1′-H), 4.79 (1H, apparent t, 2′-H), 4.37 (1H, m, 3′-H), 4.19 (1H, m, 4′-H), 3.91 (1H, dd, $J_{5'a,b}$ = 12.4 Hz, $J_{5'a,4'}$ = 2.7 Hz, 5′a-H), 3.78 (1H, dd, $J_{5'b,a}$ = 12.4 Hz, $J_{5'b,4'}$ = 2.9 Hz, 5′b-H), 2.80 (4H, q, *J* = 7.2 Hz, CH_2 TEA), 1.14 (5.9H, t, *J* = 7.3 Hz, CH_3 TEA); ^{13}C NMR (101 MHz; CD_3OD) δ: 153.04, 151.97, 149.51, 145.16, 129.65, 128.79, 125.20, 116.57, 111.86, 90.92, 87.88, 75.54, 72.46, 63.29, 47.30, 10.36; m/z (ESI) 316.1046 $[M-H]^-$, $C_{14}H_{14}N_5O_4^-$ requires 316.1051.

6-Phenyl-9*β*-(2′,3′-*O*-isopropylidene-D-ribofuranosyl)-purine (5c)

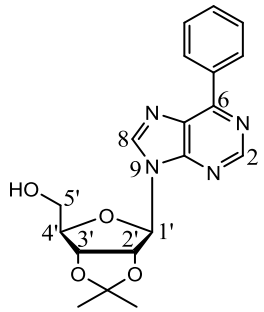

5c

The title compound was prepared according to the general synthetic procedure C, from a suspension of **5a** (0.1136 g, 1 equiv.) in acetone (8 mL), adding 70% $HClO_4$ (70 µL) and NH_4OH (70 µL). The mixture was extracted with EtOAc/brine (3x), and the organic phase dried over anhydrous $MgSO_4$; then, the solution was evaporated to dryness *in vacuo* to give **5c** as a colourless oil (0.109 g, 85% yield). ^{1}H NMR (400 MHz; CD_3OD) δ: 8.95 (1H, s, 2-H), 8.73 (1H, s, 8-H), 8.70 – 8.61 (2H, m, *Ph*), 7.62 – 7.50 (3H, m, *Ph*), 6.35 (1H, d, $J_{1',2'}$ = 3.0 Hz, 1′-H), 5.42 (1H, m, 2′-H), 5.09 (1H, m, 3′-H), 4.40 (1H, m, 4′-H), 3.80 (1H, dd, $J_{5'a,b}$ = 12.0 Hz, $J_{5'a,4'}$ = 3.8 Hz, 5′a-H), 3.73 (1H, dd, $J_{5'b,a}$ = 12.0 Hz, $J_{5'b,4'}$ = 4.4 Hz, 5′b-H), 1.64 (3H, s, *isoprop.*), 1.40 (3H, s, *isoprop.*).

6-(Pyrrol-2-yl)-9*β*-(2′,3′-*O*-isopropylidene-D-ribofuranosyl)-purine (5d)

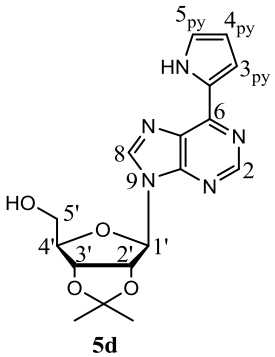

5d

The title compound was prepared according to the general synthetic procedure C, from a suspension of **5b** (0.0825 g, 1 equiv.) in acetone (8 mL), adding 70% $HClO_4$ (56 µL) and NH_4OH (56 µL). The mixture was extracted with EtOAc/brine (3x), and the organic phase dried over anhydrous $MgSO_4$; then, the solution was evaporated to dryness *in*

vacuo to give **5d** as a yellow oil (0.0367 g, 39% yield). ^{1}H NMR (400 MHz; CD_3OD) δ: 8.71 (1H, s, 2-H), 8.59 (1H, s, 8-H), 7.51 (1H, dd, $J_{5,4}$ = 3.8 Hz, $J_{5,3}$ = 1.4 Hz, 5-H *pyrrole*), 7.15 (1H, dd, $J_{3,4}$ = 2.5 Hz, $J_{3,5}$ = 1.4 Hz, 3-H *pyrrole*), 6.36 (1H, dd, $J_{4,5}$ = 3.8 Hz, $J_{4,3}$ = 2.6 Hz, 4-H *pyrrole*), 6.27 (1H, d, $J_{1',2'}$ = 3.2 Hz, 1′-H), 5.38 (1H, m, 2′-H), 5.08 (1H, m, 3′-H), 4.39 (1H, m, 4′-H), 3.80 (1H, dd, $J_{5'a,b}$ = 12.0 Hz, $J_{5'a,4'}$ = 3.7 Hz, 5′a-H), 3.73 (1H, dd, $J_{5'b,a}$ = 12.0 Hz, $J_{5'b,4'}$ = 4.3 Hz, 5′b-H), 1.63 (3H, s, *isoprop.*), 1.40 (3H, s, *isoprop.*).

Phosphoric acid mono-5′-[6-phenyl-9*β*-(2′,3′-*O*-isopropylidene-D-ribofuranosyl)-purine] (5g)

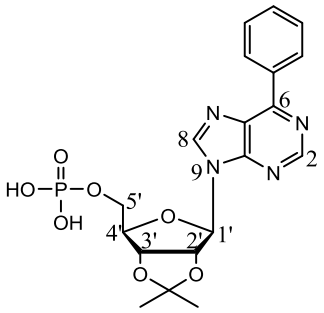

5g

The title compound was prepared according to the general synthetic procedure D1, from **5c** (0.109 g, 1 equiv.) and $POCl_3$ (0.1 mL, 3.6 equiv.) in anhydrous acetonitrile (3 mL). The crude product was purified by purification method 1 (0-50% MeOH against 0.05 M TEAB buffer over 300 mL, isocratic 50% over 50 mL, isocratic 60% over 50 mL, flow: 3 mL/min, fraction size: 5 mL), to give **5g** as a colourless oil (0.024 g, 2.4 equiv. TEA, 12% yield). **5g** was partially deprotected in the reaction conditions to give **8a** as a colourless oil (0.0448 g, 2.18 equiv. TEA, 24% yield). ^{1}H NMR (400 MHz; D_2O) δ: 8.80 (1H, s, 2-H), 8.75 (1H, s, 8-H), 8.07 (2H, m, *Ph*), 7.60 – 7.46 (3H, m, *Ph*), 6.27 (1H, d, $J_{1',2'}$ = 3.2 Hz, 1′-H), 5.36 (1H, m, 2′-H), 5.20 (1H, m, 3′-H), 4.64 (1H, br s, 4′-H), 3.91 (2H, m, 5′-H_2), 3.14 (14.4H, q, J = 7.3 Hz, CH_2 TEA), 1.69 (3H, s, *isoprop.*), 1.45 (3H, s, *isoprop.*), 1.22 (21.8H, t, J = 7.3 Hz, CH_3 TEA); ^{31}P NMR (162 MHz; D_2O) δ: 3.73.

Phosphoric acid mono-5′-[6-(pyrrol-2-yl)-9*β*-(2′,3′-*O*-isopropylidene-D-ribofuranosyl)-purine] (5h)

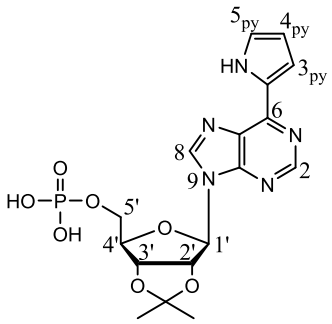

5h

The title compound was prepared according to the general synthetic procedure D1, from **5d** (0.0179 g, 1 equiv.) and $POCl_3$ (19 µL, 4 equiv.) in anhydrous acetonitrile (0.8 mL). The reaction mixture was kept at 4 °C for 48 h. The crude product was purified by purification method 1 (0-50% MeOH against 0.05 M TEAB buffer over 350 mL, then isocratic 60% over 50 mL, flow: 3 mL/min, fraction size: 5 mL) to give **5h** as a yellow oil (0.0102 g, 1.8 equiv. TEA, 33% yield). **5h** was partially deprotected in the reaction conditions to give **8b** as a yellow oil (0.0017 g, 1.8 equiv. TEA, 6% yield).^{1}H NMR (400 MHz; CD_3OD) δ: 8.79 (1H, s, 2-H), 8.71 (1H, s, 8-H), 7.50 – 7.47 (1H, dd, $J_{5,4}$ = 2.2 Hz, $J_{5,3}$ = 1.3 Hz, 5-H *pyrrole*), 7.15 (1H, dd, $J_{3,4}$ = 2.2 Hz, $J_{3,5}$ = 1.3 Hz, 3-H *pyrrole*), 6.35 (1H, m, 4-H *pyrrole*), 6.33 (1H, d, $J_{1',2'}$ = 3.2 Hz, 1′-H), 5.44 (1H, dd, $J_{2',3'}$ = 6.0 Hz, $J_{1',2'}$ = 3.2 Hz, 2′-H), 5.18 (1H, dd, $J_{2',3'}$ = 6.0 Hz, $J_{3',4'}$ = 1.8 Hz, 3′-H), 4.50 (1H, m, 4′-H), 4.07 – 3.96 (2H, m, 5′-H_2), 3.03 (10.8H, q, *J* = 7.3 Hz, CH_2 TEA), 1.63 (3H, s, *isoprop.*), 1.40 (3H, s, *isoprop.*), 1.22 (16.8H, t, *J* = 7.3 Hz, CH_3 TEA); ^{31}P NMR (162 MHz; CD_3OD) δ: 1.65.

Phosphoric acid mono-5′-[6-phenyl-9*β*-D-ribofuranosyl-purine] (8a)

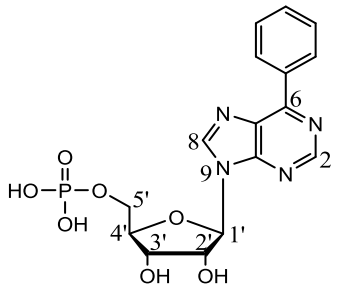

8a

The title compound was prepared according to the general synthetic procedure E, from **5g** (0.024 g, 1 equiv.). The crude product was purified by purification method 1 (0-50% MeOH against 0.05 M TEAB buffer over 300 mL, then isocratic 60% over 100 mL, flow: 3 mL/min, fraction size: 5 mL), to obtain **8a** as a colourless oil (0.0064 g, 2.1 equiv. TEA, 30% yield).

The title compound was prepared according to the general synthetic procedures D2 and E. **5c** (0.177 g, 1 equiv.) was dissolved in anhydrous CH_2Cl_2 (3 mL) and DIPEA (2.5 equiv.) and 2-cyanoethyl *N*,*N*-diisopropyl chlorophosphoramidite (1 equiv.) were added *via* syringe. The reaction was stirred under nitrogen at room temperature for 1.5 h. Then, 5.0 – 6.0 M ^{t}BuOOH in nonane solution was added to the reaction and stirred for 2 h. After extractions, the organic phase was evaporated to dryness *in vacuo* and the phosphate intermediate isolated and purified as a mixture of diastereomers by silica gel chromatography with an eluent 80:20 CH_2Cl_2/MeOH. ^{1}H NMR (400 MHz; $CDCl_3$) δ: 8.96 (1H, d, *J* = 1.1 Hz, 2-H), 8.73 – 8.65 (2H, m, *Ph*), 8.28 (0.5H, s, 8-H), 8.23 (0.5H, s, 8-H), 7.54 – 7.43 (3H, m, *Ph*), 6.21 (0.5H, d, $J_{1',2'}$ = 2.3 Hz, 1′-H), 6.18 (0.5H, d, $J_{1',2'}$ = 2.3 Hz, 1′-H), 5.44 (0.5H, dd, *J* = 6.4, 2.3 Hz, 2′-H), 5.41 (0.5H, dd, *J* = 6.4, 2.0 Hz, 2′-H), 5.12 (1H, dt, *J* = 6.5, 3.4 Hz, 3′-H), 4.50 – 4.41 (1H, m, 4′-H), 4.20 – 3.93 (4H, m, 5′-H_2, *P-O-*CH_2), 3.52 – 3.16 (4H, m, N-*CH*), 2.76 – 2.59 (2H, m, CH_2-CN), 1.59 (3H, s, *isoprop.*), 1.34 (3H, s, *isoprop.*), 1.15 (12H, d, *J* = 13.6 Hz, *N-isoprop.*); ^{31}P NMR (162 MHz; $CDCl_3$) δ: 14.17. The residue was suspended in NH_4OH under stirring at room temperature overnight. The solution was evaporated to dryness *in vacuo*, suspended in water and stirred with Dowex 88 (H^+) overnight. After filtration, the crude product was purified by purification method 1 (0-50% MeOH against 0.05 M TEAB

buffer over 300 mL, then isocratic 60% over 100 mL, flow: 3 mL/min, fraction size: 5 mL), to give **8a** as a colourless oil (0.0191 g, 1.37 equiv. TEA, 7% yield).

^{1}H NMR (400 MHz; D_2O) δ: 8.86 (1H, s, 2-H), 8.78 (1H, s, 8-H), 8.23 – 8.08 (2H, m, *Ph*), 7.58 (3H, m, *Ph*), 6.25 (1H, d, $J_{1',2'}$ = 5.3 Hz, 1′-H), 4.68 (1H, m, 2′-H), 4.51 (1H, m, 3′-H), 4.40 (1H, m, 4′-H), 4.14 (2H, m, 5′-H_2), 3.17 (8.2H, q, J = 7.3 Hz, CH_2 TEA), 1.25 (13.9H, t, J = 7.3 Hz, CH_3 TEA); ^{13}C NMR (101 MHz; D_2O) δ: 156.04, 152.66, 152.25, 145.22, 134.40, 132.36, 131.13, 130.14, 129.56, 88.31, 84.92, 75.37, 71.21, 59.70, 47.50, 23.08, 9.07, 8.23; ^{31}P NMR (162 MHz; D_2O) δ: 2.98; m/z (ESI) 407.0754 $[M-H]^-$, $C_{16}H_{16}N_4O_7P^-$ requires 407.0762.

Phosphoric acid mono-5′-[6-(pyrrol-2-yl)-9*β*-D-ribofuranosyl-purine] (8b)

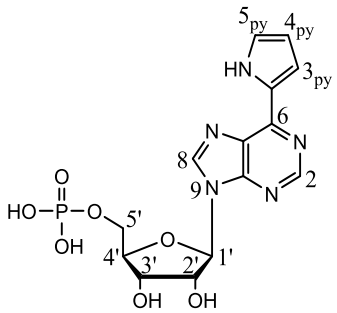

8b

The title compound was prepared from **5h** (0.0102 g, 1 equiv. TEA), dissolving it in an acetic acid solution (AcOH/H_2O, 1:9) at 90 °C for 3 h. After co-evaporation with EtOH (3x) to remove AcOH traces, the crude product gave **8b** as a colourless oil (0.0082 g, complete conversion). ^{1}H NMR (400 MHz; D_2O) δ: 8.66 (1H, s, 2-H), 8.58 (1H, s, 8-H), 7.26 (1H, dd, $J_{5,4}$ = 3.8 Hz, $J_{5,3}$ = 1.4 Hz, 5-H *pyrrole*), 7.21 (1H, dd, $J_{3,4}$ = 2.5 Hz, $J_{5,3}$ = 1.4 Hz, 3-H *pyrrole*), 6.42 (1H, dd, $J_{5,4}$ = 3.8 Hz, $J_{3,4}$ = 2.6 Hz, 4-H *pyrrole*), 6.16 (1H, d, $J_{1',2'}$ = 5.5 Hz, 1′-H), 4.75 (1H, m, 2′-H), 4.52 – 4.47 (1H, m, 3′-H), 4.40 – 4.35 (1H, m, 4′-H), 4.18 – 4.06 (2H, m, 5′-H_2); ^{13}C NMR (101 MHz; D_2O) δ: 152.94, 151.51, 148.03, 144.01, 128.03, 127.34, 126.06, 115.89, 111.94, 88.04, 75.28, 71.24; ^{31}P NMR (162 MHz; D_2O) δ: 0.63; m/z (ESI) 396.0714 $[M-H]^-$, $C_{14}H_{15}N_5O_7P^-$ requires 396.0715.

7.2.4 Preparation of 8-substituted AMP derivatives (**9b**-**n**)

Phosphoric acid mono-5′-[8-bromo-9*β*-D-ribofuranosyl-adenine] (9a)[172]

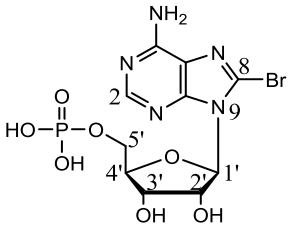

9a

To a solution of adenosine monophosphate **3a** (0.5 g, 1 equiv.) in aqueous KH_2PO_4 (50 mL, 0.25 M, pH 4), neat bromine (6.7 equiv.) was added drop-wise. The reaction was stirred at room temperature in the dark overnight. The aqueous solution was washed with CH_2Cl_2 until the colour remained pale yellow, and evaporated to dryness *in vacuo*. The crude product was purified by purification method 1 (0-10% MeOH against 0.05 M TEAB buffer over 400 mL, flow: 5 mL/min, fraction size: 5 mL) to give **9a** as a colourless oil (0.56 g, 2.2 equiv. TEA, 60% yield). ^{1}H NMR (400 MHz; D_2O) δ: 8.03 (1H, s, 2-H), 5.99 (1H, d, $J_{1',2'}$ = 6.0 Hz, 1′-H), 5.19 (1H, apparent t, 2′-H), 4.51 (1H, m, 3′-H), 4.25 – 3.93 (3H, m, 4′-H, 5′-H_2), 3.10 (13.8H, q, J = 7.3 Hz, CH_2 TEA), 1.19 (19.6H, t, J = 7.3 Hz, CH_3 TEA); m/z (ESI) 423.9670 $[M\text{-}H]^-$, $C_{10}H_{12}BrN_5O_7P^-$ requires 423.9663; TLC: R_f 0.27 (^{t}BuOH/1M TEAB buffer 6:4).

Phosphoric acid mono-5′-[8-phenyl-9*β*-D-ribofuranosyl-adenine] (9b)[172]

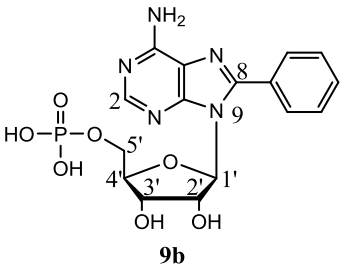

9b

The title compound was prepared according to the general synthetic procedure B2, from **9a** (0.0833 g, 1 equiv.) using Na_2PdCl_4 (0.025 equiv.), TPPTS (2.5 equiv. to Pd), phenyl boronic acid (1.7 equiv.) and K_2CO_3 (1.5 equiv.) in water (2 mL) at 80 ºC. After 1 h, the reaction was complete. The crude product was purified by purification method 1 (0-60%

MeOH against 0.05 M TEAB buffer over 400 mL, flow: 3 mL/min, fraction size: 5 mL) and 2 (0-60% 1 M TEAB buffer against H_2O over 800 mL, flow: 4 mL/min, fraction size: 5 mL) to give **9b** as a colourless oil (0.0751 g, 1.6 equiv. TEA, 82% yield). ^{1}H NMR (400 MHz; D_2O) δ: 8.18 (1H, s, 2-H), 7.68 – 7.49 (5H, m, *Ph*), 5.81 (1H, d, $J_{1',2'}$ = 6.2 Hz, 1′-H), 5.21 (1H, apparent t, 2′-H), 4.38 (1H, m, 3′-H), 4.01 (3H, m, 4′-H, 5′-H_2), 2.97 (7.8H, q, *J* = 7.3 Hz, CH_2 TEA), 1.20 (16.4H, t, *J* = 7.3 Hz, CH_3 TEA); ^{31}P NMR (162 MHz; D_2O) δ: 7.007; m/z (ESI) 422.0869 $[M-H]^-$, $C_{10}H_{12}BrN_5O_7P^-$ requires 422.0871; TLC: R_f 0.6 (iPA/H_2O/NH_4OH 6:3:1).

Phosphoric acid mono-5′-[8-(3-(*N*-Boc-aminomethyl)phenyl)-9*β*-D-ribofuranosyl-adenine] (9c)[172]

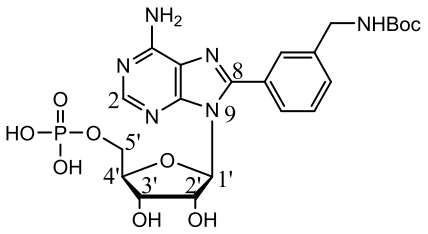

9c

The title compound was prepared according to the general synthetic procedure B2, from **9a** (0.074 g, 1 equiv.) using Na_2PdCl_4 (0.025 equiv.), TPPTS (2.5 equiv. to Pd), 3-(*N*-Boc-aminomethyl)phenyl boronic acid (1.2 equiv.) and K_2CO_3 (3 equiv.) in water (2 mL) at 80 ºC. After 1 h, the reaction was complete. The crude product was purified by purification method 1 (0-50% MeOH against 0.05 M TEAB buffer over 400 mL, flow: 3 mL/min, fraction size: 5 mL) to give **9c** as a colourless oil (0.0762 g, 1.3 equiv. TEA, 78% yield). ^{1}H NMR (400 MHz; CD_3OD) δ: 8.18 (1H, s, 2-H), 7.68 – 7.63 (2H, m, *Ph*), 7.55 – 7.46 (2H, m, *Ph*), 5.83 (1H, d, $J_{1',2'}$ = 5.8 Hz, 1′-H), 5.51 (1H, apparent t, 2′-H), 4.49 (1H, m, 3′-H), 4.31 (2H, s, CH_2NH_2), 4.27 – 4.03 (3H, m, 4′-H, 5′-H_2), 3.01 (8H, q, *J* = 7.3 Hz, CH_2 TEA), 1.42 (9H, s, CH_3 Boc), 1.19 (12.1H, t, *J* = 7.3 Hz, CH_3 TEA); ^{31}P NMR (162 MHz; D_2O) δ: 7.013; TLC: R_f 0.64 (^{t}BuOH/1M TEAB buffer 6:4).

Phosphoric acid mono-5′-[8-(3-(aminomethyl)phenyl)-9*β*-D-ribofuranosyl-adenine] (9d)

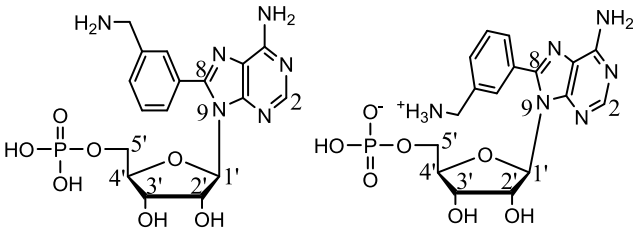

9d(a) **9d(b)**

The conformer **9d(a)** was prepared according to the general synthetic procedure B2, from **9a** (0.0712 g, 1 equiv.) using Na_2PdCl_4 (0.025 equiv.), TPPTS (2.5 equiv. to Pd), 3-(*N*-Boc-aminomethyl)phenyl boronic acid (1.2 equiv.) and K_2CO_3 (3 equiv.) in water (6 mL) at 40 °C. After 2 days, the reaction seemed complete and the crude product was purified by purification method 1 (0-8% MeOH against 0.05 M TEAB buffer over 350 mL, flow: 3 mL/min, fraction size: 5 mL) to give **9d(a)** as a colourless oil (0.047 g, 0.5 equiv. TEA, 85% yield).

The two conformers, **9d(a)** and **9d(b)**, of the title compound were prepared according to the general synthetic procedure B2, from **9a** (0.042 g, 1 equiv.) using Na_2PdCl_4 (0.025 equiv.), TPPTS (2.5 equiv. to Pd), 3-(aminomethyl)phenyl boronic acid (1.2 equiv.) and K_2CO_3 (3 equiv.) in water (3 mL) at 80 °C. After 2 h, the reaction seemed complete and the crude product was purified by purification method 1 (0-8% MeOH against 0.05 M TEAB buffer over 350 mL, flow: 3 mL/min, fraction size: 5 mL) and 2 (0-60% 1 M TEAB buffer against H_2O over 700 mL, flow: 3 mL/min, fraction size: 5 mL).

The conformer **9d(a)** was prepared treating **9c** with TFA in MeOH under reflux (pH 1) until to almost complete disappearance of the starting material. The mixture was evaporated to dryness and the crude product purified by purification method 1 (0-8% MeOH against 0.05 M TEAB buffer over 350 mL, flow: 3 mL/min, fraction size: 5 mL).

Conformer **9d(a)**: ^{1}H NMR (400 MHz; D_2O) δ: 8.24 (1H, s, 2-H), 7.75 – 7.58 (4H, m, *Ph*), 5.82 (1H, d, $J_{1',2'}$ = 6.2 Hz, 1′-H), 5.17 (1H, apparent t, 2′-H), 4.36 (1H, m, 3′-H), 4.23 (2H, s, CH_2NH_2), 4.17 – 3.95 (3H, m, 4′-H, 5′-H_2), 3.35 (8.1H, q, *J* = 7.3 Hz, CH_2

TEA), 1.23 (12.2H, t, *J* = 7.3 Hz, *CH*$_3$ TEA); m/z **(**ESI) 451.1150 [M-H]$^-$, $C_{17}H_{20}N_6O_7P^-$ requires 451.1137; TLC: R_f 0.52 (iPA/H_2O/NH_4OH 6:3:1).

Conformer **9d(b)**: ^{1}H NMR (400 MHz; D_2O) δ: 8.21 (1H, s, 2-H), 7.72 – 7.55 (4H, m, *Ph*), 5.80 (1H, d, $J_{1',2'}$ = 6.4 Hz, 1′-H), 5.17 (1H, apparent t, 2′-H), 4.37 (1H, m, 3′-H), 4.21 (2H, d, *CH*$_2$NH$_2$), 4.19 – 3.98 (3H, m, 4′-H, 5′-H$_2$), 1.22 (4.9H, t, *J* = 7.3 Hz *CH*$_3$ TEA); m/z (ESI) 451.1130 [M-H]$^-$, $C_{17}H_{20}N_6O_7P^-$ requires 451.1137; TLC: R_f 0.81 (iPA/H_2O/NH_4OH 6:3:1).

Phosphoric acid mono-5′-[8-(pyridin-3-yl)-9*β*-D-ribofuranosyl-adenine] (9e)[172]

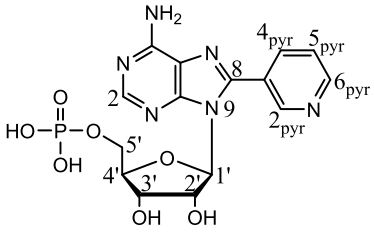

9e

The title compound was prepared according to the general synthetic procedure B2, from **9a** (0.0175 g, 1 equiv.) using Na_2PdCl_4 (0.02 equiv.), TPPTS (3 equiv. to Pd), 3-pyridinyl boronic acid (1.2 equiv.) and K_2CO_3 (3 equiv.) in water (1 mL) at 100 ºC. After 24 h, the reaction was complete. The crude product was purified by purification method 1 (0-10% MeOH against 0.05 M TEAB buffer over 400 mL, flow: 3 mL/min, fraction size: 5 mL) and 2 (0-25% 1 M TEAB buffer against H_2O over 350 mL, flow: 2 mL/min, fraction size: 3 mL) to give **9e** as a colourless oil (0.0123 g, 2 equiv. TEA, 70% yield). ^{1}H NMR (400 MHz; D_2O) δ: 8.82 (1H, br s, 2-H *pyridine*), 8.70 (1H, br s, 6-H *pyridine*), 8.22 (1H, s, 2-H), 8.18 (1H, m, 4-H *pyridine*), 7.64 (1H, br s, 5-H *pyridine*), 5.77 (1H, d, 1′-H), 5.22 (1H, apparent t, 2′-H), 4.38 (1H, m, 3′-H), 4.27 – 3.88 (3H, m, 4′-H, 5′-H$_2$), 3.14 (12.5H, q, *J* = 7.3 Hz, *CH*$_2$ TEA), 1.21 (18.6H, t, *J* = 7.3 Hz, *CH*$_3$ TEA); ^{31}P NMR (162 MHz; D_2O) δ: 7.013; TLC: R_f 0.34 (^{t}BuOH/1M TEAB buffer 6:4).

Phosphoric acid mono-5′-[8-(pyridin-4-yl)-9*β*-D-ribofuranosyl-adenine] (9f)

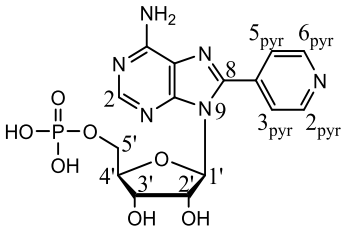

9f

The title compound was prepared according to general synthetic procedure B2, from **9a** (0.045 g, 1 equiv.) using Na_2PdCl_4 (0.09 equiv.), TPPTS (3 equiv. to Pd), 4-pyridinyl boronic acid (1.5 equiv.) and K_2CO_3 (3.5 equiv.) in water (2 mL) at 100 °C. After 12 h, the reaction seemed complete. The crude product was purified by purification method 1 (0-18% MeOH against 0.05 M TEAB buffer over 400 mL, flow: 3 mL/min, fraction size: 5 mL) and 2 (0-60% 1 M TEAB buffer against H_2O over 400 mL, flow: 2 mL/min, fraction size: 5 mL) to give **9f** as a colourless oil (0.0324 g, 1.58 equiv. TEA, 80% yield). ^{1}H NMR (400 MHz; D_2O) δ: 8.72 (2H, br s, 2-H *pyridine*, 6-H *pyridine*), 8.27 (1H, s, 2-H), 7.78 (2H, br s, 3-H *pyridine*, 5-H *pyridine*), 5.86 (1H, d, $J_{1',2'}$ = 5.1 Hz, 1′-H), 5.27 (1H, apparent t, 2′-H), 4.46 (1H, m, 3′-H), 4.14 (3H, m, 4′-H, 5′-H_2), 3.17 (8.7H, q, *J* = 7.3 Hz, *CH*$_2$ TEA), 1.27 (13.1H, t, *J* = 7.3 Hz, *CH*$_3$ TEA); ^{31}P NMR (162 MHz; D_2O) δ: 7.019; m/z (ESI) 423.0821 $[M-H]^-$, $C_{15}H_{16}N_6O_7P^-$ requires 423.0824.

Phosphoric acid mono-5′-[8-(2,4-*DMT*-pyrimidin-5-yl)-9*β*-D-ribofuranosyl-adenine] (9g)[172]

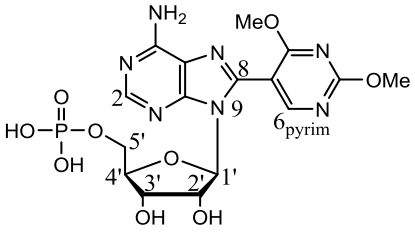

9g

The title compound was prepared according to the general synthetic procedure B2, from **9a** (0.0675 g, 1 equiv.) using Na_2PdCl_4 (0.025 equiv.), TPPTS (2.5 equiv. to Pd), 2,4-*DMT*-5-pyrimidinyl boronic acid (1.2 equiv.) and K_2CO_3 (3 equiv.) in water (3 mL) at 80 ºC. After 1 h, the reaction was complete. The crude product was purified by

purification method 1 (0-40% MeOH against 0.05 M TEAB buffer over 400 mL, flow: 3 mL/min, fraction size: 5 mL) to give **9g** as a colourless oil (0.074 g, 1.4 equiv. TEA, 75% yield). ^{1}H NMR (400 MHz; D_2O) δ: 8.43 (1H, s, 6-H *pyrimidine*), 8.23 (1H, s, 2-H), 5.56 (1H, d, $J_{1',2'}$ = 6.2 Hz, 1′-H), 5.19 (1H, apparent t, 2′-H), 4.44 (1H, m, 3′-H), 4.14 – 3.82 (9H, m, 4′-H, 5′-H_2, 2 OCH_3), 2.83 (8.4H, q, J = 7.3 Hz, CH_2 TEA), 1.09 (12.3H, t, J = 7.3 Hz, CH_3 TEA); ^{31}P NMR (162 MHz; D_2O) δ: 7.000; m/z (ESI) 484.0976 $[M-H]^-$, $C_{16}H_{19}N_7O_9P^-$ requires 484.0987; TLC: R_f 0.35 (^{t}BuOH/1M TEAB buffer 6:4).

Phosphoric acid mono-5′-[8-(pyrrol-2-yl)-9*β*-D-ribofuranosyl-adenine] (9h)[172]

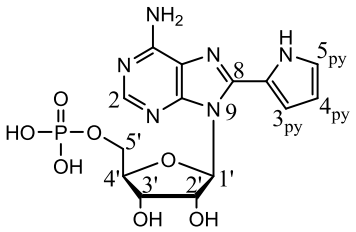

9h

The title compound was prepared according to the general synthetic procedure B2, from **9a** (0.0175 g, 1 equiv.) using Na_2PdCl_4 (0.02 equiv.), TPPTS (3 equiv. to Pd), *N*-Boc-2-pyrrole boronic acid (1.5 equiv.) and K_2CO_3 (3 equiv.) in water (1 mL) at 100 ºC. After 24 h, the reaction was complete. The crude product was purified by purification method 1 (0-12% MeOH against 0.05 M TEAB buffer over 150 mL, 12-40% over 200 mL, flow: 3 mL/min, fraction size: 5 mL) and 2 (0-5% 1 M TEAB buffer against H_2O over 50 mL, 5-28% over 75 mL, 28-40% over 20 mL, isocratic 40% over 20 mL, flow: 2 mL/min, fraction size: 5 mL), to give **9h** as a colourless oil (0.0098 g, 2.2 equiv. TEA, 57% yield). ^{1}H NMR (400 MHz; D_2O) δ: 8.07 (1H, s, 2-H), 7.14 (1H, dd, $J_{5,4}$ = 2.5 Hz, $J_{5,3}$ = 1.4 Hz, 5-H *pyrrole*), 6.79 (1H, dd, $J_{3,4}$ = 3.7 Hz, $J_{3,5}$ = 1.3 Hz, 3-H *pyrrole*), 6.33 (1H, dd, $J_{4,3}$ = 3.5 Hz, $J_{4,5}$ = 2.8 Hz, 4-H *pyrrole*), 6.05 (1H, d, $J_{1',2'}$ = 6.2 Hz, 1′-H), 5.19 (1H, apparent t, 2′-H), 4.48 (1H, m, 3′-H), 4.22 (1H, m, 4′-H), 4.06 (2H, m, 5′-H_2), 3.14 (13.8H, q, J = 7.3 Hz, CH_2 TEA), 1.20 (19.6H, t, J = 7.3 Hz, CH_3 TEA); ^{31}P NMR (162 MHz; D_2O) δ: 7.032; m/z (ESI) 411.0812 $[M-H]^-$, $C_{14}H_{16}N_6O_7P^-$ requires 411.2871; TLC: R_f 0.65 (^{t}BuOH/1M TEAB buffer 6:4).

Phosphoric acid mono-5′-[8-(furan-2-yl)-9*β*-D-ribofuranosyl-adenine] (9i)

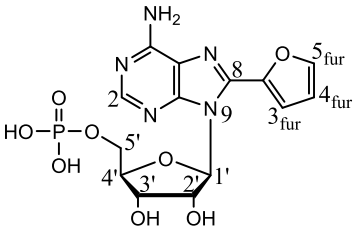

9i

The title compound was prepared according to the general synthetic procedure B2, from **9a** (0.0554 g, 1 equiv.) using Na_2PdCl_4 (0.09 equiv.), TPPTS (2.3 equiv. to Pd), 2-furanyl boronic acid (1.5 equiv.) and K_2CO_3 (3 equiv.) in water (6 mL) at 100 °C. After 12 h, the reaction seemed complete. The crude product was purified by purification method 1 (0-30% MeOH against 0.05 M TEAB buffer over 400 mL, flow: 3 mL/min, fraction size: 5 mL) to give **9i** as a colourless oil (0.031 g, 1.7 equiv. TEA, 67% yield). ^{1}H NMR (400 MHz; D_2O) δ: 8.10 (1H, s, 2-H), 7.69 (1H, br s, 5-H *furan*), 7.09 (1H, br s, 3-H *furan*), 6.60 (1H, br s, 4-H *furan*), 6.20 (1H, d, $J_{1',2'}$ = 5.7 Hz, 1′-H), 5.31 (1H, apparent t, 2′-H), 4.56 (1H, m, 3′-H), 4.13 (3H, m, 4′-H, 5′-H_2), 3.12 (10.2H, q, *J* = 7.3 Hz, CH_2 TEA), 1.21 (15.2H, t, *J* = 7.3 Hz, CH_3 TEA); ^{31}P NMR (162 MHz; D_2O) δ: 6.975; m/z (ESI) 412.0652 $[M-H]^-$, $C_{14}H_{15}N_5O_8P^-$ requires 412.0664.

Phosphoric acid mono-5′-[8-(1*H*-pyrazol-4-yl)-9*β*-D-ribofuranosyl-adenine] (9j)

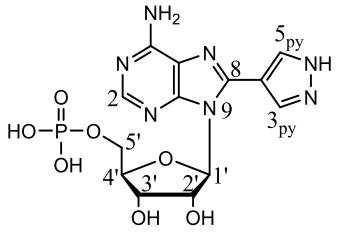

9j

The title compound was prepared according to the general synthetic procedure B2, from **9a** (0.1068 g, 1 equiv.) using Na_2PdCl_4 (0.1 equiv.), TPPTS (2.5 equiv. to Pd), 1*H*-Pyrazole-4-boronic acid (2 equiv.) and K_3PO_4 (1.5 equiv.) in water (10 mL) at 100 °C. After 12 h, the reaction seemed complete. The crude product was purified by purification method 1 (0-40% MeOH against 0.05 M TEAB buffer over 300 mL, then

isocratic 45% over 100 mL, flow: 3 mL/min, fraction size: 5 mL) and 2 (0-100% 1 M TEAB buffer against H_2O over 300 mL, flow: 2 mL/min, fraction size: 5 mL) to give **9j** as a colourless oil (0.0569 g, 1.7 equiv. TEA, 57% yield). ^{1}H NMR (400 MHz; D_2O) δ: 8.12 (1H, s, 2-H), 8.07 (2H, s, 3-H *pyrazole*, 5-H *pyrazole*), 5.90 (1H, d, $J_{1',2'}$ = 6.2 Hz, 1′-H), 5.25 (1H, apparent t, 2′-H), 4.48 – 4.43 (1H, m, 3′-H), 4.23 (1H, m, 4′-H), 4.11 (2H, m, 5′-H_2), 3.15 (6.1H, q, J = 7.3 Hz, CH_2 TEA), 1.23 (9.9H, t, CH_3 TEA); ^{31}P NMR (162 MHz; D_2O) δ: 0.25; m/z (ESI) 412.0745 $[M-H]^-$, $C_{13}H_{15}N_7O_7P^-$ requires 412.0776.

Phosphoric acid mono-5′-[8-(5-formyl-thien-2-yl)-9*β*-D-ribofuranosyl-adenine] (9k)

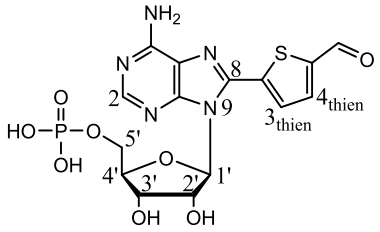

9k

The title compound was prepared according to the general synthetic procedure B2, from **9a** (0.0554 g, 1 equiv.) using Na_2PdCl_4 (0.09 equiv.), TPPTS (2.3 equiv. to Pd), 5-formyl-2-thienyl boronic acid (1.5 equiv.) and K_2CO_3 (3 equiv.) in water (6 mL) at 100 °C. After 12 h, the reaction was not finished, however the crude product was evaporated and purified by purification method 1 (0-30% MeOH against 0.05 M TEAB buffer over 400 mL, flow: 3 mL/min, fraction size: 5 mL) and 2 (0-60% 1 M TEAB buffer against H_2O over 400 mL, flow: 2 mL/min, fraction size: 5 mL) to give **9k** as a colourless oil (0.0275 g, 1.6 equiv. TEA, 52% yield). ^{1}H NMR (400 MHz; D_2O) δ: 9.58 (1H, s, *CHO*), 8.05 (1H, s, 2-H), 7.69 (1H, s, 4-H *thienyl*), 7.53 (1H, 1s, 3-H *thienyl*), 5.89 (1H, d, 1′-H), 5.30 (1H, apparent t, 2′-H), 4.53 (1H, m, 3′-H), 4.16 (3H, m, 4′-H, 5′-H_2), 3.10 (9.6H, q, J = 7.3 Hz, CH_2 TEA), 1.18 (14.6H, t, J = 7.3 Hz, CH_3 TEA); ^{31}P NMR (162 MHz; D_2O) δ: 7.019; m/z (ESI) 423.0376 $[M-H]^-$, $C_{15}H_{15}N_5O_8PS^-$ requires 456.0384.

Phosphoric acid mono-5′-[8-(5-bromo-thien-2-yl)-9*β*-D-ribofuranosyl-adenine] (9l)

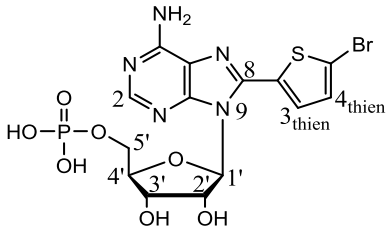

9l

The title compound was prepared according to the general synthetic procedure B2, from **9a** (0.0792 g, 1 equiv.) using Na_2PdCl_4 (0.1 equiv.), TPPTS (2.5 equiv. to Pd), 5-bromo-2-thienyl boronic acid (0.5 equiv.) and K_3PO_4 (1.5 equiv.) in water (15 mL) at 100 °C. After 12 h, the reaction seemed complete. The crude product was purified by purification method 1 (0-40% MeOH against 0.05 M TEAB buffer over 250 mL, 40-50% over 150 mL, flow: 3 mL/min, fraction size: 5 mL) to give **9l** as a colourless oil (0.015 g, 1.9 equiv. TEA, 17% yield). ^{1}H NMR (400 MHz; D_2O) δ: 8.23 (1H, s, 2-H), 7.43 (1H, d, $J_{3,4}$ = 4.0 Hz, 4-H *thienyl*), 7.24 (1H, d, $J_{3,4}$ = 4.0 Hz, 3-H *thienyl*), 6.02 (1H, d, $J_{1',2'}$ = 6.1 Hz, 1′-H), 5.42 (1H, apparent t, 2′-H), 4.56 – 4.50 (1H, m, 3′-H), 4.28 – 4.20 (1H, m, 4′-H), 4.07 (2H, m, 5′-H_2), 3.17 (11.2H, q, CH_2 TEA), 1.25 (17.9H, t, CH_3 TEA); ^{31}P NMR (162 MHz; D_2O) δ: 2.73; m/z (ESI) 505.9554 $[M-H]^-$, $C_{14}H_{14}BrN_5O_7PS^-$ requires 505.9540.

Phosphoric acid mono-5′-[8-(indol-2-yl)-9*β*-D-ribofuranosyl-adenine] (9m)

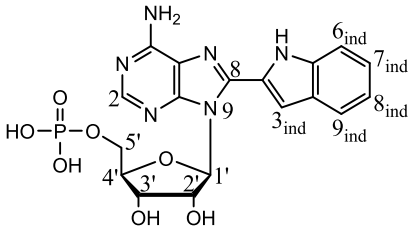

9m

The title compound was prepared according to the general synthetic procedure B2, from **9a** (0.1068 g, 1 equiv.) using Na_2PdCl_4 (0.09 equiv.), TPPTS (3.5 equiv. to Pd), *N*-Boc-indole-2-boronic acid (1.6 equiv.) and K_2CO_3 (3 equiv.) in water (6 mL) at 100 °C.

After 12 h, the reaction seemed complete. The crude product was purified by purification method 1 (0-45% MeOH against 0.05 M TEAB buffer over 500 mL, flow: 3 mL/min, fraction size: 5 mL) to give **9m** as a colourless oil (0.0966 g, 2.2 equiv. TEA, 83% yield). ^{1}H NMR (400 MHz; D_2O) δ: 7.88 (1H, s, 2-H), 7.53 (1H, d, *J* = 8.0 Hz, 6-H *indole*), 7.33 (1H, d, *J* = 8.3 Hz, 9-H *indole*), 7.13 (1H, t, *J* = 7.5 Hz, 3-H *indole*), 7.02 – 6.94 (2H, m, 7-H *indole*, 8-H *indole*), 6.17 (1H, d, $J_{1',2'}$ = 5.7 Hz, 1′-H), 5.42 (1H, apparent t, 2′-H), 4.55 (1H, m, 3′-H), 4.36 – 4.28 (1H, m, 4′-H), 4.09 (2H, m, 5′-H_2), 3.12 (13.2H, q, *J* = 7.3 Hz, CH_2 TEA), 1.21 (20.4H, t, *J* = 7.3 Hz, CH_3 TEA); ^{31}P NMR (162 MHz; D_2O) δ: 3.37; m/z (ESI) 461.0955 [M-H]$^-$, $C_{18}H_{18}N_6O_7P^-$ requires 461.0980.

Phosphoric acid mono-5′-[8-(benzofuran-2-yl)-9*β*-D-ribofuranosyl-adenine] (9n)

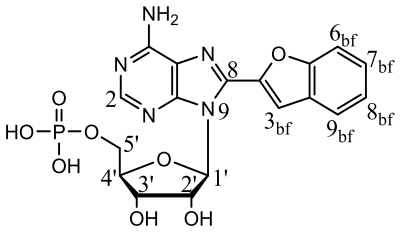

9n

The title compound was prepared according to the general synthetic procedure B2, from **9a** (0.0396 g, 1 equiv.) using Na_2PdCl_4 (0.09 equiv.), TPPTS (3 equiv. to Pd), 2-benzofuranyl boronic acid (2 equiv.) and K_2CO_3 (2 equiv.) in water (3 mL) at 100 °C. After 12 h, the conversion seemed at 50%. The crude product was purified by purification method 1 (0-40% MeOH against 0.05 M TEAB buffer over 400 mL, isocratic 50% over 50 mL, flow: 3 mL/min, fraction size: 5 mL) to give **9n** as a colourless oil (0.0038 g, 1.4 equiv. TEA, 10% yield). ^{1}H NMR (400 MHz; D_2O) δ: 7.89 (1H, s, 2-H), 7.40 (2H, m, 6-H *benzofuran*, 9-H *benzofuran*), 7.29 (1H, s, 3-H *benzofuran*), 7.20 (1H, m, 7-H *benzofuran*), 7.04 (1H, m, 8-H *benzofuran*), 6.28 (1H, d, $J_{1',2'}$ = 5.3 Hz, 1′-H), 5.39 (1H, apparent t, 2′-H), 4.63 (1H, m, 3′-H), 4.32 (1H, d, 4′-H), 4.27 – 4.06 (2H, m, 5′-H_2), 3.15 (8.5H, q, *J* = 7.3 Hz, CH_2 TEA), 1.23 (16.6H, t, *J* = 7.3 Hz, CH_3 TEA); ^{31}P NMR (162 MHz; D_2O) δ: 0.82; m/z (ESI) 462.0848 [M-H]$^-$, $C_{18}H_{17}N_5O_8P^-$ requires 462.0820.

7.2.5 Preparation of aryl/heteroaryl adenine-modified NAD^+ derivatives (**13a**-**b**, **14a**-**b**, **15b**,**c**,**e**,**g**,**h**)

Morpholin-4-yl-phosphonic acid mono-5′-[2-iodo-9*β*-D-ribofuranosyl-adenine] (10a)

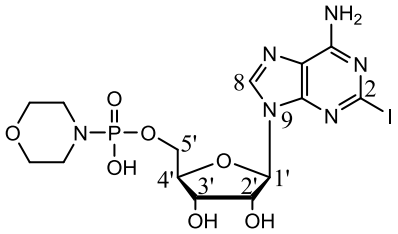

10a

The title compound was prepared according to the general synthetic procedure F, from **7a** (0.009 g, 1 equiv.). The crude product was purified by purification method 1 (100% 0.05 M TEAB over 60 mL, 0-60% MeOH against 0.05 M TEAB buffer over 300 mL, isocratic 60% over 100 mL, flow: 3 mL/min, fraction size: 5 mL) to give **10a** as a colourless oil (0.0089 g, 1.1 equiv. TEA, 97% yield). ^{1}H NMR (400 MHz; D_2O) δ: 8.30 (1H, s, 8-H), 6.01 (1H, d, $J_{1',2'}$ = 4.7 Hz, 1′-H), 4.76 (1H, m, 2′-H), 4.51 (1H, t, *J* = 4.9 Hz, 3′-H), 4.31 (1H, m, 4′-H), 4.08 – 3.93 (2H, m, 5′-H_2), 3.53 (4H, m, *CH_2 morpholine*), 3.17 (6.8H, q, *J* = 7.3 Hz, *CH_2* TEA), 2.88 (4H, m, *CH_2 morpholine*), 1.24 (9.8H, t, *CH_3* TEA); ^{31}P NMR (162 MHz; D_2O) δ: 7.37; m/z (ESI) 541.0105 $[M-H]^-$, $C_{14}H_{19}IN_6O_7P^-$ requires 541.0103.

Morpholin-4-yl-phosphonic acid mono-5′-[2-phenyl-9*β*-D-ribofuranosyl-adenine] (10b)

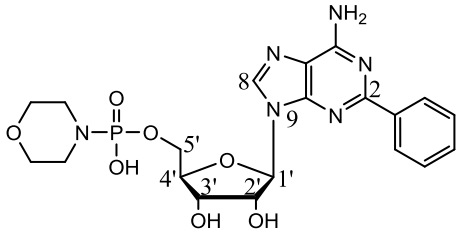

10b

The title compound was prepared according to the general synthetic procedure F, from **7b** (0.0075 g, 1 equiv.). The crude product was purified by purification method 1 (100% 0.05 M TEAB over 100 mL, 0-50% MeOH against 0.05 M TEAB buffer over 250 mL,

isocratic 60% over 50 mL, flow: 2.5 mL/min, fraction size: 5 mL) to give **10b** as a colourless oil (0.0086 g, 1.1 equiv. TEA, 98% yield). ^{1}H NMR (400 MHz; D_2O) δ: 8.28 (1H, s, 8-H), 8.01 (2H, m, *Ph*), 7.45 (3H, m, *Ph*), 6.10 (1H, d, $J_{1',2'}$ = 4.2 Hz, 1′-H), 4.87 (1H, apparent t, 2′-H), 4.63 (1H, apparent t, 3′-H), 4.30 (1H, m, 4′-H), 4.00 (2H, m, 5′-H_2), 3.37 (4H, m, *CH_2 morpholine*), 2.98 (6.6H, q, *J* = 7.3 Hz, *CH_2* TEA), 2.76 (4H, m, *CH_2 morpholine*), 1.16 (10.1H, t, *J* = 7.3 Hz, *CH_3* TEA); ^{31}P NMR (162 MHz; D_2O) δ: 7.42; m/z (ESI) 491.1452 $[M-H]^-$, $C_{20}H_{24}N_6O_7P^-$ requires 491.1450.

Morpholin-4-yl-phosphonic acid mono-5′-[6-phenyl-9*β*-D-ribofuranosyl-purine] (11a)

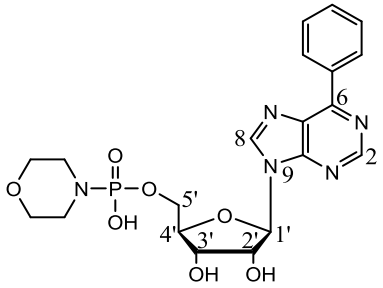

11a

The title compound was prepared according to the general synthetic procedure F, from **8a** (0.0191 g, 1 equiv.). The crude product was purified by purification method 1 (100% 0.05 M TEAB over 100 mL, 0-50% MeOH against 0.05 M TEAB buffer over 250 mL, isocratic 60% over 50 mL, flow: 3 mL/min, fraction size: 5 mL) to give **11a** as a colourless oil (0.0172 g, 1.2 equiv. TEA, 82% yield). ^{1}H NMR (400 MHz; D_2O) δ: 8.78 (1H, s, 2-H), 8.68 (1H, s, 8-H), 8.05 (2H, m, *Ph*), 7.58 – 7.45 (3H, m, *Ph*), 6.16 (1H, d, $J_{1',2'}$ = 4.6 Hz, 1′-H), 4.53 (1H, t, *J* = 4.9 Hz, 3′-H), 4.35 (1H, m, 4′-H), 4.12 – 3.96 (2H, m, 5′-H_2), 3.48 (4H, m, *CH_2 morpholine*), 3.16 (7.4H, q, *J* = 7.3 Hz, *CH_2* TEA), 2.87 (4H, m, *CH_2 morpholine*), 1.24 (11.6H, t, *J* = 7.2 Hz, *CH_3* TEA); ^{31}P NMR (162 MHz; D_2O) δ: 7.40; m/z (ESI) 476.1339 $[M-H]^-$, $C_{20}H_{23}N_5O_7P^-$ requires 476.1341.

Morpholin-4-yl-phosphonic acid mono-5′-[6-(pyrrol-2-yl)-9*β*-D-ribofuranosyl-purine] (11b)

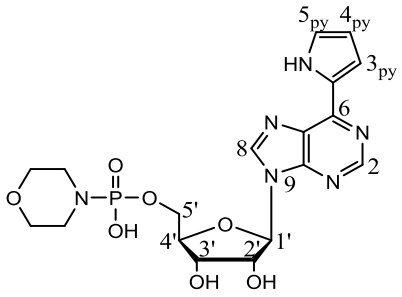

11b

The title compound was prepared according to the general synthetic procedure F, from **8b** (0.015 g, 1 equiv.). The crude product was purified by purification method 1 (100% 0.05 M TEAB over 100 mL, 0-50% MeOH against 0.05 M TEAB buffer over 250 mL, isocratic 60% over 50 mL, flow: 3 mL/min, fraction size: 5 mL) to give **11b** as a colourless oil (0.0132 g, 1.1 equiv. TEA, 88% yield). ^{1}H NMR (400 MHz; D_2O) δ: 8.54 (1H, s, 2-H), 8.52 (1H, s, 8-H), 7.19 (2H, m, 5-H *pyrrole*, 3-H *pyrrole*), 6.39 (1H, s, 4-H *pyrrole*), 6.09 (1H, d, $J_{1',2'}$ = 4.6 Hz, 1′-H), 4.52 (1H, t, *J* = 4.9 Hz, 3′-H), 4.34 (1H, m, 4′-H), 4.11 – 3.92 (2H, m, 5′-H_2), 3.49 (4H, m, *CH_2 morpholine*), 3.15 (6.3H, q, *J* = 7.3 Hz, *CH_2* TEA), 2.85 (4H, m, *CH_2 morpholine*), 1.23 (10.1H, t, *J* = 7.3 Hz, *CH_3* TEA); ^{31}P NMR (162 MHz; D_2O) δ: 7.41.

Morpholin-4-yl-phosphonic acid mono-5′-[8-phenyl-9*β*-D-ribofuranosyl-adenine] (12b)[112]

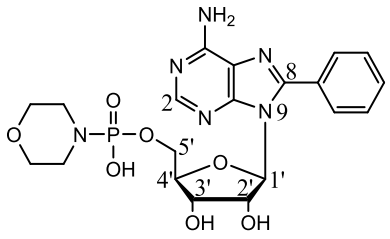

12b

The title compound was prepared according to the general synthetic procedure F, from **9b** (0.0092 g, 1 equiv.) by NaI precipitation. **12b** was obtained as sodium salt in quantitative yield. ^{1}H NMR (400 MHz; D_2O) δ: 8.23 (1H, s, 2-H), 7.74 – 7.46 (5H, m, *Ph*), 5.86 (1H, d, $J_{1',2'}$ = 5.3 Hz, 1′-H), 5.30 (1H, apparent t, 2′-H), 4.58 (1H, m, 3′-H),

4.17 – 3.95 (3H, m, 4′-H, 5′-H_2), 3.46 (4H, m, *CH_2 morpholine*), 2.82 (4H, m, *CH_2 morpholine*); m/z (ESI) 491.1452 $[M\text{-}Na]^-$, $C_{20}H_{24}N_6O_7P^-$ requires 491.1450.

Morpholin-4-yl-phosphonic acid mono-5′-[8-(3-(*N*-Boc-aminomethyl)phenyl)-9*β*-D-ribofuranosyl-adenine] (12c)

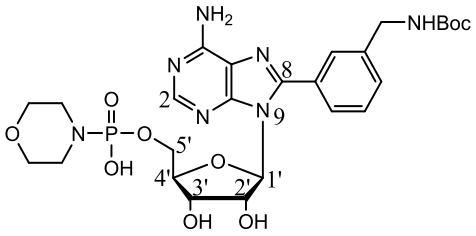

12c

The title compound was prepared according to the general synthetic procedure F, from **9c** (0.0425 g, 1 equiv.). The crude product was purified by purification method 1 (0-50% MeOH against 0.05 M TEAB buffer over 300 mL, then 50-60% over 100 mL, flow: 3 mL/min, fraction size: 5 mL) to give **12c** as a colourless oil (1.3 equiv. TEA, quantitative yield). ^{1}H NMR (400 MHz; CD_3OD) δ: 8.26 (1H, s, 2-H), 7.89 – 7.48 (4H, m, *Ph*), 5.86 (1H, d, 1′-H), 5.58 (1H, apparent t, 2′-H), 4.60 (1H, m, 3′-H), 4.51 – 3.85 (5H, m, 4′-H, 5′-H_2, *CH_2*NHBoc), 3.55 (4H, m, *CH_2 morpholine*), 2.91 (4H, m, *CH_2 morpholine*), 3.06 (8H, q, *J* = 7.3 Hz, *CH_2* TEA), 1.45 (9H, s, *CH_3* Boc), 1.24 (11.8H, t, *J* = 7.3 Hz, *CH_3* TEA).

Morpholin-4-yl-phosphonic acid mono-5′-[8-(pyridin-3-yl)-9*β*-D-ribofuranosyl-adenine] (12e)

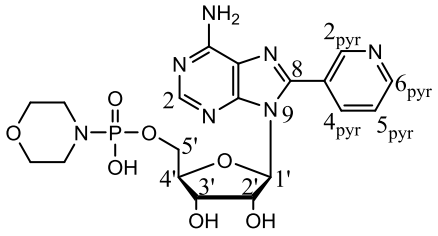

12e

The title compound was prepared according to the general synthetic procedure F, from **9e** (0.0123 g, 1 equiv.) by NaI precipitation. **12e** was obtained as sodium salt in quantitative yield. ^{1}H NMR (400 MHz; D_2O) δ: 8.84 (1H, m, 2-H *pyridine*), 8.71 (1H,

m, 6-H *pyridine*), 8.20 (1H, s, 2-H), 8.19 – 8.04 (1H, m, 5-H *pyridine*), 5.81 (1H, d, 1′-H), 5.38 (1H, m, 2′-H), 4.62 (1H, m, 3′-H), 4.26 – 3.90 (3H, m, 4′-H, 5′-H_2), 3.48 (4H, m, CH_2 *morpholine*), 2.84 (4H, m, CH_2 *morpholine*).

Morpholin-4-yl-phosphonic acid mono-5′-[8-(pyrrol-2-yl)-9*β*-D-ribofuranosyl-adenine] (12h)

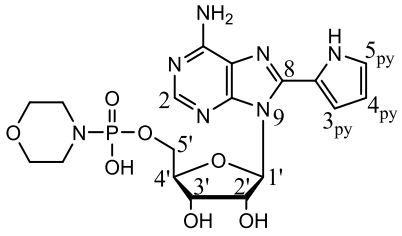

12h

The title compound was prepared according to the general synthetic procedure F, from **9h** (0.0417 g, 1 equiv.) by purification method 1 (0-50% MeOH against 0.05 M TEAB buffer over 300 mL, then 50-60% over 100 mL, flow: 3 mL/min, fraction size: 5 mL) to give **12h** as a colourless oil (1.3 equiv. TEA, quantitative yield). ^{1}H NMR (400 MHz; D_2O) δ: 8.16 (1H, s, 2-H), 7.13 (1H, s, 5-H *pyrrole*), 6.82 (1H, s, 3-H *pyrrole*), 6.35 (1H, s, 4-H *pyrrole*), 6.08 (1H, br s, 1′-H), 5.44 (1H, br s, 2′-H), 4.42 – 3.89 (4H, m, 3′-H, 4′-H, 5′-H_2), 3.36 (4H, m, CH_2 *morpholine*), 2.72 (4H, m, CH_2 *morpholine*), 3.15 (7.6H, q, J = 7.3 Hz, CH_2 TEA), 1.21 (11.4H, t, J = 7.3 Hz, CH_3 TEA).

P^1-(2-Iodo-adenine-9β-D-ribofuranos-5′-yl)-P^2-(nicotinamide-1β-D-ribofuranos-5′-yl) pyrophosphate (13a)

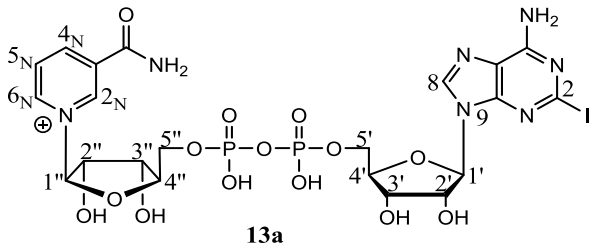

13a

The title compound was prepared according to the general synthetic procedure G, from **10a** (0.0134 g, 1 equiv.) and β-NMN (2.4 equiv.). The reaction was stirred overnight. The crude product was purified by purification method 1 (0-50% MeOH against 0.05 M TEAB buffer over 360 mL, isocratic 50% over 40 mL, flow: 3 mL/min, fraction size: 5 mL) and treated with Chelex to give **13a** as a colourless oil (0.0093 g, 0.2 equiv. TEA, 53% yield). ^{1}H NMR (400 MHz; D_2O) δ: 9.31 (1H, s, 2_N-H), 9.06 (1H, s, 6_N-H), 8.87 (1H, m, 4_N-H), 8.31 (1H, s, 8-H), 8.21 (1H, m, 5_N-H), 6.02 (1H, d, $J_{1'',2''}$ = 5.0 Hz, 1″-H), 5.91 (1H, d, $J_{1',2'}$ = 5.3 Hz, 1′-H), 4.74 (1H, br s, 2′-H), 4.54 – 3.98 (9H, m, 2″-H, 3′-H, 3″-H, 4′-H, 4″-H, 5′-H_2, 5″-H_2), 1.24 (1.8H, t, J = 7.3 Hz, CH_3 TEA); ^{13}C NMR (126 MHz; D_2O) δ: 156.87, 147.44, 143.83, 141.65, 138.06, 130.41, 121.21, 101.62, 98.90, 88.71, 88.27, 85.50, 79.19, 75.49, 72.29, 71.99, 67.03, 66.57, 60.58, 9.07; ^{31}P NMR (162 MHz; D_2O) δ: -11.4, -11.2; m/z (ESI) 787.9967 $[M-2H]^-$, $C_{21}H_{25}IN_7O_{14}P_2^-$ requires 787.9985.

P^1-(2-Phenyl-adenine-9β-D-ribofuranos-5′-yl)-P^2-(nicotinamide-1β-D-ribofuranos-5′-yl) pyrophosphate (13b)

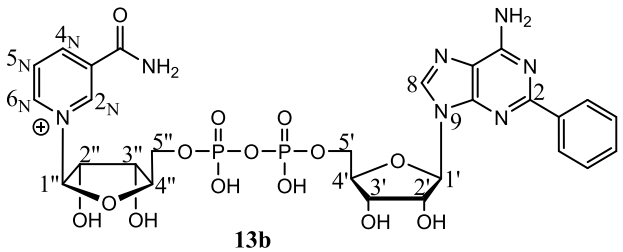

13b

The title compound was prepared according to the general synthetic procedure G, from **10b** (1.7 equiv.) and β-NMN (0.0234 g, 1 equiv.). The reaction was stirred overnight. The crude product was purified by purification method 1 (0-50% MeOH against 0.05 M TEAB buffer over 400 mL, flow: 3 mL/min, fraction size: 5 mL) to give **13b** as a colourless oil (0.017 g, 1.18 equiv. TEA, 28% yield). ^{1}H NMR (400 MHz; D_2O) δ: 9.04 (1H, br s, 2_N-H), 8.83 (1H, br s, 6_N-H), 8.61 (1H, m, 4_N-H), 8.09 – 7.86 (3H, m, 5_N-H, 8-H, *Ph*), 7.45 (4H, m, *Ph*), 6.08 (1H, br s, 1″-H), 5.76 (1H, br s, 1′-H), 4.84 (1H, br s, 2′-H), 4.56 (1H, br s, 2″-H), 4.43 – 4.01 (6H, m, 3′-H, 3″-H, 4′-H, 4″-H, 5′-H_2, 5″-H_2), 3.16 (7H, q, J = 7.2 Hz, CH_2 TEA), 1.22 (10.6H, t, J = 7.2 Hz, CH_3 TEA); ^{13}C NMR (101 MHz; D_2O) δ: 146.30, 142.68, 140.55, 138.29, 137.55, 137.23, 135.59, 131.55, 131.52, 129.56, 129.49, 128.80, 100.61, 93.30, 87.75, 84.39, 78.37, 74.32, 71.26, 65.04, 53.17, 52.17, 47.51, 9.07; ^{31}P NMR (162 MHz; D_2O) δ: -11.5, -11.7; m/z (ESI) 738.1324 $[M-H]^-$, $C_{27}H_{30}N_7O_{14}P_2^-$ requires 738.1331.

P^1-(6-Phenyl-purine-9β-D-ribofuranos-5′-yl)-P^2-(nicotinamide-1β-D-ribofuranos-5′-yl) pyrophosphate (14a)

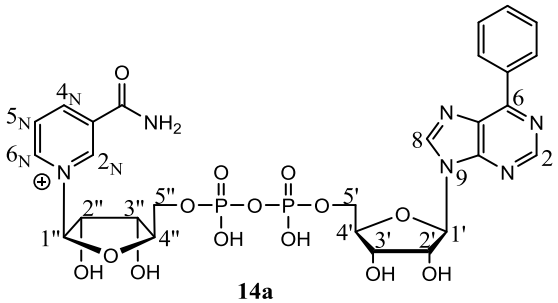

14a

The title compound was prepared according to the general synthetic procedure G, from **11a** (0.019 g, 1 equiv.) and β-NMN (1.8 equiv.). The reaction was stirred overnight. The crude product was purified twice by purification method 1 (0-50% MeOH against 0.05 M TEAB buffer over 400 mL, flow: 3 mL/min, fraction size: 5 mL) and treated with Chelex to give **14a** as a colourless oil (0.0171 g, 0.4 equiv. TEA, 56% yield). ^{1}H NMR (400 MHz; D_2O) δ: 9.18 (1H, s, 2_N-H), 9.01 (1H, d, $J_{6,5}$ = 5.8 Hz, 6_N-H), 8.82 (1H, s, 2-H), 8.78 (1H, s, 8-H), 8.66 (1H, d, $J_{4,5}$ = 8.0 Hz, 4_N-H), 8.11 (2H, d, J = 7.3 Hz, *Ph*), 8.06 – 8.01 (1H, m, 5_N-H), 7.57 (3H, m, *Ph*), 6.21 (1H, d, $J_{1'',2''}$ = 5.4 Hz, 1″-H), 5.88 (1H, d, J = 4.2 Hz, 1′-H), 4.55 – 4.09 (10H, m, 2′-H, 2″-H, 3′-H, 3″-H, 4′-H, 4″-H, 5′-H_2, 5″-H_2), 3.24 (2.4H, q, J = 7.3 Hz, CH_2 TEA), 1.22 (4.1H, t, J = 7.2 Hz, CH_3 TEA). ^{13}C NMR (126 MHz; D_2O) δ: 162.12, 156.90, 153.67, 153.43, 147.40, 146.20, 144.11, 141.19, 138.05, 135.24, 133.34, 132.02, 131.14, 131.00, 130.54, 130.10, 101.56, 98.89, 88.75, 85.62, 79.13, 75.74, 72.09, 67.00, 66.49, 60.58, 48.24, 9.07; ^{31}P NMR (162 MHz; D_2O) δ: -11.3 (d, $J_{P,P}$ = 20.3 Hz), -11.7 (d, $J_{P,P}$ = 20.7 Hz); m/z (ESI) 723.1210 $[M-2H]^-$, $C_{27}H_{29}N_6O_{14}P_2^-$ requires 723.1222.

P^1-[6-(Pyrrol-2-yl)-purine-9β-D-ribofuranos-5′-yl]-P^2-[nicotinamide-1β-D-ribofuranos-5′-yl] pyrophosphate (14b)

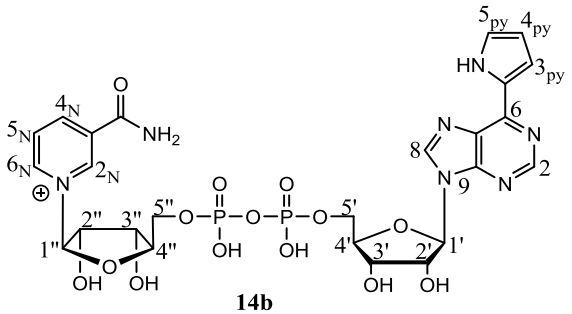

14b

The title compound was prepared according to the general synthetic procedure G, from **11b** (0.0084 g, 1 equiv.) and β-NMN (2.1 equiv.). The reaction was stirred overnight. The crude product was purified by purification method 1 (0-50% MeOH against 0.05 M TEAB buffer over 400 mL, flow: 3 mL/min, fraction size: 5 mL) to give **14b** as a colourless oil (0.0132 g, 1.3 equiv. TEA, 87% yield). ^{1}H NMR (400 MHz; D_2O) δ: 9.11 (1H, s, 2_N-H), 8.94 (1H, d, $J_{6,5}$ = 5.1 Hz, 6_N-H), 8.69 (1H, s, 2-H), 8.61 (1H, s, 8-H), 8.57 (1H, d, J = 7.7 Hz, 4_N-H), 7.90 (1H, m, 5_N-H), 7.23 (1H, s, 5-H *pyrrole*), 7.20 (1H, d, $J_{3,4}$ = 3.1 Hz, 3-H *pyrrole*), 6.43 (1H, m, 4-H *pyrrole*), 6.17 (1H, d, $J_{1'',2''}$ = 5.8 Hz, 1″-H), 5.91 (1H, d, $J_{1',2'}$ = 4.4 Hz, 1′-H), 4.60 – 4.12 (10H, m, 2′-H, 2″-H, 3′-H, 3″-H, 4′-H, 4″-H, 5′-H_2, 5″-H_2), 3.18 (6.2H, q, J = 7.3 Hz, CH_2 TEA), 1.25 (12H, t, J = 7.3 Hz, CH_3 TEA); ^{13}C NMR (126 MHz; D_2O) δ: 153.21, 151.85, 147.85, 146.39, 144.16, 143.33, 143.31, 140.35, 129.02, 127.81, 127.11, 126.18, 116.04, 112.16, 101.03, 98.14, 87.89, 87.59, 85.07, 78.47, 74.90, 71.57, 71.37, 59.83, 47.50, 9.07; ^{31}P NMR (162 MHz; D_2O) δ: -11.4, -11. 6; m/z (ESI) 714.1311 $[M]^+$, $C_{25}H_{30}N_7O_{14}P_2^+$ requires 714.1320.

P^1-(8-Phenyl-adenine-9β-D-ribofuranos-5′-yl)-P^2-(nicotinamide-1β-D-ribofuranos-5′-yl) pyrophosphate (15b)[112, 172]

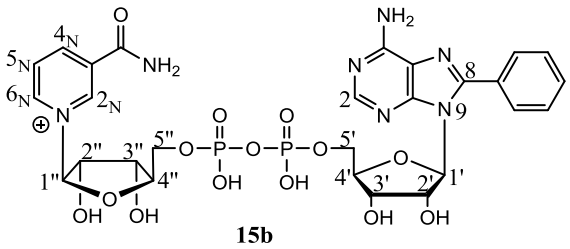

15b

The title compound was prepared according to the general synthetic procedure G, from **12b** (1.2 equiv.) and β-NMN (0.0038 g, 1 equiv.). The reaction was stirred overnight. The crude product was purified by purification method 1 (0% MeOH over 50 mL, 0-40% MeOH against 0.05 M TEAB buffer over 350 mL, flow: 3 mL/min, fraction size: 5 mL) to give **15b** as a colourless oil (0.004 g, 1.18 equiv. TEA, 41% yield). ^{1}H NMR (400 MHz; D_2O) δ: 9.21 (1H, s, 2_N-H), 9.06 (1H, d, $J_{6,5}$ = 6.4 Hz, 6_N-H), 8.68 (1H, m, $J_{4,5}$ = 8.1 Hz, $J_{4,6}$ = 1.3 Hz, $J_{4,2}$ = 1.5 Hz, 4_N-H), 8.18 (1H, s, 2-H), 8.16 – 8.10 (1H, m, 5_N-H), 7.65 – 7.50 (5H, m, *Ph*), 5.90 (1H, d, $J_{1'',2''}$ = 5.1 Hz, 1″-H), 5.79 (1H, d, $J_{1',2'}$ = 5.9 Hz, 1′-H), 5.14 (1H, apparent t, 2′-H), 4.43 – 4.06 (9H, m, 2″-H, 3′-H, 3″-H, 4′-H, 4″-H, 5′-H_2, 5″-H_2), 3.14 (6.8H, q, J = 7.3 Hz, CH_2 TEA), 1.22 (10.6H, t, J = 7.3 Hz, CH_3 TEA); ^{13}C NMR (150.90 MHz; D_2O) δ: 154.05, 153.70, 153.30, 150.91, 146.55, 143.18, 140.61, 132.04, 130.39, 130.25, 129.92, 129.63, 128.46, 119.14, 100.88, 89.82, 89.61, 87.85, 83.78, 78.41, 71.32, 71.23, 71.14, 70.38, 70.23, 66.61, 65.69, 59.73, 47.51, 9.07; ^{31}P NMR (162 MHz; D_2O) δ: -11.7 (d, $J_{P,P}$ = 20.6 Hz); -11.3 (d, $J_{P,P}$ = 20.6 Hz); m/z (ESI) 738.1332 $[M-2H]^-$, $C_{27}H_{30}N_7O_{14}P_2^-$ requires 738.1331; HPLC: retention time 10.34 min (79.4%); TLC: R_f 0.43 (iPA/H_2O/NH_4OH 6:3:1).

P^1-{8-[3-(*N*-Boc-aminomethyl)phenyl]-adenine-9*β*-D-ribofuranos-5′-yl}-P^2-{nicotinamide-1*β*-D-ribofuranos-5′-yl} pyrophosphate (15c)[172]

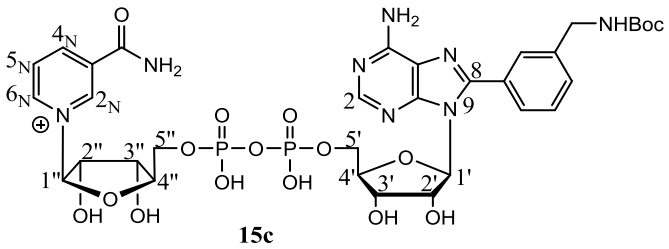

15c

The title compound was prepared according to the general synthetic procedure G, from **12c** (1.2 equiv.) and *β*-NMN (0.0176 g, 1 equiv.). The reaction was stirred overnight. The crude product was purified by purification method 1 (0-10% MeOH against 0.05 M TEAB buffer over 190 mL, 10-30% over 50 mL, isocratic 30% over 50 mL, flow: 3 mL/min, fraction size: 5 mL) to give **15c** as a colourless oil (0.0331 g, 1.7 equiv. TEA, 61% yield) and treated with Chelex to obtain the sodium salt. ^{1}H NMR (400 MHz; D_2O) δ: 9.16 (1H, s, 2_N-H), 8.99 (1H, br s, 6_N-H), 8.60 (1H, m, 4_N-H), 8.07 (2H, m, 2-H, 5_N-H), 7.54 – 7.26 (4H, m, *Ph*), 5.85 (1H, br s, 1″-H), 5.71 (1H, br s, 1′-H), 5.16 (1H, br s, 2′-H), 4.49 – 3.77 (11H, m, 2″-H, 3′-H, 3″-H, 4′-H, 4″-H, 5′-H_2, 5″-H_2, CH_2NH_2), 1.33 (9H, s, CH_3 Boc); ^{13}C NMR (150.90 MHz; D_2O) δ: 158.95, 155.55, 153.21, 152.45, 150.65, 148.28, 146.33, 142.95, 140.67, 140.41, 137.07, 134.10, 130.20 – 128.23, 124.83, 118.92, 101.81, 100.66, 96.99, 89.71, 87.67, 83.67, 81.92, 78.22, 75.81, 71.34 – 70.15, 66.34, 65.39, 44.10, 28.36; ^{31}P NMR (162 MHz; D_2O) δ: -11.3 (d, $J_{P,P}$ = 20.6 Hz); -11.1 (d, $J_{P,P}$ = 20.6 Hz); m/z (ESI) 867.2120 $[M-2H]^-$, $C_{33}H_{41}N_8O_{16}P_2^-$ requires 867.2121; HPLC: retention time 17.96 min (99.5%); TLC: R_f 0.75 (iPA/H_2O/ NH_4OH 6:3:1).

P^1-[8-(Pyridin-3-yl)-adenine-9β-D-ribofuranos-5′-yl]-P^2-[nicotinamide-1β-D-ribofuranos-5′-yl] pyrophosphate (15e)[172]

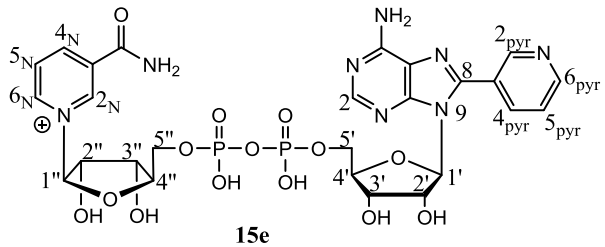

15e

The title compound was prepared according to the general synthetic procedure G, from **12e** (0.0143 g, 1 equiv.) and β-NMN (1.1 equiv.). The reaction was stirred overnight. The crude product was purified by purification method 1 (0-10% MeOH against 0.05 M TEAB buffer over 300 mL, then 10-12% MeOH over 100 mL, flow: 3 mL/min, fraction size: 5 mL) to give **15e** as a colourless oil (0.0068 g, 1.18 equiv. TEA, 24% yield). ^{1}H NMR (400 MHz; D_2O) δ: 9.29 (1H, s, 2_N-H), 9.14 (1H, d, $J_{6,5}$ = 6.0 Hz, 6_N-H), 9.01 – 8.65 (3H, m, 4_N-H, 2-H *pyridine*, 6-H *pyridine*), 8.34 – 8.13 (3H, m, 2-H, 5_N-H, 4-H *pyridine*), 7.70 (1H, br s, 5-H *pyridine*), 6.01 (1H, d, $J_{1'',2''}$ = 5.1 Hz, 1″-H), 5.80 (1H, d, $J_{1',2'}$ = 5.7 Hz, 1′-H), 5.24 (1H, apparent t, 2′-H), 4.51 – 4.11 (9H, m, 2″-H, 3′-H, 3″-H, 4′-H, 4″-H, 5′-H_2, 5″-H_2), 3.19 (6.9H, q, J = 7.3 Hz, CH_2 TEA), 1.27 (10.6H, t, J = 7.3 Hz, CH_3 TEA); ^{13}C NMR (150.90 MHz; D_2O) δ: 155.89, 153.53, 151.01, 150.53, 149.62, 146.60, 143.28, 140.56, 139.32, 134.53, 129.60, 119.50, 100.89, 89.71, 87.92, 84.08, 78.44, 71.38, 70.28, 66.41, 65.65, 47.52, 9.07; m/z (ESI) 739.1300 $[M-2H]^-$, $C_{26}H_{29}N_8O_{14}P_2^-$ requires 739.1284; HPLC: retention time 7.07 min (95.8%); TLC: R_f 0.62 (iPA/H_2O/NH_4OH 6:3:1).

P^1-[8-(2,4-*DMT*-pyrimidin-5-yl)-adenine-9*β*-D-ribofuranos-5′-yl]-P^2-[nicotinamide-1*β*-D-ribofuranos-5′-yl] pyrophosphate (15g)[172]

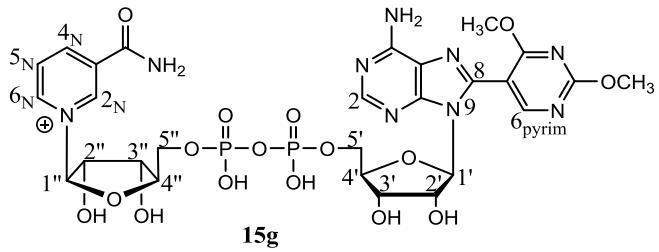

15g

The title compound was prepared according to the general synthetic procedure G, from **12g** (1.5 equiv.) and *β*-NMN (0.0112 g, 1 equiv.). The reaction was stirred overnight. The crude product was purified by purification method 1 (0-22% MeOH against 0.05 M TEAB buffer over 300 mL, 22-40% over 50 mL, isocratic 40% over 50 mL, flow: 3 mL/min, fraction size: 5 mL) to give **15g** as a colourless oil (0.0139 g, 1.7eq TEA, 43% yield) and treated with Chelex to obtain the sodium salt. ^{1}H NMR (400 MHz; D_2O) δ: 9.25 (1H, s, 2_N-H), 9.08 (1H, m, 6_N-H), 8.68 (1H, m, 4_N-H), 8.33 (1H, m, 6-H *pyrimidine*), 8.10 (2H, br s, 2-H, 5_N-H), 6.01 (1H, d, $J_{1'',2''}$ = 5.4 Hz, 1″-H), 5.49 (1H, d, $J_{1',2'}$ = 5.5 Hz, 1′-H), 5.08 (1H, apparent t, 2′-H), 4.53 – 3.85 (15H, m, 2″-H, 3′-H, 3″-H, 4′-H, 4″-H, 5′-H_2, 5″-H_2, 2 *OCH_3*); ^{13}C NMR (150.90 MHz; D_2O) δ: 169.85, 167.00, 161.02, 155.64, 153.60, 152.48, 150.47, 148.31, 146.40, 143.03, 137.11, 134.25, 129.37, 124.87, 119.49, 104.96, 101.81, 100.69, 97.02, 90.06, 87.71, 83.85, 81.78, 78.28, 75.82, 71.78 – 70.43, 66.90 – 65.50, 59.66, 56.29, 55.60; ^{31}P NMR (162 MHz; D_2O) δ: -11.3 (d, $J_{P,P}$ = 20.6 Hz); -11.1 (d, $J_{P,P}$ = 20.6 Hz); m/z (ESI) 800.1447 $[M-2H]^-$, $C_{27}H_{32}N_9O_{16}P_2^-$ requires 800.1448; HPLC: retention time 11.41 min (96.5%); TLC: R_f 0.69 (iPA/H_2O/ NH_4OH 6:3:1).

P^1-[8-(Pyrrol-2-yl)-adenine-9β-D-ribofuranos-5′-yl]-P^2-[nicotinamide-1β-D-ribofuranos-5′-yl] pyrophosphate (15h)[172]

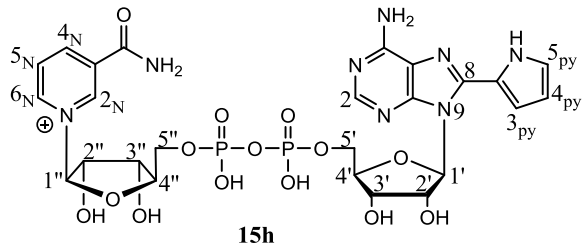

15h

The title compound was prepared according to the general synthetic procedure G, from **12h** (1.5 equiv.) and β-NMN (0.0332 g, 1 equiv.). The reaction was stirred overnight. The crude product was purified by purification method 1 (0-10% MeOH against 0.05 M TEAB buffer over 400 mL, flow: 3 mL/min, fraction size: 5 mL) and 2 (0-80% 1 M TEAB buffer against H_2O over 400 mL, flow: 3 mL/min, fraction size: 5 mL), to give **15h** as a colourless oil (0.0245 g, 1.01 equiv. TEA, 30% yield). ^{1}H NMR (400 MHz; D_2O) δ: 9.09 (1H, s, 2_N-H), 8.92 (1H, d, $J_{5,6}$ = 6.2 Hz, 6_N-H), 8.60 (1H, d, $J_{4,5}$ = 8.1 Hz, 4_N-H), 8.09 (1H, s, 2-H), 8.05 (1H, dd, $J_{5,6}$ = 6.5 Hz, $J_{5,4}$ = 7.8 Hz, 5_N-H), 7.05 (1H, dd, $J_{5,4}$ = 2.4 Hz, $J_{5,3}$ = 1.2 Hz, 5-H *pyrrole*), 6.57 (1H, dd, $J_{3,4}$ = 3.6 Hz, $J_{3,5}$ = 1.1 Hz, 3-H *pyrrole*), 6.24 (1H, dd, $J_{3,4}$ = 3.4 Hz, $J_{5,4}$ = 2.9 Hz, 4-H *pyrrole*), 5.91 (1H, d, $J_{1'',2''}$ = 6.1 Hz, 1″-H), 5.73 (1H, d, $J_{1',2'}$ = 4.8 Hz, 1′-H), 5.33 (1H, apparent t, 2′-H), 4.54 (1H, dd, J = 4.56 and 6.1 Hz, 3′-H), 4.41 – 3.98 (8H, m, 2″-H, 3″-H, 4′-H, 4″-H, 5′-H_2, 5″-H_2), 3.15 (6.08H, q, J = 7.3 Hz, CH_2 TEA), 1.24 (9.14H, t, J = 7.3 Hz, CH_3 TEA); ^{13}C NMR (150.90 MHz; D_2O) δ: 154.89, 151.98, 150.90, 147.10, 146.40, 142.91, 140.48, 134.14, 129.64, 124.27, 119.43, 113.82, 110.00, 100.81, 89.46, 87.79, 87.73, 83.81, 83.76, 78.41, 71.24, 70.89, 70.02, 66.47, 65.61, 59.60, 47.52, 9.07; ^{31}P NMR (162 MHz; D_2O) δ: -11.9 (d, $J_{P,P}$ = 20.9 Hz); -11.4 (d, $J_{P,P}$ = 21.0 Hz); m/z (ESI) 727.1276 $[M-2H]^-$, $C_{25}H_{29}N_8O_{14}P_2^-$ requires 727.1284; HPLC: retention time 7.68 min (99.8%).

7.2.6 Synthesis of 8-(pyrrol-2-yl) *c*ADPR (**24**)

8-(Pyrrol-2-yl)-adenine-[*P*^{1}-(9*β*-D-ribofuranos-5′-yl)-*P*^{2}-(1*β*-D-ribofuranos-5′-yl)] pyrophosphate (24)[246]

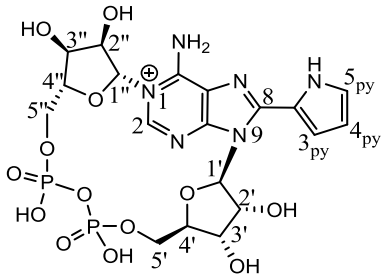

24

A stock solution of ADPRC from *Aplysia californica* (50 U/mL) was prepared in HEPES buffer (50 mM, pH 7.4). To a solution of **15h** (0.005 g) in HEPES buffer (13 mL, 50 mM, pH 7.4) an appropriate volume of ADPRC stock was added to have a final enzyme concentration of 0.192 U/mL. The reaction was incubated for 1 h at room temperature until HPLC analysis indicated completion of the reaction. Afterwards, the solution was evaporated to dryness and the crude product purified by purification method 2 (0-80% 1 M TEAB buffer against H_2O over 240 mL, flow rate: 2 mL/min, fraction size: 3 mL) to give **24** as a white residue (0.0051 g, 2.76 equiv. TEA, 96% yield). ^{1}H NMR (400 MHz; D_2O) δ: 8.98 (1H, s, 2-H), 7.23 (1H, dd, $J_{5,3}$ = 1.4 Hz, 5-H *pyrrole*), 6.92 (1H, dd, $J_{3,4}$ = 3.0 Hz, 3-H *pyrrole*), 6.45 (1H, dd, $J_{4,3}$ = 3.1 Hz, $J_{4,5}$ = 2.9 Hz, 4-H *pyrrole*), 6.42 (1H, d, *J* = 5.3 Hz, 1′-H), 6.16 (1H, d, *J* = 3.3 Hz, 1″-H), 5.53 (1H, apparent t, 2′-H), 4.50 – 4.09 (9H, m, 2″-H, 3′-H, 3″-H, 4′-H, 4″-H, 5′-H_2, 5″-H_2), 3.26 (16.6H, q, *J* = 7.3 Hz, CH_2 TEA), 1.24 (24.8H, t, *J* = 7.3 Hz, CH_3 TEA); ^{31}P NMR (162 MHz; CD_3OD) δ: -10.2 (d, $J_{P,P}$ = 11.7 Hz), -9.8 (d, $J_{P,P}$ = 11.3 Hz); m/z (ESI) 607.0947 $[M]^+$, $C_{19}H_{25}N_6O_{13}P_2^+$ requires 607.0949; HPLC: retention time 8.7 min.

7.3 Quantum yield measurements for AMP and NAD^+ derivatives

Fluorescence quantum yields (Φ_x) of AMP and NAD^+ derivatives were determined by the comparative method,[204, 205] using 2-amino pyridine in 0.1 M H_2SO_4 (Φ = 0.60) and tryptophan in water, pH 7.2 (Φ = 0.14), as reference standards. Absorbance spectra for all the compounds were recorded at room temperature from the most concentrated (Abs ≤ 1) to the most diluted solution between 200 and 800 nm. Emission spectra of the same solutions were recorded at room temperature between 200 and 900 nm at λ_{ex} maxima; the emission spectra for the same compound must be recorded with constant slit width to make valid the obtained quantum yield values. The integrated areas under the emission spectra were plotted as function of the integrated areas under the absorbance spectra at corresponding concentrations. The obtained gradient, $Grad_x$, was then substituted in equation [1] (see page 94), where $Grad_{st}$ is known from the calibration of the two standards, performed with the same protocol, and Φ_{st} is known from the literature. After correction for the refractive index, η, of the solvents used in the measurements, it is possible to calculate Φ_x from equation [1].

7.4 Chemical hydrolysis of NAD^+ derivatives[172]

For the monitoring by fluorescence of the chemical hydrolysis of NAD^+ derivatives, 0.1 N NaOH solution was added to the cuvette and the reaction was started by the addition of a requisite volume of aqueous solution of the compounds to give a final concentration of 0.8 μM. The basic hydrolysis was monitored at λ_{ex} and λ_{em} maxima for each compound at room temperature. In the case of **15h**, the whole emission spectra at λ_{ex} maxima was recorded over time (data not shown).

The HPLC time-course for the basic hydrolysis of **15h** was performed on a 49.5 μM solution in 0.1 N NaOH at room temperature. Each sample was quenched with an equivalent volume of 0.1 N HCl prior to injection into the HPLC. (for the HPLC method, see 7.1.2; retention times: NaM 3.8 min, **15h** 7.3 min, **23** 8.0 min). Peak areas were fitted to a 1st order rate equation using GraFit5. The estimated rate constant for the formation of NaM, k_{NaM}, from fitting the peak areas to a 1st order rate equation is 0.0672 min^{-1}, and the $t_{1/2}$ = 10.31 min, in agreement within error of each other with the

estimated rate constant for the formation of **23**, k_{23}, 0.0586 min^{-1}, and the $t_{1/2}$ = 11.83 min.

7.5 Protocols for HPLC assays of enzyme activities[172]

7.5.1 Nucleotide pyrophosphatase (NPP)

Separate stock solutions of **15h** (82.48 μM) and NPP from *Crotalus adamanteus* venom (8.39 U/mL) were prepared in Tris/HCl buffer (50 mM, pH 8) containing $MgCl_2$ (10 mM). The reaction was started by addition of an appropriate volume of **15h** stock (300 μL, 24.74 μM) to the enzyme solution (1.2 μL, 0.01 U/mL) in the reaction buffer to give a final volume of 1 mL (all concentrations are final concentrations). The reaction was incubated at 30 ºC for 90 min. Samples were drawn at different time points and stored immediately on dry-ice for 20 min, to stop the enzymatic reaction. Samples were diluted as appropriate and analysed by HPLC (for the HPLC method, see 7.1.2; retention times: **15h** 6.5 min, *β*-NMN 1.8 min, **9h** 7.7 min). The estimated rate constant *k* for the formation of **9h** was obtained by fitting the peak areas to a 1st order rate equation (k_{9h} 0.2457 min^{-1}, $t_{1/2}$ 2.82 min) using Grafit5.

7.5.2 NAD^+-glycohydrolase (NADase)

A stock solution of **15h** (82.48 μM) was prepared in Tris/HCl buffer (50 mM, pH 8). NADase from porcine brain (0.01 U/mg) was accurately weighed and suspended in Tris/HCl buffer (50 mM, pH 8) and incubated for a few minutes at 37 ºC. The reaction was started by addition of an appropriate volume of **15h** stock (300 μL, 24.74 μM) to the enzyme suspension (0.9 mg, 0.009 U/mL) in the reaction buffer to give a final volume of 1 mL (all concentrations are final concentrations). Samples were drawn at different time points and stored immediately on dry-ice for 20 min, to stop the enzymatic reaction. Samples were centrifuged, diluted as appropriate and analysed by HPLC (for the HPLC method, see 7.1.2; retention times: **15h** 7.3 min, NaM 3.8 min, **23** 8.0 min). The estimated rate constants for the formation of NaM, k_{NaM}, and the formation of **23**, k_{23}, were obtained by fitting the peak areas to a 1st order rate equation (k_{NaM} 0.1750 min^{-1}, $t_{1/2}$ 3.96 min; k_{23} 0.1696 min^{-1}, $t_{1/2}$ = 4.09 min) using Grafit5. In a

control experiment, **15h** was incubated in Tris/HCl buffer (50 mM, pH 8) at 37 ºC over 1 h without degradation.

7.5.3 ADP-ribosyl cyclase (ADPRC)

Separate stock solutions of **15h** (82.48 μM) and ADPRC from *Aplysia californica* (50 U/mL) were prepared in HEPES buffer (50 mM, pH 7.4). The reaction was started by addition of an appropriate volume of **15h** stock (75 μL, 12.37 μM) to the enzyme solution (0.5 μL, 0.05 U/mL) in the reaction buffer to give a final volume of 500 μL (all concentrations are final concentrations). The reaction was incubated at 26 ºC for 1 h. Samples were drawn at different time points and stored immediately on dry-ice for 20 min, to stop the enzymatic reaction. Samples were diluted as appropriate and analysed by HPLC (for the HPLC method, see 7.1.2; retention times: **15h** 6.6 min, NaM 3.8 min, **24** 8.7 min). The estimated rate constants for the formation of NaM, k_{NaM}, and the formation of 24, k_{24}, were obtained by fitting the peak areas to a 1st order rate equation (k_{NaM} 0.3525 min^{-1}, $t_{1/2}$ 1.97 min; k_{24} 0.1700 min^{-1}, $t_{1/2}$ 4.08 min) using Grafit5.

7.6 Protocols for fluorescent assays of enzyme activities[172]

7.6.1 Nucleotide pyrophosphatase (NPP)

Separate stock solutions of **15h** (17.6 μM), **9h** (9.4 μM) and NPP from *Crotalus adamanteus* venom (8.39 U/mL) were prepared in Tris/HCl buffer (50 mM, pH 8) containing $MgCl_2$ (10 mM), unless stated otherwise. β-NAD^+ (964.7 μM), AMP (1730 μM) and β-NMN (478.8 μM) stock solutions were prepared in Milli-Q water, unless stated otherwise. In the kinetic experiments, the requisite volume of substrate **15h** or product **9h** was added to individual wells of a 96-well plate, and Tris/HCl buffer (50 mM, pH 8) containing $MgCl_2$ (10 mM) was added as required to give a final volume of 100 μL. In the inhibition experiments, the requisite volume of substrate **15h** and β-NAD^+, or AMP, or β-NMN was added to individual wells of a 96-well plate, and Tris/HCl buffer (50 mM, pH 8) containing $MgCl_2$ (10 mM) was added as required to give a final volume of 100 μL. In each experiment, two calibration wells were included for the determination of sample concentration from fluorescence intensity: one well

contained only Tris/HCl buffer (50 mM, pH 8) and $MgCl_2$ (10 mM) and gave the 'zero' readout (negative control), and the second contained **9h** (3 μM) inTris/HCl buffer (50 mM, pH 8) and $MgCl_2$ (10 mM) (positive control). Samples and fluorimeter readings were allowed to stabilize by placing the plate in the microplate reader at 30 ºC and taking readings (excitation 300 ± 5 nm, emission 410 ± 5 nm, gain 15%) until a stable signal was obtained (typically *ca* 60 min). The data collection program was re-started and, after 7 min, the enzyme reaction was initiated by addition of enzyme stock solution (20 μL, 0.007 U/mL per well). Fluorescence emission was recorded for 60 min. All samples, including controls, were recorded in duplicate, and the mean of the two readings processed. To convert [RFU] to **9h** concentration [μM], it was assumed that there is very little contribution to fluorescence from **15h** related to **9h**. For each assay point, the fluorescence emission [RFU], F_t, was converted to **9h** concentration [μM], $[\boldsymbol{9h}]_t$, using the equation [2] and with reference to the fluorescence from **9h** (3 μM), $F_{3\mu M}$. From the resulting plot of [**9h**] *vs* time, initial velocity can be calculated from linear region at the beginning of each trace.

$$[\boldsymbol{9h}]_t = \frac{F_t - F_{buffer\ alone}}{F_{3\mu M} - F_{buffer\ alone}} \times 3\ \mu M \quad [2]$$

For the determination of kinetic parameters, K_m and V_{max}, enzyme (0.007 U/mL) and **15h** (0.2 μM – 6.5 μM) in Tris/HCl buffer (50 mM, pH 8) containing $MgCl_2$ (10 mM) were used (total volume per well: 120 μL, all concentrations are final concentrations). Kinetic parameters were reported as the mean (± SD) of at least two data sets. For the IC_{50} determination of *β*-NAD^+, increasing concentrations of *β*-NAD^+ (0 – 350 μM) were introduced into assays of **15h** (4.4 μM) and NPP (0.007 U/mL). For the kinetic analysis of *β*-NAD^+ inhibition, enzyme (0.007 U/mL), **15h** (0.2 μM – 5 μM) and *β*-NAD^+ (8 μM – 15 μM) in Tris/HCl buffer (50 mM, pH 8) containing $MgCl_2$ (10 mM) were used (total volume per well: 120 μL, all concentrations are final concentrations). For the kinetic analysis of AMP inhibition, enzyme (0.007 U/mL), **15h** (0.2 μM – 5 μM) and AMP (8 μM – 40 μM) in Tris/HCl buffer (50 mM, pH 8) containing $MgCl_2$ (10 mM) were used (total volume per well: 120 μL, all concentrations are final concentrations). For the kinetic analysis of *β*-NMN inhibition, enzyme (0.007 U/mL), **15h** (0.2 μM – 5 μM) and

β-NMN (7 μM – 17 μM) in Tris/HCl buffer (50 mM, pH 8) containing $MgCl_2$ (10 mM) were used (total volume per well: 120 μL, all concentrations are final concentrations).

7.6.2 NAD^+-glycohydrolase (NADase)

A stock solution of **15h** (6.3 μM) was prepared in Tris/HCl buffer (50 mM, pH 8), unless stated otherwise. In the kinetic experiments, an appropriate volume of Tris/HCl buffer (150 μL, 50 mM, pH 8) was added to individual wells of a 96-well plate. NADase from porcine brain (0.01 U/mg) was accurately weighed and suspended in Tris/HCl buffer (50 mM, pH 8) and incubated for several minutes at 37 ºC. The reaction was started by addition of an appropriate volume of **15h** stock (1 mL, 5.25 μM) to the enzyme suspension (0.9 mg, 0.0075 U/mL) in the reaction buffer to give a final volume of 1.2 mL (all concentrations are final concentrations). Samples (100 μL) were drawn at different time points and stored immediately on dry-ice for 20 min, to stop the enzymatic reaction. Then, from each one, 50 μL was drawn and added to the wells to give a final volume of 200 μL. Fluorescence emission was recorded at 37 ºC (excitation 300 ± 5 nm, emission 410 ± 5 nm, gain 15%).

7.6.3 ADP-ribosyl cyclase (ADPRC)

Separate stock solutions of **15h** (82.48 μM) and ADPRC (50 U/mL) from *Aplysia californica* were prepared in HEPES buffer (50 mM, pH 7.4), unless stated otherwise. In the kinetic experiments, the requisite volume of substrate **15h** was added to individual wells of a 96-well plate, and HEPES buffer (50 mM, pH 7.4) was added as required to give a final volume of 198 μL. In each experiment, two calibration wells were included for the determination of sample concentration from fluorescence intensity: one well contained only HEPES buffer (50 mM, pH 7.4) and gave the 'zero' readout (negative control), and the second contained **15h** (34 μM) in HEPES buffer (50 mM, pH 7.4) (positive control). Samples and fluorimeter readings were allowed to stabilize by placing the plate in the microplate reader at 25 ºC and taking readings (excitation 300 ± 5 nm, emission 410 ± 5 nm, gain 15%) until a stable signal was obtained (typically *ca* 40 min). The data collection program was re-started and, after 17 min, the enzyme reaction was initiated by addition of enzyme stock solution (2 μL,

0.075 U/mL per well). Fluorescence emission was recorded for 80 min. All samples, including controls, were recorded in duplicate, and the mean of the two readings processed. To convert [RFU] to **15h** concentration [μM], it was assumed that there is very little contribution to fluorescence from the reaction product, **24**. For each assay point, the fluorescence emission [RFU], F_t, was converted to **15h** concentration [μM], $[\boldsymbol{15h}]_t$, using the equation [3] and with reference to the fluorescence from **15h** (34 μM), $F_{34\mu M}$: From the resulting plot of [**15h**] *vs* time, initial velocity can be calculated from linear region at the beginning of each trace.

$$[\mathbf{15}\boldsymbol{h}]_t = \frac{F_t - F_{buffer\ alone}}{F_{34\mu M} - F_{buffer\ alone}} \times 34\ \mu M \quad [3]$$

For the determination of kinetic parameters, K_m and V_{max}, enzyme (0.075 U/mL) and **15h** (2.1 μM – 33.9 μM) in HEPES buffer (50 mM, pH 7.4) were used (total volume per well: 200 μL, all concentrations are final concentrations). Kinetic parameters were reported as the mean (± SD) of at least two data sets.

7.7 *Escherichia coli* DNA ligase (EcLigA)

7.7.1 Expression and purification[250]

The gene encoding DNA ligase from *Escherichia coli* (EcLigA) was previously cloned into pET-16b vector to introduce 10-His-tag at the N terminus of the protein and ampicillin resistance. The resulting plasmid, pRB20, was transformed in competent *E. coli* BL21 pLysS cells, plated on LB-agar containing chloramphenicol and ampicillin antibiotics. The plates were incubated at 37 °C overnight. Single colonies were inoculated into 5 mL LB media containing antibiotics, and incubated at 30 °C overnight. 1 mL of overnight culture was inoculated into 100 mL LB media containing antibiotics, and incubated at 37 °C until growth had reached mid log phase (OD_{600} 0.4 – 0.6). Therefore, IPTG was added to 400 μM final concentration to induce the protein over-expression, and the culture incubated at 25 °C overnight. The culture was centrifuged and the pellets re-suspended in binding buffer (Table 7.2) and sonicated; the insoluble fraction was separated by centrifugation. The supernatant was filtered through a 0.45 μm filter, then applied to a His-tag binding column, previously equilibrated with

binding buffer, to purify the over-expressed protein by affinity chromatography. Following sample loading, the column was rinsed with 10 mL binding buffer and 10 mL wash buffer to remove eventual proteins not-specifically interacting with the column resin; finally, the protein was eluted with 5 mL elution buffer (Table 7.2). The protein purity was confirmed by SDS-PAGE analysis. To desalt the protein from imidazole, size-exclusion chromatography was used. The protein concentration was determined using the Bradford method. Glycerol (30%) and DTT (1 mM) were added to the obtained protein, that was aliquoted and stored at -80 °C.

Buffer	*Composition*
Binding buffer	5 mM imidazole, 0.5 M NaCl, 20 mM Tris/HCl pH 7.9
Wash buffer	60 mM imidazole, 0.5 M NaCl, 20 mM Tris/HCl pH 7.9
Elution buffer	1 M imidazole, 0.5 M NaCl, 20 mM Tris/HCl pH 7.9

Table 7.2 Composition of buffers used for nickel-affinity chromatography.

7.7.2 Preparation of DNA substrate

A 40 bp double-stranded oligonucleotide containing a single-strand nick between bases 18 and 19 was used as a substrate for the DNA ligation. It was obtained by annealing a 18-mer (LigSub1) and a 22-mer (LigSub2) to a complementary 40-mer (LigSub1+2) in ratio 1:3:3 in 10 x TBE/KCl buffer (1.1 M Tris/borate pH 8.3, 25 mM EDTA, 1 M KCl): in particular, the 18-mer contained a fluorescein (F) molecule in 5′-position, and the 22-mer a phosphate group (P_i) in 5′-position (Table 7.3). The annealing was checked by native PAGE and the substrate stored at -20 °C.

Oligonucleotide	*Sequence (5′ to 3′)*
LigSub1	**F**-GTA AAA CGA CGG CCA GTG
LigSub2	**P_i**-AAT TCG AGC TCG GTA CCC GGG G
LigSub1+2	CCC CGG GTA CCG AGC TCG AAT TCA CTG GCC GTC GTT TTA C

Table 7.3 Oligonucleotides sequence used for the preparation of substrate for ligation assay.

7.7.3 Ligation assay

Separate stock solutions of DNA substrate (5 μM), EcLigA (0.2 μM), β-NAD^+ (181 μM) and the different compounds (1 mM) were prepared in Milli-Q water. To test EcLigA activity, the requisite volumes of DNA substrate (0.75 μL, 0.125 μM) and β-NAD^+ (4.3 μL, 26 μM) were added to an appropriate volume of 1 x buffer (22 μL, 30 mM Tris/HCl pH 8, 4 mM $MgCl_2$, 1 mM DTT, 50 μg/mL BSA) and incubated at 30 °C under shaking: the reaction was started with EcLigA addition (3 μL, 0.1 μM) to give a final volume of 30 μL (all concentrations are final concentrations). For the inhibition and the NNS activity experiments of C-2 and C-6 substituted derivatives, the requisite volumes of DNA substrate (1.5 μL, 0.5 μM), C-2 substituted derivatives (3 μL, 200 μM), or C-6 substituted derivatives (3.75 μL, 250 μM), with/without β-NAD^+ (2.15 μL, 26 μM), were added to an appropriate volume of 1 x buffer (30 mM Tris/HCl pH 8, 4 mM $MgCl_2$, 1 mM DTT, 50 μg/mL BSA) to give a final volume of 11.25 μL; the reaction, incubated at 30 °C under shaking, was started with EcLigA addition (3.75 μL, 0.05 μM) to give a final volume of 15 μL (all concentrations are final concentrations). For the inhibition and the NNS activity experiments of C-8 substituted derivatives, the requisite volumes of DNA substrate (0.75 μL, 0.125 μM), C-8 substituted derivatives (7.5 μL, 250 μM), with/without β-NAD^+ (4.3 μL, 26 μM), were added to an appropriate volume of 1 x buffer (30 mM Tris/HCl pH 8, 4 mM $MgCl_2$, 1 mM DTT, 50 μg/mL BSA) to give a final volume of 27 μL; the reaction, incubated at 30 °C under shaking, was started with EcLigA addition (3 μL, 0.1 μM) to give a final volume of 30 μL (all concentrations are final concentrations). For the NNS activity experiments of **13a** and **13b**, the requisite volumes of DNA substrate (1.5 μL, 0.5 μM), and **13a** or **13b** (0.75 – 3.75 μL, 50 – 250 μM) were added to an appropriate volume of 1 x buffer (30 mM Tris/HCl pH 8, 4 mM $MgCl_2$, 1 mM DTT, 50 μg/mL BSA) to give a final volume of 11.25 μL; the reaction, incubated at 30 °C under shaking, was started with EcLigA addition (3.75 μL, 0.05 μM) to give a final volume of 15 μL (all concentrations are final concentrations). In all the set of experiments, a control reaction was included to test EcLigA activity with only β-NAD^+, not containing any tested compound. Samples were drawn at different time points and mixed with an equal volume of 1 x stop solution (deionized formamide, 0.5 M EDTA, 1 M NaOH, 20 mg bromophenol blue), then put in

ice. Afterwards, samples were run on a pre-warmed 15% polyacrylamide/urea denaturing gel.

7.7.4 Gel electrophoresis

For protein analysis, SDS-PAGE with 10% SDS-polyacrylamide resolving gel and 5% stacking gel was used. The protein samples were diluted with 4 x SDS-loading dye (200 mM Tris, 8% SDS, 0.4% bromophenol blue, 40% glycerol, 20% DME) and loaded into the wells; a potential of 200 V was applied for 1 h in TGS buffer (25 mM Tris pH 8.3, 192 mM glycine, 0.1% (w/v) SDS buffer). The gel was visualized by staining with Coomassie blue.

For non-denaturing gel electrophoresis of DNA, or native PAGE, a 12% polyacrylamide gel was used. The DNA samples were diluted with 6 x loading dye (10 mM Tris/HCl pH 7.6, 0.03% bromophenol blue, 0.03% xylene, cyanol FF, 60% glycerol, 60 mM EDTA) and loaded into the wells; a potential of 50 V was applied for 3 h in TBE buffer (45 mM Tris/borate pH 8.3, 1.25 mM EDTA). The gel was visualized by fluorescence imaging using Molecular Dynamics Storm Phosphorimager.

For denaturing gel electrophoresis of DNA, a 15% polyacrylamide/urea gel was used. The reaction samples were diluted with 1 x stop solution (20 mL deionized formamide, 400 µL 0.5 M EDTA, 40 µL 1 M NaOH, 20 mg bromophenol blue), incubated at 95 °C for 5 min, and loaded into the wells of a pre-warmed denaturing gel; a potential of 400 V was applied for 20 min in TBE buffer (45 mM Tris/borate pH 8.3, 1.25 mM EDTA). The gel was visualized by fluorescence imaging using Molecular Dynamics Storm Phosphorimager.

7.7.5 Molecular modeling for DNA ligase

All calculations were performed on an Intel Core Duo 2.8 Ghz MacBook Pro. The crystal structure of β-NAD^+-bound DNA ligase from *E.faecalis* was obtained from the RCSB Protein Data Bank (PDB 1TAE). The protein was prepared for molecular modeling analysis using the MOE modeling package (CCG, Montreal, Canada). The ligand β-NAD^+ and crystallographic water molecules were removed, leaving an empty

active center. Hydrogen atoms were added to the heavy atoms, and the residues were assigned with the appropriate protonation states at pH 7.4. The final protein was saved in TriposMol2 format and directly imported into the GOLD software package (CCDC,Cambridge, UK, Version 3.2) for subsequent docking calculations. **15h** was built with the Builder module of MOE, and hydrogen atoms were assigned to all heavy atoms in the molecule: then, it was energy minimized using the MMFF94s force field and the conjugate gradient method, until the default derivative convergence criterion of 0.01 kcal·mol^{-1}·A was met. The phosphate groups were assigned a charge of −1, as appropriate at pH 7.4. The ligand file was exported into GOLD as Tripos Mol2 files. The ligand dockings into the catalytic site of 1TAE were performed using Gold Suite 4.12 (CCDC, Cambridge, UK). The binding site was defined by the position of β-NAD$^+$ in the original structure and the radius was set to 15 Å. All torsion angles in **15h** were allowed to rotate freely. GoldScore was chosen as the scoring function, and the solutions were rescored using the ChemScore scoring function. 100 docking runs were performed for **15h**. The resulting solutions were clustered on the basis of heavy atom rmsd values (1 Å). The top-ranked solutions were visually analysed using PyMol (PyMOL Molecular Graphics System, Version 1.1, Schrödinger, LLC). To validate the docking protocol, β-NAD$^+$ was redocked into the empty catalytic pocket of 1TAE using the above protocol, and the conformations of the top scored poses were compared to the crystal structure position of the ligand. All docking poses were exported as sdf files and imported into MOE as a database (mdb file).

7.8 Sequence alignment and 3D alignment of protein structures

A sequence alignment was undertaken for ADPRC from *Aplysia californica* (PDB 3ZWM, Uniprot ID P29241), archeal Sir2-Af2 (PDB 1YC2, Uniprot ID O30124) and DNA ligase from *E.faecalis* (PDB 1TAE, Uniprot ID Q837V6) using the sequence alignment tool provided by Uniprot (Universal Protein Resource, http://www.uniprot.org).[275] Pairwise 3D alignment for the chains A of the three proteins mentioned above was undertaken using the protein comparison tools, jFATCAT-rigid and jFATCAT-flexible, provided by RCSB Protein Data Bank (http://www.rcsb.org/).

8 APPENDIX

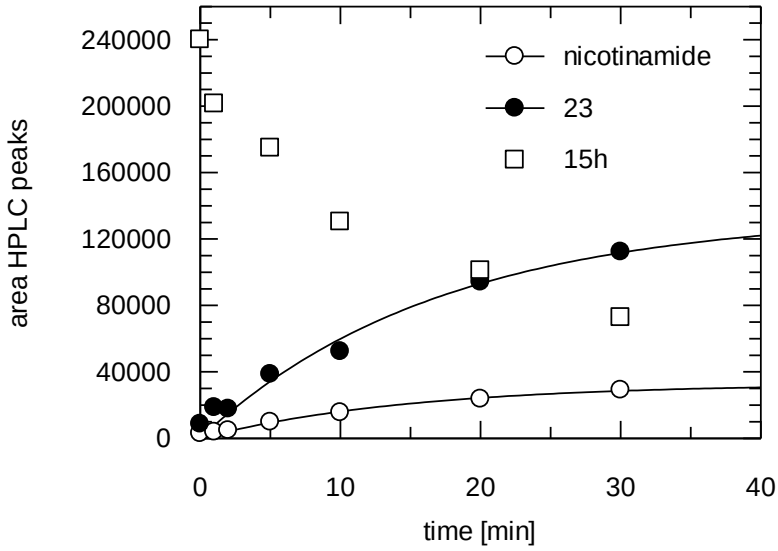

Figure A1 HPLC time-course for the basic hydrolysis of **15h**. *Conditions*: **15h** (49.5 µM) in 0.1 N NaOH, rt. Data from single experiment, peak area *vs* time [min], data plotting to a 1st order rate equation with Grafit5.

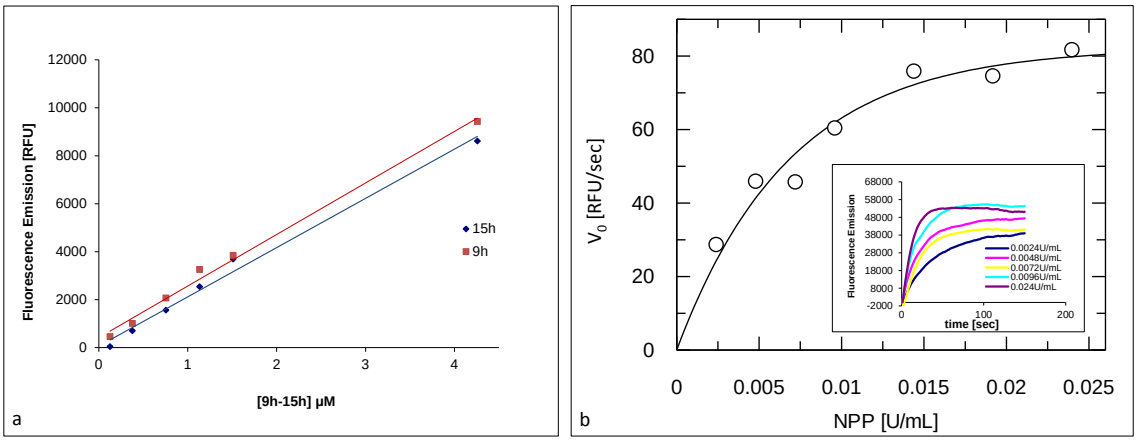

Figure A2 **a)** Fluorescence calibration curves for **15h** and **9h**. *Conditions*: **15h** or **9h** (0.13 – 4.26 µM), $MgCl_2$ (10 mM), Tris/HCl buffer (50 mM, pH 8), 30 ºC, λ_{ex} = 300 nm, λ_{em} = 410 nm, gain 15%; all concentrations are final concentrations. Fluorescence intensity values were fitted to a linear equation with Excel. The estimated linear equations are, respectively: y = 2149.4x + 418.93 (r^2 = 0.994) for **9h**, and y = 2052.9x + 62.892 (r^2 = 0.991) for **15h**. Each data point is the mean (± SD) of experiments run in duplicate. **b)** Fluorimetric assay of NPP from *Crotalus adamanteus* venom and **15h**: initial velocity (V_0) as function of NPP concentration. *Conditions*: NPP (0.0024 – 0.024 U/mL), **15h** (0.09 µM), $MgCl_2$ (10 mM), Tris/HCl buffer (50 mM, pH 8), 30 ºC, λ_{ex} = 300 nm, λ_{em} = 410 nm; all concentrations are final concentrations. Initial velocity values (V_0) were calculated from the reaction time-courses (insert) measuring the fluorescence signals generated when 10% product was formed. Initial velocity values were fitted to a polynomial equation with GraFit5.

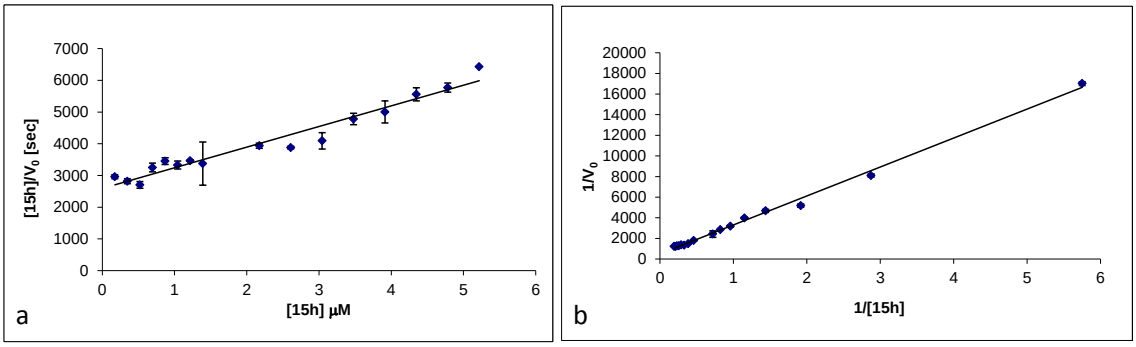

Figure A3 Fluorimetric assay of NPP from *Crotalus adamanteus* venom and **15h**: **a)** Hanes-Woolf and **b)** Lineweaver-Burk plot. *Conditions*: NPP (0.007 U/mL), **15h** (0.2 – 5.2 µM), $MgCl_2$ (10 mM), Tris/HCl buffer (50 mM, pH 8), 30 ºC, λ_{ex} = 300 nm, λ_{em} = 410 nm, gain 15%; all concentrations are final concentrations. Initial velocity values (V_0) were calculated from the corresponding time-courses measuring the fluorescence signals generated when 10% product is formed. Initial velocity values were then fitted to linear equations with Excel. The estimated linear equation for Hanes-Woolf plot is y = 651.08x + 2591.9 (r^2 = 0.9519); for Lineweaver-Burk plot, y = 2808.6x + 495.98 (r^2 = 0.9958). Each data point is the mean (± SD) of experiments run in duplicate.

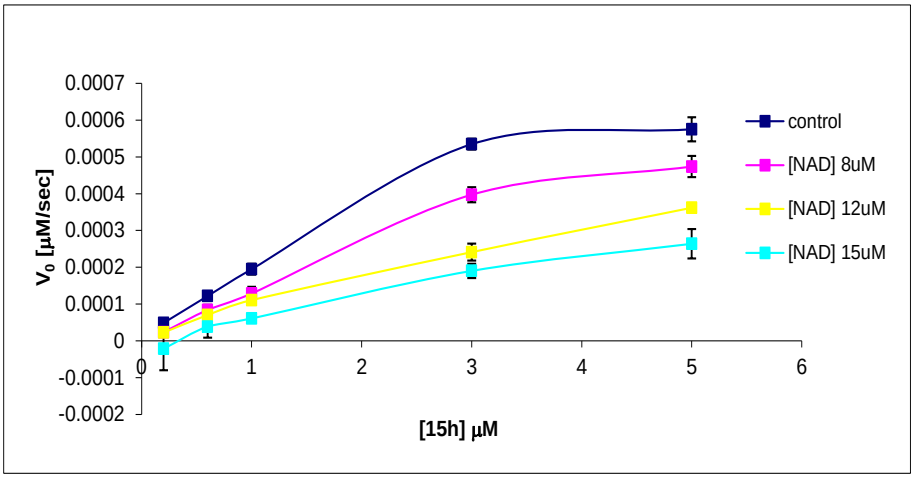

Figure A4 Fluorimetric assay of NPP from *Crotalus adamanteus* venom and **15h**: Michaelis-Menten plot for *β*-NAD^+ inhibition toward the activity of NPP from *Crotalus adamanteus* venom and **15h**. *Conditions*: NPP (0.007 U/mL), **15h** (0.2 – 5 µM), *β*-NAD^+ (8 – 15 µM), $MgCl_2$ (10 mM), Tris/HCl buffer (50 mM, pH 8), 30 ºC, λ_{ex} = 300 nm, λ_{em} = 410 nm, gain 15%; all concentrations are final concentrations. Initial velocity values (V_0) were calculated from the corresponding time-courses measuring the fluorescence signals generated when 10% product was formed. Each data point is the mean (± SD) of experiments run in duplicate, data plotting with Excel.

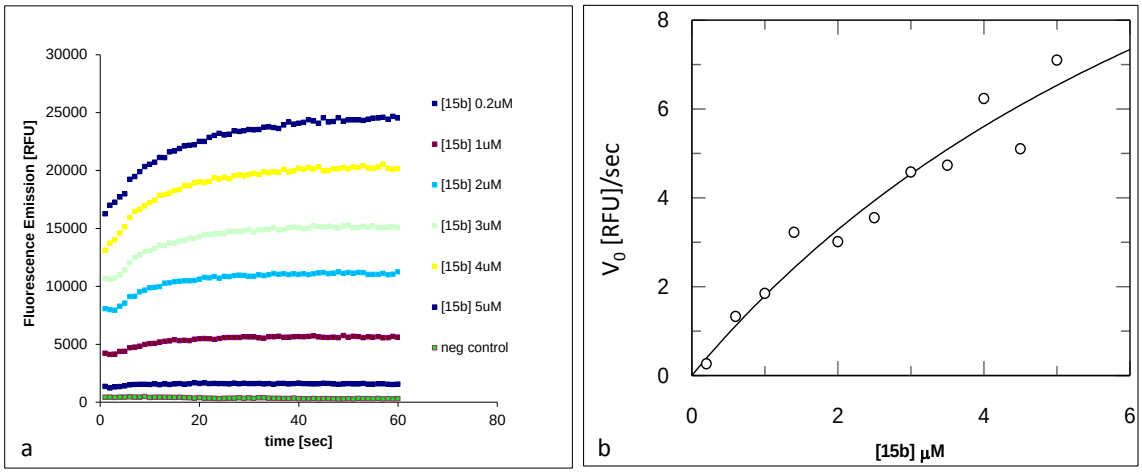

Figure A5 Fluorimetric assay of NPP from *Crotalus* a*damanteus* venom and **15b**: **a)** fluorescence time-course as fluorescence emission [RFU] *vs* time [sec]; **b)** Michaelis-Menten plot. *Conditions*: NPP (0.007 U/mL), **15b** (0.2 – 5 µM), $MgCl_2$ (10 mM), Tris/HCl buffer (50 mM, pH 8), 30 ºC, λ_{ex} = 300 nm, λ_{em} = 410 nm, gain 15%; all concentrations are final concentrations. Initial velocity values (V_0) were calculated from the time-courses measuring the fluorescence signals generated when 10% product is formed. Initial velocity values were fitted to the Michaelis-Menten equation with Grafit5.

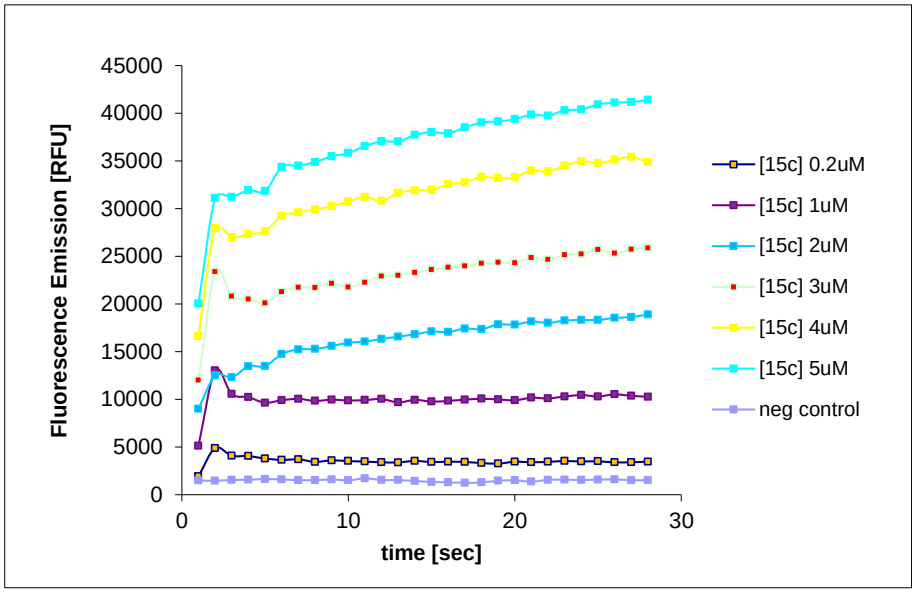

Figure A6 Fluorimetric assay of NPP from *Crotalus* a*damanteus* venom and **15c**: fluorescence time-course as fluorescence emission [RFU] *vs* time [sec]. *Conditions*: NPP (0.007 U/mL), **15c** (0.2 – 5 µM), $MgCl_2$ (10 mM), Tris/HCl buffer (50 mM, pH 8), 30 ºC, λ_{ex} = 300 nm, λ_{em} = 410 nm, gain 15%; all concentrations are final concentrations.

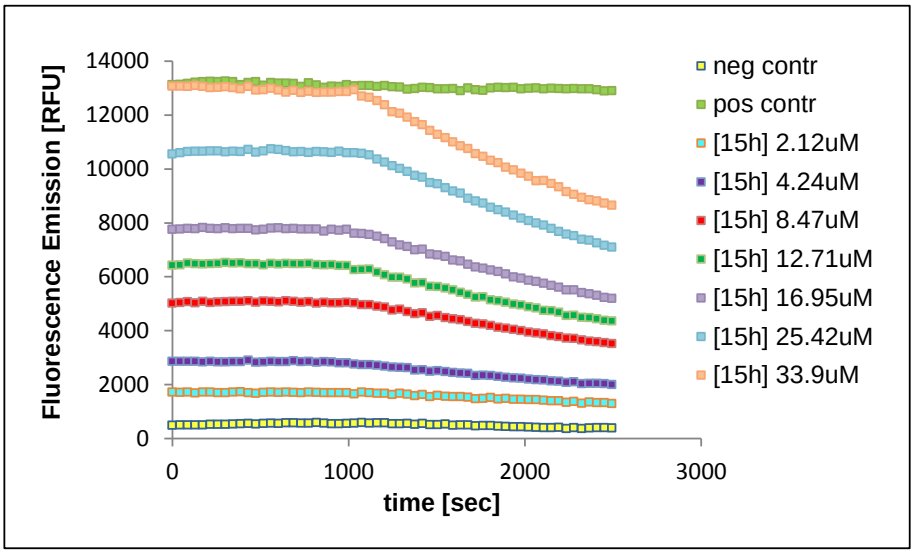

Figure A7 Fluorimetric assay of ADPRC from *Aplysia californica* and **15h**: ADPR-cyclase activity; fluorescence time-course as fluorescence emission [RFU] *vs* time [sec]. *Conditions*: ADPRC (0.075 U/mL), **15h** (2.12 – 33.9 µM), HEPES buffer (50 mM, pH 7.4), 26 ºC, λ_{ex} = 300 nm, λ_{em} = 410 nm, gain 15%. Enzyme addition at 1030 sec. Positive control: **15h** (33.9 µM). Negative control: buffer. All concentrations are final concentrations. Each data point is the mean of experiments run in duplicate.

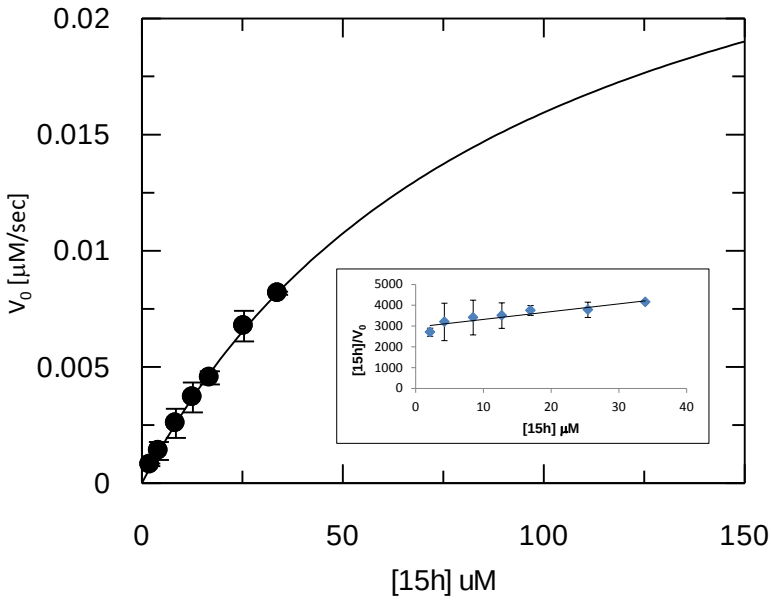

Figure A8 Fluorimetric assay of ADPRC from *Aplysia californica* and **15h**: Michaelis-Menten and Hanes-Woolf plot (insert). *Conditions*: ADPRC (0.075 U/mL), **15h** (2.12 – 33.9 µM), HEPES buffer (50 mM, pH 7.4), 26 ºC, λ_{ex} = 300 nm, λ_{em} = 410 nm, gain 15%; all concentrations are final concentrations. Initial velocity values (V_0) were calculated from the corresponding reaction time-courses measuring the fluorescence signals generated when 10% product is formed. Initial velocity values were fitted to the Michaelis-Menten plot with Grafit5, and to the Hanes-Woolf plot (insert) with Excel (estimated linear equation: y = 37.26x + 2947.7, r^2 = 0.8568). Each data point is the mean (± SD) of experiments run in duplicate.

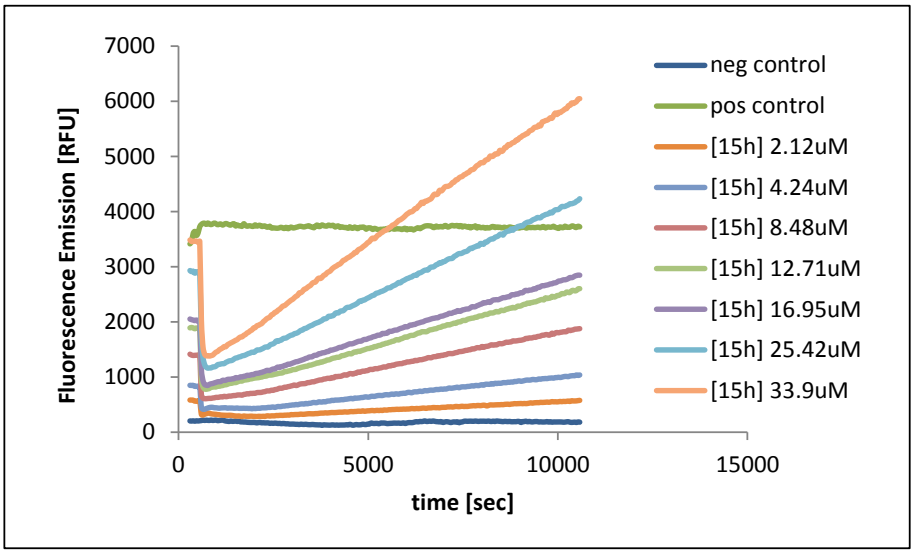

Figure A9 Fluorimetric assay of ADPRC from *Aplysia californica* and **15h**: *c*ADPR-hydrolase activity; fluorescence time-course as fluorescence emission [RFU] *vs* time [sec]. *Conditions*: ADPRC (1.75 U/mL), **15h** (2.12 – 33.9 μM), HEPES buffer (50 mM, pH 7.4), 26 ºC, λ_{ex} = 300 nm, λ_{em} = 410 nm, gain 15%; all concentrations are final concentrations. Each data point is the mean of experiments run in duplicate.

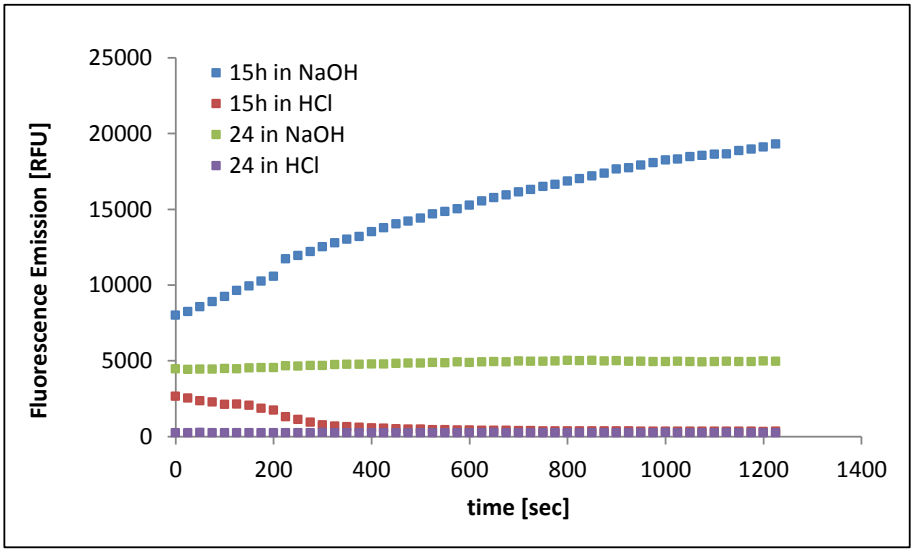

Figure A10 Comparison of hydrolytic stability for **15h** and **24**. *Conditions*: **15h** and **24** respectively in NaOH (0.1 N) and HCl (0.1 N), 26 ºC, λ_{ex} = 300 nm, λ_{em} = 410 nm, gain 15%.

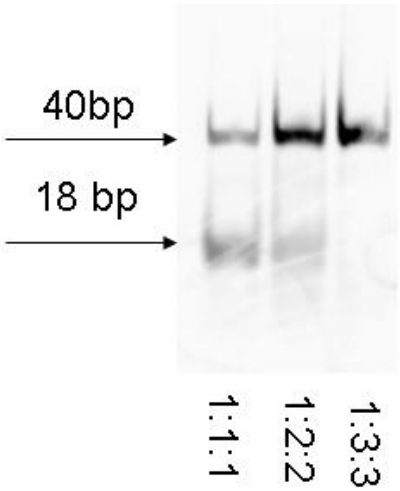

Figure A11 Preparation of annealed substrate for ligation assay at different ratio LigSub1:LigSub2:LigSub1+2. *Conditions*: LigSub1 at 5 µM in 10 x TBE/KCl (50 mM) buffer; analysis by native PAGE and gel visualization by fluorescence imaging.

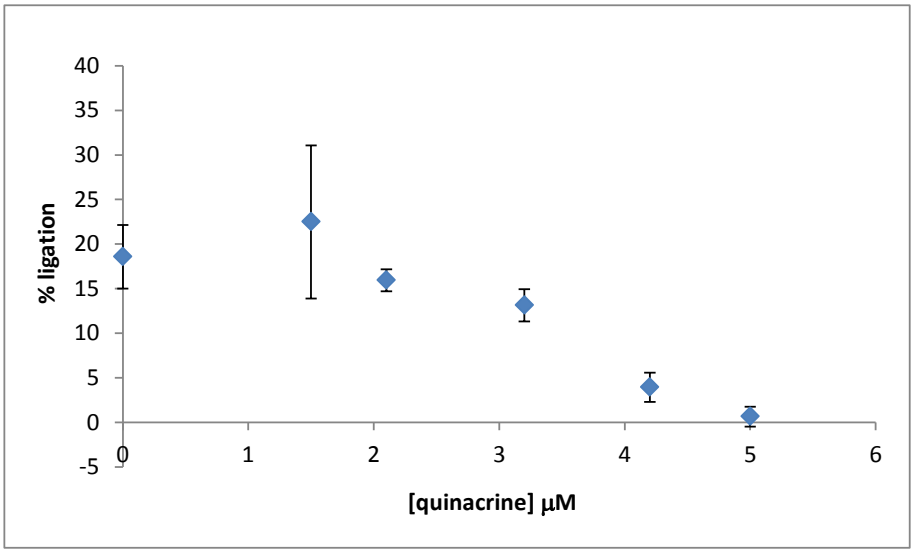

Figure A12 IC_{50} estimation for quinacrine. *Conditions*: DNA substrate (0.5 µM), *β*-NAD^+ (26 µM), EcLigA (0.05 µM), quinacrine·2HCl (0 – 5 µM) in 1 x buffer (30 mM Tris/HCl pH 8, 4 mM $MgCl_2$, 1 mM DTT, 50 µg/mL BSA) incubated at 30 °C under shaking and sampled at 5 min; all concentrations are final concentrations. Analysis of assay run on denaturing PAGE and visualized by fluorescence imaging. Data analysed using ImageJ. Each data point is the mean (± SD) of a set of experiments run in triplicate; data plotting with Excel.

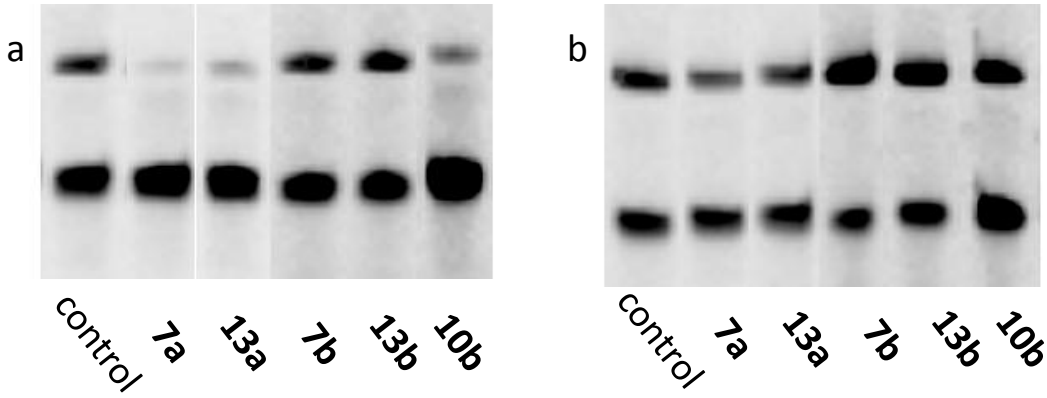

Figure A13 Denaturing PAGE for the inhibition of 2-substituted AMP/AMP-morpholidate/NAD^+ derivatives at 200 µM. *Conditions*: DNA substrate (0.5 µM), *β*-NAD^+ (26 µM), EcLigA (0.05 µM), 2-substituted derivative (200 µM) in 1 x buffer (30 mM Tris/HCl pH 8, 4 mM $MgCl_2$, 1 mM DTT, 50 µg/mL BSA) incubated at 30 °C under shaking and sampled at 5 (**a**) and 15 min (**b**); all concentrations are final concentrations. Control reaction at the same conditions without any 2-substituted derivative. Gel visualization by fluorescence imaging.

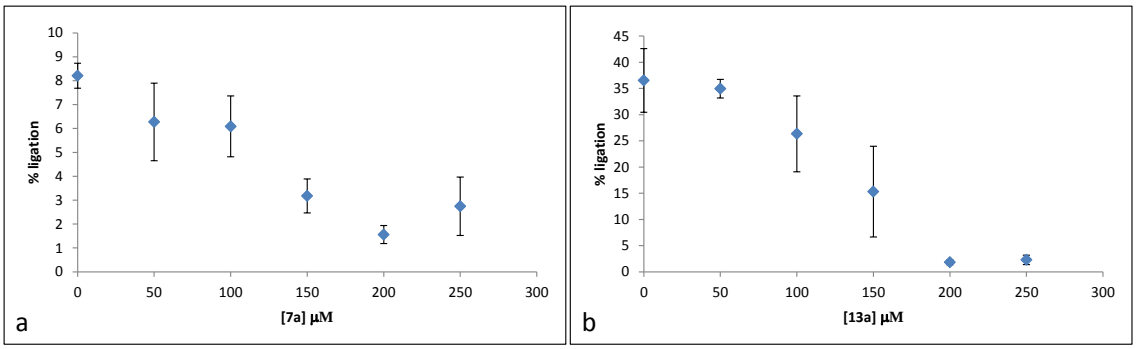

Figure A14 IC_{50} estimation for **7a** (**a**) and **13a** (**b**). *Conditions*: DNA substrate (0.5 µM), *β*-NAD^+ (26 µM), EcLigA (0.05 µM), **7a** or **13a** (0 – 250 µM) in 1 x buffer (30 mM Tris/HCl pH 8, 4 mM $MgCl_2$, 1 mM DTT, 50 µg/mL BSA) incubated at 30 °C under shaking and sampled at 5 min; all concentrations are final concentrations. Analysis of assays run by denaturing PAGE; visualization by fluorescence imaging and data analysis by ImageJ. Each data point is the mean (± SD) of a set of experiments run in triplicate; data plotting with Excel.

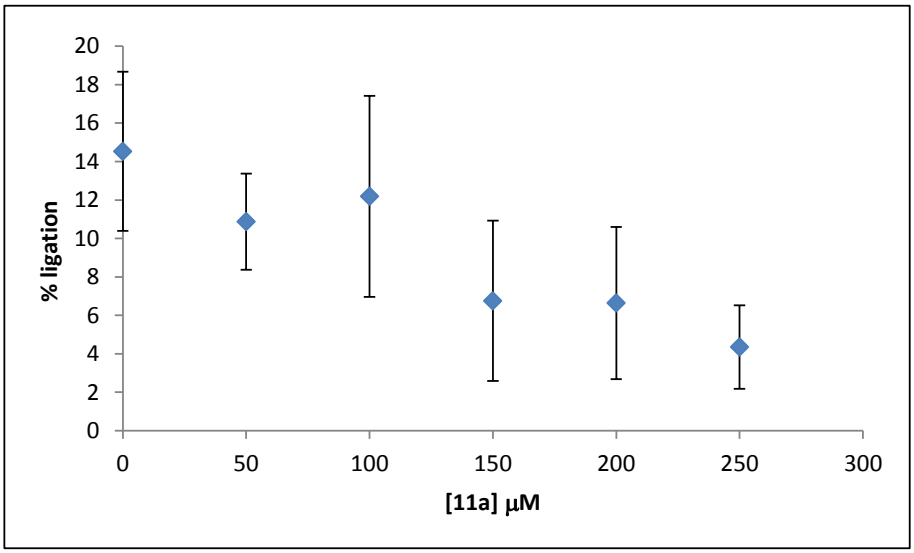

Figure A15 IC_{50} estimation for **11a**. *Conditions*: DNA substrate (0.5 µM), *β*-NAD^+ (26 µM), EcLigA (0.05 µM), **11a** (0 – 250 µM) in 1 x buffer (30 mM Tris/HCl pH 8, 4 mM $MgCl_2$, 1 mM DTT, 50 µg/mL BSA) incubated at 30 °C under shaking and sampled at 5 min. Analysis of assays run by denaturing PAGE; visualization by fluorescence imaging and data analysis by ImageJ. Each data point is the mean (± SD) of a set of experiments run in triplicate; data plotting with Excel.

Enzyme (PBD)	*Twists*	*P*	*RMSD*	*Score*	*% Id*	*% Similarity*
1TAE (chain A)	0	0.454	8.96	108.39	2.5	13.57
1YC2 (chain A)	5	0.199	3.98	163.83	4.1	12.03
1TAE (chain A)	0	0.460	9.58	100.28	2.08	7.72
3ZWM (chain A)	5	0.525	4.98	131.42	4.59	10.09
1YC2 (chain A)	0	0.181	11.12	135.22	8.27	17.29
3ZWM (chain A)	4	0.0916	18.64	150.27	4.17	12.50

Table A1 Structure pairwise alignment of ADPRC from *Aplysia californica* (PDB 3ZWM), archaeal Sir2-Af2 (PDB 1YC2), and DNA ligase from *E. faecalis* (PDB 1TAE) by rigid FATCAT and flexible FATCAT. The flexible structure alignment works by identifying aligned fragment pairs and allowing flexibility in connecting them by twists in the structure. The more twists that are introduced in the structure, the less is the similarity between the two proteins. *Twists = 0* in rigid FATCAT; *twists ≥ 0* in flexible FATCAT. *P* is the probability value that two structures are similar (values < 0.05 indicates significant similarities); *RMSD* is the average distance between the Cα atoms of superimposed proteins; *Score* is the raw score of the alignment; *% Id* is the percent sequence identity in the alignment; *% Similarity* is the percent structure similarity in the alignment.

9 REFERENCES

1. D. Voet, C. W. Pratt and J. G. Voet, *Fundamentals of Biochemistry*, 2008.
2. R. F. Anderson, *Biochim. Biophys. Acta - Bioenergetics*, 1980, **590**, 277-281.
3. J. A. Farrington, E. J. Land and A. J. Swallow, *Biochim. Biophys. Acta - Bioenergetics*, 1980, **590**, 273-276.
4. M. Ziegler, *Eur. J. Biochem.*, 2000, **267**, 1550-1564.
5. P. Belenky, K. L. Bogan and C. Brenner, *Trends Biochem. Sci.*, 2007, **32**, 12-19.
6. A. Legutko, P. Lekeux and F. Bureau, *Open Immunol. J.*, 2009, **2**, 42-51.
7. H. Lin, *Org. Biomol. Chem.*, 2007, **5**, 2541-2554.
8. N. J. Oppenheimer, *Mol. Cell. Biochem.*, 1994, **138**, 245-251.
9. R. W. Johnson, T. M. Marschner and N. J. Oppenheimer, *J. Am. Chem. Soc.*, 1988, **110**, 2257-2263.
10. C. C. Guilbert and S. L. Johnson, *Biochemistry*, 1977, **16**, 335-344.
11. S. L. Johnson and D. L. Morrison, *J. Biol. Chem.*, 1970, **245**, 4519-4524.
12. S.-J. Lin and L. Guarente, *Curr. Opin. Cell Biol.*, 2003, **15**, 241-246.
13. N. Pollak, C. Dolle and M. Ziegler, *Biochem. J.*, 2007, **402**, 205-218.
14. J. Du, H. Jiang and H. Lin, *Biochemistry*, 2009, **48**, 2878-2890.
15. S. Shuman, *J. Biol. Chem.*, 2009, **284**, 17365-17369.
16. M. Bollen, R. Gijsbers, H. Ceulemans, W. Stalmans and C. Stefan, *Crit. Rev. Biochem. Mol. Biol.*, 2000, **35**, 393-432.
17. G. G. Yegutkin, *Biochim. Biophys. Acta - Mol. Cell Res.*, 2008, **1783**, 673-694.
18. G. Magni, A. Amici, M. Emanuelli, G. Orsomando, N. Raffaelli and S. Ruggieri, *Cell. Mol. Life Sci.*, 2004, **61**, 19-34.
19. J. W. Rowen and A. Kornberg, *J. Biol. Chem.*, 1951, **193**, 497-507.
20. B. D. Bennett, E. H. Kimball, M. Gao, R. Osterhout, S. J. Van Dien and J. D. Rabinowitz, *Nat. Chem. Biol.*, 2009, **5**, 593-599.
21. J. A. Khan, F. Forouhar, X. Tao and L. Tong, *Expert Opin. Ther. Targets*, 2007, **11**, 695-705.
22. A. Mattevi, *Nat. Struct. Mol. Biol.*, 2006, **13**, 563-564.

23. J. R. Revollo, A. A. Grimm and S.-i. Imai, *J. Biol. Chem.*, 2004, **279**, 50754-50763.

24. L. J. Zatman, N. O. Kaplan and S. P. Colowick, *J. Biol. Chem.*, 1953, **200**, 197-212.

25. J. C. Tanny and D. Moazed, *Proc. Natl. Acad. Sci. USA*, 2001, **98**, 415-420.

26. M. Kotaka, R. Graeff, Z. Chen, L. H. Zhang, H. C. Lee and Q. Hao, *J. Mol. Biol.*, 2012, **415**, 514-526.

27. G. T. Marsischky, B. A. Wilson and R. J. Collier, *J. Biol. Chem.*, 1995, **270**, 3247-3254.

28. D. Slade, M. S. Dunstan, E. Barkauskaite, R. Weston, P. Lafite, N. Dixon, M. Ahel, D. Leys and I. Ahel, *Nature*, 2011, **477**, 616-620.

29. A. Ruf, V. Rolli, G. de Murcia and G. E. Schulz, *J. Mol. Biol.*, 1998, **278**, 57-65.

30. Q. Liu, I. A. Kriksunov, H. Jiang, R. Graeff, H. Lin, H. C. Lee and Q. Hao, *Chem. Biol.*, 2008, **15**, 1068-1078.

31. K. Zhao, R. Harshaw, X. Chai and R. Marmorstein, *Proc. Natl. Acad. Sci. USA*, 2004, **101**, 8563-8568.

32. B. C. Smith and J. M. Denu, *J. Am. Chem. Soc.*, 2007, **129**, 5802-5803.

33. L. Franco, L. Guida, S. Bruzzone, E. Zocchi, C. Usai and A. D. Flora, *FASEB J.*, 1998, **12**, 1507-1520.

34. H. Maruta, N. Matsumura and S.-i. Tanuma, *Biochem. Biophys. Res. Comm.*, 1997, **236**, 265-269.

35. E. N. Chini, *Curr. Pharm. Des.*, 2009, **15**, 57-63.

36. M. Kruszewski and I. Szumiel, *DNA Repair*, 2005, **4**, 1306-1313.

37. A. Grahnert, A. Grahnert, C. Klein, E. Schilling, J. Wehrhahn and S. Hauschildt, *Innate Immun.*, 2011, **17**, 212-233.

38. F. Malavasi, S. Deaglio, G. Zaccarello, A. L. Horenstein, A. Chillemi, V. Audrito, S. Serra, M. Gandione and A. a. T. Zitella, A, *J. Mol. Endocrinol.*, 2010, **45**, 183-191.

39. T. Vaisitti, V. Audrito, S. Serra, C. Bologna, D. Brusa, F. Malavasi and S. Deaglio, *FEBS Lett.*, 2011, **585**, 1514-1520.

40. S. Bruzzone, L. Guida, E. Zocchi, L. Franco and A. De Flora, *FASEB J.*, 2001, **15**, 10-12.

41. A. Gerth, K. Nieber, N. J. Oppenheimer and S. Hauschildt, *Biochem. J.*, 2004, **382**, 849-856.

42. L. Guida, S. Bruzzone, L. Sturla, L. Franco, E. Zocchi and A. De Flora, *J. Biol. Chem.*, 2002, **277**, 47097-47105.

43. I. Lange, S. Yamamoto, S. Partida-Sanchez, Y. Mori, A. Fleig and R. Penner, *Sci. Signal.*, 2009, **2**.

44. R. A. Billington, E. A. Bellomo, E. M. Floriddia, J. Erriquez, C. Distasi and A. A. Genazzani, *FASEB J.*, 2006, **20**, 521-523.

45. S. Todisco, G. Agrimi, A. Castegna and F. Palmieri, *J. Biol. Chem.*, 2006, **281**, 1524-1531.

46. A. Leskovar and J. Reinstein, *Arch. Biochem. Biophys.*, 2008, **473**, 16-24.

47. D. M. Jameson and J. F. Eccleston, in *Methods Enzymol.*, ed. M. L. J. Ludwig Brand, Academic Press, 1997, pp. 363-390.

48. S. E. Pollack, T. Uchida and D. S. Auld, *J. Protein Chem.*, 1983, **2**, 1-12.

49. J. Zhang, in *Methods Enzymol.*, ed. J. W. S. C. W. Donald B. McCormick, Academic Press, 1997, pp. 255-265.

50. K. W. Pankiewicz, *Pharmacol. Therapeut.*, 1997, **76**, 89-100.

51. P. Franchetti, L. Cappellacci, P. Perlini, H. N. Jayaram, A. Butler, B. P. Schneider, F. R. Collart, E. Huberman and M. Grifantini, *J. Med. Chem.*, 1998, **41**, 1702-1707.

52. L. Bonnac, L. Chen, R. Pathak, G. Gao, Q. Ming, E. Bennett, K. Felczak, M. Kullberg, S. E. Patterson, F. Mazzola, G. Magni and K. W. Pankiewicz, *Bioorg. Med. Chem. Lett.*, 2007, **17**, 1512-1515.

53. V. Cepeda, M. A. Fuertes, J. Castilla, C. Alonso, C. Quevedo, M. Soto and J. M. Perez, *Recent Pat. Anti-Cancer Drug Discov.*, 2006, **1**, 39-53.

54. R. J. Griffin, N. J. Curtin, D. R. Newell, B. T. Golding, B. W. Durkacz and A. H. Calvert, *Biochimie*, 1995, **77**, 408-422.

55. J. L. Avalos, K. M. Bever and C. Wolberger, *Mol. Cell*, 2005, **17**, 855-868.

56. K. Inageda, K. Takahashi, K.-i. Tokita, H. Nishina, Y. Kanaho, I. Kukimoto, K. Kontani, S.-i. Hoshino and T. Katadat, *J. Biochem.*, 1995, **117**, 125-131.

57. M. T. Schmidt, B. C. Smith, M. D. Jackson and J. M. Denu, *J. Biol. Chem.*, 2004, **279**, 40122-40129.

58. M. E. Migaud, R. L. Pederick, V. C. Bailey and B. V. L. Potter, *Biochemistry*, 1999, **38**, 9105-9114.

59. J. T. Slama and A. M. Simmons, *Biochemistry*, 1988, **27**, 183-193.

60. K. A. Wall, M. Klis, J. Kornet, D. Coyle, J. C. Amé, M. K. Jacobson and J. T. Slama, *Biochem. J.*, 1998, **335**, 631-636.

61. A. A. Sauve and V. L. Schramm, *Biochemistry*, 2002, **41**, 8455-8463.

62. H. M. Muller-Steffner, O. Malver, L. Hosie, N. J. Oppenheimer and F. Schuber, *J. Biol. Chem.*, 1992, **267**, 9606-9611.

63. Q. Liu, R. Graeff, I. A. Kriksunov, H. Jiang, B. Zhang, N. Oppenheimer, H. Lin, B. V. L. Potter, H. C. Lee and Q. Hao, *J. Biol. Chem.*, 2009, **284**, 27637-27645.

64. P. E. Smith, *J. Am. Chem. Soc.*, 1999, **121**, 8637-8644.

65. J. K. Crane, I. Shulgina and T. M. Naeher, *Purinergic Signal.*, 2007, **3**, 233-246.

66. K. W. Pankiewicz, K. Lesiak and K. A. Watanabe, *J. Am. Chem. Soc.*, 1997, **28**, 3691-3695.

67. K. Felczak, L. Chen, D. Wilson, J. Williams, R. Vince, R. Petrelli, H. N. Jayaram, P. Kusumanchi, M. Kumar and K. W. Pankiewicz, *Bioorg. Med. Chem.*, 2011, **19**, 1594-1605.

68. R. Petrelli, Y. Y. Sham, L. Chen, K. Felczak, E. Bennett, D. Wilson, C. Aldrich, J. S. Yu, L. Cappellacci, P. Franchetti, M. Grifantini, F. Mazzola, M. Di Stefano, G. Magni and K. W. Pankiewicz, *Bioorg. Med. Chem.*, 2009, **17**, 5656-5664.

69. R. M. Graeff, T. F. Walseth, H. K. Hill and H. C. Lee, *Biochemistry*, 1996, **35**, 379-386.

70. T. Pesnot, J. Kempter, J. r. Schemies, G. Pergolizzi, U. Uciechowska, T. Rumpf, W. Sippl, M. Jung and G. K. Wagner, *J. Med. Chem.*, 2011, **54**, 3492-3499.

71. B. Zhang, H. Muller-Steffner, F. Schuber and B. V. L. Potter, *Biochemistry*, 2007, **46**, 4100-4109.

72. J. Trapp, A. Jochum, R. Meier, L. Saunders, B. Marshall, C. Kunick, E. Verdin, P. Goekjian, W. Sippl and M. Jung, *J. Med. Chem.*, 2006, **49**, 7307-7316.

73. S. D. Mills, A. E. Eakin, E. T. Buurman, J. V. Newman, N. Gao, H. Huynh, K. D. Johnson, S. Lahiri, A. B. Shapiro, G. K. Walkup, W. Yang and S. S. Stokes, *Antimicrob. Agents Chemother.*, 2011, **55**, 1088-1096.

74. S. S. Stokes, H. Huynh, M. Gowravaram, R. Albert, M. Cavero-Tomas, B. Chen, J. Harang, J. T. Loch Iii, M. Lu, G. B. Mullen, S. Zhao, C.-F. Liu and S. D. Mills, *Bioorg. Med. Chem. Lett.*, 2011, **21**, 4556-4560.

75. J. Hendle, A. F. Buckmann, W. Aehle, D. Schomburg and R. D. Schmid, *Eur. J. Biochem.*, 1993, **213**, 947-956.

76. G. W. E. Plaut, C. P. Cheung, R. J. Suhadolnik and T. Aogaichi, *Biochemistry*, 1979, **18**, 3430-3438.

77. N. O. Kaplan, M. M. Ciotti and F. E. Stolzenbach, *J. Biol. Chem.*, 1956, **221**, 833-844.

78. B. M. Anderson and N. O. Kaplan, *J. Biol. Chem.*, 1959, **234**, 1226-1232.

79. S. L. Oei, J. Griesenbeck, G. Buchlow, D. Jorcke, P. Mayer-Kuckuk, T. Wons and M. Ziegler, *FEBS Lett.*, 1996, **397**, 17-21.

80. H. Jiang, J. H. Kim, K. M. Frizzell, W. L. Kraus and H. Lin, *J. Am. Chem. Soc.*, 2010, **132**, 9363-9372.

81. H. Jiang, J. Congleton, Q. Liu, P. Merchant, F. Malavasi, H. C. Lee, Q. Hao, A. Yen and H. Lin, *J. Am. Chem. Soc.*, 2009, **131**, 1658-1659.

82. A. C. Nottbohm, R. S. Dothager, K. S. Putt, M. T. Hoyt and P. J. Hergenrother, *Angew. Chem. Int. Ed.*, 2007, **46**, 2066-2069.

83. N. J. Leonard, *Crit. Rev. Biochem.*, 1984, **15**, 125-199.

84. S. P. Colowick, N. O. Kaplan and M. M. Ciotti, *J. Biol. Chem.*, 1951, **191**, 447-459.

85. W. Lohmann, C. Lohmann and M. Ibrahim, *Naturwissenschaften*, 1988, **75**, 141-142.

86. A. A. Heikal, *Biomark. Med.*, 2010, **4**, 241-263.

87. J. R. Barrio, J. A. Secrist and N. J. Leonard, *Proc. Natl. Acad. Sci. USA*, 1972, **69**, 2039–2042.

88. B. A. Gruber and N. J. Leonard, *Proc. Natl. Acad. Sci. USA*, 1975, **72**, 3966-3969.

89. C. D. Muller, C. Tarnus and F. Schuber, *Biochem. J.*, 1984, **223**, 715-721.

90. Z. Fang-Jie and C. J. Sih, *Bioorg. Med. Chem. Lett.*, 1995, **5**, 1701-1706.

91. B. M. Anderson and D. A. Yost, in *Methods Enzymol.*, ed. D. B. M. Frank Chytil, Academic Press, 1986, pp. 169-173.

92. B. M. Klebl and D. Pette, *Anal. Biochem.*, 1996, **239**, 145-152.

93. S. Armstrong and A. R. Merrill, *Anal. Biochem.*, 2001, **292**, 26-33.

94. K. Schweitzer, G. W. Mayr and A. H. Guse, *Anal. Biochem.*, 2001, **299**, 218-226.

95. R. E. Davis, V. Mysore, J. C. Browning, J. C. Hsieh, Q.-A. T. Lu and P. D. Katsikis, *J. Histochem. Cytochem.*, 1998, **46**, 1279-1289.

96. M. Shirato, S. Tozawa, D. Maeda, M. Watanabe, H. Nakagama and M. Masutani, *Biochem. Biophys. Res. Comm.*, 2007, **355**, 451-456.

97. J. L. Sims, H. Juarez-Salinas and M. K. Jacobson, *Anal. Biochem.*, 1980, **106**, 296-306.

98. K. Ikai, K. Ueda and O. Hayaishi, *J. Histochem. Cytochem.*, 1980, **28**, 670-676.

99. K. S. Putt and P. J. Hergenrother, *Anal. Biochem.*, 2004, **326**, 78-86.

100. Y. Feng, J. Wu, L. Chen, C. Luo, X. Shen, K. Chen, H. Jiang and D. Liu, *Anal. Biochem.*, 2009, **395**, 205-210.

101. H. Nakamura and Z. Tamura, *Anal. Chem.*, 1978, **50**, 2047-2051.

102. D. Wegener, F. Wirsching, D. Riester and A. Schwienhorst, *Chem. Biol.*, 2003, **10**, 61-68.

103. D. Wegener, C. Hildmann, D. Riester and A. Schwienhorst, *Anal. Biochem.*, 2003, **321**, 202-208.

104. B. Heltweg, F. Dequiedt, E. Verdin and M. Jung, *Anal. Biochem.*, 2003, **319**, 42-48.

105. B. O. S. Scott, M. Lavesa-Curto, D. R. Bullard, J. N. Butt and R. P. Bowater, *Anal. Biochem.*, 2006, **358**, 90-98.

106. L. Liu, Z. Tang, K. Wang, W. Tan, J. Li, Q. Guo, X. Meng and C. Ma, *Analyst*, 2005, **130**, 350-357.

107. C.-Y. Lee, D. A. Lappi, B. Wermuth, J. Everse and N. O. Kaplan, *Arch. Biochem. Biophys.*, 1974, **163**, 561-569.

108. J. L. Panza, A. J. Russell and E. J. Beckman, *Tetrahedron*, 2002, **58**, 4091-4104.

109. R. Parkesh, A. M. Lewis, P. K. Aley, A. Arredouani, S. Rossi, R. Tavares, S. R. Vasudevan, D. Rosen, A. Galione, J. Dowden and G. C. Churchill, *Cell Calcium*, 2008, **43**, 531-538.

110. J. Lee, H. Churchil, W.-B. Choi, J. E. Lynch, F. E. Roberts, R. P. Volante and P. J. Reider, *Chem. Commun.*, 1999, 729-730.

111. N. E. Batoux, F. Paradisi, P. C. Engel and M. E. Migaud, *Tetrahedron*, 2004, **60**, 6609-6617.

112. B. Zhang, G. K. Wagner, K. Weber, C. Garnham, A. J. Morgan, A. Galione, A. H. Guse and B. V. L. Potter, *J. Med. Chem.*, 2008, **51**, 1623-1636.

113. H. Gold, P. van Delft, N. Meeuwenoord, J. D. C. Codée, D. V. Filippov, G. Eggink, H. S. Overkleeft and G. A. van der Marel, *J. Org. Chem.*, 2008, **73**, 9458-9460.

114. L. A. Agrofoglio, I. Gillaizeau and Y. Saito, *Chem. Rev.*, 2003, **103**, 1875-1916.

115. H. Rosemeyer, *Chem. Biodivers.*, 2004, **1**, 361-401.

116. M. Legraverend, *Tetrahedron*, 2008, **64**, 8585-8603.

117. J. H. Lister, *The chemistry of heterocyclic compounds*, Wiley Interscience, 1971.

118. E. Y. Sutcliffe and R. K. Robins, *J. Org. Chem.*, 1963, **28**, 1662-1666.

119. B. C. Pal, *Biochemistry*, 1962, **1**, 558-563.

120. M. J. J. Jacob Strouse, and Jeffrey B. Arterburn, *Acta Chim. Slov.*, 2005, **52**, 187–199.

121. M. Hocek, *Eur. J. Org. Chem.*, 2003, **2**, 245-254.

122. J. Liu and M. J. Robins, *Org. Lett.*, 2005, **7**, 1149-1151.

123. M. Hocek, *Nucleic Acids Symp. Ser.*, 2005, **49**, 29-30.

124. M. K. Lakshman, *J. Organomet. Chem.*, 2002, **653**, 234-251.

125. M. K. Lakshman, *Curr. Org. Synth.*, 2005, **2**, 83-112.

126. P. Gunda, L. M. Russon and M. K. Lakshman, *Angew. Chem. Int. Ed.*, 2004, **43**, 6372-6377.

127. M. K. Lakshman, J. H. Hilmer, J. Q. Martin, J. C. Keeler, Y. Q. V. Dinh, F. N. Ngassa and L. M. Russon, *J. Am. Chem. Soc.*, 2001, **123**, 7779-7787.

128. I. Era, R. Pohl, B. Klepetov and M. Hocek, *Org. Lett.*, 2006, **8**, 5389-5392.

129. I. Cerna, R. Pohl and M. Hocek, *Chem. Commun.*, 2007, 4729-4730.

130. T. E. Storr, J. A. Strohmeier, C. G. Baumann and I. J. S. Fairlamb, *Chem. Commun.*, 2010, **46**, 6470-6472.

131. N. Miyaura and A. Suzuki, *Chem. Rev.*, 1995, **95**, 2457-2483.

132. J. K. Stille, *Angew. Chem. Int. Ed.*, 1986, **25**, 508-524.

133. S. Kotha, K. Lahiri and D. Kashinath, *Tetrahedron*, 2002, **58**, 9633–9695.

134. A. Matsuda, M. Shinozaki, T. Yamaguchi, H. Homma, R. Nomoto, T. Miyasaka, Y. Watanabe and T. Abiru, *J. Med. Chem.*, 1992, **35**, 241-252.

135. H. Homma, Y. Watanabe, T. Abiru, T. Murayama, Y. Nomura and A. Matsuda, *J. Med. Chem.*, 1992, **35**, 2881-2890.

136. L. Chen, G. Gao, K. Felczak, L. Bonnac, S. E. Patterson, D. Wilson, E. M. Bennett, H. N. Jayaram and L. Hedstrom, *J. Med. Chem.*, 2007, **50**, 5743-5751.

137. T. Persson, S. Gronowitz, A.-B. Hörnfeldt and N. G. Johansson, *Bioorg. Med. Chem.*, 1995, **3**, 1377-1382.

138. J. o. Neres, N. P. Labello, R. V. Somu, H. I. Boshoff, D. J. Wilson, J. Vannada, L. Chen, C. E. Barry, E. M. Bennett and C. C. Aldrich, *J. Med. Chem.*, 2008, **51**, 5349-5370.

139. V. Nair and D. A. Young, *J. Org. Chem.*, 1985, **50**, 406-408.

140. M. J. Robins and B. Uznanski, *Can. J. Chem.*, 1981, **59**, 2601-2607.

141. Y. Xu, H. Jin, Z. Yang, L. Zhang and L. Zhang, *Tetrahedron*, 2009, **65**, 5228-5239.

142. C. N. Johnson, G. Stemp, N. Anand, S. C. Stephen and T. Gallagher, *Synlett*, 1998, 1025-1027.

143. K. L. Billingsley, K. W. Anderson and Buchwald, *Angew. Chem. Int. Ed.*, 2006, **45**, 3484-3488.

144. A. Collier and G. Wagner, *Org. Biomol. Chem.*, 2006, **4**, 4526-4532.

145. M. Yoshikawa, T. Kato and T. Takenishi, *Bull. Chem. Soc. Jpn*, 1969, **42**, 3505-3508.

146. T. Sowa and S. Ouchi, *Bull. Chem. Soc. Jpn*, 1975, **48**, 2084-2090.

147. M. Hocek, A. Holý, I. Votruba and H. Dvořáková, *J. Med. Chem.*, 2000, **43**, 1817-1825.

148. M. Hocek, P. Nauš, R. Pohl, I. Votruba, P. A. Furman, P. M. Tharnish and M. J. Otto, *J. Med. Chem.*, 2005, **48**, 5869-5873.

149. P. Nauš, R. Pohl, I. Votruba, P. Džubák, M. n. Hajdúch, R. Ameral, G. Birkuš, T. Wang, A. S. Ray, R. Mackman, T. Cihlar and M. Hocek, *J. Med. Chem.*, 2009, **53**, 460-470.

150. P. Capek, R. Pohl and M. Hocek, *Org. Biomol. Chem.*, 2006, **4**, 2278-2284.

151. A. Collier and G. K. Wagner, *Chem. Commun.*, 2008, **2**, 178-180.

152. T. Pesnot and G. K. Wagner, *Org. Biomol. Chem.*, 2008, **6**, 2884-2891.

153. I. Hasan, E. R. Marinelli, L.-C. C. Lin, F. W. Fowler and A. B. Levy, *J. Org. Chem.*, 1981, **46**, 157-164.

154. S. R. Dandepally and A. L. Williams, *Tetrahedron Lett.*, 2009, **50**, 1071-1074.

155. M. Ikehara, S. Uesugi and M. Kaneko, *Chem. Commun. (London)*, 1967, **1**, 17-18.

156. K. Mikhailov, N. Marchenkov, V. Chichikina, V. Orlova and N. Myasoedov, *Chem. Nat. Compd.*, 1976, **12**, 461-464.

157. E. C. Western, J. R. Daft, E. M. Johnson, P. M. Gannett and K. H. Shaughnessy, *J. Org. Chem.*, 2003, **68**, 6767-6774.

158. A. Collier and G. K. Wagner, *ChemInform*, 2007, **38**, 3713-3721.

159. K. H. Shaughnessy, *Chem. Rev.*, 2009, **109**, 643-710.

160. N. Kohyama, T. Katashima and Y. Yamamoto, *Synthesis*, 2004, 2799-2804.

161. N. Kudo and M. Perseghini, *Angew. Chem. Int. Ed.*, 2006, **45**, 1282–1284.

162. C. A. Fleckenstein and H. Plenio, *Chemistry*, 2008, **14**, 4267–4279.

163. D. G. Hall, *Structure, Properties, and Preparation of Boronic Acid Derivatives: Overview of Their Reactions and Applications.*, Wiley-VCH Verlag GmbH & Co KGaA, Weinheim, Germany, Boronic Acids, 2005.

164. R. B. Bedford, M. E. Blake, C. P. Butts and D. Holder, *Chem. Commun.*, 2003, **4**, 466-467.

165. B. H. Lipshutz and A. R. Abela, *Org. Lett.*, 2008, **10**, 5329-5332.

166. B. H. Lipshutz, T. B. Petersen and A. R. Abela, *Org. Lett.*, 2008, **10**, 1333-1336.

167. V. A. Bloomfield, D. M. Crothers and I. Tinoco, *Nucleic Acids: Structures, Properties, and Functions*, Sausalito, Calif, University Science Books, 2000.

168. J. G. Moffatt and H. G. Khorana, *J. Am. Chem. Soc.*, 1961, **83**, 663-675.

169. S. Roseman, J. J. Distler, J. G. Moffatt and H. G. Khorana, *J. Am. Chem. Soc.*, 1961, **83**, 659-663.

170. T. Mukaiyama and M. Hashimoto, *Bull. Chem. Soc. Jpn*, 1971, **44**, 2284.

171. M. Hashimoto, M. Ueki and T. Mukaiyama, *Chem. Lett.*, 1976, **5**, 157-160.

172. G. Pergolizzi, J. N. Butt, R. P. Bowater and G. K. Wagner, *Chem. Commun.*, 2011, **47**, 12655-12657.

173. S. L. Beaucage and M. H. Caruthers, *Tetrahedron Lett.*, 1981, **22**, 1859-1862.

174. R. L. Letsinger and W. B. Lunsford, *J. Am. Chem. Soc.*, 1976, **98**, 3655–3661.

175. M. D. Matteucci and M. H. Caruther, *J. Am. Chem. Soc.*, 1981, **103**, 3185-3191.

176. M. L. Paul, D. L. Miles and M. A. Cook, *J. Pharm. Exp. Ther.*, 1982, **222**, 241-245.

177. C. D. Jardetzky, *J. Am. Chem. Soc.*, 1960, **82**, 229-233.

178. C. F. G. C. Geraldes and H. Santos, *Perkin Trans. 2*, 1983, **11**, 1693-1697.

179. R. Stolarski, L. Dudycz and D. Shugar, *Eur. J. Biochem.*, 1980, **108**, 111-121.

180. C. Altona and M. Sundaralingam, *J. Am. Chem. Soc.*, 1973, **95**, 2333-2244.

181. J. R. Lakowicz, *Principles of Fluorescence Spectroscopy*, Springer, 2006.

182. E. L. Wehry, in *Handbook of Instrumental Techniques for Analytical Chemistry*, ed. F. A. Settle, Prentice Hall PTR, 1997.

183. M. Sauer, J. Hofkens and J. Enderlein, *Handbook of Fluorescence Spectroscopy and Imaging*, Wiley VCH, 2011.

184. R. W. Sinkeldam, N. J. Greco and Y. Tor, *Chem. Rev.*, 2010, **110**, 2579-2619.

185. L. J. Kricka and P. Fortina, *Clin. Chem.*, 2009, **55**, 670-683.

186. J. W. Longworth, R. O. Rahn and R. G. Shulman, *J. Chem. Phys.*, 1966, **45**, 2930-2939.

187. E. Nir, K. Kleinermanns, L. Grace and M. S. de Vries, *J. Phys. Chem. A*, 2001, **105**, 5106-5110.

188. J.-M. L. Pecourt, J. Peon and B. Kohler, *J. Am. Chem. Soc.*, 2001, **123**, 10370-10378.

189. A. M. Ababneh, C. C. Large and S. Georghiou, *J. Appl. Sci. Res.*, 2007, **3**, 1288-1295.

190. J. N. Wilson and E. T. Kool, *Org. Biomol. Chem.*, 2006, **4**, 4265-4274.

191. J. N. Wilson, J. Gao and E. T. Kool, *Tetrahedron*, 2007, **63**, 3427-3433.

192. S. Paszyc and M. Rafalska, *Nucleic Acids Res.*, 1979, **6**, 385–397.

193. D. S. S. Zhou, S. C. Pomerantz, P. F. Crain, J. A. McCloskey, *Nucleosides Nucleotides Nucleic Acids*, 2004, **23**, 41-50.

194. L. M. Wilhelmsson, P. Sandin, A. Holmén, B. Albinsson, P. Lincoln and B. Nordén, *J. Phys. Chem. B*, 2003, **107**, 9094-9101.

195. J. C. Greenfield, N. J. Leonard and R. I. Gumport, *Biochemistry*, 1975, **14**, 698-706.

196. E. Sharon, S. A. Lévesque, M. N. Munkonda, J. Sévigny, D. Ecke, G. Reiser and B. Fischer, *ChemBioChem*, 2006, **7**, 1361-1374.

197. Y. Shinohara, K. Matsumoto, K. Kugenuma, T. Morii, Y. Saito and I. Saito, *Bioorg. Med. Chem. Lett.*, 2010, **20**, 2817-2820.

198. A. G. Firth, I. J. S. Fairlamb, K. Darley and C. G. Baumann, *Tetrahedron Lett.*, 2006, **47**, 3529-3533.

199. D. W. Dodd, K. N. Swanick, J. T. Price, A. L. Brazeau, M. J. Ferguson, N. D. Jones and R. H. E. Hudson, *Org. Biomol. Chem.*, 2010, **8**, 663-666.

200. L. Zilbershtein, A. Silberman and B. Fischer, *Org. Biomol. Chem.*, 2011, **9**, 7763-7773.

201. S. G. Srivatsan, H. Weizman and Y. Tor, *Org. Biomol. Chem.*, 2008, **6**, 1334-1338.

202. Y. T. Nicholas J. Greco, *Tetrahedron*, 2007, **63**, 3515-3527.

203. T. M. Michiko Kimoto, Yoko Harada, Akira Sato, Shigeyuki Yokoyama, and Ichiro Hirao, *Nucleic Acids Res.*, 2007, **35**, 5360–5369.

204. A. T. R. Williams, S. A. Winfield and J. N. Miller, *Analyst*, 1983, **108**, 1067-1071.

205. Jobin Yvon Ltd, *http://www.horiba.com/fileadmin/uploads/Scientific/Documents/Fluorescence/quantumyieldstrad.pdf*, 1996.

206. P. I. Vestues and R. B. Martin, *J. Am. Chem. Soc.*, 1981, **103**, 806-809.

207. A. J. Lees, *Chem. Rev.*, 1987, **87**, 711-743.

208. C. E. Moore Jr and A. L. Underwood, *Anal. Biochem.*, 1969, **29**, 149-153.

209. P. E. Smith and J. J. Tanner, *J. Mol. Recogn.*, 2000, **13**, 27-34.

210. J. E. Roberts, Y. Aizono, M. Sonenberg and N. I. Swislocki, *Bioorg. Chem.*, 1975, **4**, 181-187.

211. D. G. Cross and H. F. Fisher, *Biochemistry*, 1969, **8**, 1147-1155.

212. A. Schmidt, A. Lindner, M. Nieger, M. Ruiz-Delgado and F. J. Ramirez, *Org. Biomol. Chem.*, 2006, **4**, 3056-3066.

213. P. R. Mitchell and H. Sigel, *Eur. J. Biochem.*, 1978, **88**, 149-154.

214. R. H. Sarma and R. J. Mynott, *J. Am. Chem. Soc.*, 1973, **95**, 7470-7480.

215. O. Jardetzky and N. G. Wade-Jardetzky, *J. Biol. Chem.*, 1966, **241**, 85-91.

216. G. Zieger, R. Konrat and H. Sterk, *Magn. Res. Chem.*, 1992, **30**, S3-S6.

217. R. M. Riddle, T. J. Williams, T. A. Bryson, R. B. Dunlap, R. R. Fisher and P. D. Ellis, *J. Am. Chem. Soc.*, 1976, **98**, 4286-4290.

218. C.-H. Lee and I. Tinoco, *Biochemistry*, 1977, **16**, 5403-5414.

219. C. Stefan, S. Jansen and M. Bollen, *Purinergic Signal.*, 2006, **2**, 361–370.

220. J. W. Goding, B. Grobben and H. Slegers, *Biochim. Biophys. Acta - Mol. Basis Dis.*, 2003, **1638**, 1-19.

221. J. S. Culp and L. G. Butler, *Arch. Biochem. Biophys.*, 1986, **246**, 245-249.

222. R. Gijsbers, H. Ceulemans, W. Stalmans and M. Bollen, *J. Biol. Chem.*, 2001, **276**, 1361-1368.

223. E. Bischoff, T. Tran-Thi and K. F. A. Decker, *Eur. J. Biochem.*, 1975, **51**, 353-361.

224. L. H. Schliselfeld, J. van Eys and O. Touster, *J. Biol. Chem.*, 1965, **240**, 811-818.

225. W. Hensel, D. Rakow and W. Christ, *Anal. Biochem.*, 1975, **68**, 128-137.

226. D. W. Kahn and B. M. Anderson, *J. Biol. Chem.*, 1986, **261**, 6016-6025.

227. D. J. Wise, C. D. Anderson and B. M. Anderson, *Vet. Microbiol.*, 1997, **58**, 261-276.

228. R. K. Haroz, J. S. Twu and R. K. Bretthauer, *J. Biol. Chem.*, 1972, **247**, 1452-1457.

229. M. Bartkiewicz, H. Sierakowska and D. Shugar, *Eur. J. Biochem.*, 1984, **143**, 419-426.

230. J. Wierzchowski, H. Sierakowska and D. Shugar, *Biochim. Biophys. Acta - Protein Struct. Mol. Enzymol.*, 1985, **828**, 109-115.

231. H.-p. Cheng, S. Wei, L.-p. Wei and A. Verkhratsky, *Acta Pharmacol. Sin.*, 2006, **27**, 767-772.

232. H. C. Lee, R. Graeff and T. F. Walseth, *Biochimie*, 1995, **77**, 345-355.

233. H. C. Lee, *Physiol. Rev.*, 1997, **77**, 1133-1164.

234. F.-J. Zhang, Q.-M. Gu and C. J. Sih, *Bioorg. Med. Chem.*, 1999, **7**, 653-664.

235. Q.-M. Gu and C. J. Sih, *J. Am. Chem. Soc.*, 1994, **116**, 7481-7486.

236. H. C. Lee and R. Aarhus, *Cell Regul.*, 1991, **2**, 203-209.

237. H. C. Lee and R. Aarhus, *Biochim. Biophys. Acta - Protein Struct. Mol. Enzymol.*, 1993, **1164**, 68-74.

238. C. Cakir-Kiefer, H. Muller-Steffner and F. Schuber, *Biochem. J.*, 2000, **349**, 203-210.

239. R. M. Graeff, T. F. Walseth, K. Fryxell, W. D. Branton and H. C. Lee, *J. Biol. Chem.*, 1994, **269**, 30260-30267.

240. H. Kim, E. L. Jacobson and M. K. Jacobson, *Mol. Cell. Biochem.*, 1994, **138**, 237-243.

241. H. l. n. M. Muller-Steffner, A. l. Augustin and F. Schuber, *J. Biol. Chem.*, 1996, **271**, 23967-23972.

242. M. Ziegler, D. Jorcke, J. Zhang, R. Schneider, H. Klocker, B. Auer and M. Schweiger, *Biochemistry*, 1996, **35**, 5207-5212.

243. P. H. Pekala and B. M. Anderson, *J. Biol. Chem.*, 1978, **253**, 7453-7459.

244. H. M. Muller, C. D. Muller and F. Schuber, *Biochem. J.*, 1983, **212**, 459–464.

245. H. C. Lee, R. M. Graeff, C. B. Munshi, T. F. Walseth and R. Aarhus, in *Methods Enzymol.*, ed. J. W. S. C. W. Donald B. McCormick, Academic Press, 1997, pp. 331-340.

246. S. Zahringer, *Novel non-natural dinucleotides as chemical tools for biological studies*, 2012, **Diploma thesis**.

247. S. P. Jackson and J. Bartek, *Nature*, 2009, **461**, 1071-1078.

248. N. Dwivedi, D. Dube, J. Pandey, B. Singh, V. Kukshal, R. Ramachandran and R. P. Tripathi, *Med. Res. Rev.*, 2008, **28**, 545-568.

249. J. M. Pascal, *Curr. Opin. Struct. Biol.*, 2008, **18**, 96-105.

250. A. Wilkinson, H. Sayer, D. Bullard, A. Smith, J. Day, T. Kieser and R. Bowater, *Proteins*, 2003, **51**, 321-326.

251. J. Y. Lee, C. Chang, H. K. Song, J. Moon, J. K. Yang, H.-K. Kim, S.-T. Kwon and S. W. Suh, *EMBO J.*, 2000, **19**, 1119-1129.

252. L. K. Wang, H. Zhu and S. Shuman, *J. Biol. Chem.*, 2009, **284**, 8486-8494.

253. K. S. Gajiwala and C. Pinko, *Structure*, 2004, **12**, 1449-1459.

254. H. Zhu and S. Shuman, *J. Biol. Chem.*, 2005, **280**, 12137-12144.

255. J. Nandakumar, P. A. Nair and S. Shuman, *Mol. Cell*, 2007, **26**, 257-271.

256. L. K. Wang, P. A. Nair and S. Shuman, *J. Biol. Chem.*, 2008, **283**, 23343-23352.

257. A. Wilkinson, A. Smith, D. Bullard, M. Lavesa-Curto, H. Sayer, A. Bonner, A. Hemmings and R. Bowater, *Biochim. Biophys. Acta - Proteins Proteomics*, 2005, **1749**, 113-122.

258. T. I. Meier, D. Yan, R. B. Peery, K. A. McAllister, C. Zook, S.-B. Peng and G. Zhao, *FEBS J.*, 2008, **275**, 5258-5271.

259. R. P. Tripathi, J. Pandey, V. Kukshal, A. Ajay, M. Mishra, D. Dube, D. Chopra, R. Dwivedi, V. Chaturvedi and R. Ramachandran, *MedChemComm*, 2011, **2**, 378-384.

260. G. Ciarrocchi, D. G. MacPhee, L. W. Deady and L. Tilley, *Antimicrob. Agents Chemother.*, 1999, **43**, 2766-2772.

261. W. Gu, T. Wang, F. Maltais, B. Ledford, J. Kennedy, Y. Wei, C. H. Gross, J. Parsons, L. Duncan, S. J. Ryan Arends, C. Moody, E. Perola, J. Green and P. S. Charifson, *Bioorg. Med. Chem. Lett.*, 2012, **22**, 3693-3698.

262. T. Wang, L. Duncan, W. Gu, H. O'Dowd, Y. Wei, E. Perola, J. Parsons, C. H. Gross, C. S. Moody, S. J. Ryan Arends and P. S. Charifson, *Bioorg. Med. Chem. Lett.*, 2012, **22**, 3699-3703.

263. L. Miesel, C. Kravec, A.-T. Xin, P. McMonagle, S. Ma, J. Pichardo, B. Feld, E. Barrabee and R. Palermo, *Anal. Biochem.*, 2007, **366**, 9-17.

264. A. Bondi, *J. Phys. Chem. B*, 1964, **68**, 441-451.

265. D. L. Miles and H. Eyring, *Int. J. Quantum Chem.*, 1978, **14**, 173-190.

266. T. Kouzarides, *EMBO J.*, 2000, **19**, 1176-1179.

267. J. Schemies, U. Uciechowska, W. Sippl and M. Jung, *Med. Res. Rev.*, 2010, **30**, 861-889.

268. T. Finkel, C.-X. Deng and R. Mostoslavsky, *Nature*, 2009, **460**, 587-591.

269. B. J. North and E. Verdin, *Genome Biol.*, 2004, **5**, 224.

270. N. Dali-Youcef, M. Lagouge, S. Froelich, C. Koehl, K. Schoonjans and J. Auwerx, *Ann. Med.*, 2007, **39**, 335-345.

271. K. T. Howitz, K. J. Bitterman, H. Y. Cohen, D. W. Lamming, S. Lavu, J. G. Wood, R. E. Zipkin, P. Chung, A. Kisielewski, L.-L. Zhang, B. Scherer and D. A. Sinclair, *Nature*, 2003, **425**, 191-196.

272. Y. Ye and A. Godzik, *Nucleic Acids Res.*, 2004, **32**, 582-585.

273. Y. Ye and A. Godzik, *Protein Sci.*, 2004, **13**, 1841-1850.

274. B. J. North, B. Schwer, N. Ahuja, B. Marshall and E. Verdin, *Methods*, 2005, **36**, 338-345.

275. M. Magrane and U. Consortium, *Database*, 2011, **2011**.